

## *Advanced structural mechanics*

# *Advanced structural mechanics*

An introduction to continuum mechanics  
and structural mechanics

**David Johnson**

*Principal Lecturer in Structural Engineering  
Nottingham Trent University*



Thomas Telford

Published by Thomas Telford Publishing, Thomas Telford Ltd, 1 Heron Quay, London E14 4JD.  
URL: <http://www.t-telford.co.uk>

Distributors for Thomas Telford books are

*USA:* ASCE Press, 1801 Alexander Bell Drive, Reston, VA 20191-4400

*Japan:* Maruzen Co. Ltd, Book Department, 3-10 Nihonbashi 2-chome, Chuo-ku, Tokyo 103

*Australia:* DA Books and Journals, 648 Whitehorse Road, Mitcham 3132, Victoria

First published 1986 by Collins Professional and Technical Books

This edition 2000

A catalogue record for this book is available from the British Library

ISBN: 0 7277 2860 1

© D. Johnson and Thomas Telford Limited 2000

All rights, including translation, reserved. Except as permitted by the Copyright, Designs and Patents Act 1988, no part of this publication may be reproduced, stored in a retrieval system or transmitted in any form or by any means, electronic, mechanical, photocopying or otherwise, without the prior written permission of the Publishing Director, Thomas Telford Publishing, Thomas Telford Ltd, 1 Heron Quay, London E14 4JD

This book is published on the understanding that the author is solely responsible for the statements made and opinions expressed in it and that its publication does not necessarily imply that such statements and/or opinions are or reflect the views or opinions of the publishers. While every effort has been made to ensure that the statements made and the opinions expressed in this publication provide a safe and accurate guide, no liability or responsibility can be accepted in this respect by the author or publishers

Typeset by Helius, Brighton

Printed and bound in Great Britain by MPG Books, Bodmin

# Contents

<b>Preface to the first edition</b>	<b>v</b>
<b>Preface to the second edition</b>	<b>vii</b>
<b>Examination question sources</b>	<b>ix</b>
<b>1 Elasticity</b>	<b>1</b>
1.1 Introduction	1
1.2 Elasticity theory	2
1.2.1 Stress	3
1.2.2 Displacements and strains	4
1.2.3 Stresses and strains	6
1.3 Plane stress	9
1.3.1 Introduction	9
1.3.2 Theory	10
1.3.3 Stress function solution	15
1.4 Finite element method	16
1.4.1 Triangular element theory	16
1.4.2 Example 1.1 – concrete cube analysis	20
1.4.3 Finite element types	36
1.4.4 Eight-noded isoparametric element	37
1.4.5 Assessment of solution accuracy	45
1.5 Plane strain	48
1.5.1 Introduction	48
1.5.2 Stresses and strains	49
References and further reading	50
Problems	51
<b>2 Torsion</b>	<b>59</b>
2.1 Introduction	59
2.2 Torsional behaviour	61
2.3 Solid sections	62
2.3.1 Circular section	62
2.3.2 Non-circular sections	63

2.3.3	Finite difference solutions	69
2.3.4	Comparison of solution methods	76
2.3.5	Properties of solid sections	77
2.4	Thin-walled sections	77
2.4.1	Singly closed sections	78
2.4.2	Multiply closed sections	81
2.4.3	Open sections	87
2.4.4	Properties of thin-walled sections	91
2.5	Soap-bubble (membrane) analogy	91
2.6	Non-uniform torsion	93
	References and further reading	94
	Problems	95
<b>3</b>	<b>Plates and slabs</b>	<b>101</b>
3.1	Introduction	101
3.2	Physical behaviour	102
3.2.1	Beam analogy	102
3.2.2	Grid analogy	103
3.2.3	Poisson's ratio effect	104
3.3	Elastic plate theory	105
3.3.1	Introduction	105
3.3.2	Displacements and strains	106
3.3.3	Strains, stresses and stress resultants	107
3.3.4	Moments, curvatures and stresses	109
3.3.5	Equilibrium	110
3.3.6	General elastic plate equation	112
3.3.7	Boundary conditions	113
3.3.8	Classical solutions to the plate problem	117
3.4	Finite difference method	118
3.4.1	Introduction	118
3.4.2	Boundary conditions	118
3.4.3	Evaluation of moments and shear forces	120
3.4.4	Examples	120
3.4.5	Extensions and refinements	126
3.5	Grid representation method	126
3.5.1	Grid properties	126
3.5.2	Boundary conditions	128
3.5.3	Load representation	129
3.5.4	Evaluation of moments and shear forces	129
3.5.5	Evaluation of reactions	130
3.5.6	Examples	130
3.5.7	Extensions and refinements	136
3.6	Finite element method	136
3.6.1	Rectangular element theory	136

3.6.2	Example	145
3.6.3	Extensions and refinements	151
3.7	Comparison of analyses	152
3.8	Design moments	152
3.8.1	Introduction	152
3.8.2	Recommendations	153
3.8.3	Example 3.7 – simply supported slab design moments	154
3.8.4	Example 3.8 – fixed-edge slab design moments	154
	References and further reading	154
	Problems	156
<b>4</b>	<b>Thin shells</b>	<b>165</b>
4.1	Introduction	165
4.1.1	Generation, classification and application	165
4.1.2	Structural behaviour	167
4.1.3	Scope of the chapter	168
4.2	Membrane theory for axisymmetric shells	169
4.2.1	Basic properties	169
4.2.2	Example 4.1 – spherical dome under dead load	176
4.2.3	Limitations of membrane theory	178
4.2.4	Example 4.2 – paraboloid dome under internal pressure	180
4.2.5	Example 4.3 – conical shell under fluid pressure	182
4.3	Bending of circular cylindrical shells	186
4.3.1	Finite element method	186
4.3.2	Example 4.4 – circular tank of uniform thickness	193
4.3.3	Example 4.5 – circular tank of non-uniform thickness	199
4.4	Finite elements for non-cylindrical shells	204
	References and further reading	205
	Problems	206
<b>5</b>	<b>Structural dynamics</b>	<b>217</b>
5.1	Introduction	217
5.2	Types of vibration	218
5.2.1	Free, undamped vibration	218
5.2.2	Free, damped vibration	221
5.2.3	Forced, damped vibration	223
5.3	Determination of natural frequencies and modes	228
5.3.1	Modelling	228
5.3.2	Theory	228
5.3.3	Example 5.1 – single-storey sway frame	231
5.3.4	Simplified analysis of sway frames	235
5.3.5	Analysis of beams	240

5.3.6	Example 5.4 – cantilever slab	244
5.3.7	Orthogonality of the principal modes	247
5.3.8	Rayleigh quotient	248
5.3.9	Distributed-mass models	250
5.4	Free, undamped vibration analysis	250
5.4.1	Analysis by mode superposition	251
5.4.2	Example 5.5 – three-storey sway frame	253
5.5	Forced, undamped vibration analysis	255
5.5.1	Analysis by mode superposition	256
5.5.2	Example 5.6 – sway frame under ground motion	258
5.6	Harmonically forced, undamped vibration analysis	261
5.6.1	Analysis by mode superposition	261
5.6.2	Example 5.7 – harmonically forced cantilever beam	262
5.7	Specialized problems	263
	References and further reading	264
	Problems	266
<b>Appendix A Finite difference method</b>		<b>273</b>
A.1	Theory	273
A.1.1	Functions of a single variable	273
A.1.2	Functions of two variables	275
A.2	Practical application	277
	References and further reading	280
<b>Appendix B Finite element method</b>		<b>281</b>
B.1	Introduction	281
B.2	Theory	282
	References and further reading	285
<b>Solutions to problems</b>		<b>287</b>
<b>Index</b>		<b>299</b>

## *Preface to the first edition*

In recent years an increasing emphasis has been placed on numerically based methods of structural analysis. This has been reflected in the production of structural mechanics texts which are orientated towards particular numerical methodologies, especially the finite element method. Whilst this approach serves the needs of potential 'research' engineers, a concentration on the numerical analysis aspects of structural mechanics is of less relevance to future 'professional' engineers, who are likely to be concerned with the use and interpretation of numerical analyses, but not in the development of the methodologies.

It is to this latter group that the present text is especially addressed, and the intention is to give a broad introduction to the principal themes of continuum mechanics and structural dynamics, with an emphasis on the description of physical behaviour and on the use of analytical techniques to illumine and quantify the performance of structural systems.

In an introductory work such as this, a breadth of coverage is desirable from the standpoints of both the needs of the student and of the possibilities provided for exploring the relevance of structural concepts to differing geometric forms. Breadth, within a manageable text, does, however, require that rather brutal decisions be made in the selection of the material to be covered. In addition to the very limited treatment of the theory, as opposed to the use, of numerical methods, it has only been possible to mention solutions based on classical methods of differential calculus due to the limited applicability of such solutions and the often lengthy and intricate nature of the mathematical arguments involved.

A perhaps more serious cause for regret is that space has required a restriction to a linear elastic behavioural model. Whilst commonly used for practical analysis purposes, and convenient as a model which can be readily adapted to different structural forms and materials, linear elasticity is, of course, unable to represent many aspects of structural behaviour which are of practical concern, especially when non-metallic materials are employed. As a partial remedy for this and other deficiencies, the author has been able to do no more



than indicate at the end of each chapter a selection of texts which may be used to augment the material covered.

In brief, then, the text aims to be a ‘taster’ in linear elastic continuum mechanics and structural dynamics, and it is hoped that, having acquired the taste, the student will be encouraged to tackle the more substantial fare that is available in the texts cited in the further reading sections of the book. The preliminary knowledge assumed is that usually covered in the first two years of undergraduate courses in structural mechanics, strength of materials and mathematics. In particular, an acquaintance with matrix algebra and the finite difference and element methods is presumed, although outlines of the latter two topics are included as appendices for the benefit of those who may not have been previously exposed to these techniques.

For the purely numerical analysis operations of linear equation solution and eigenvalue determination, it has been assumed that standard computer routines are readily available. For the more structurally orientated aspects of numerical methods, it has, however, been considered desirable to give and set examples solved by ‘hand’ in order to develop a feel for the techniques involved. For solutions to be practical by hand, coarse nets must be used so that the results may be liable to substantial error. As far as possible, the nets used have been sufficiently fine so as to produce acceptable approximations, but this is not the case for some of the problems for student solution, which must be accepted as being of teaching value only.

Finally, a pleasant task: to acknowledge those whose assistance has been so generously given in the preparation of this book. Professor Arthur Bolton of Heriot-Watt University, Costas Ioannou of NELP and Dave Phillips of Glasgow University have all read chapters in proof and I have profited greatly from their advice and comments. Fred Marris and Brian Whiting, both of NELP, patiently provided ‘driving instruction’ on the MEDUSA drafting system and DIABLO printer used to prepare the diagrams and text respectively. An author’s family have to tolerate an even greater than normal level of absence and abstraction of mind, and I am grateful to record that this has been cheerfully accorded me. In particular, I must thank my daughter Ruth, who prepared some of the diagrams and a considerable number of the equations.

## *Preface to the second edition*

The aims of the text have remained unchanged for this edition, although the major addition, that of covering the application of isoparametric finite elements to plane elasticity, has inevitably tended to increase the proportion of material devoted to the numerical analysis aspect of this topic in relation to the material treating the structural behavioural aspect. This is a cause for minor regret but has been accepted due to the wide use made of this particular finite element and the need therefore for future 'professional' engineers to have at least an outline appreciation of its theoretical foundations. In common with the other elements covered, a numerical example of the use of an isoparametric element has been provided, although this certainly represents the limit to which it is reasonably possible to contemplate example hand solutions.

The number of problems for student solution has been increased to provide a wider range and the opportunity has been taken to update material and to correct errors in the previous editions, without, it is hoped, introducing too many new ones. Comments on this edition are always welcome and I am grateful, in particular, for advice from Professor Ian May of Heriot-Watt University and Dr Angus Ramsay of Nottingham Trent University regarding its preparation.

## *Examination question sources*

A number of the problems for student solution have been taken from degree, or equivalent, examination questions set by different institutions and are reproduced by kind permission of the relevant authorities. The sources of such problems are indicated in the text as follows:

BRIGHTON: University of Brighton

CITY: City University, London

EC: Engineering Council

KCL: King's College (University of London)

LIVERPOOL: Liverpool University

NTU: Nottingham Trent University

UCL: University College (University of London)

UEL: University of East London

The solutions provided are, however, my own and the responsibility for any errors in these therefore lies solely with myself.

# 1. *Elasticity*

## 1.1 Introduction

Elementary structural mechanics is primarily concerned with the behaviour of *line* elements, such as rods or beams, and with assemblies of these elements in the form of skeletal structures. Line elements are characterized by having cross-sectional dimensions which are of a different order to the length of the element. The structural analysis of line elements is simplified by several properties, the most pertinent of which is that the deformed shape of the element may often be completely described by the displaced shape of its longitudinal axis. This is so if the deformation of the cross-section may be assumed to bear a simple geometric relationship to the axis deformation. An example of such a relationship is the *plane sections* assumption of simple bending theory in which sections normal to the axis are presumed to remain normal in the deformed position. In these circumstances, the displacement of the element may be expressed in terms of one independent position variable, namely distance along the axis, and the resulting differential equation for the displacement will be of the *ordinary* form, as in the case of beam bending.

As the name suggests, *continuum mechanics* is concerned with structures which are continuous in space. The simplest elements of this type are *surface* elements which have a thickness of a different order to the other two dimensions. Surface elements are termed *plates* if they have a plane form, and *shells* if the form is a general surface. The deformation throughout the thickness of a plate or shell may still usually be related to the deformation of a single point within the thickness by the assumption of suitable geometric relationships. It is not therefore necessary to treat these elements as three-dimensional solids, it being sufficient to examine the deformation of a, usually central, surface. At least two independent variables will, however, be needed to specify a position on such a surface, and the differential equations governing its deformation therefore become more complex than for line elements and are also of the *partial* variety. The deformed state of a general solid is variable throughout its volume, and three independent position variables are involved with correspondingly more complex governing partial differential equations.

Overall geometric form thus allows structures to be categorized into line, surface or solid elements, and analytic models may then be developed which are best suited to the different types. In producing models, the nature of the constructional material must, however, be carefully considered. If the structural geometry, material and loads are such that the displacements under the expected loads can reasonably be expected to be so small as not to influence the structural behaviour, then a *small-deflection/small-strain* theory is produced in which, in particular, elastic instability (buckling) effects are excluded. If the loads and material are also such that the deformations are of a linear elastic nature (as assumed throughout this volume), so that plasticity, for example, does not occur, then the analysis of plates, shells and solids on this basis is simply termed the *theory of elasticity*.

The purposes of the present chapter are to develop some fundamental theory of elasticity ideas and relationships and to apply these to the analysis of structural forms which are such that either the stresses or the strains are confined to a plane. Chapter 2 considers line elements but again uses elasticity theory, since the subject matter is torsion, for which it is not possible to assume a simple relationship between the axial and cross-sectional displacements in the case of non-circular sections. Chapter 3 deals with plates which are normally loaded so that bending and twisting actions predominate. Shells are discussed in Chapter 4, where the detailed treatment is restricted to axisymmetric forms and loading. Finally, line elements are considered once more in Chapter 5, which deals with the dynamic response of, mainly, skeletal structures.

## 1.2 Elasticity theory

In structural analysis, the objective is to determine the *response* (deformations and stresses) to a specified *causation* effect, which will here be taken to be

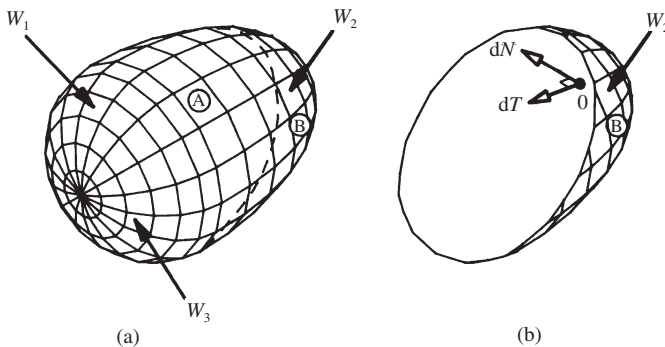


Fig. 1.1 (a) Solid body. (b) Part body

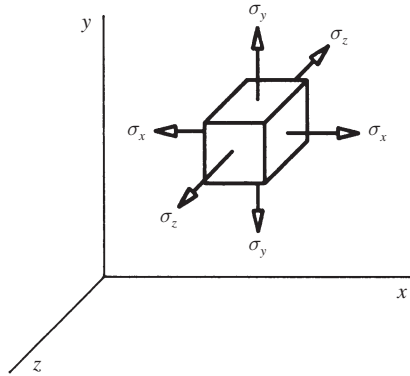


Fig. 1.2 Direct stress components

applied loading but could, more generally, include temperature changes, support movements and similar influences. This section defines the response variables which are of interest in the theory of elasticity and establishes general relationships between these variables, based on both geometrical and elastic material law considerations.

### 1.2.1 Stress

The solid of Fig. 1.1(a) is considered to consist of the two parts A and B separated by the plane shown dotted. The effect of part A on a small element  $dA$  of the separation plane on B may be represented by a force,  $dP$ , and  $dP$  may be represented by components  $dN$  and  $dT$  (Fig. 1.1(b)) which act along the normal to the plane and within the plane respectively. The direct (normal) and shear (tangential) components of stress at O are then defined to be

$$\sigma = \lim_{dA \rightarrow 0} \left( \frac{dN}{dA} \right) \quad (1.1)$$

$$\tau = \lim_{dA \rightarrow 0} \left( \frac{dT}{dA} \right) \quad (1.2)$$

If a stressed element in a set of rectangular Cartesian axes is now considered, then the direct stress on the element may be represented by the three pairs of self-equilibrating stress components shown, in their positive directions, in Fig. 1.2. The shear stress may be represented by the three *sets* of pairs of stress components shown, also in their positive directions, in Fig. 1.3. In Fig. 1.3, it should be noted that the two pairs of shear stress components involved in each set are of equal magnitude. This *complementary* property of

shear stress components is required for the moment equilibrium of the element, since, for example, in Fig. 1.3(a), taking the element sides to be  $dx$ ,  $dy$  and  $dz$ :

By moments about the  $z$ -axis:

$$-\tau_{xy}(dz dx)dy + \tau_{yx}(dz dy)dx = 0$$

Hence

$$\tau_{yx} = \tau_{xy}$$

In Fig. 1.3, it should be noted that the planes on which the shear stresses act are perpendicular to the plane formed by the pair of axes specified by the relevant double suffix. Thus  $\tau_{yz}$ , for example, acts on planes which are normal to the  $y$ - $z$  plane.

### 1.2.2 Displacements and strains

The deformation at any point of a body will be defined by its displacement components  $u$ ,  $v$  and  $w$  parallel to the  $x$ ,  $y$  and  $z$  axes respectively. The deformation of an element of a body will be represented by a set of strain components corresponding to the stress components which have just been described. If the deformation of an element in the  $x$ - $y$  plane, for example, is considered then it is possible to geometrically relate strain and displacement components.

In Fig. 1.4(a), direct strain in the  $x$ -direction is illustrated, extension being considered positive so as to correspond to the tensile positive stress convention adopted earlier. The  $x$ -displacement component at the beginning of the element is  $u$  and, since the rate of increase in  $u$  is mathematically represented by  $\partial u/\partial x$ , the total increase in  $u$  over the length of the element,  $dx$ , will be

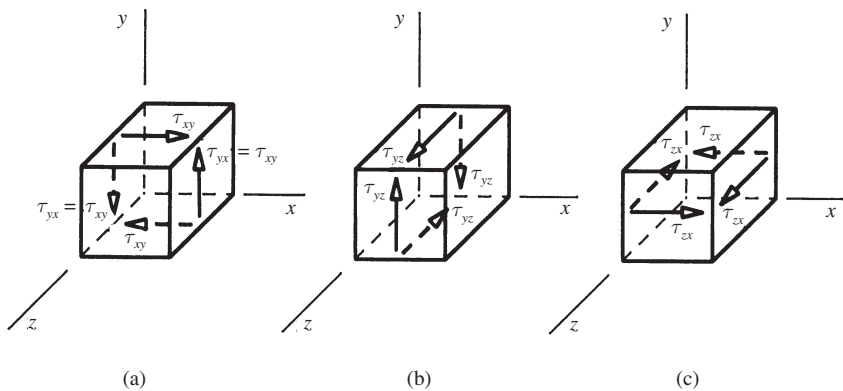


Fig. 1.3 Shear stress components

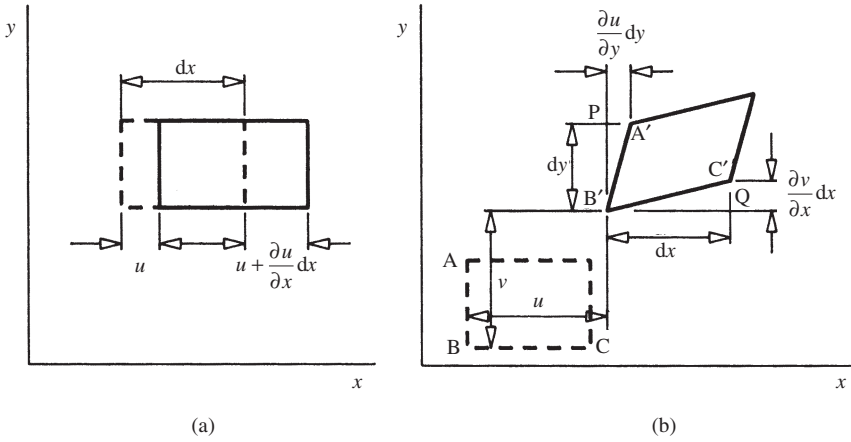


Fig. 1.4 (a) Direct strain. (b) Shear strain

$(\partial u/\partial x)dx$ . The  $x$ -direction strain may therefore be represented as

$$\varepsilon_x = \frac{(\partial u/\partial x)dx}{dx} = \frac{\partial u}{\partial x}$$

The shear strain illustrated in Fig. 1.4(b) may also be related to the displacement components. It is first noted that positive shear strain is caused by positive shear stress (Fig. 1.3) and is defined as the change in the angle ABC in Fig. 1.4(b). The shear stress components have, in fact, been taken such that a positive shear stress causes a *decrease* in the relevant element angle closest to (or furthest from) the origin. The expressions given in Fig. 1.4(b) for the  $u$  and  $v$  displacements of  $A'$  and  $C'$  relative to  $B'$  follow from a similar mathematical argument to that used for direct strain. Thus, to obtain the  $x$ -displacement of  $A'$  relative to  $B'$  it is necessary to consider the rate of increase of  $u$  with  $y$  which is given by  $\partial u/\partial y$ , the total relative displacement then being as indicated in the figure. A corresponding argument results in the expression shown for the relative  $y$ -displacement of  $C'$  to  $B'$ . Assuming small angles, the shear strain may therefore be determined as

$$\begin{aligned}\gamma_{xy} &= \hat{P}B'A' + C'\hat{B}'Q \\ &= \frac{(\partial u/\partial y)dy}{dy} + \frac{(\partial v/\partial x)dx}{dx}\end{aligned}$$

Hence

$$\gamma_{xy} = \frac{\partial u}{\partial y} + \frac{\partial v}{\partial x}$$



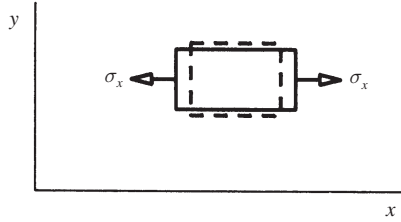


Fig. 1.5  $x$ -direction stress

From similar considerations to the above, the complete three-dimensional strain–displacement relationships are

$$\varepsilon_x = \frac{\partial u}{\partial x}, \quad \varepsilon_y = \frac{\partial v}{\partial y}, \quad \varepsilon_z = \frac{\partial w}{\partial z} \quad (1.3)$$

for direct strains and

$$\begin{aligned} \gamma_{xy} &= \frac{\partial u}{\partial y} + \frac{\partial v}{\partial x} \\ \gamma_{yz} &= \frac{\partial v}{\partial z} + \frac{\partial w}{\partial y} \\ \gamma_{zx} &= \frac{\partial w}{\partial x} + \frac{\partial u}{\partial z} \end{aligned} \quad (1.4)$$

for shear strains.

### 1.2.3 Stresses and strains

In seeking relationships between stresses and strains, material law considerations must be employed. Under linear conditions, a direct stress produces a proportional strain, so that, for a stress in the  $x$ -direction (Fig. 1.5), stress and strain may, typically, be related by

$$\varepsilon_x = \frac{\sigma_x}{E}$$

where the material constant  $E$  is known as *Young's modulus* or the *modulus of elasticity*.

From experience of rubbery materials, it may however be visualized that a positive  $x$ -direction stress will cause a contraction in the  $y$ -direction as well as an extension in the  $x$ -direction. This phenomenon is known as the *Poisson's ratio* effect and the two strains are related by

$$\varepsilon_y = -\nu\varepsilon_x = -\nu\frac{\sigma_x}{E}$$

where the material constant  $\nu$  is known as *Poisson's ratio*.

The effects of Poisson's ratio are significant in the case of metals, which have an average ratio of approximately 0.3, but are of less importance, and can sometimes be neglected, for concrete and masonry, which, typically, have ratios in the range 0.1–0.2. As already noted, rubber has a particularly high ratio, approaching 0.5. If the general three-dimensional direct stress case is considered (Fig. 1.2), then the total strain in any given direction may be obtained by superimposing the individual strains in the specified direction due to the three stress components. If a restriction is made to a *homogeneous, isotropic* material, that is, one which is uniform throughout its volume and has identical material properties in all directions, then, at any point in the material

$$\begin{aligned}\varepsilon_x &= \frac{1}{E}(\sigma_x - \nu\sigma_y - \nu\sigma_z) \\ \varepsilon_y &= \frac{1}{E}(-\nu\sigma_x + \sigma_y - \nu\sigma_z) \\ \varepsilon_z &= \frac{1}{E}(-\nu\sigma_x - \nu\sigma_y + \sigma_z)\end{aligned}\quad (1.5)$$

A linear relationship between shear stress and strain is also presumed, so that

$$\gamma_{xy} = \frac{1}{G}\tau_{xy}, \quad \gamma_{yz} = \frac{1}{G}\tau_{yz}, \quad \gamma_{zx} = \frac{1}{G}\tau_{zx}\quad (1.6)$$

where the material constant  $G$  is known as the *shear modulus* or *modulus of rigidity*.

The three elastic material constants  $E$ ,  $\nu$  and  $G$  cannot, in fact, be specified independently and it is shown in elementary strength of materials texts (Megson, 1996) that

$$G = \frac{E}{2(1+\nu)}\quad (1.7)$$

It is sometimes necessary to determine stresses from known strains, in which case the dependent and independent variables of equations (1.5) and (1.6) may be changed to give (as the reader may verify)

$$\begin{aligned}\sigma_x &= \frac{E(1-\nu)}{(1+\nu)(1-2\nu)}\left[\varepsilon_x + \frac{\nu}{(1-\nu)}\varepsilon_y + \frac{\nu}{(1-\nu)}\varepsilon_z\right] \\ \sigma_y &= \frac{E(1-\nu)}{(1+\nu)(1-2\nu)}\left[\frac{\nu}{(1-\nu)}\varepsilon_x + \varepsilon_y + \frac{\nu}{(1-\nu)}\varepsilon_z\right] \\ \sigma_z &= \frac{E(1-\nu)}{(1+\nu)(1-2\nu)}\left[\frac{\nu}{(1-\nu)}\varepsilon_x + \frac{\nu}{(1-\nu)}\varepsilon_y + \varepsilon_z\right]\end{aligned}\quad (1.8a)$$

$$\begin{aligned}\tau_{xy} &= G\gamma_{xy}, \quad \tau_{yz} = G\gamma_{yz}, \quad \tau_{zx} = G\gamma_{zx}\end{aligned}\quad (1.8b)$$

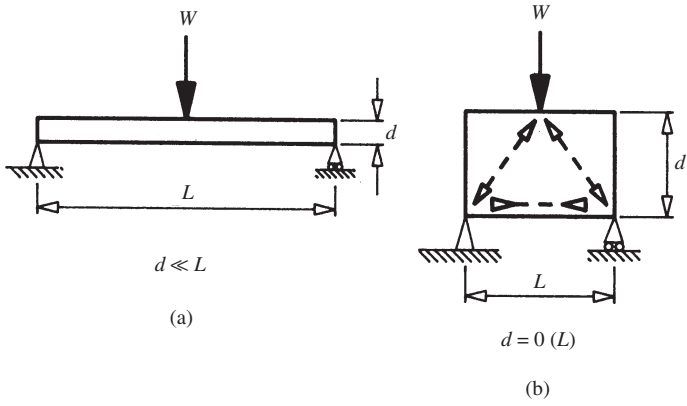


Fig. 1.6 (a) Normal beam. (b) Deep beam

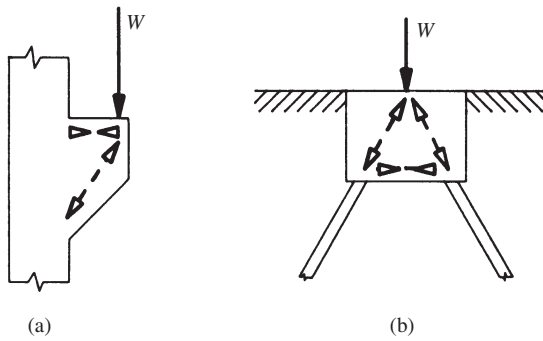


Fig. 1.7 (a) Corbel. (b) Pile cap

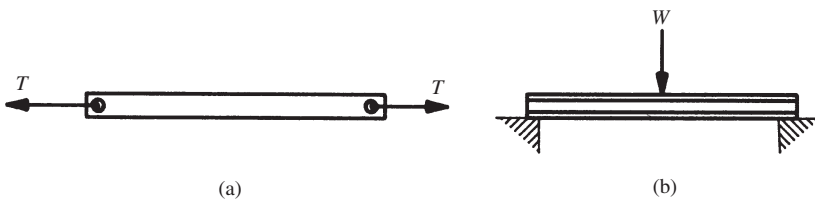


Fig. 1.8 (a) Tie. (b) Simple beam

## 1.3 Plane stress

### 1.3.1 Introduction

The relationships developed in the previous section provide a basis on which specific, more restricted elasticity problems may be studied. The limitations are imposed in the interests of simplicity, and perhaps the most straightforward case to study is that of *plane stress* in which all stresses other than those acting in a particular plane are assumed to be zero. Plane stress occurs when a thin plate is subjected to loading in its own plane only, say along its edges. The faces of the plate are then free of normal or tangential stresses and, for a thin plate, it may reasonably be presumed that this situation persists throughout the plate thickness. A classic problem of this type is to determine the stress concentration around a hole introduced into the stressed hull of a ship or aircraft. Similar stress concentrations occur around a notch or idealized crack and also in the neighbourhood of re-entrant plate corners, all of which situations fall within the scope of plane stress analysis.

Another way of producing plane stress problems is to take a plane line element and make two of its leading dimensions be of the same order so as to produce a plate problem. Thus, if the depth of the beam element of Fig. 1.6(a) is made of the same order as the span, while the thickness remains small, then a plane stress problem of the *deep beam* variety (Fig. 1.6(b)) is produced. Deep beams cannot be accurately analysed by simple bending theory, since loads tend to be resisted by internal ‘truss’ action (Fig. 1.6(b)) rather than by the familiar combined shear and bending action of normal beam theory. Deep beams occur in practice whenever loads are relatively large and spans short. Typical examples are the crane supporting corbel and the pile cap of Fig. 1.7.

Even when the overall behaviour of line elements may be satisfactorily described by simple theories, elasticity theory may be needed to investigate local effects. Thus, while the tensile stress in the tie of Fig. 1.8(a) is uniform along the major part of its length, a non-uniform stress distribution will exist on cross-sections close to the ends, since the end cross-sections must be stress-free, and high bearing stresses will exist at the points of load application. A further example of an important local effect is provided by the simple beam of Fig. 1.8(b). Normal bending theory predicts that the load is resisted by longitudinal direct stresses and shear stresses, there being no direct stress in the vertical direction. Clearly this is not the case in the neighbourhood of the applied load (or near the supports) where direct vertical compressive stresses must exist and can cause local buckling if the web is insufficiently stiff.

The region in which local effects need to be considered may be identified from *Saint-Venant’s* principle. This principle states that if a loading system be replaced by a statically equivalent system, then the response is unaffected at a distance which is of the order of the length over which the statically equivalent system is applied. So, if the load  $T$  in Fig. 1.8(a) were replaced by a statically

equivalent set of uniform direct stresses of magnitude  $T/A$  distributed over the end cross-sections, then uniform stress would persist throughout the tie, and Saint–Venant’s principle indicates that the non-uniformity due to point application of  $T$  can be expected to be small at a distance along the tie of about once or twice its width.

### 1.3.2 Theory

If the faces of a plate are stress-free (Fig. 1.9), then only the three co-planar stress components  $\sigma_x$ ,  $\sigma_y$  and  $\tau_{xy}$  are non-zero and these stresses may be considered to be uniformly distributed through the (small) plate thickness,  $t$ . The plate displacement, at any given point, will be constant throughout its thickness and will be in the plane of the plate. Thus, the displacement at any point will be fully represented by the two displacement components  $u$  and  $v$ . The determination of the stresses  $\sigma_x$ ,  $\sigma_y$  and  $\tau_{xy}$  and the displacements  $u$  and  $v$  throughout the plate for a specified in-plane loading constitutes the general plane stress problem.

It should be emphasized that the stress and displacement components determined will relate only to the chosen  $x$ - and  $y$ -axes. The components in any other directions, say  $x'$  and  $y'$  of Fig. 1.10(a), may, however, be determined by suitable resolution. In the case of stresses, it may be shown (Megson, 1996) that there will exist two mutually perpendicular directions at any point, for which the shear stress component disappears, leaving only two direct *principal stresses* in these directions. The principal stresses may further be shown to be the algebraically greatest and smallest stresses acting at the point. The orientation angle of the principal stresses is given by

$$\tan 2\theta = \frac{2\tau_{xy}}{\sigma_y - \sigma_x} \quad (1.9)$$

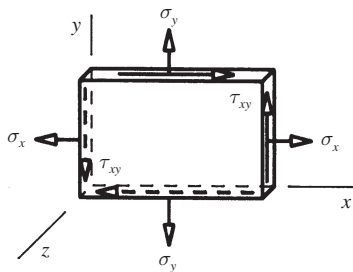


Fig. 1.9 Plane stress components

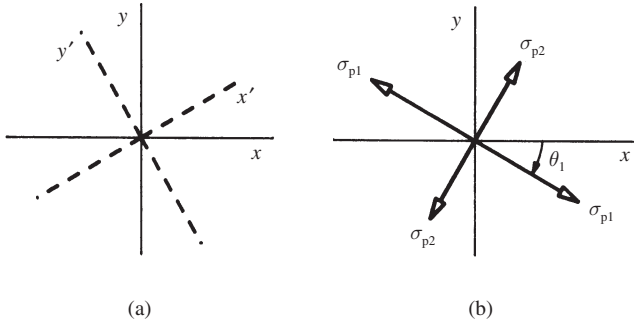


Fig. 1.10 (a) Axes rotation. (b) Principal stress directions

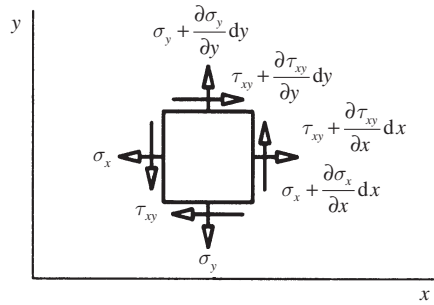


Fig. 1.11 Stress component variation

The solution to equation (1.9) provides two mutually perpendicular orientation angles:

$$\theta_1 = \theta, \quad \theta_2 = \theta + 90^\circ \quad (1.10)$$

where  $-45^\circ \leq \theta \leq 45^\circ$ . Using these two angles successively, the two principal stresses are given by

$$\sigma_{p1,2} = \sigma_x \cos^2 \theta_{1,2} + \sigma_y \sin^2 \theta_{1,2} - \tau_{xy} \sin 2\theta_{1,2} \quad (1.11)$$

The direction of the first principal stress makes an angle  $\theta_1$  (clockwise positive) with the positive  $x$ -axis (Fig. 1.10(b)), and the direction of the second principal stress is perpendicular to that of the first. As with the analysis of skeletal structures, the solution of a plane stress problem requires simultaneous satisfaction of conditions of equilibrium, compatibility and material behaviour. The governing equations for these three sets of conditions are therefore developed in the following sections.

### Equilibrium

Using the same sort of differential technique as with displacements and strains (see Section 1.2.2), the variation of the plane stress components acting on a rectangular element of size  $dx$ ,  $dy$  (thickness,  $t$ ) may be represented in the manner shown in Fig. 1.11. In Fig. 1.11, it has been assumed, for simplicity, that the plate is not subjected to *body* forces which are distributed throughout its volume. Gravitational, pore pressure, magnetic and inertial fields all give rise to body forces, for the treatment of which the reader is referred to more advanced texts (e.g. see Timoshenko and Goodier, 1982). The equilibrium of the element may be ensured by:

Resolving horizontal forces:

$$\left( \sigma_x + \frac{\partial \sigma_x}{\partial x} dx \right) (t dy) - \sigma_x (t dy) + \left( \tau_{xy} + \frac{\partial \tau_{xy}}{\partial y} dy \right) (t dx) - \tau_{xy} (t dx) = 0$$

Whence

$$\frac{\partial \sigma_x}{\partial x} + \frac{\partial \tau_{xy}}{\partial y} = 0 \quad (1.12a)$$

Similarly, resolving vertical forces:

$$\frac{\partial \sigma_y}{\partial y} + \frac{\partial \tau_{xy}}{\partial x} = 0 \quad (1.12b)$$

### Compatibility

In a state of plane stress, the deformation at any point may either be represented by the *two* displacement components  $u$  and  $v$  or by the *three* strain components  $\varepsilon_x$ ,  $\varepsilon_y$  and  $\gamma_{xy}$  and, by extraction from equations (1.3) and (1.4), these variables are related by

$$\varepsilon_x = \frac{\partial u}{\partial x}, \quad \varepsilon_y = \frac{\partial v}{\partial y}, \quad \gamma_{xy} = \frac{\partial u}{\partial y} + \frac{\partial v}{\partial x} \quad (1.13)$$

The disparity in the numbers of the displacement and strain variables indicates that a unique deformation may be specified by only two independent deformation variables and that the three strain variables must be inter-related. This is indeed the case, since:

From equations (1.13)

$$\frac{\partial^2 \varepsilon_x}{\partial y^2} = \frac{\partial^3 u}{\partial y^2 \partial x}, \quad \frac{\partial^2 \varepsilon_y}{\partial x^2} = \frac{\partial^3 v}{\partial x^2 \partial y}, \quad \frac{\partial^2 \gamma_{xy}}{\partial x \partial y} = \frac{\partial^3 u}{\partial x \partial y^2} + \frac{\partial^3 v}{\partial x^2 \partial y}$$

Hence

$$\frac{\partial^2 \varepsilon_x}{\partial y^2} + \frac{\partial^2 \varepsilon_y}{\partial x^2} = \frac{\partial^2 \gamma_{xy}}{\partial x \partial y} \quad (1.14)$$

Equation (1.14) is the *compatibility* equation, since it expresses the geometric integrity requirement that the plate material remain free from discontinuities such as ‘gaps’ or ‘overlaps’ between adjacent elements.

### Material laws

The relevant material laws assumed here are those of linear elasticity, and the relationships for plane stress may be obtained by setting  $\sigma_z$ ,  $\tau_{yz}$  and  $\tau_{zx}$  to zero in the more general equations (1.5) and (1.6) to give

$$\varepsilon_x = \frac{1}{E}(\sigma_x - \nu\sigma_y), \quad \varepsilon_y = \frac{1}{E}(-\nu\sigma_x + \sigma_y), \quad \gamma_{xy} = \frac{1}{G}\tau_{xy} \quad (1.15)$$

Also, if stresses are required in terms of strains, then, by changing the subjects of equations (1.15),

$$\sigma_x = \frac{E}{1-\nu^2}(\varepsilon_x + \nu\varepsilon_y), \quad \sigma_y = \frac{E}{1-\nu^2}(\nu\varepsilon_x + \varepsilon_y), \quad \tau_{xy} = G\gamma_{xy} \quad (1.16)$$

The strain–stress relationships may be combined with the compatibility equation to produce a general condition in terms of the stress components. Thus, substituting in equation (1.14) from equation (1.15) yields

$$\frac{1}{E} \left( \frac{\partial^2 \sigma_x}{\partial y^2} - \nu \frac{\partial^2 \sigma_y}{\partial y^2} \right) + \frac{1}{E} \left( -\nu \frac{\partial^2 \sigma_x}{\partial x^2} + \frac{\partial^2 \sigma_y}{\partial x^2} \right) = \frac{1}{G} \frac{\partial^2 \tau_{xy}}{\partial x \partial y} \quad (1.17)$$

But, from the equilibrium equations (1.12a) and (1.12b),

$$\frac{\partial^2 \tau_{xy}}{\partial x \partial y} = -\frac{\partial^2 \sigma_x}{\partial x^2}$$

$$\frac{\partial^2 \tau_{xy}}{\partial y \partial x} = -\frac{\partial^2 \sigma_y}{\partial y^2}$$

So that

$$2 \frac{\partial^2 \tau_{xy}}{\partial x \partial y} = -\frac{\partial^2 \sigma_x}{\partial x^2} - \frac{\partial^2 \sigma_y}{\partial y^2} \quad (1.18)$$

Substituting in equation (1.17) from equations (1.18) and (1.7):

$$\frac{1}{E} \left( \frac{\partial^2 \sigma_x}{\partial y^2} - \nu \frac{\partial^2 \sigma_y}{\partial y^2} \right) + \frac{1}{E} \left( -\nu \frac{\partial^2 \sigma_x}{\partial x^2} + \frac{\partial^2 \sigma_y}{\partial x^2} \right) = \frac{-(1+\nu)}{E} \left( \frac{\partial^2 \sigma_x}{\partial x^2} + \frac{\partial^2 \sigma_y}{\partial y^2} \right)$$



Whence

$$\left( \frac{\partial^2}{\partial x^2} + \frac{\partial^2}{\partial y^2} \right) (\sigma_x + \sigma_y) = 0 \quad (1.19)$$

Equation (1.19) is of the Laplace form and is of fundamental importance, not only in elasticity but also in wave and flow mechanics as well as several other physical fields.

### Virtual work

In connection with the finite element method, it will be necessary to make use of the principle of virtual displacements, and it is convenient to consider here how internal virtual work may be determined for a plane stress system. An expression will therefore be established for the virtual work expended when the plane stress system of Fig. 1.9 is subjected to a set of virtual strains  $(\varepsilon_x, \varepsilon_y, \gamma_{xy})_v$ . It is first noted that only corresponding strains and stresses produce net work, since, for example,  $x$ -direction strain produces no displacement in the direction of the normal  $y$ -direction stresses and the works done by the shear stresses on the upper and lower horizontal edges of the element are equal and opposite. Taking the element sides to be  $dx$ ,  $dy$  and  $t$ , it is therefore found that, for  $x$ -direction strain,

$$\begin{aligned} x\text{-direction virtual work} &= \text{force} \times \text{displacement} \\ &= \sigma_x (t \, dy) \times (\varepsilon_{xv} \, dx) = \varepsilon_{xv} \sigma_x \, dv \end{aligned}$$

where  $dv$  is the volume of the element. Similarly,

$$y\text{-direction virtual work} = \varepsilon_{yv} \sigma_y \, dv$$

In the case of work due to shear strain, the contributions from the distortions shown in Figs 1.12(a) and 1.12(b) will be summed. Thus, for the distortion of Fig. 1.12(a):

$$\begin{aligned} \text{shear}_a \text{ virtual work} &= \text{shear force} \times AA' = (\tau_{xy} t \, dx) \times (\alpha \, dy) \\ &= \tau_{xy} \alpha t \, dx \, dy = \tau_{xy} \alpha \, dv \end{aligned}$$

Similarly for the distortion of Fig. 1.12(b):

$$\text{shear}_b \text{ virtual work} = \tau_{xy} \beta \, dv$$

Hence

$$\text{shear virtual work} = \tau_{xy} (\alpha + \beta) \, dv = \gamma_{xyv} \tau_{xy} \, dv$$

and, by summing contributions,

$$\text{total virtual work} = (\varepsilon_{xv} \sigma_x + \varepsilon_{yv} \sigma_y + \gamma_{xyv} \tau_{xy}) \, dv \quad (1.20)$$

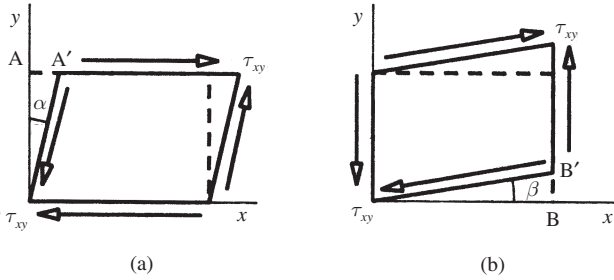


Fig. 1.12 Shear distortions

Equation (1.20) therefore provides the required expression for the virtual work undertaken by the stresses  $\sigma_x$ ,  $\sigma_y$  and  $\tau_{xy}$  acting on an element of volume  $dV$  when the element is subjected to a set of virtual strains  $(\varepsilon_x, \varepsilon_y, \gamma_{xy})_v$ .

### 1.3.3 Stress function solution

To achieve a solution to a plane stress problem, it is necessary to satisfy simultaneously the equations of equilibrium (1.12), compatibility (1.14) and the material laws (1.15) at every point in the plate and also to ensure that whatever special conditions may exist at the edges (*boundaries*) of the plate are also satisfied. Initially, the *closed-form* (analytical) solution of the governing equations by the methods of classical calculus will be considered. The most convenient approach here is to make use of a *stress function* so that the equilibrium equations are automatically satisfied and attention may be concentrated on the two remaining sets of conditions. In the plane stress case, this desirable object may be achieved by defining a stress function,  $\phi$ , such that, at any point in the plate,

$$\sigma_x = \frac{\partial^2 \phi}{\partial y^2}, \quad \sigma_y = \frac{\partial^2 \phi}{\partial x^2}, \quad \tau_{xy} = \frac{-\partial^2 \phi}{\partial x \partial y} \quad (1.21)$$

Substitution from equations (1.21) into the equilibrium equations (1.12) proves the adequacy of the stress function. If these stress function expressions are now substituted in the compatibility equation in terms of stresses (equation (1.19), which subsumes the material law conditions), the general plane stress equation in terms of the stress function may be obtained as

$$\frac{\partial^4 \phi}{\partial x^4} + 2 \frac{\partial^4 \phi}{\partial x^2 \partial y^2} + \frac{\partial^4 \phi}{\partial y^4} = 0 \quad (1.22)$$

Thus, if a stress function is found which satisfies equation (1.22) and also the boundary conditions for a given plane stress problem, then the problem is

solved, since the stress components may be obtained from equations (1.21), the strains from equations (1.15), and, by integration, the displacements from equations (1.13).

Direct solutions along these lines, using the methods of classical calculus, are, however, extremely arduous in rectangular coordinates and the commonest approach is to use a *semi-inverse* method (Timoshenko and Goodier, 1982), in which an assumed form of stress function is employed (usually a polynomial) which incorporates a number of undetermined coefficients. The coefficients are determined by enforcement of the general plane stress equation (1.22) and the boundary conditions. The stress function is then fully defined and the solution proceeds as just described. Even with this approach, the problems which may be tackled are restricted to relatively simple rectangular or triangular shapes. The use of different coordinate systems allows the range of problems to be extended, but many features of practical importance such as boundary irregularities, variable material properties, complex loadings or cut-outs cause insuperable difficulties. Non-standard problems, the norm in practice, are therefore usually tackled by the perhaps less elegant but more versatile numerical methods. The stress function approach can be adapted to the finite difference method but is limited by the difficulties involved in expressing boundary conditions in terms of the stress function and in automatically generating conditions along irregular boundaries. The finite element method is much more amenable to general automatic implementation and is therefore the usual current tool for plane stress analysis.

## 1.4 Finite element method

The reader who has not studied the finite element method previously is referred to Appendix B which gives an outline of the method and defines the notation used here where the application of the method to plane stress analysis is presented.

### 1.4.1 Triangular element theory

As noted above, the distortion of a point, under plane stress conditions, may be represented by the two displacement components  $u$  and  $v$  in the  $x$ - and  $y$ -directions respectively. Thus, for a triangular element (Fig. 1.13), each node has two displacement components and the total number of nodal displacement components to be considered is six. In choosing a polynomial displacement function to represent the variation of the displacements throughout the element, just six undetermined coefficients can therefore be included. Further, since  $u$  and  $v$  are independent of each other, their polynomial functions should

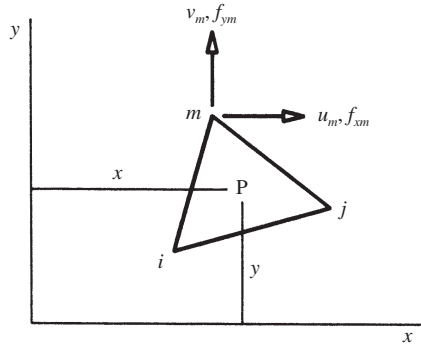


Fig. 1.13 Triangular element

not incorporate the same coefficients so that three distinct coefficients are available for each of the two displacement component polynomials. The simplest polynomial involving three coefficients in the position variables  $x$  and  $y$  is linear, so it will be assumed that the displacement of a general point, P, within the element may be represented by

$$u = \alpha_1 + \alpha_2 x + \alpha_3 y, \quad v = \alpha_4 + \alpha_5 x + \alpha_6 y \quad (1.23)$$

Equations (1.23) may be expressed in the matrix form

$$\{\partial\} = \begin{Bmatrix} u \\ v \end{Bmatrix} = \begin{bmatrix} 1 & x & y & 0 & 0 & 0 \\ 0 & 0 & 0 & 1 & x & y \end{bmatrix} \{\alpha\} \quad (1.24)$$

where  $\{\alpha\} = \{\alpha_1, \alpha_2, \dots, \alpha_6\}^T$  is the column vector of undetermined coefficients.

By successively letting P be the three element nodes  $i, j$  and  $m$ , the six nodal displacement components may be related to the six undetermined coefficients by

$$\{\partial^e\} = \begin{Bmatrix} u_i \\ v_i \\ u_j \\ v_j \\ u_m \\ v_m \end{Bmatrix} = \begin{bmatrix} 1 & x_i & y_i & 0 & 0 & 0 \\ 0 & 0 & 0 & 1 & x_i & y_i \\ 1 & x_j & y_j & 0 & 0 & 0 \\ 0 & 0 & 0 & 1 & x_j & y_j \\ 1 & x_m & y_m & 0 & 0 & 0 \\ 0 & 0 & 0 & 1 & x_m & y_m \end{bmatrix} \{\alpha\} = [C^e] \{\alpha\} \quad (1.25)$$

For convenience in inverting matrix  $[C^e]$ , equation (1.25) may be temporarily rearranged as

$$\begin{Bmatrix} u_i \\ u_j \\ u_m \\ v_i \\ v_j \\ v_m \end{Bmatrix} = \begin{bmatrix} 1 & x_i & y_i & 0 & 0 & 0 \\ 1 & x_j & y_j & 0 & 0 & 0 \\ 1 & x_m & y_m & 0 & 0 & 0 \\ 0 & 0 & 0 & 1 & x_i & y_i \\ 0 & 0 & 0 & 1 & x_j & y_j \\ 0 & 0 & 0 & 1 & x_m & y_m \end{bmatrix} \{\alpha\} \quad (1.26)$$

By using the co-factor (Stroud, 1995) or other method of inversion, the polynomial coefficients may now be expressed in terms of the element nodal displacements as shown by

$$\{\alpha\} = \frac{1}{2A} \begin{bmatrix} x_j y_m - x_m y_j & x_m y_i - x_i y_m & x_i y_j - x_j y_i & 0 & 0 & 0 \\ y_j - y_m & y_m - y_i & y_i - y_j & 0 & 0 & 0 \\ x_m - x_j & x_i - x_m & x_j - x_i & 0 & 0 & 0 \\ 0 & 0 & 0 & x_j y_m - x_m y_j & x_m y_i - x_i y_m & x_i y_j - x_j y_i \\ 0 & 0 & 0 & y_j - y_m & y_m - y_i & y_i - y_j \\ 0 & 0 & 0 & x_m - x_j & x_i - x_m & x_j - x_i \end{bmatrix} \begin{Bmatrix} u_i \\ u_j \\ u_m \\ v_i \\ v_j \\ v_m \end{Bmatrix} \quad (1.27)$$

where

$$A = \frac{1}{2} \det \begin{bmatrix} 1 & x_i & y_i \\ 1 & x_j & y_j \\ 1 & x_m & y_m \end{bmatrix}$$

which may be shown to be equal to the area of the triangular element  $i, j, m$ . Reverting to the original ordering of the variables,

$$\begin{aligned} \{\alpha\} &= \frac{1}{2A} \begin{bmatrix} x_j y_m - x_m y_j & 0 & x_m y_i - x_i y_m & 0 & x_i y_j - x_j y_i & 0 \\ y_j - y_m & 0 & y_m - y_i & 0 & y_i - y_j & 0 \\ x_m - x_j & 0 & x_i - x_m & 0 & x_j - x_i & 0 \\ 0 & x_j y_m - x_m y_j & 0 & x_m y_i - x_i y_m & 0 & x_i y_j - x_j y_i \\ 0 & y_j - y_m & 0 & y_m - y_i & 0 & y_i - y_j \\ 0 & x_m - x_j & 0 & x_i - x_m & 0 & x_j - x_i \end{bmatrix} \begin{Bmatrix} u_i \\ v_i \\ u_j \\ v_j \\ u_m \\ v_m \end{Bmatrix} \\ &= [C^e]^{-1} \{\partial^e\} \end{aligned} \quad (1.28)$$

It is now necessary to relate the strain components at P which, for plane stress, are  $\varepsilon_x, \varepsilon_y, \gamma_{xy}$ , to the element nodal displacement components. This may be achieved by first substituting the expressions for  $u$  and  $v$  from equation (1.24) into equations (1.13) to give

$$\{\varepsilon\} = \begin{Bmatrix} \varepsilon_x \\ \varepsilon_y \\ \gamma_{xy} \end{Bmatrix} = \begin{Bmatrix} \frac{\partial u}{\partial x} \\ \frac{\partial v}{\partial y} \\ \frac{\partial u}{\partial y} + \frac{\partial v}{\partial x} \end{Bmatrix} = \begin{bmatrix} 0 & 1 & 0 & 0 & 0 & 0 \\ 0 & 0 & 0 & 0 & 0 & 1 \\ 0 & 0 & 1 & 0 & 1 & 0 \end{bmatrix} \{\alpha\} = [Q]\{\alpha\} \quad (1.29)$$

Hence, using equation (1.28),

$$\begin{aligned} \{\varepsilon\} &= [Q][C^e]^{-1}\{\partial^e\} \\ &= \frac{1}{2A} \begin{bmatrix} y_j - y_m & 0 & y_m - y_i & 0 & y_i - y_j & 0 \\ & x_m - x_j & 0 & x_i - x_m & 0 & x_j - x_i \\ x_m - x_j & y_j - y_m & x_i - x_m & y_m - y_i & x_j - x_i & y_i - y_j \end{bmatrix} \\ &= [B]\{\partial^e\} \end{aligned} \quad (1.30)$$

It should be noted that the strain matrix  $[B]$  is independent of the variables  $x$  and  $y$  and hence of the position of  $P$ . The matrix  $[B]$  is, in fact, a function of the known nodal coordinate positions only and hence, for a given element,  $[B]$  is a constant matrix and the strain is therefore constant throughout the element. For this reason, the triangular plane stress element is often referred to as the constant-strain element. Equations (1.16) provide the elasticity relationships, which, recast in matrix form and incorporating equation (1.7), are

$$\{\sigma\} = \begin{Bmatrix} \sigma_x \\ \sigma_y \\ \tau_{xy} \end{Bmatrix} = \frac{E}{1-\nu^2} \begin{bmatrix} 1 & \nu & 0 \\ \nu & 1 & 0 \\ 0 & 0 & \frac{1-\nu}{2} \end{bmatrix} \{\varepsilon\} = [D]\{\varepsilon\} \quad (1.31)$$

To relate the stress components at  $P$  to the nodal displacement components, substitution from equation (1.30) into equation (1.31) gives

$$\{\sigma\} = [D][B]\{\partial^e\} \quad (1.32)$$

Having related both the stress and the strain components at  $P$  to the element nodal displacement components by equations (1.30) and (1.32), the remainder of the analysis follows directly from the general finite element theory given in Appendix B. In particular, it should be noted that the stress and strain vectors defined above do satisfy the requirement (Appendix B, equation (B.7)) that  $\{\varepsilon\}^T\{\sigma\}$  represent a work scalar (see equation (1.20)), and the principle of virtual displacements may therefore be invoked to establish the element stiffness matrix as (equation (B.11)):

$$[k] = \int_{\text{vol}} [B]^T [D] [B] dv \quad (1.33)$$

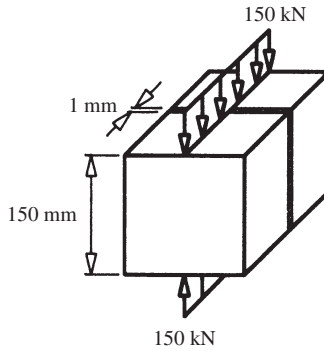


Fig. 1.14 Concrete cube test

However, for this particular element, it has already been shown that  $[B]$  is independent of  $x$  and  $y$  as, if a homogeneous material and uniform element are presumed, are  $[D]$  and  $t$ , hence

$$[k] = [B]^T [D] [B] t \iint dx dy = (At) [B]^T [D] [B] \quad (1.34)$$

where  $A$  is the area of the triangular element.

For the case of zero Poisson's ratio, an explicit form of the plane stress element stiffness matrix is given as equation (1.35) (page 21); for the non-zero Poisson's ratio case, the reader is referred to other texts (Ross, 1996). As with all stiffness matrices, the reciprocal theorem assures the symmetry of the matrix. The element stiffness matrix of equation (1.35) is, however, given in full for convenience of use.

For practical analysis purposes, finite element theory, such as the above, is incorporated into completely automated, standard, analysis 'packages' which are mounted on computers. The function of the engineer is to idealize the structure, possibly to devise a suitable element sub-division and, most importantly, to critically assess the validity of the results against engineering judgement. The element sub-divisions required for acceptable accuracy are always so fine as to render hand solutions impractical. However, a full understanding of the method, including the manner in which the complete structure stiffness matrix is assembled from the element stiffness matrices, is perhaps most easily obtained from numerical examples. The following hand solution is therefore undertaken to illustrate the basic theory described above.

#### 1.4.2 Example 1.1 – concrete cube analysis

One form of concrete test is to subject a cube to a central compressive line load as illustrated in Fig. 1.14. This is usually done by placing square steel rods

$$[k] = \frac{Et}{4A} \begin{bmatrix}
 Y_{jm}^2 + 0.5X_{mj}^2 & 0.5X_{mj}Y_{jm} & Y_{jm}Y_{mi} + 0.5X_{mj}X_{im} & 0.5X_{mj}Y_{mi} & Y_{ij}Y_{jm} + 0.5X_{ji}X_{mj} & 0.5X_{mj}Y_{ij} \\
 0.5X_{mj}Y_{jm} & X_{mj}^2 + 0.5Y_{jm}^2 & 0.5X_{im}Y_{jm} & X_{im}X_{mj} + 0.5Y_{jm}Y_{mi} & 0.5X_{ji}Y_{jm} & X_{jm}X_{mj} + 0.5Y_{ij}Y_{jm} \\
 Y_{jm}Y_{mi} + 0.5X_{mj}X_{im} & 0.5X_{im}Y_{jm} & Y_{mi}^2 + 0.5X_{im}^2 & 0.5X_{im}Y_{mi} & Y_{ij}X_{mj} + 0.5X_{im}X_{ji} & 0.5X_{im}Y_{ij} \\
 0.5X_{mj}Y_{mi} & X_{im}X_{mj} + 0.5Y_{jm}Y_{mi} & 0.5X_{im}Y_{im} & X_{im}^2 + 0.5Y_{mi}^2 & 0.5X_{ji}Y_{mi} & X_{im}X_{ji} + 0.5Y_{ij}Y_{mi} \\
 Y_{ij}Y_{jm} + 0.5X_{ji}X_{mj} & 0.5X_{jm}Y_{jm} & Y_{jm}Y_{mi} + 0.5X_{im}X_{ji} & 0.5X_{jm}Y_{mi} & Y_{ij}^2 + 0.5X_{ji}^2 & 0.5X_{jm}Y_{ij} \\
 0.5X_{mj}Y_{jm} & X_{jm}X_{mj} + 0.5Y_{ij}Y_{jm} & 0.5X_{im}Y_{jm} & X_{im}X_{ji} + 0.5Y_{ij}Y_{mi} & 0.5X_{ji}Y_{jm} & X_{ji}^2 + 0.5Y_{ij}^2
 \end{bmatrix} \quad (1.35)$$

where  $X_{ji} = (x_j - x_i)$ ,  $Y_{mi} = (y_m - y_i)$ , etc.



between the cube and the platens of the testing machine as shown in Fig. 1.15(a). The object of the present example is to analyse a typical 150 mm cube under such loading conditions and to assess the likely failure behaviour of the cube in the light of the results obtained. The *total* load applied will be taken as 150 kN and plane stress conditions will be assumed with  $E = 30 \text{ kN/mm}^2$  and  $\nu = 0$ .

It may not be immediately apparent as to how as solid an object as a concrete block may be analysed as a *plane* stress problem. However, it should be clear that, for the given loading, the stress distribution in the plane of a thin slice such as that shown in Fig. 1.14 will be independent of the position of the slice. Furthermore, it may be shown (see Section 1.5.1) that, for zero Poisson's ratio, the normal direct stress on the slice will be zero and plane stress conditions will therefore prevail. For convenience, a 1 mm slice of the cube (Fig. 1.14) will be considered, so that the load on the slice is 1 kN (Fig. 1.15(b)). Taking account of symmetry, only one quarter of the slice need be analysed and this will be divided into triangular elements as shown in Fig. 1.15(b).

### Idealization

The quarter-cube slice to be analysed is shown in Fig. 1.16 with a system of node and element numbering. The numbering systems are arbitrary, excepting that there is some advantage in this case in making the element numbering such that all the even-numbered elements are similar and that the same applies to the odd-numbered elements. A system of  $i, j$  and  $m$  element node designation is also shown. Again, odd- and even-numbered elements have been treated consistently. The choice of an element node  $i$  is arbitrary but, once designated,  $j$  and  $m$  must follow in an anti-clockwise sense, since the theory was based on this assumption (Fig. 1.13). An arbitrary, but convenient, set of axes

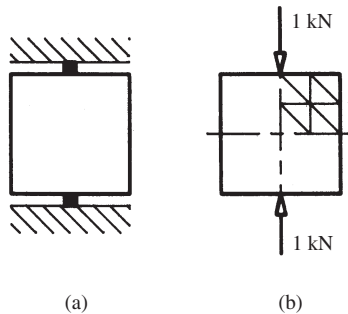


Fig. 1.15 (a) Cube test. (b) Cube idealization

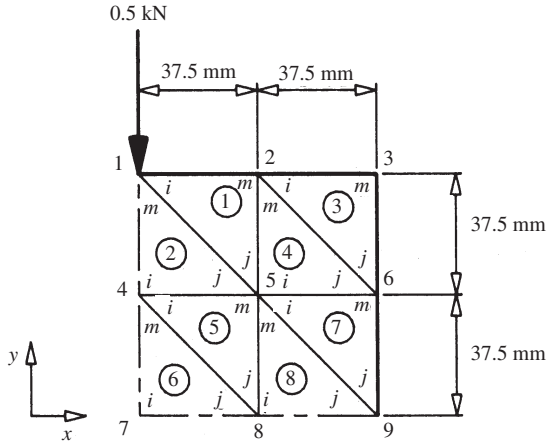


Fig. 1.16 Finite element sub-division

are shown, as is the load acting on the quarter slice, which, because of the use of symmetry, is one half the load applied to the full slice.

The first stage of the analysis is to evaluate the element stiffness matrices for the odd- and even-numbered elements. These element stiffness matrices will then be assembled into structure stiffness equations, the solution of which provides the nodal displacements. Finally, the element stresses are determined from the nodal displacements.

### Element stiffness matrices

For an *odd*-numbered element, using kilonewton and millimetre units throughout:

The strain–nodal displacement matrix,  $[B]$ , for the element may be obtained by substitution in equation (1.30):

$$\begin{aligned}
 [B] &= \frac{1}{2A} \begin{bmatrix} y_j - y_m & 0 & y_m - y_i & 0 & y_i - y_j & 0 \\ 0 & x_m - x_j & 0 & x_i - x_m & 0 & x_j - x_i \\ x_m - x_j & y_j - y_m & x_i - x_m & y_m - y_i & x_j - x_i & y_i - y_j \end{bmatrix} \\
 &= \frac{37.5}{2A} \begin{bmatrix} -1 & 0 & 0 & 0 & 1 & 0 \\ 0 & 0 & 0 & -1 & 0 & 1 \\ 0 & -1 & -1 & 0 & 1 & 1 \end{bmatrix} \quad (1.36)
 \end{aligned}$$

where  $A = \text{element area} = 37.5^2/2 \text{ mm}^2$ .

The stress–strain (elasticity) matrix,  $[D]$ , is produced by substituting the specified material constants in equation (1.31):

$$[D] = \frac{E}{1-\nu^2} \begin{bmatrix} 1 & \nu & 0 \\ \nu & 1 & 0 \\ 0 & 0 & \frac{1-\nu}{2} \end{bmatrix} = \frac{E}{2} \begin{bmatrix} 2 & 0 & 0 \\ 0 & 2 & 0 \\ 0 & 0 & 1 \end{bmatrix} \quad (\text{since } \nu = 0) \quad (1.37)$$

The element stiffness matrix then follows by substitution for  $[B]$  and  $[D]$  from equations (1.36) and (1.37) in equation (1.34) to give

$$\begin{aligned} [k]_{\text{odd}} &= (At)[B]^T[D][B] \\ &= (At) \left( \frac{E}{2} \right) \left( \frac{37.5}{2A} \right)^2 \times \\ &\quad \begin{bmatrix} -1 & 0 & 0 \\ 0 & 0 & -1 \\ 0 & 0 & -1 \\ 0 & -1 & 0 \\ 1 & 0 & 1 \\ 0 & 1 & 1 \end{bmatrix} \begin{bmatrix} 2 & 0 & 0 \\ 0 & 2 & 0 \\ 0 & 0 & 1 \end{bmatrix} \begin{bmatrix} -1 & 0 & 0 & 0 & 1 & 0 \\ 0 & 0 & 0 & -1 & 0 & 1 \\ 0 & -1 & -1 & 0 & 1 & 1 \end{bmatrix} \end{aligned}$$

Since the pre-multiplication of a matrix by a diagonal matrix results in scaling the rows of the matrix by the corresponding diagonal terms:

$$[k]_{\text{odd}} = \frac{1 \times 30 \times 37.5^2}{8 \times 37.5^2 / 2} \begin{bmatrix} -1 & 0 & 0 \\ 0 & 0 & -1 \\ 0 & 0 & -1 \\ 0 & -1 & 0 \\ 1 & 0 & 1 \\ 0 & 1 & 1 \end{bmatrix} \begin{bmatrix} -2 & 0 & 0 & 0 & 2 & 0 \\ 0 & 0 & 0 & -2 & 0 & 2 \\ 0 & -1 & -1 & 0 & 1 & 1 \end{bmatrix}$$

Whence

$$[k]_{\text{odd}} = 7.5 \begin{bmatrix} 2 & 0 & 0 & 0 & -2 & 0 \\ 0 & 1 & 1 & 0 & -1 & -1 \\ \hline 0 & 1 & 1 & 0 & -1 & -1 \\ 0 & 0 & 0 & 2 & 0 & -2 \\ \hline -2 & -1 & -1 & 0 & 3 & 1 \\ 0 & -1 & -1 & -2 & 1 & 3 \end{bmatrix} \quad (1.38)$$

Following the same procedure for the even-numbered elements, it may be shown that

$$[k]_{\text{even}} = 7.5 \begin{bmatrix} 3 & 1 & -2 & -1 & -1 & 0 \\ 1 & 3 & 0 & -1 & -1 & -2 \\ \hline -2 & 0 & 2 & 0 & 0 & 0 \\ -1 & -1 & 0 & 1 & 1 & 0 \\ \hline -1 & -1 & 0 & 1 & 1 & 0 \\ 0 & -2 & 0 & 0 & 0 & 2 \end{bmatrix} \quad (1.39)$$

The above element stiffness matrices could, of course, have alternatively been produced by direct substitution in equation (1.35).

### Structure stiffness matrix

The element stiffness matrices link *element* nodal forces to *element* nodal displacement components. The element nodal forces must be such as to produce a quantity of work (see Appendix B) when the force components are multiplied by the corresponding displacement components. Element nodal force components in the  $x$ - and  $y$ -axes (Fig. 1.13) will therefore correspond to the chosen  $u$  and  $v$  displacement components, and, by subdividing  $[k]$ , equation (B.11) may be rewritten as

$$\begin{Bmatrix} f_i \\ f_j \\ f_m \end{Bmatrix} = \begin{bmatrix} k_{ii} & k_{ij} & k_{im} \\ k_{ji} & k_{jj} & k_{jm} \\ k_{mi} & k_{mj} & k_{mm} \end{bmatrix} \begin{Bmatrix} \partial_i \\ \partial_j \\ \partial_m \end{Bmatrix} \quad (1.40)$$

where

$$f_i = \begin{Bmatrix} f_{xi} \\ f_{yi} \end{Bmatrix}$$

the force components at node  $i$ ;

$$\partial_i = \begin{Bmatrix} u_i \\ v_i \end{Bmatrix}$$

and  $k_{mj}$  relates force components at node  $m$  due to displacement at node  $j$ .

The structure stiffness equations relate the *total* nodal force components for the complete *structure* to the nodal displacement components for the complete *structure*. Since there are nine nodes in the present analysis and each node has two force (or displacement) components, there will be a total of 18 stiffness equations. However, it is convenient initially to construct the

stiffness matrix in terms of the element stiffness sub-matrices of equation (1.40). Since these sub-matrices are  $2 \times 2$ , the structure stiffness matrix, so formed, will be  $9 \times 9$ . The general form of the structure stiffness equations is then

$$\begin{Bmatrix} F_1 \\ \vdots \\ F_9 \end{Bmatrix} = [K] \begin{Bmatrix} \partial_1 \\ \vdots \\ \partial_9 \end{Bmatrix} \quad (1.41)$$

where

$$F_1 = \begin{Bmatrix} F_{x1} \\ F_{y1} \end{Bmatrix}$$

the total force components at node 1.

To construct the structure stiffness matrix in terms of the element stiffness sub-matrices, each node in turn is considered and the sum is obtained of the force contributions made at the node by the elements which the node interconnects. Thus, node 1 connects elements 1 and 2 so that it is the sum of the forces produced at node 1 by each of these two elements which gives the total force at the node.

For element 1, since the  $i, j, m$  designation for this element is 1, 5, 2 (Fig. 1.16), its element stiffness equations, from equation (1.40), may be written as

$$\begin{Bmatrix} f_1 \\ f_5 \\ f_2 \end{Bmatrix} = \begin{bmatrix} k_{ii} & k_{ij} & k_{im} \\ k_{ji} & k_{jj} & k_{jm} \\ k_{mi} & k_{mj} & k_{mm} \end{bmatrix} \begin{Bmatrix} \partial_1 \\ \partial_5 \\ \partial_2 \end{Bmatrix} \quad (1.42)$$

The first of the above set of three equations relates the forces at node 1 to the element nodal displacement components and may be written out in expanded form as

$$\{f_1^1\} = [k_{ii}^1]\{\partial_1\} + [k_{ij}^1]\{\partial_5\} + [k_{im}^1]\{\partial_2\} \quad (1.43)$$

where <sup>1</sup> indicates evaluation for element 1.

It should be noted that, since node 1 is node 'i' for element 1, it is the sub-matrices with initial suffix  $i$  which are involved in equation (1.43). The first row of the structure stiffness matrix may now be partially assembled by allocating the sub-matrices of equation (1.43) to their appropriate column locations in the structure stiffness matrix. The columns of the structure stiffness matrix are in nodal displacement order so that it is the displacement suffixes in equation (1.43) which identify the relevant columns. Thus,  $k_{ii}$  is located in column 1 of the structure stiffness matrix;  $k_{ij}$  is located in column 5; and  $k_{im}$  is in column 2. Hence, the partially completed first structure stiffness equation becomes

$$\{f_1^1\} = \begin{bmatrix} 1 & 2 & 3 & 4 & 5 & 6 & 7 & 8 & 9 \\ k_{ii}^1 & k_{im}^1 & 0 & 0 & k_{ij}^1 & 0 & 0 & 0 & 0 \end{bmatrix} \{\Delta\} \quad (1.44)$$

where  $\{\Delta\} = \{\partial_1, \partial_2, \dots, \partial_9\}^T$ .

Element 2 has its node 'm' at node 1 and it is therefore the third of its element stiffness equations (equation (1.40)) which relates to the element forces at node 1. The  $i, j, m$  designation for the element (Fig. 1.16) is 4, 5, 1 so that the expanded relationship between the element forces at node 1 and the element nodal displacement components is

$$\{f_1^2\} = [k_{mi}^2] \{\partial_4\} + [k_{mj}^2] \{\partial_5\} + [k_{mm}^2] \{\partial_1\} \quad (1.45)$$

The total force components at node 1 are obtained by summing the contributions from elements 1 and 2. Thus, adding equation (1.45) to equation (1.44), which involves allocating the stiffness sub-matrices of equation (1.45) to their appropriate columns in equation (1.44), gives the completed first stiffness equation as

$$\begin{aligned} \{F_1\} &= \{f_1^1 + f_1^2\} \\ &= \begin{bmatrix} 1 & 2 & 3 & 4 & 5 & 6 & 7 & 8 & 9 \\ k_{ii}^1 + k_{mm}^2 & k_{im}^1 & 0 & k_{mi}^2 & k_{ij}^1 + k_{mj}^2 & 0 & 0 & 0 & 0 \end{bmatrix} \{\Delta\} \end{aligned}$$

The same procedure is followed for all the nodes, nodes 2 and 4 having three contributory elements, node 5 six elements, and so on. In this way, the complete structure stiffness matrix, in sub-matrix form, may be built up as given by equation (1.46) (page 28).

Several general properties of stiffness matrices may be used to check a matrix such as that of equation (1.46). The symmetrical property is perhaps the most basic and may be used either for checking purposes or to reduce the labour involved in matrix assembly by limiting the matrix formation to an upper (or lower) triangular matrix.

Second, the number of sub-matrices in any diagonal position will be equal to the number of elements which the relevant node interconnects, since displacement of a node will produce force contributions at the same node from all the elements joined to it. Thus, node 6 of the example (Fig. 1.16) connects three elements, and three sub-matrices are therefore located in the diagonal position of the sixth row of equation (1.46). Also, all the sub-matrices on the diagonal will possess repeated suffixes, since the forces and displacements they relate occur at the same node.

Off-diagonal sub-matrices will not involve repeated suffixes since the related forces and displacements are at separate nodes. Further, the number of sub-matrices in any off-diagonal location will be equal to the number of elements which connect the node specified by the matrix column to the node specified by the matrix row. For a plane set of elements, the maximum number

1	$k_{ji}^1 + k_{nm}^2$	0	0	0	0	0	0	0	0
2	$k_{mi}^1$	$k_{im}^1 + k_{nm}^4 + k_{ji}^3$	$k_{im}^3$	$k_{mi}^2$	$k_{nj}^1 + k_{mj}^2$	0	0	0	0
3	$k_{mi}^1$	$k_{mi}^3$	$k_{nm}^3$	0	0	$k_{ij}^3 + k_{nj}^4$	0	0	0
4	$k_{im}^2$	0	0	$k_{ji}^2 + k_{ii}^5 + k_{nm}^6$	$k_{ij}^2 + k_{im}^5$	0	$k_{mi}^6$	$k_{ij}^5 + k_{mj}^6$	0
5	$k_{ji}^1 + k_{jm}^2$	$k_{jm}^1 + k_{im}^4$	0	$k_{ji}^2 + k_{ij}^2 + k_{ii}^4 + k_{nm}^8$	$k_{ij}^1 + k_{jj}^2 + k_{ii}^4 + k_{nm}^8$	$k_{ij}^4 + k_{im}^7$	0	$k_{mj}^5 + k_{mi}^8$	$k_{ij}^7 + k_{mj}^8$
6	0	$k_{ji}^3 + k_{jm}^4$	$k_{jm}^3$	0	$k_{ji}^4 + k_{mi}^7$	$k_{ij}^3 + k_{jj}^4 + k_{nm}^7$	0	0	$k_{mj}^7$
7	0	0	0	$k_{im}^6$	0	0	$k_{ii}^6$	$k_{ij}^6$	0
8	0	0	0	$k_{ji}^5 + k_{jm}^6$	$k_{jm}^5 + k_{im}^8$	0	$k_{ji}^6$	$k_{jj}^5 + k_{jj}^6 + k_{ii}^8$	$k_{ij}^8$
9	0	0	0	0	$k_{ji}^7 + k_{jm}^8$	$k_{jm}^7$	0	$k_{ji}^8$	$k_{ij}^7 + k_{ji}^8$

(1.46)

of elements which can so connect two nodes is two, so that a maximum of two sub-matrices can occur in any off-diagonal position. For example, with reference to Fig. 1.16, two elements connect node 5 to node 2 so that two sub-matrices are found in the fifth column of row two in equation (1.46).

To produce the full stiffness matrix in numeric form, substitution is made for the element sub-matrices of equation (1.46) from equation (1.38) or (1.39), according to whether an odd- or an even-numbered element is being dealt with.

Thus, for example,

$$k_{mi}^7 = \begin{bmatrix} -2 & -1 \\ 0 & -1 \end{bmatrix}$$

and

$$k_{jm}^4 = \begin{bmatrix} 0 & 0 \\ 1 & 0 \end{bmatrix}$$

The resulting complete structure stiffness matrix is given by equation (1.47) (page 30).

### *Solution of the stiffness equations*

Prior to solving the structure stiffness equations, the appropriate boundary restraints must be applied to the stiffness matrix. Boundary restraints need particular care when, as here, use of symmetry is being made. If the centre point of the block (Fig. 1.15(b)) is fully restrained to provide a reference point, then the vertical centre-line of the cube must remain vertical under symmetrical loading and the horizontal centre-line must remain horizontal. These conditions imply that there is no horizontal displacement along the vertical centre-line (although vertical displacement can occur along this line) and, similarly, that vertical movements cannot take place along the horizontal centre-line (but horizontal movements can). In terms of the chosen nodal numbering, these conditions require that

$$u_1 = u_4 = u_7 = v_7 = v_8 = v_9 = 0 \quad (1.48)$$

Restraining boundary displacement components implies that, at the relevant boundary points, there are restraint forces which physically represent the reactions from the adjacent portions of the block. By making these reaction components and the applied load equivalent to the total nodal forces, the stiffness equations may be represented by equation (1.49) (page 31). In equation (1.49), the restrained displacement components (equation (1.48)) have been set to zero. Since these displacement components are effectively determined, while the reaction components are unknown, the equations involving the



$$\begin{array}{c}
 \begin{array}{cccccccccc}
 & 1 & 2 & 3 & 4 & 5 & 6 & 7 & 8 & 9 \\
 \begin{array}{c} 1 \\ 2 \\ 3 \\ 4 \\ 7.5 \\ 6 \\ 7 \\ 8 \\ 9 \end{array} & \begin{bmatrix} 3 & 0 & -2 & 0 & 0 & 0 & -1 & -1 & 0 & 1 & 0 & 0 & 0 & 0 & 0 \\
 0 & 3 & -1 & -1 & 0 & 0 & 0 & -2 & 1 & 0 & 0 & 0 & 0 & 0 & 0 \\
 -2 & -1 & 6 & 1 & -2 & 0 & 0 & 0 & -2 & -1 & 0 & 1 & 0 & 0 & 0 \\
 0 & -1 & 1 & 6 & -1 & -1 & 0 & 0 & -1 & -4 & 1 & 0 & 0 & 0 & 0 \\
 0 & 0 & -2 & -1 & 3 & 1 & 0 & 0 & 0 & 0 & -1 & 0 & 0 & 0 & 0 \\
 0 & 0 & 0 & -1 & 1 & 3 & 0 & 0 & 0 & 0 & -1 & -2 & 0 & 0 & 0 \\
 -1 & 0 & 0 & 0 & 0 & 0 & 6 & 1 & -4 & -1 & 0 & 0 & -1 & -1 & 0 & 0 \\
 -1 & -2 & 0 & 0 & 0 & 0 & 1 & 6 & -1 & -2 & 0 & 0 & 0 & -2 & 1 & 0 & 0 \\
 0 & 1 & -2 & -1 & 0 & 0 & -4 & -1 & 12 & 2 & -4 & -1 & 0 & 0 & -2 & -1 & 0 & 1 \\
 1 & 0 & -1 & -4 & 0 & 0 & -1 & -2 & 2 & 12 & -1 & -2 & 0 & 0 & -1 & -4 & 1 & 0 \\
 0 & 0 & 0 & 1 & -1 & -1 & 0 & 0 & -4 & -1 & 6 & 1 & 0 & 0 & 0 & 0 & -1 & 0 \\
 0 & 0 & 1 & 0 & 0 & -2 & 0 & 0 & 0 & -1 & -2 & 1 & 6 & 0 & 0 & 0 & -1 & -2 \\
 0 & 0 & 0 & 0 & 0 & 0 & -1 & 0 & 0 & 0 & 0 & 0 & 3 & 1 & -2 & -1 & 0 & 0 \\
 0 & 0 & 0 & 0 & 0 & 0 & -1 & -2 & 0 & 0 & 0 & 0 & 1 & 3 & 0 & -1 & 0 & 0 \\
 0 & 0 & 0 & 0 & 0 & 0 & 0 & 1 & -2 & -1 & 0 & 0 & -2 & 0 & 6 & 1 & -2 & -1 \\
 0 & 0 & 0 & 0 & 0 & 0 & 1 & 0 & -1 & -4 & 0 & 0 & -1 & -1 & 1 & 6 & 0 & -1 \\
 0 & 0 & 0 & 0 & 0 & 0 & 0 & 0 & 0 & 1 & -1 & -1 & 0 & 0 & -2 & 0 & 3 & 0 \\
 0 & 0 & 0 & 0 & 0 & 0 & 0 & 0 & 0 & 1 & 0 & 0 & -2 & 0 & -1 & -1 & 0 & 3
 \end{bmatrix}
 \end{array}
 \end{array}
 \tag{1.47}$$

$$\left. \begin{array}{l} R_{x1} \\ -0.5 \\ 0 \\ 0 \\ 0 \\ 0 \\ R_{x4} \\ 0 \\ 0 \\ 0 \\ 0 \\ 0 \\ R_{x7} \\ R_{y7} \\ 0 \\ R_{y8} \\ 0 \\ R_{y9} \end{array} \right\} = 7.5 \left[ \begin{array}{cccccccccccc} 3 & 0 & -2 & 0 & 0 & 0 & -1 & -1 & 0 & 1 & 0 & 0 & 0 & 0 & 0 \\ 0 & 3 & -1 & -1 & 0 & 0 & 0 & -2 & 1 & 0 & 0 & 0 & 0 & 0 & 0 \\ -2 & -1 & 6 & 1 & -2 & 0 & 0 & 0 & -2 & -1 & 0 & 1 & 0 & 0 & 0 \\ 0 & -1 & 1 & 6 & -1 & -1 & 0 & 0 & -1 & -4 & 1 & 0 & 0 & 0 & 0 \\ 0 & 0 & -2 & -1 & 3 & 1 & 0 & 0 & 0 & 0 & -1 & 0 & 0 & 0 & 0 \\ 0 & 0 & 0 & -1 & 1 & 3 & 0 & 0 & 0 & 0 & -1 & -2 & 0 & 0 & 0 \\ -1 & 0 & 0 & 0 & 0 & 0 & 6 & 1 & -4 & -1 & 0 & 0 & -1 & -1 & 0 & 0 \\ -1 & -2 & 0 & 0 & 0 & 0 & 1 & 6 & -1 & -2 & 0 & 0 & 0 & -2 & 1 & 0 & 0 \\ 0 & 1 & -2 & -1 & 0 & 0 & -4 & -1 & 12 & 2 & -4 & -1 & 0 & 0 & -2 & -1 & 0 & 1 \\ 1 & 0 & -1 & -4 & 0 & 0 & -1 & -2 & 2 & 12 & -1 & -2 & 0 & 0 & 0 & -1 & -4 & 1 & 0 \\ 0 & 0 & 0 & 1 & -1 & -1 & 0 & 0 & -4 & -1 & 6 & 1 & 0 & 0 & 0 & 0 & 0 & -1 & 0 \\ 0 & 0 & 1 & 0 & 0 & -2 & 0 & 0 & -1 & -2 & 1 & 6 & 0 & 0 & 0 & 0 & 0 & -1 & -2 \\ 0 & 0 & 0 & 0 & 0 & 0 & -1 & 0 & 0 & 0 & 0 & 0 & 3 & 1 & -2 & -1 & 0 & 0 & 0 \\ 0 & 0 & 0 & 0 & 0 & 0 & -1 & -2 & 0 & 0 & 0 & 0 & 1 & 3 & 0 & -1 & 0 & 0 & 0 \\ 0 & 0 & 0 & 0 & 0 & 0 & 0 & 1 & -2 & -1 & 0 & 0 & -2 & 0 & 6 & 1 & -2 & -1 & 0 \\ 0 & 0 & 0 & 0 & 0 & 0 & 1 & 0 & -1 & -4 & 0 & 0 & -1 & -1 & 1 & 6 & 0 & -1 & 0 \\ 0 & 0 & 0 & 0 & 0 & 0 & 0 & 0 & 0 & 0 & -1 & -1 & 0 & 0 & -2 & 0 & 3 & 0 & 0 \\ 0 & 0 & 0 & 0 & 0 & 0 & 0 & 0 & 1 & 0 & 0 & -2 & 0 & 0 & -1 & -1 & 0 & 3 & 0 \end{array} \right] \left. \begin{array}{l} v_1 \\ u_2 \\ v_2 \\ u_3 \\ v_3 \\ 0 \\ v_4 \\ u_5 \\ v_5 \\ u_6 \\ v_6 \\ 0 \\ 0 \\ u_8 \\ 0 \\ u_9 \end{array} \right\} \quad (1.49)$$

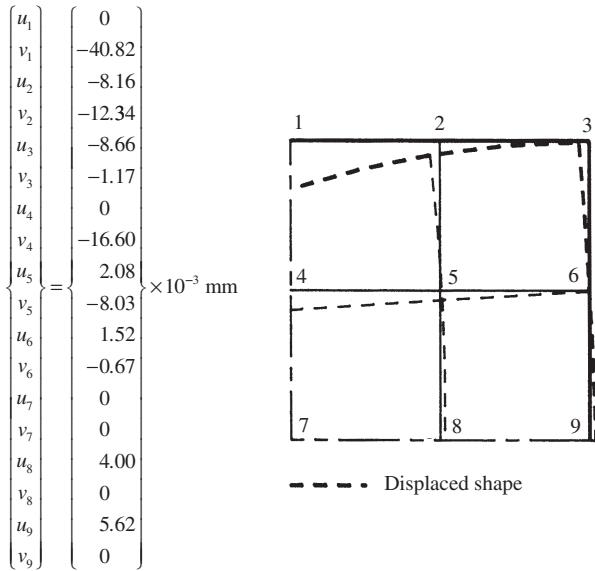


Fig. 1.17 Displacement solution

unknown reactions and the columns of the stiffness matrix corresponding to the zero displacements may be deleted, to give a constrained set of stiffness equations which is presented as

$$\begin{Bmatrix} -0.5 \\ 0 \\ 0 \\ 0 \\ 0 \\ 0 \\ 0 \\ 0 \\ 0 \\ 0 \end{Bmatrix} = 7.5 \begin{bmatrix} 3 & -1 & -1 & 0 & 0 & -2 & 1 & 0 & 0 & 0 & 0 & 0 \\ -1 & 6 & 1 & -2 & 0 & 0 & -2 & -1 & 0 & 1 & 0 & 0 \\ -1 & 1 & 6 & -1 & -1 & 0 & -1 & -4 & 1 & 0 & 0 & 0 \\ 0 & -2 & -1 & 3 & 1 & 0 & 0 & 0 & -1 & 0 & 0 & 0 \\ 0 & 0 & -1 & 1 & 3 & 0 & 0 & 0 & -1 & -2 & 0 & 0 \\ -2 & 0 & 0 & 0 & 0 & 6 & -1 & -2 & 0 & 0 & 1 & 0 \\ 1 & -2 & -1 & 0 & 0 & -1 & 12 & 2 & -4 & -1 & -2 & 0 \\ 0 & -1 & -4 & 0 & 0 & -2 & 2 & 12 & -1 & -2 & -1 & 1 \\ 0 & 0 & 1 & -1 & -1 & 0 & -4 & -1 & 6 & 1 & 0 & -1 \\ 0 & 0 & 1 & 0 & 0 & -2 & 0 & -1 & -2 & 1 & 6 & 0 & -1 \\ 0 & 0 & 0 & 0 & 0 & 1 & -2 & -1 & 0 & 0 & 6 & -2 \\ 0 & 0 & 0 & 0 & 0 & 0 & 0 & 1 & -1 & -1 & -2 & 3 \end{bmatrix} \begin{Bmatrix} v_1 \\ u_2 \\ v_2 \\ u_3 \\ v_3 \\ v_4 \\ u_5 \\ v_5 \\ u_6 \\ v_6 \\ u_8 \\ u_9 \end{Bmatrix} \tag{1.50}$$

A computer solution of equations (1.50), augmented by the restrained displacement components, is given in Fig. 1.17. Once a finite element displacement solution has been achieved, it is essential that the values are carefully inspected for 'reasonableness'. Order of magnitude and general directions of movement apart, checks are most easily made by sketching a displacement diagram of the type shown in Fig. 1.17. The diagram does agree with expectations in that the greatest vertical deflection occurs under the load, while reducing vertical displacements are found at increasing distance from the loaded node. It should also be noted that the horizontal displacements are inward at the top of the block, but outward along the centre-line.

### Element stress solution

Equation (1.32) relates element stresses to element nodal displacements. Thus, for an odd-numbered element, substituting from equations (1.36) and (1.37) in equation (1.32) gives

$$\{\sigma\} = [D][B]\{\partial^e\} = \frac{E}{2} \frac{37.5}{2A} \begin{bmatrix} 2 & 0 & 0 \\ 0 & 2 & 0 \\ 0 & 0 & 1 \end{bmatrix} \begin{bmatrix} -1 & 0 & 0 & 0 & 1 & 0 \\ 0 & 0 & 0 & -1 & 0 & 1 \\ 0 & -1 & -1 & 0 & 1 & 1 \end{bmatrix} \{\partial^e\}$$

Whence

$$\{\sigma\} = 0.4 \times 10^3 \begin{bmatrix} -2 & 0 & 0 & 0 & 2 & 0 \\ 0 & 0 & 0 & -2 & 0 & 2 \\ 0 & -1 & -1 & 0 & 1 & 1 \end{bmatrix} \{\partial^e\} \text{ N/mm}^2 \quad (1.51)$$

Similarly, for an even-numbered element,

$$\{\sigma\} = 0.4 \times 10^3 \begin{bmatrix} -2 & 0 & 2 & 0 & 0 & 0 \\ 0 & -2 & 0 & 0 & 0 & 2 \\ -1 & -1 & 0 & 1 & 1 & 0 \end{bmatrix} \{\partial^e\} \text{ N/mm}^2 \quad (1.52)$$

Equations (1.51) and (1.52) allow the element stresses to be determined once the nodal displacement vector for a particular element has been extracted from the structure nodal displacement component solution (Fig. 1.17). Thus, for element 1,

$$\begin{aligned} \{\partial^e\} &= \{\partial_1, \partial_5, \partial_2\}^T \\ &= \{0, -40.82, 2.08, -8.03, -8.16, -12.34\}^T \times 10^{-3} \text{ mm} \end{aligned}$$

So that, from equation (1.51),

$$\{\sigma\} = \begin{Bmatrix} \sigma_x \\ \sigma_y \\ \tau_{xy} \end{Bmatrix} = 0.4 \times 10^3 \times 10^{-3} \begin{bmatrix} -2 & 0 & 0 & 0 & 2 & 0 \\ 0 & 0 & 0 & -2 & 0 & 2 \\ 0 & -1 & -1 & 0 & 1 & 1 \end{bmatrix} \begin{Bmatrix} 0 \\ -40.82 \\ 2.08 \\ -8.03 \\ -8.16 \\ -12.34 \end{Bmatrix} \text{ N/mm}^2$$

Whence

$$\begin{Bmatrix} \sigma_x \\ \sigma_y \\ \tau_{xy} \end{Bmatrix} = \begin{Bmatrix} -6.53 \\ -3.45 \\ 7.29 \end{Bmatrix} \text{ N/mm}^2$$

Repeating this procedure for the remaining elements, the full set of element stresses can be shown to be as given in Table 1.1.

The stress components of Table 1.1 confirm expectations in that the vertical direct stress components are all compressive and increase in magnitude towards the region under the applied load. The horizontal direct stress components are compressive above the diagonal connecting nodes 1–5–9 (Fig. 1.16) and tensile below this line. This behaviour may be directly related to the displacement solution in this case, since, for zero Poisson’s ratio, stress is directly related to the strain in the relevant direction and the presence of horizontal contraction and extension, respectively, above and below the quarter-cube diagonal may be confirmed from the displacement diagram (Fig. 1.17).

The stress solution is, however, generally more easily inspected if expressed in terms of principal stresses. Equations (1.9) and (1.11) have been

Table 1.1 Element stresses (N/mm<sup>2</sup>)

Element	$\sigma_x$	$\sigma_y$	$\tau_{xy}$
1	-6.53	-3.45	7.29
2	1.67	-19.37	3.43
3	-0.40	-0.40	0.40
4	-0.45	-3.45	-1.16
5	1.67	-6.42	2.66
6	3.20	-13.28	0
7	-0.45	-0.54	1.30
8	1.30	-6.42	-0.77

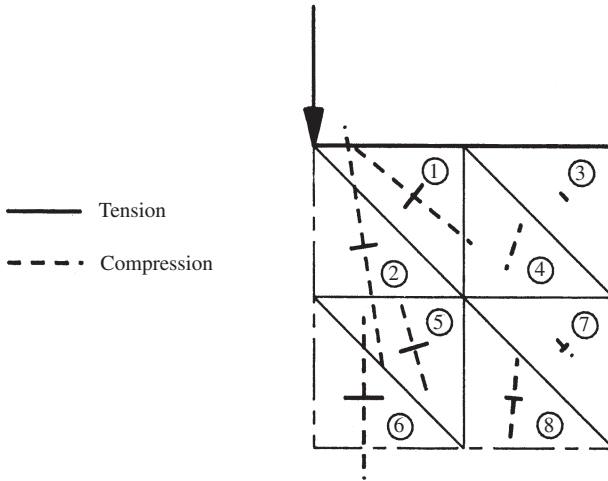


Fig. 1.18 Principal stress diagram

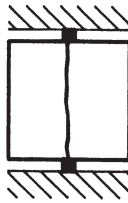


Fig. 1.19 Splitting test

used to determine the principal stress directions and values corresponding to the stress component solution of Table 1.1. The resulting values are shown on a vector principal stress plot as Fig. 1.18, where the stresses are located at the element centroids, this being usually considered the most appropriate location for the stresses of a constant stress element.

As with the stress components, the magnitudes of the principal stresses (Fig. 1.18) decay with distance from the point load. In each element, the numerically greater principal stress is compressive and acts (with the exception of elements 4 and 8) towards the position of the point load. This is the general form of behaviour one might expect, but, of equal significance in view of the low tensile strength of concrete, the smaller principal stresses are tensile. The likely mode of failure of the block is therefore by tensile cracking initiated at the point of greatest tensile principal stress, which the analysis indicates is in

the element closest to the centre of the complete block. This is indeed the type of failure found experimentally, where this form of ‘splitting’ test results in the formation of a vertical tensile crack (Fig. 1.19) and can be used to estimate the tensile strength of concrete.

### 1.4.3 Finite element types

The triangular constant-strain element used above is one of the simplest elements which may be employed for plane stress analysis but many more possibilities exist. Other element types may be based on different geometric shapes of element, a rectangle being an obvious possibility. For a rectangular element (Fig. 1.20(a)), there are eight nodal displacement components in total (two at each of the four nodes), and eight undetermined coefficients are therefore used in the displacement function (equation (B.1)). As usually formulated, the resulting finite element is such that strain, and stress, vary linearly over the element. This represents an enhancement over the constant-strain–stress representation of the triangular element, but is obtained at the expense of reduced geometric freedom, since rectangular elements cannot easily model irregularly shaped plates, and the possibilities for the production of graded, irregular element meshes are much more limited than in the case of triangular elements (Fig. B.1). If it is desired to retain the triangular shape but improve the accuracy of the representation, then additional, mid-side nodes may be used (Fig. 1.20(b)) to give a total of 12 nodal displacements and a similar number of undetermined coefficients.

A further refinement is to employ a transformation such that the element is formulated in a set of local element coordinates and is then *mapped* onto its true structural position in a set of global coordinates (Fig. 1.21). The mapping should be such that the nodes are exactly mapped onto their actual positions, while other element locations will generally be approximately positioned. One advantage of such a mapping is the ability it provides for the better approximation of curved boundaries. An elegant approach to this mapping operation is to use the same function for the transformation as is used for the displacement function and elements so derived are termed *isoparametric* (Zienkiewicz and Taylor, 1989).

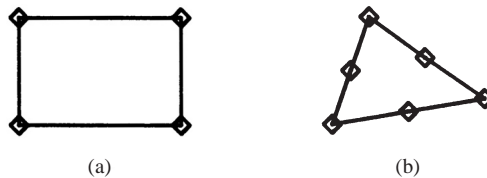


Fig. 1.20 Element types: (a) rectangular; (b) triangular with mid-side nodes

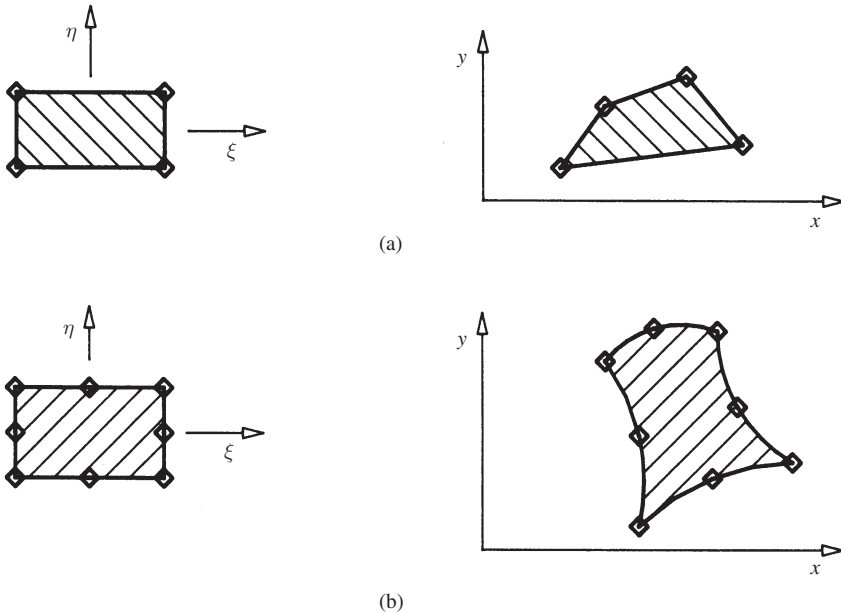


Fig. 1.21 Isoparametric elements: (a) linear; (b) quadratic

If an isoparametric transformation is applied to a four-noded rectangular element, then the normal formulation for this element utilizes linear displacement functions along the element boundaries. Consequently, the isoparametric transformation will also be linear along the boundaries and will allow the rectangular element to model a quadrilateral area on the structural mesh (Fig. 1.21(a)). Similarly, a rectangular element with mid-side nodes uses a quadratic displacement function along its edges, and the corresponding transformation results in a structural mesh shape with curved boundaries (Fig. 1.21(b)), so permitting actual curved edges to be represented as a series of quadratic approximations by the elements located along the edge. The versatility and accuracy of this eight-noded isoparametric element has made it one of the most popular in practice. The formulation and use of the element is given in the following section.

#### 1.4.4 Eight-noded isoparametric element

The concrete splitting test described in relation to testing a concrete cube in example 1.1 is in fact more usually undertaken with a cylindrical specimen. Should it be required to analyse this form of the test using triangular elements, then a mesh such as that shown in Fig. 1.22(a) could be employed but the



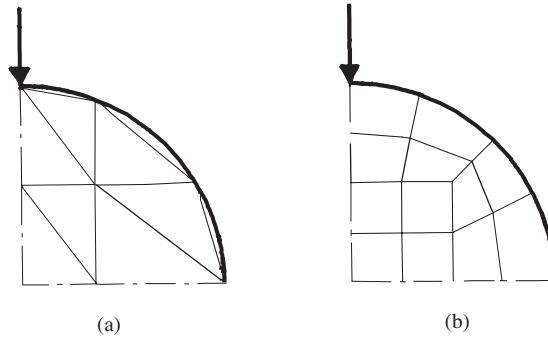


Fig. 1.22 Element meshes: (a) triangular; (b) isoparametric

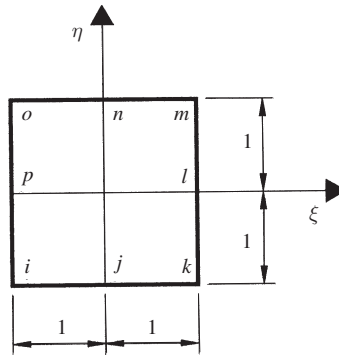


Fig. 1.23 Basis element

circular boundary would be rather crudely approximated. Isoparametric elements provide the opportunity for much better boundary representation (Fig. 1.22(b)) and will, in general, produce a more accurate solution both for this reason and also because the element is more powerful.

### Theory

A central concept of the eight-noded isoparametric element is that, for simplicity, its properties are established with reference to a basis element and the properties are subsequently mapped (Fig. 1.21) onto the geometry each element actually occupies in the finite element mesh. For the typical square

basis element shown in Fig. 1.23, there are eight nodes with two displacement components ( $u, v$ ) at each node, so that a total of 16 undetermined coefficients can be used in the displacement component polynomials, or eight to each of  $u$  and  $v$ . The lowest order of polynomial containing eight coefficients, which is also symmetric in  $x$  and  $y$ , is to take

$$u = \alpha_1 + \alpha_2\xi + \alpha_3\eta + \alpha_4\xi^2 + \alpha_5\xi\eta + \alpha_6\eta^2 + \alpha_7\xi^2\eta + \alpha_8\xi\eta^2 \quad (1.53)$$

and

$$v = \alpha_9 + \alpha_{10}\xi + \alpha_{11}\eta + \alpha_{12}\xi^2 + \alpha_{13}\xi\eta + \alpha_{14}\eta^2 + \alpha_{15}\xi^2\eta + \alpha_{16}\xi\eta^2$$

In the following, the formulation will be established with respect to the  $u$  displacement component and the  $x$ -coordinate, since  $v, y$  expressions may be inferred from the corresponding  $u, x$  ones. Thus, by letting the general point  $P$  take the positions of the eight element nodes,  $i-p$ , in turn, the displacement components may be related to the undetermined coefficients by

$$\{\delta_u^e\} = \begin{bmatrix} 1 & -1 & -1 & 1 & 1 & 1 & -1 & -1 \\ 1 & 0 & -1 & 0 & 0 & 1 & 0 & 0 \\ 1 & 1 & -1 & 1 & -1 & 1 & -1 & 1 \\ 1 & 1 & 0 & 1 & 0 & 0 & 0 & 0 \\ 1 & 1 & 1 & 1 & 1 & 1 & 1 & 1 \\ 1 & 0 & 1 & 0 & 0 & 1 & 0 & 0 \\ 1 & -1 & 1 & 1 & -1 & 1 & 1 & -1 \\ 1 & -1 & 0 & 1 & 0 & 0 & 0 & 0 \end{bmatrix} \{\alpha_u\} = [C^e] \{\alpha_u\} \quad (1.54)$$

where  $\{\alpha_u\} = \{\alpha_1, \alpha_2, \dots, \alpha_8\}^T$ , the column vector of undetermined  $u$  coefficients.

A computer inversion of  $[C^e]$  gives

$$\{\alpha_u\} = \frac{1}{4} \begin{bmatrix} -1 & 2 & -1 & 2 & -1 & 2 & -1 & 2 \\ 0 & 0 & 0 & 2 & 0 & 0 & 0 & -2 \\ 0 & -2 & 0 & 0 & 0 & 2 & 0 & 0 \\ 1 & -2 & 1 & 0 & 1 & -2 & 1 & 0 \\ 1 & 0 & -1 & 0 & 1 & 0 & -1 & 0 \\ 1 & 0 & 1 & -2 & 1 & 0 & 1 & -2 \\ -1 & 2 & -1 & 0 & 1 & -2 & 1 & 0 \\ -1 & 0 & 1 & -2 & 1 & 0 & -1 & 2 \end{bmatrix} \{\delta_u\} = [C^e]^{-1} \{\delta_u\} \quad (1.55)$$

The determination of the strain components requires the evaluation of  $\partial u/\partial x, \partial u/\partial y$ , which poses some immediate problems since the axes  $\xi$  and  $\eta$

are currently being employed. To overcome this difficulty, the chain rule of differentiation may be used to give

$$\begin{aligned}\frac{\partial u}{\partial \xi} &= \frac{\partial u}{\partial x} \frac{\partial x}{\partial \xi} + \frac{\partial u}{\partial y} \frac{\partial y}{\partial \xi} \\ \frac{\partial u}{\partial \eta} &= \frac{\partial u}{\partial x} \frac{\partial x}{\partial \eta} + \frac{\partial u}{\partial y} \frac{\partial y}{\partial \eta}\end{aligned}\tag{1.56}$$

or

$$\begin{Bmatrix} \frac{\partial u}{\partial \xi} \\ \frac{\partial u}{\partial \eta} \end{Bmatrix} = \begin{bmatrix} \frac{\partial x}{\partial \xi} & \frac{\partial y}{\partial \xi} \\ \frac{\partial x}{\partial \eta} & \frac{\partial y}{\partial \eta} \end{bmatrix} \begin{Bmatrix} \frac{\partial u}{\partial x} \\ \frac{\partial u}{\partial y} \end{Bmatrix} \quad \text{or} \quad \begin{Bmatrix} \frac{\partial u}{\partial \xi} \\ \frac{\partial u}{\partial \eta} \end{Bmatrix} = [J] \begin{Bmatrix} \frac{\partial u}{\partial x} \\ \frac{\partial u}{\partial y} \end{Bmatrix}\tag{1.57}$$

If it is presumed for the moment that it is possible to evaluate the *Jacobian* matrix,  $[J]$ , and that  $[J]$  is non-singular, then, since  $u$  derivatives with respect to  $\xi$  and  $\eta$  are readily available from equation (1.53), the  $x$ - and  $y$ -derivatives may be obtained as

$$\begin{Bmatrix} \frac{\partial u}{\partial x} \\ \frac{\partial u}{\partial y} \end{Bmatrix} = [J]^{-1} \begin{Bmatrix} \frac{\partial u}{\partial \xi} \\ \frac{\partial u}{\partial \eta} \end{Bmatrix}\tag{1.58}$$

The evaluation of  $[J]$  requires the  $\xi$ - and  $\eta$ -coordinates to be mapped onto the  $x, y$  system. The 'iso-' prefix in the term isoparametric comes from the concept of using the same function for this mapping as that used for the displacement function (equation (1.53)). Thus, it is assumed that

$$x = \alpha_1 + \alpha_2 \xi + \alpha_3 \eta + \alpha_4 \xi^2 + \alpha_5 \xi \eta + \alpha_6 \eta^2 + \alpha_7 \xi^2 \eta + \alpha_8 \xi \eta^2\tag{1.59}$$

and

$$y = \alpha_9 + \alpha_{10} \xi + \alpha_{11} \eta + \alpha_{12} \xi^2 + \alpha_{13} \xi \eta + \alpha_{14} \eta^2 + \alpha_{15} \xi^2 \eta + \alpha_{16} \xi \eta^2$$

Just as the displacement components are made to coincide exactly with the nodal components, so the nodal geometric components are made to coincide exactly with the nodal coordinate positions. Hence

$$\{x^e\} = [C^e] \{\alpha_x\}, \quad \{\alpha_x\} = [C^e]^{-1} \{x^e\}\tag{1.60}$$

where

$$\{x^e\} = \{x_i, x_j, x_k, x_l, x_m, x_n, x_o, x_p\}^T$$

Now, from equation (1.59),

$$\begin{Bmatrix} \frac{\partial x}{\partial \xi} \\ \frac{\partial x}{\partial \eta} \end{Bmatrix} = \begin{bmatrix} 0 & 1 & 0 & 2\xi & \eta & 0 & 2\xi\eta & \eta^2 \\ 0 & 0 & 1 & 0 & \xi & 2\eta & \xi^2 & 2\xi\eta \end{bmatrix} \{\alpha_x\} = [Q]\{\alpha_x\} \quad (1.61)$$

But, using equations (1.60) and (1.55),

$$\begin{Bmatrix} \frac{\partial x}{\partial \xi} \\ \frac{\partial x}{\partial \eta} \end{Bmatrix} = [Q][C^e]^{-1}\{x^e\} = [S]\{x^e\} \quad (1.62)$$

where

$$\begin{aligned} S_{11} &= (1-\eta)(2\xi+\eta)/4, & S_{12} &= -\xi(1-\eta), & S_{13} &= (1-\eta)(2\xi-\eta)/4, \\ S_{14} &= (1-\eta^2)/2, & S_{15} &= (1+\eta)(2\xi+\eta)/4, & S_{16} &= -\xi(1+\eta), \\ S_{17} &= (1+\eta)(2\xi-\eta)/4, & S_{18} &= -(1-\eta^2)/2, & S_{21} &= (1-\xi)(\xi+2\eta)/4, \\ S_{22} &= -(1-\xi^2)/2, & S_{23} &= (1+\xi)(-\xi+2\eta)/4, & S_{24} &= -\eta(1+\xi), \\ S_{25} &= (1+\xi)(\xi+2\eta)/4, & S_{26} &= (1+\xi^2)/2, & S_{27} &= (1-\xi)(-\xi+2\eta)/4, \\ S_{28} &= -\eta(1-\xi) \end{aligned}$$

The  $x$ -derivatives provided by equation (1.62), together with the corresponding  $y$ -derivatives, enable the Jacobian matrix to be evaluated at any given point within the isoparametric element from equation (1.57). In turn, the Jacobian allows the  $u$  displacement derivatives with respect to  $x$  and  $y$  to be obtained from equation (1.58), since, by the iso- nature of the formulation, the derivatives with respect to  $\xi$  and  $\eta$  are given (see equation (1.62)) by

$$\begin{Bmatrix} \frac{\partial u}{\partial \xi} \\ \frac{\partial u}{\partial \eta} \end{Bmatrix} = [Q][C^e]^{-1}\{u^e\} = [S]\{u^e\} \quad (1.63)$$

Once the  $u$  displacement derivatives have been found, the  $v$  ones follow by correspondence and the strain matrix,  $[B]$ , is obtained by using the standard plane stress expression (equation (1.13))

$$\begin{Bmatrix} \varepsilon_x \\ \varepsilon_y \\ \gamma_{xy} \end{Bmatrix} = \begin{Bmatrix} \frac{\partial u}{\partial x} \\ \frac{\partial v}{\partial y} \\ \frac{\partial u}{\partial y} + \frac{\partial v}{\partial x} \end{Bmatrix} \quad (1.64)$$

The standard concepts of the finite element method may then be invoked (see Appendix B) but require some modification to adapt the method to  $\xi$ - and  $\eta$ -coordinates and also due to the fact that  $[B]$  is no longer constant, as with the previous triangular element, but, as may be seen from equation (1.63) and the form of  $[S]$  (equation (1.61)), a fairly complex function of  $\xi$  and  $\eta$ . To cope with these features, the standard element stiffness relationship (equation (B.11)) may be first converted to  $\xi$ - and  $\eta$ -coordinates by further use of the Jacobian matrix, since it may be shown (Stroud, 1995) that

$$d\xi d\eta = \det[J] dx dy \tag{1.65}$$

Thus

$$[k] = t \iint [B]^T [D] [B] \det[J] d\xi d\eta \tag{1.66}$$

Equation 1.66 will obviously reflect  $[B]$  and be an even more complicated function of  $\xi$  and  $\eta$  than  $[B]$  itself. It is therefore necessary to resort to numerical integration to evaluate the integral of equation (1.66), and *Gaussian* integration is normally employed for this purpose. The Gauss method (Zienkiewicz and Taylor, 1989) requires the function to be integrated to be evaluated at a number of *Gauss points*. The number of points employed can be varied according to the accuracy desired but a common choice is nine points. Once the number of points has been selected, the integration rule designates

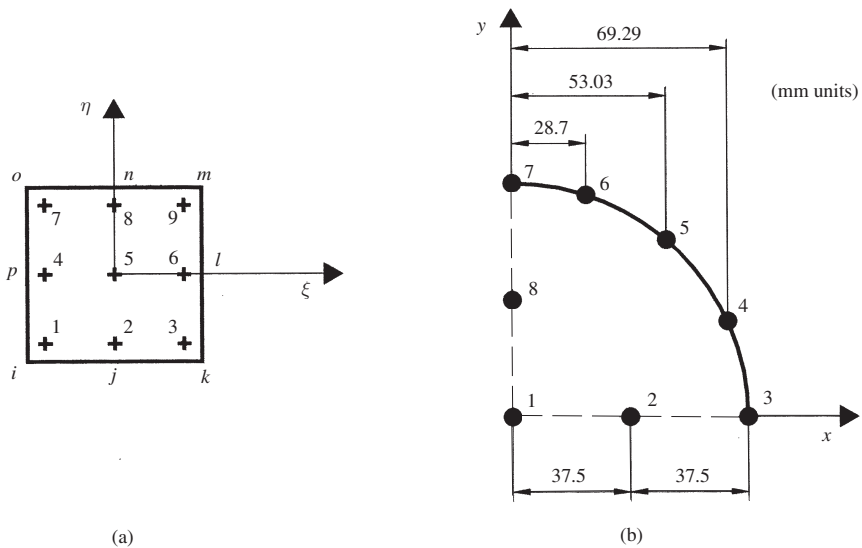


Fig. 1.24 (a) Gauss points. (b) Cylinder representation

Table 1.2 Gauss point positions and weights

$i$	$\xi_i$	$\eta_i$	$w_i$
1	-0.7746	-0.7746	0.3086
2	0	-0.7746	0.4938
3	0.7746	-0.7746	0.3086
4	-0.7746	0	0.4938
5	0	0	0.7901
6	0.7746	0	0.4938
7	-0.7746	0.7746	0.3086
8	0	0.7746	0.4938
9	0.7746	0.7746	0.3086

the position of these such that optimal accuracy results, and, for the basis element (Fig. 1.24(a)) equation (1.66) would be evaluated as

$$[k] = \sum_{i=1}^9 w_i t [B_i]^T [D] [B_i] \det[J_i] \quad (1.67)$$

where the positions of the Gauss points and the values of the weights,  $w_i$ , are, for the nine-point rule, to be taken as given in Table 1.2.

#### Application to cylinder analysis

Since it is more powerful, the isoparametric element is consequently much more complex than the linear triangular type and is certainly not intended for hand calculations. However, for demonstration purposes only, the very simplest one-element isoparametric representation of the quarter-cylinder analysis (Fig. 1.24(b)) will be undertaken in outline.

For this element, the nodal  $x$ -coordinates are given by

$$\{x^e\} = \{0 \quad 37.5 \quad 75 \quad 69.29 \quad 53.03 \quad 28.7 \quad 0 \quad 0 \quad 0\}^T \text{ mm} \quad (1.68)$$

and at Gauss point 1, where  $\xi = \eta = -0.7746$ ,

$$\begin{aligned} \begin{Bmatrix} \frac{\partial x}{\partial \xi} \\ \frac{\partial x}{\partial \eta} \end{Bmatrix}_1 &= [S]_1 \{x^e\} \\ &= \begin{bmatrix} -1.032 & 1.376 & -0.344 & -0.200 & -0.131 & 0.174 & -0.044 & -0.200 \\ -1.032 & -0.200 & -0.044 & 0.174 & -0.131 & 0.200 & -0.344 & 1.376 \end{bmatrix} \{x^e\} \\ &= \begin{Bmatrix} 37.70 \\ 0.12 \end{Bmatrix} \end{aligned} \quad (1.69)$$

Using similar results for the derivatives of  $y$ , the Jacobian matrix becomes

$$[J]_1 = \begin{bmatrix} 37.70 & 0.12 \\ 0.12 & 37.70 \end{bmatrix} \quad \text{whence} \quad (1.70)$$

$$[J]_1^{-1} = \frac{1}{1421} \begin{bmatrix} 37.70 & -0.12 \\ -0.12 & 37.70 \end{bmatrix} \quad \text{and} \quad \det[J]_1 = 1421$$

Hence

$$\left\{ \begin{array}{c} \frac{\partial u}{\partial x} \\ \frac{\partial u}{\partial y} \end{array} \right\}_1 = [J]_1^{-1} [S]_1 \{u^e\} = \frac{1}{1421} \begin{bmatrix} 37.70 & -0.12 \\ -0.12 & 37.70 \end{bmatrix} \times \quad (1.71)$$

$$\begin{bmatrix} -1.031 & 1.375 & -0.344 & -0.200 & -0.131 & 0.175 & -0.044 & -0.200 \\ -1.031 & -0.200 & -0.044 & 0.175 & -0.131 & 0.200 & -0.344 & 1.375 \end{bmatrix} \{u^e\}$$

$$= \begin{bmatrix} -0.02726 & 0.03638 & -0.00911 & 0.00529 & -0.00346 & 0.0462 & -0.00113 & -0.00542 \\ -0.02726 & -0.00542 & -0.00113 & 0.00462 & -0.00346 & 0.00529 & -0.00911 & 0.03648 \end{bmatrix} \{u^e\}$$

Using equation (1.71), and the corresponding result for the  $v$ -derivatives, allows the strain matrix,  $[B]$ , to be obtained by substitution in equation (1.64). Equation (1.67) then provides the contribution from Gauss point 1 to the

Table 1.3 Comparative displacement solutions

Node (refer to Fig. 1.16)		Displacement ( $\times 10^{-3}$ mm)			
		8 tri.	9 iso.	16 iso.	64 iso.
1	$u$	0	0	0	0
	$v$	-40.82	-76.72	-76.76	-91.47
2	$u$	-8.16	-10.56	-10.59	-10.92
	$v$	-12.33	-10.11	-10.14	-10.10
3	$u$	-8.66	-9.13	-9.20	-9.24
	$v$	-1.17	2.53	2.46	2.48
4	$u$	0	0	0	0
	$v$	-16.60	-18.11	-18.18	-18.06
5	$u$	2.08	1.80	1.81	1.82
	$v$	-8.03	-7.72	-7.73	-7.75
6	$u$	1.51	1.23	1.34	1.33
	$v$	-0.67	1.29	1.27	1.27
7	$u$	0	0	0	0
	$v$	0	0	0	0
8	$u$	4.00	3.89	3.97	3.97
	$v$	0	0	0	0
9	$u$	5.62	4.70	4.66	4.66
	$v$	0	0	0	0

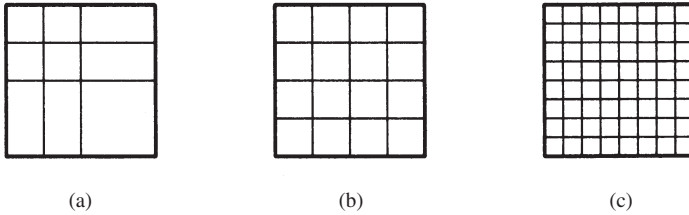


Fig. 1.25 Element meshes

element stiffness matrix, and the whole procedure must be repeated at the other eight Gauss points to complete the stiffness matrix computation. Solution of the stiffness equations will then produce the nodal displacement values. Element stresses are obtained from the general relationship  $\{\sigma\} = [D][B]\{\delta^e\}$  (equation (1.32)). Since the strain matrix is available at the Gauss points, these are the obvious, and, in fact, by far the most accurate positions at which to calculate the stresses. Computer packages therefore calculate the stress components at Gauss points but will then normally extrapolate these values to the nodes of the element and may undertake various other ‘smoothing’ operations, to ensure, for instance, that stresses are continuous between elements, which would not otherwise necessarily be the case.

#### 1.4.5 Assessment of solution accuracy

Commercial packages often provide ‘error estimators’ which give an indication of the likely error in the results, particularly stresses, generated by an analysis. There are then three principal ways in which the accuracy of a finite element analysis may be improved. The simplest is to make the mesh finer so that smaller elements are used. The elements may also be graded so that a closer mesh is formed in areas where rapid change in strain is expected. Such regions will be the most difficult to model and will have the greatest significance on the overall accuracy achieved. The final possibility is to employ more powerful elements, fewer of which may be needed. Some packages provide ‘adaptive meshing’, which automatically generates an enhanced mesh in order that improved accuracy can be obtained.

The application of these ideas for improved accuracy will be applied to the concrete block analysis of example 1.1 to assess the adequacy of the solution obtained previously, which was based on eight triangular elements.

The quarter block (Fig. 1.15) is now divided into a mesh of nine rectangular elements (Fig. 1.25(a)), graded such that the mesh is finest in the neighbourhood of the point load, where intuition and the previous solution suggest that the strain changes most quickly. A quadrilateral isoparametric element with mid-side nodes was used for this solution, and comparative nodal displacements are given in Table 1.3.



It will be seen that the displacements produced by the two solutions ('8 tri.' and '9 iso.' in Table 1.3) generally correspond in sense and order of magnitude, but otherwise differ markedly, this being most pronounced at node 1, to which the load was applied. The displacement under a perfect point load is theoretically indeterminate, and the discrepancy at node 1 may therefore be disregarded. To resolve the remaining differences, a further isoparametric analysis was undertaken using the finer net of Fig. 1.25(b), and the displacement results are given in Table 1.3 under the column headed '16 iso.'. These latter two sets of displacements correlate well, and the corresponding nodal principal stress values are given in Table 1.4.

The principal stress values derived from the two analyses ('9 iso.' and '16 iso.' in Table 1.4) correlate less well than the displacement solutions, so that a further, more refined analysis was performed in which the quarter block was divided into 64 quadrilateral isoparametric elements as shown in Fig. 1.25(c). The displacements and principal stresses resulting from this analysis are also presented in Tables 1.3 and 1.4 respectively. There is good agreement with the displacement solutions from the two previous isoparametric solutions, and the principal stresses correlate with those of the 16-element solution in regions of

Table 1.4 Comparative principal stresses

Node (refer to Fig. 1.16)		Principal stress (N/mm <sup>2</sup> )		
		9 iso.	16 iso.	64 iso.
1	$\sigma_1$	1.04	1.00	-1.57
	$\sigma_2$	-149.3	-149.0	-300.7
2	$\sigma_1$	6.18	6.35	3.48
	$\sigma_2$	-1.71	-2.37	-0.17
3	$\sigma_1$	1.31	0.33	-0.09
	$\sigma_2$	-0.36	-0.39	-0.12
4	$\sigma_1$	2.80	2.54	4.06
	$\sigma_2$	-15.2	-15.7	-18.0
5	$\sigma_1$	0.40	0.41	0.54
	$\sigma_2$	-6.22	-5.99	-6.13
6	$\sigma_1$	1.59	1.80	1.73
	$\sigma_2$	-0.22	0.10	0.02
7	$\sigma_1$	4.79	4.19	4.24
	$\sigma_2$	-11.94	-12.5	-12.8
8	$\sigma_1$	1.58	1.63	1.60
	$\sigma_2$	-7.30	-6.82	-6.77
9	$\sigma_1$	0.64	0.44	0.46
	$\sigma_2$	-0.43	-0.09	-0.02

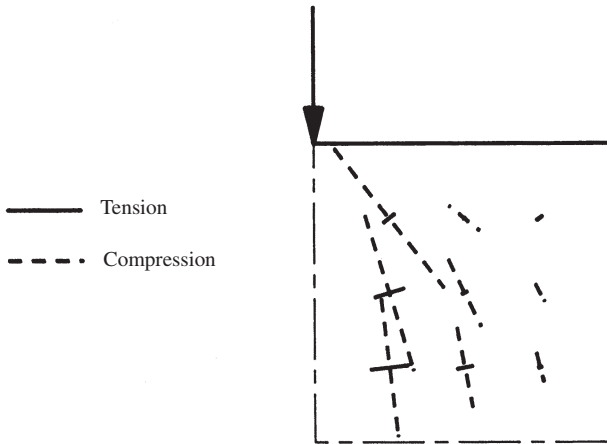


Fig. 1.26 Principal stress diagrams

the block remote from the load. Close agreement will never be obtained at the load position, but it is of some interest that the discrepancies persist until the mid-points of the quarter-block sides (nodes 2 and 4 in Fig. 1.16).

A principal stress diagram based on the 64-element results is given in Fig. 1.26, and it may be seen that all the compressive principal stresses are inclined towards the general direction of the load, without the occasional anomalous behaviour detected in the earlier triangular element analysis (Fig. 1.18). From the material behaviour point of view, the final analysis does substantiate experimental evidence that the greatest tensile principal stress is located at the centre of the block, and not at node 2 as indicated by the 16-element analysis. The 16- and 64-element analyses correlate in respect of the magnitude of this maximum tensile stress which, under increasing load, will initiate the splitting failure referred to previously.

The general conclusions to be drawn from this example assessment of solution accuracy are threefold. First, in the absence of prior experience, progression to successively finer nets is essential to ensure confidence in solution accuracy. Second, correlation of displacements is an indication, but not a guarantee, of stress correlation. Finally, solutions will generally not be reliable in the immediate vicinity of point loads. If this latter feature is of significance, then point loads should be represented as pressure loads over the length they can be expected to be applied to in practice. A detailed analysis of the area local to the load should then be undertaken using a fine element mesh.

## 1.5 Plane strain

### 1.5.1 Introduction

Just as stresses may be confined to act within a plane, so strains may be similarly restricted, giving rise to problems of *plane strain*. Plane stress is associated with elements in which the thickness of the element is of an order smaller than its other dimensions, while the reverse applies in plane strain, in that the thickness is of an order *greater* than the cross-sectional dimensions. The other requirements for plane stress apply equally to plane strain, namely that the loading on all cross-sections should be the same and should act in the plane of the cross-section.

Plane strain conditions are encountered in practice in the analysis of long dams, pipelines, culverts and other structures (Fig. 1.27). To appreciate that these forms of structure and loading do imply a plane strain condition, consider three equal, adjacent, thin slices from a typical structure (Fig. 1.27). Then, given the constancy of the cross-section and loading along the length of the structure, the strains must be similar for each of the slices. However, equal longitudinal extensional strains in the outer slices would imply a dissimilar contraction in the central slice. Conversely, similar longitudinal contractional strains in the outer slices imply an extension of the central slice. Hence it must be concluded that direct longitudinal strain cannot exist in such circumstances, and the situation does indeed resolve itself into one in which the strains are confined to the plane of the cross-section, since the symmetrical, co-planar nature of the loading and the cross-sections also prevents the development of shear strains other than in the  $x$ - $y$  plane.

To summarize, plane stress is characterized by the three stress components  $\sigma_x$ ,  $\sigma_y$  and  $\tau_{xy}$  which act in the  $x$ - $y$  plane. The direct stress components will, in general, produce strains in the normal  $z$ -direction by the Poisson's ratio effect but the stress component in this direction will be zero everywhere. Plane strain, on the other hand, is characterized by the three co-planar strain components  $\varepsilon_x$ ,  $\varepsilon_y$  and  $\gamma_{xy}$ , with zero strain in the longitudinal ( $z$ -) direction, but, as is shown below, longitudinal direct *stress* components will generally exist for non-zero Poisson's ratio.

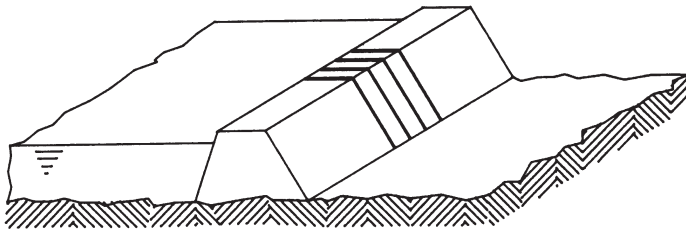


Fig. 1.27 Dam structure

### 1.5.2 Stresses and strains

By using the zero  $z$ -direction strain condition in the relevant (third) stress–strain relationship from general elasticity (equations (1.5)), the  $z$ -direction direct stress component may be determined as

$$\sigma_z = \nu(\sigma_x + \sigma_y) \quad (1.72)$$

Equation (1.72) shows that longitudinal direct stress will exist under plane strain conditions, provided that Poisson’s ratio is non-zero. The equation may also be used to determine the longitudinal direct stresses, once a solution for  $\sigma_x$  and  $\sigma_y$  has been established. The plane strain strain–stress relationships may be obtained by substituting from equation (1.72) in the first two of equations (1.5) to give

$$\begin{aligned} \varepsilon_x &= \frac{1}{E}[(1-\nu^2)\sigma_x - \nu(1+\nu)\sigma_y] = \frac{1-\nu^2}{E} \left( \sigma_x - \frac{\nu}{1-\nu}\sigma_y \right) \\ \varepsilon_y &= \frac{1}{E}[-\nu(1+\nu)\sigma_x + (1-\nu^2)\sigma_y] = \frac{1-\nu^2}{E} \left( -\frac{\nu}{1-\nu}\sigma_x + \sigma_y \right) \\ \gamma_{xy} &= \frac{1}{G}\tau_{xy} \end{aligned} \quad (1.73)$$

By comparing equations (1.73) with the corresponding plane stress strain–stress relationships (equations (1.15)), it may be seen that the plane strain case becomes analogous to one of plane stress if modified elastic constants are used such that

$$E' = \frac{E}{1-\nu^2}, \quad \nu' = \frac{\nu}{1-\nu}, \quad G' = G \quad (1.74)$$

Equations (1.74) show that plane stress and plane strain solutions are identical for the case of zero Poisson’s ratio. The concrete block example considered earlier (example 1.1) is intermediate between plane stress and strain, since its thickness is equal to its other dimensions. However, since zero Poisson’s ratio was assumed, the plane stress solution obtained will be equally applicable to plane strain conditions. The relationships given by equations (1.74) enable any general plane stress solution to be converted to plane strain by appropriate substitution for the elastic constants. It should be noted, however, that, in the absence of body forces, the general plane stress equation in terms of the stress components (equation (1.22)) is independent of the elastic constants. Consequently, the stress solution will also be independent of the elastic constants, so that plane strain and plane stress result in identical  $\sigma_x$ ,  $\sigma_y$  and  $\tau_{xy}$  values if no body forces are present. The strain and displacement solutions will obviously differ due to the different stress–strain relationships, and a longitudinal direct stress given by equation (1.72) will exist in the plane strain case but be absent under plane stress conditions. Should relationships for the stress components be

required in terms of the corresponding plane strains, then changing the subject of equations (1.73) yields the elasticity relationships given by equations (1.75).

If the finite element method is being employed, then a purpose-made plane strain program may be constructed by forming the stress–strain matrix,  $[D]$  (see equation (1.31)) from

$$\begin{aligned}\sigma_x &= \frac{E(1-\nu)}{(1+\nu)(1-2\nu)} \left( \varepsilon_x + \frac{\nu}{1-\nu} \varepsilon_y \right) \\ \sigma_y &= \frac{E(1-\nu)}{(1+\nu)(1-2\nu)} \left( \frac{\nu}{1-\nu} \varepsilon_x + \varepsilon_y \right) \\ \tau_{xy} &= G\gamma_{xy}\end{aligned}\tag{1.75}$$

Alternatively, if there are no body forces, then a plane stress program may be used for plane strain provided that use is made of the modified elastic constants defined by equation (1.74).

## References and further reading

- Astley, R. J. (1992) *Finite Elements in Solids and Structures*. Chapman and Hall, London.
- Brown, D. K. (1990) *An Introduction to the Finite Element Method using Basic Programming*, 2nd edn. Chapman and Hall, London. Chapter 4 describes a triangular plane stress–strain element computer program and a numerical hand-solved example is given.
- Cheung, Y. K. and Yeo, M. F. (1979) *A Practical Introduction to Finite Element Analysis*. Pitman, London. ‘Practical’ is here to be interpreted in a program construction sense; the programming language used is FORTRAN.
- Heyman, J. (1984) *Elements of Stress Analysis*. Cambridge University Press, Cambridge. Elasticity theory is presented in tensor notation and the limitations of Saint–Venant’s principle are explored in detail.
- Megson, T. H. G. (1996) *Structural and Stress Analysis*. Arnold, London. Chapters 5 and 14 cover the analysis of stress and strain.
- Ove Arup and Partners (1977) *The Design of Deep Beams in Reinforced Concrete*. CIRIA, London. Includes plane stress analyses of a variety of deep beams.
- Ross, C. T. F. (1996) *Finite Element Techniques in Structural Mechanics*. Albion, Chichester. Chapter 3 provides a stiffness matrix for a constant strain triangular element with non-zero Poisson’s ratio.
- Stroud, K. A. (1995) *Engineering Mathematics*. Macmillan, Basingstoke. Covers matrix theory including inversion by the adjoint (co-factor) method.
- Timoshenko, S. P. and Goodier, J. N. (1982) *Theory of Elasticity*, 3rd edn. McGraw-Hill, New York. The standard engineering text on classical elasticity theory.

Zienkiewicz, O. Z. and Taylor, R. L. (1989) *The Finite Element Method*, 4th edn, Vol. 1. *Basic Formulation and Linear Problems*. McGraw-Hill, London. The most comprehensive of the many available finite element texts.

## Problems

- 1.1 Briefly describe, with appropriate matrix equations, the principal steps in the construction of the stiffness matrix for a constant-strain triangular finite element for plane stress analysis. The  $[B]$  matrix for element 1,  $[B^1]$ , in the plane stress plate problem shown in Fig. 1.28 is given by

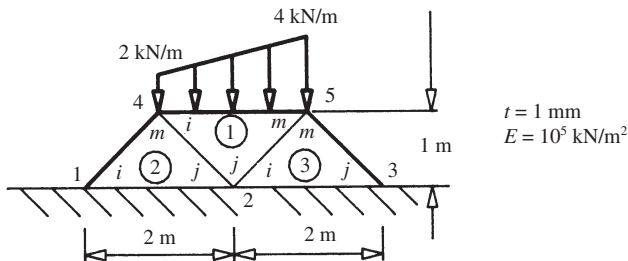
$$[B^1] = \frac{1}{2A} \begin{bmatrix} -1 & 0 & 0 & 0 & 1 & 0 \\ 0 & 1 & 0 & -2 & 0 & 1 \\ 1 & -1 & -2 & 0 & 1 & 1 \end{bmatrix}$$

where  $A$  is the element area, and, for both elements 2 and 3,

$$[B^2] = [B^3] = \frac{1}{2A} \begin{bmatrix} -1 & 0 & 1 & 0 & 0 & 0 \\ 0 & -1 & 0 & -1 & 0 & 2 \\ -1 & -1 & -1 & 1 & 2 & 0 \end{bmatrix}$$

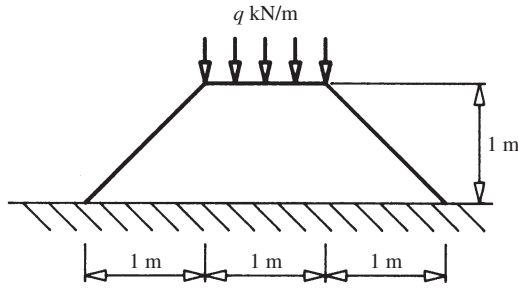
If  $\nu = 0$ , construct the two different stiffness matrices. What checks can be made on these matrices?

(KCL)



$$[D] = \frac{E}{(1-\nu^2)} \begin{bmatrix} 1 & \nu & 0 \\ \nu & 1 & 0 \\ 0 & 0 & \frac{1-\nu}{2} \end{bmatrix}$$

Fig. 1.28



$$[k] = \begin{bmatrix} k_{11}^n & k_{12}^n & k_{13}^n & k_{14}^n & k_{15}^n & k_{16}^n \\ k_{21}^n & k_{22}^n & - & - & - & k_{26}^n \\ k_{31}^n & k_{32}^n & - & - & - & - \\ k_{41}^n & - & - & - & k_{ij}^n & - \\ k_{51}^n & - & - & - & - & - \\ k_{61}^n & - & - & - & - & k_{66}^n \end{bmatrix}$$

Fig. 1.29

- 1.2 Choose a suitable, simple finite element mesh (no more than four elements) of triangular plane strain stiffness elements for the stress analysis of the plate problem shown in Fig. 1.29. With suitable node numbering and referring to the global stiffness matrix components of an element  $n$  as

$$k_{ij}^n; \quad i = 1, \dots, 6, \quad j = 1, \dots, 6$$

- (a) Give the assembled global stiffness matrix.  
 (b) Modify the matrix for the displacement boundary conditions.

(KCL)

- 1.3 Figure 1.30(a) shows a finite element idealization for a thin plate analysis. If the element stiffness matrices are as given on Fig. 1.30(b), construct the part of the structure stiffness matrix which relates the forces at nodes 1–4 to the displacements at nodes 1–8.

(UEL)

- 1.4 Figure 1.31 shows a plane stress finite element idealization of a thin, uniform plate analysis. The displacements obtained from the analysis are given, in part, in Table 1.5. Calculate the stresses in elements 1, 5 and 9 and relate these stresses to the expected behaviour of the plate ( $E = 200$  kN/mm<sup>2</sup>,  $\nu = 0$ ,  $t = 2.5$  mm).

(UEL)

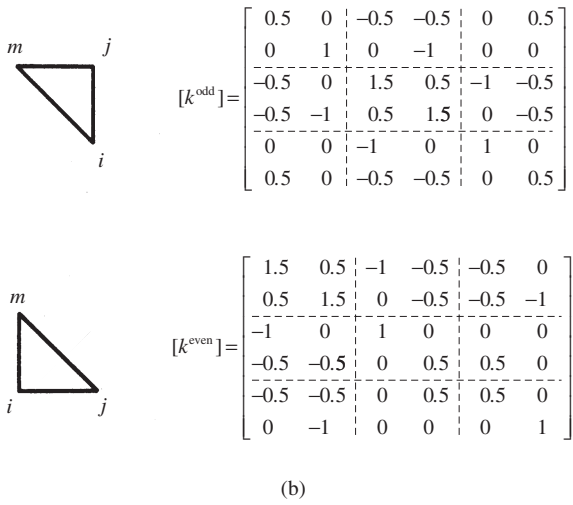
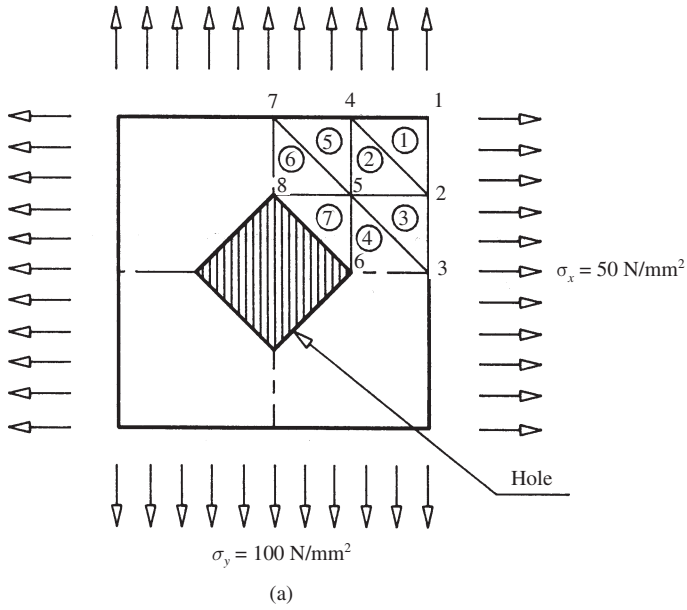


Fig. 1.30



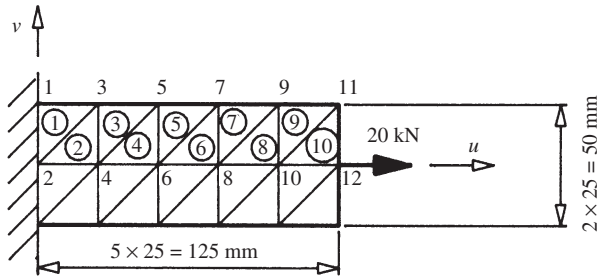


Fig. 1.31

Table 1.5

Node	3	5	6	7	9	10	11
$u$ ( $\times 10^{-2}$ mm)	2.00	3.98	4.02	5.91	7.65	8.35	8.82
$v$ ( $\times 10^{-5}$ mm)	-3.34	-11.8	0	-34.5	-56.7	0	215

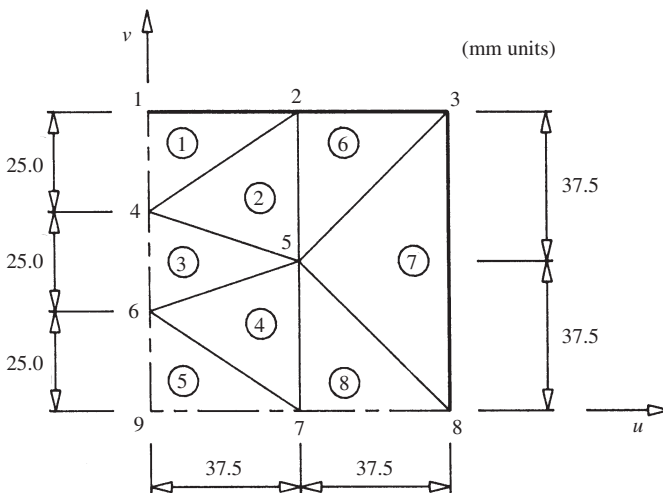
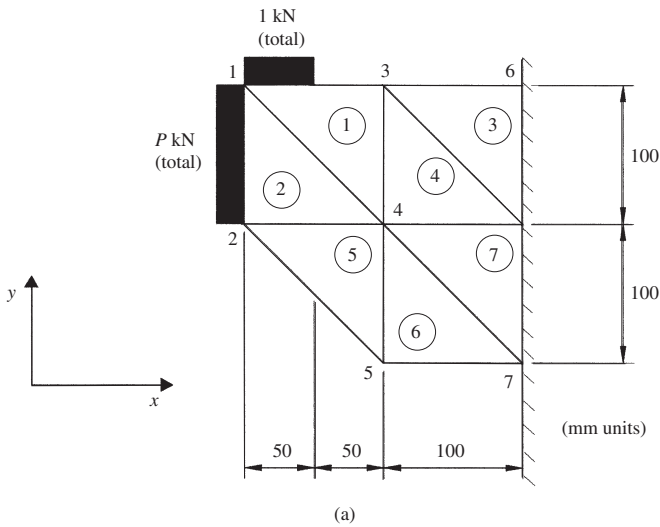


Fig. 1.32

1.5 A 1 mm slice of a quarter of the concrete block shown in Fig. 1.14 has been analysed by the finite element method using constant-strain triangular elements arranged in the graded mesh shown in Fig. 1.32. The displacement results from the analysis are given, in part, in Table 1.6. Determine the stresses in elements 3, 4 and 5, and compare the values obtained with those of Tables 1.1 and 1.3, giving reasons for any discrepancies.

Table 1.6

Node	$u$ (mm)	$v$ (mm)
4	0	-0.023132
5	0.001234	-0.007472
6	0	-0.010444
7	0.003067	0



$$\{\Delta\} = [K]^{-1}\{W\} \text{ where } [K]^{-1} = 10^{-3} \begin{bmatrix} 97 & 53 & 22 & 57 & 46 & 12 & 14 & 13 & -8 & 15 \\ 53 & 169 & -9 & 134 & 44 & 56 & -5 & 54 & -35 & 49 \\ 22 & -9 & 50 & -10 & 13 & 0 & 21 & 0 & 12 & 1 \\ 57 & 134 & -10 & 154 & 42 & 52 & -2 & 55 & -38 & 51 \\ 46 & 44 & 13 & 42 & 49 & 11 & 11 & 14 & -5 & 15 \\ 12 & 56 & 0 & 52 & 11 & 54 & 0 & 36 & -12 & 31 \\ 14 & -5 & 21 & -2 & 11 & 0 & 22 & -1 & 11 & 2 \\ 13 & 54 & 0 & 55 & 14 & 36 & -1 & 44 & -13 & 37 \\ -8 & -35 & 12 & -38 & -5 & -12 & 11 & -13 & 50 & -18 \\ 15 & 49 & 1 & 51 & 15 & 31 & 2 & 37 & -18 & 60 \end{bmatrix} \text{ mm/kN}$$

(b)

$$[B] = \frac{1}{2A} \begin{bmatrix} y_j - y_m & 0 & y_m - y_i & 0 & y_i - y_j & 0 \\ 0 & x_m - x_j & 0 & x_i - x_m & 0 & x_j - x_i \\ x_m - x_j & y_j - y_m & x_i - x_m & y_m - y_i & x_j - x_i & y_i - y_j \end{bmatrix}$$

(c)

Fig. 1.33

- 1.6 Under the action of the 1 kN load alone, the  $x$ -direction direct stress component in element 3 of the corbel analysis shown in Fig. 1.33 is  $10.7 \text{ N/mm}^2$ . It is proposed that this tensile stress component be eliminated by application of the uniformly distributed pre-stress shown in Fig. 1.33(a). Determine the required value of  $P$  if the inverse structure stiffness matrix for the analysis is as given in Fig. 1.33(b) and the element strain matrix is as given in Fig. 1.33(c) ( $E = 30 \text{ kN/mm}^2, \nu = 0$ ).
- Would the pre-stress acting alone produce a tensile principal stress in element 7?

(UEL)

- 1.7 For the rectangular plane stress finite element shown in Fig. 1.34, it is proposed to use an assumed displacement function such that the displacement components  $u$  and  $v$  at a general point, P, are given by

$$u = \alpha_1 + \alpha_2 x + \alpha_3 y + \alpha_4 xy$$

$$v = \alpha_5 + \alpha_6 x + \alpha_7 y + \alpha_8 xy$$

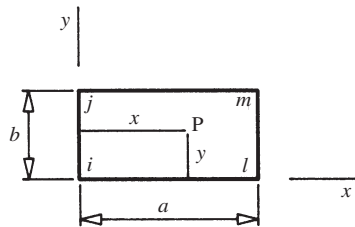


Fig. 1.34

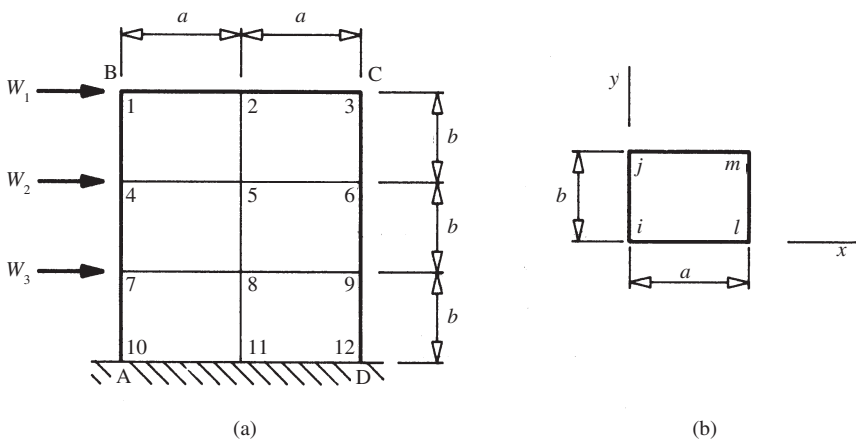


Fig. 1.35

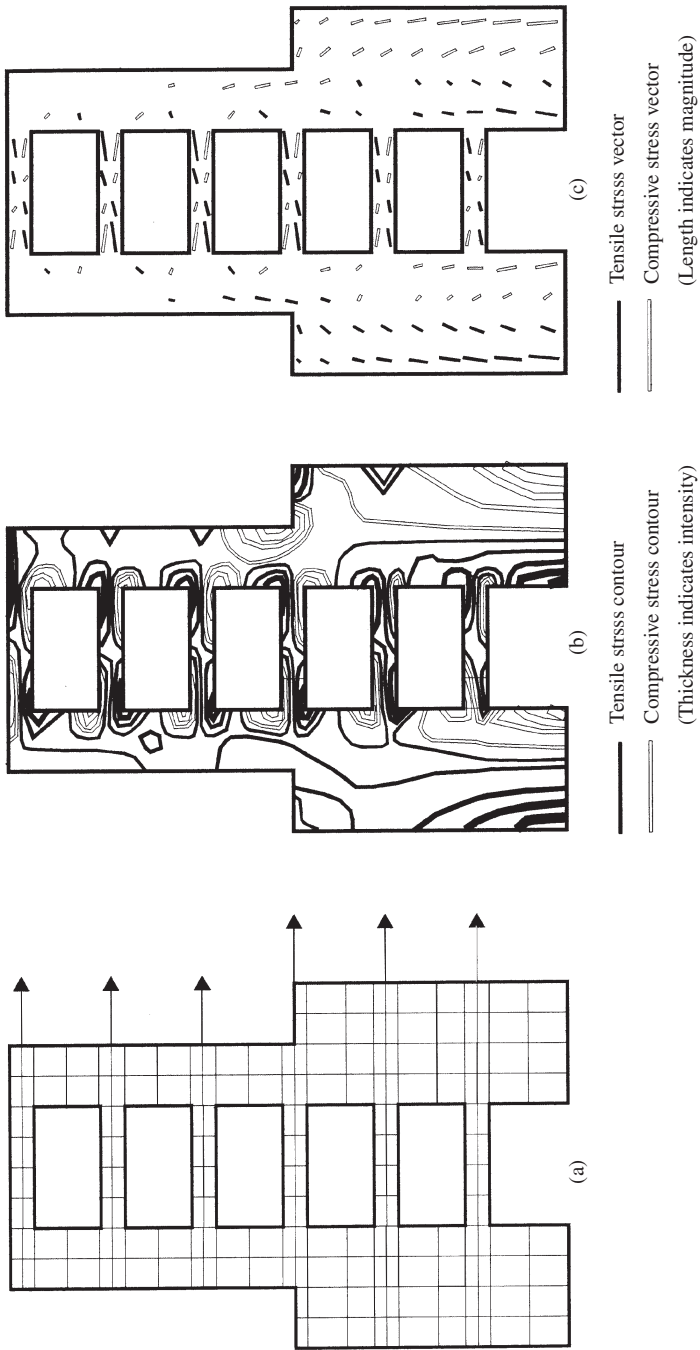


Fig. 1.36

Determine the general form of the strain matrix,  $[B]$ , which relates the three strain components at P,  $\varepsilon_x$ ,  $\varepsilon_y$  and  $\gamma_{xy}$ , to the eight nodal displacement components. What form of strain variation within the element may be represented accurately? Indicate, without detailed evaluation, how an expression for the element stiffness matrix could be obtained.

- 1.8 A shear wall, ABCD, is fully restrained at the base and is loaded as shown in Fig. 1.35(a). It is to be analysed with rectangular plane stress finite elements of the form shown in Fig. 1.35(b). The dimensions and the order of the nodal displacements are as shown in the figure.

The stiffness matrix for an element is

$$[k] = t \int_0^b \int_0^a [B]^T [D] [B] dx dy = \begin{bmatrix} k_{ii} & & & & & & & & \\ & k_{jj} & & & & & & & \\ & & k_{li} & & & & & & \\ & & & k_{mj} & & & & & \\ & & & & k_{mi} & & & & \\ & & & & & k_{mm} & & & \\ & & & & & & & & \\ & & & & & & & & \\ & & & & & & & & \end{bmatrix} \text{symmetric}$$

- (a) Describe briefly the matrices  $[B]$  and  $[D]$  and define a typical element  $2 \times 2$  sub-matrix.  
 (b) Assemble the global stiffness matrix for the wall.

(UEL)

- 1.9 An eight-noded isoparametric finite element mesh for a shear wall is shown in Fig. 1.36(a). The structure is subjected to the horizontal nodal loads shown in the figure. Figures 1.36(b) and 1.36(c) show output results in the form of contours of *absolute* maximum principal stress values and principal stress vectors, respectively.

Use the figures to describe the response of the structure to the applied loading.

## 2. Torsion

### 2.1 Introduction

The twisting of rods used as drive shafts, or of girders which support loads eccentric to their longitudinal axes, is a familiar concept. Less obvious is the role of torsion in slabs and grillages, where the torsional stiffness assists in the distribution of load through the structure. Torsion is also an important aspect of box girder design, since this form of section (Fig. 2.1(a)) is particularly stiff in torsion and is therefore well able to resist eccentric loads. Box girders also possess the twisting rigidity required to avoid the torsional oscillations which dramatically destroyed the Tacoma Narrows bridge. This suspension bridge was susceptible to wind-induced vibrations and collapsed in a moderate wind only months after its completion in 1939.

A somewhat curious feature of *closed* sections, such as box girders, is that, if they possess more than one cell and are therefore *multiply connected* (Fig. 2.1(b)), then torsion theory is needed to determine the shear stress response even if the load is applied through the girder axis and the section is not therefore twisted.

The considerations applicable to box girder design are also relevant to the analysis of multi-storey buildings constructed on the structural core principle if the concrete core forms a closed section (Fig. 2.2(a)). Should a closed core be architecturally inappropriate, then cores consisting of one or more *open* sections (Fig. 2.2(b)) are used. Open sections are typically less stiff in torsion than closed sections and the distribution of shear stress across the section also



Fig. 2.1 (a) Singly-connected box girder. (b) Multiply-connected box girder

differs in the two cases. Open sections therefore require separate consideration from closed ones. Open section torsion theory will also apply to standard structural steel sections, since, tubes and rectangular hollow sections apart, these are of an open form.

Elastic stability problems (Trahair, 1993) also often require a knowledge of torsional behaviour. The commonest example is lateral beam instability, in which a beam bent about its major axis buckles sideways by a combination of twisting and minor axis bending.

Torsional action is therefore important in a wide variety of applications, and the purpose of this chapter is to describe how the torsional response of different structural sections may be evaluated.

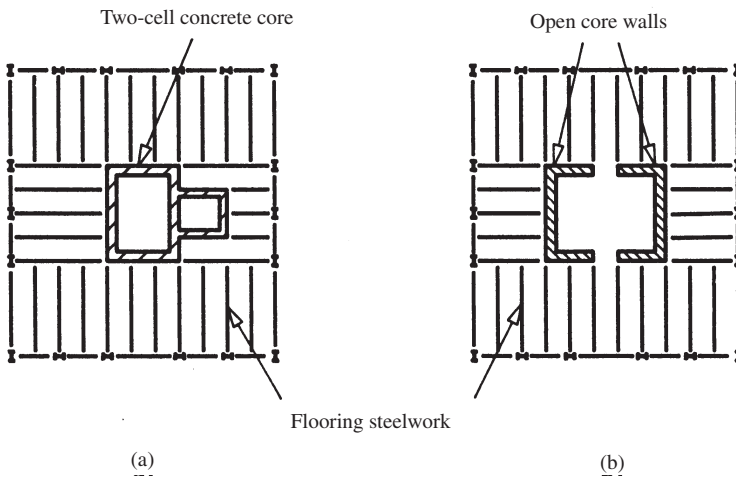


Fig. 2.2 Concrete core construction plans

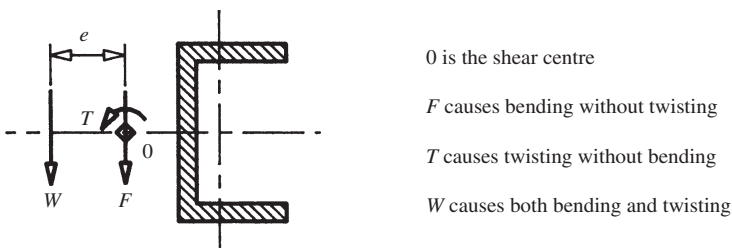


Fig. 2.3 Shear centre

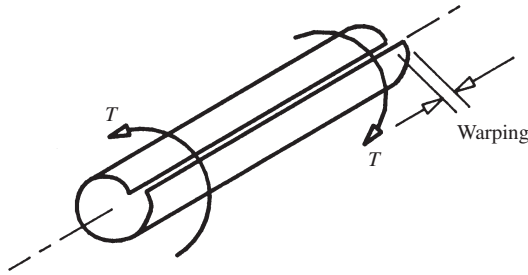


Fig. 2.4 Saint-Venant torsion

## 2.2 Torsional behaviour

When twisting occurs, it will do so about the *centre of rotation* of the section, and it is about this point that the torque due to eccentric forces is calculated. The centre of rotation coincides with the *shear centre* (Fig. 2.3), since, by the reciprocal theorem, the point about which moments can be applied so as to cause twisting without bending is the same as the point through which a load must be applied to cause bending without twisting, that is, the shear centre (Megson, 1996a).

The form of the torsional response depends upon both the type of torque and the nature of the end restraints applied to the structural member. The simplest case is when the bar is subjected to *uniform torsion* by the application of equal and opposite twisting moments at its ends. It is assumed that the cross-section does not deform in its own plane, so that the displacements in this plane may be readily obtained from the twist as rigid-body movements. In addition to these in-plane displacements, however, nearly all sections displace along their axes when subjected to torsion (Fig. 2.4). If these *warping* displacements are free to occur unhindered, then the warping is said to be *free* or *unrestrained*. Taken together, the case of uniform torsion and unrestrained warping is generally referred to as *Saint-Venant* torsion and is such as to produce a uniform rate of twist along the length of the bar. Saint-Venant torsion is the simplest case to examine and is the only one to be considered in detail here.

The response required is usually the stresses caused by the torque, sometimes the twist, and, occasionally, the warping movements. The stress and rotational characteristics are easier to determine for *thin-walled* sections (Fig. 2.1) than for solid sections, since the limited wall thickness effectively predetermines the direction of the stress at any point. The more general solid section will be considered first, using the elasticity theory developed in Chapter 1. Attention will then be given to the simplifications which are possible for thin sections. Finally, some indication will be provided of the (considerable) complications which ensue if the Saint-Venant restrictions are relaxed.



## 2.3 Solid sections

### 2.3.1 Circular section

The circular section is the only one normally considered in introductory texts (Megson, 1996b), for the excellent reason that it is the only solid section which may be simply discussed. For this case, the response to uniform torsion (Fig. 2.5) must be radially symmetric, which requires originally straight radii to remain straight in the deformed position. Also, since warping does not occur along lines of symmetry, there is no warping displacement whatsoever, so that plane sections remain plane.

Under these conditions, it may readily be demonstrated that the shearing distortion suffered by elements on cylindrical surfaces concentric to the rod axis (Fig. 2.5) corresponds to a shear stress distribution which varies linearly from the centre of the section (Fig. 2.6), acts in the plane of the element, and the magnitude,  $\tau$ , of which is given by

$$\tau = \frac{Tr}{J} \quad (2.1)$$

where  $T$  is the torque and  $J$  is the torsion constant (= second polar moment of area (*circular section only*)).

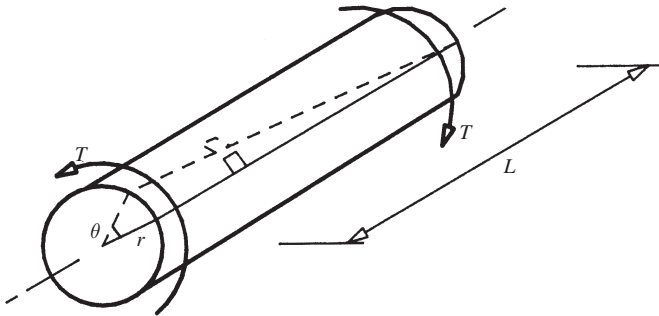


Fig. 2.5 Torsion of circular rod

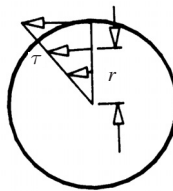


Fig. 2.6 Shear stresses on circular section

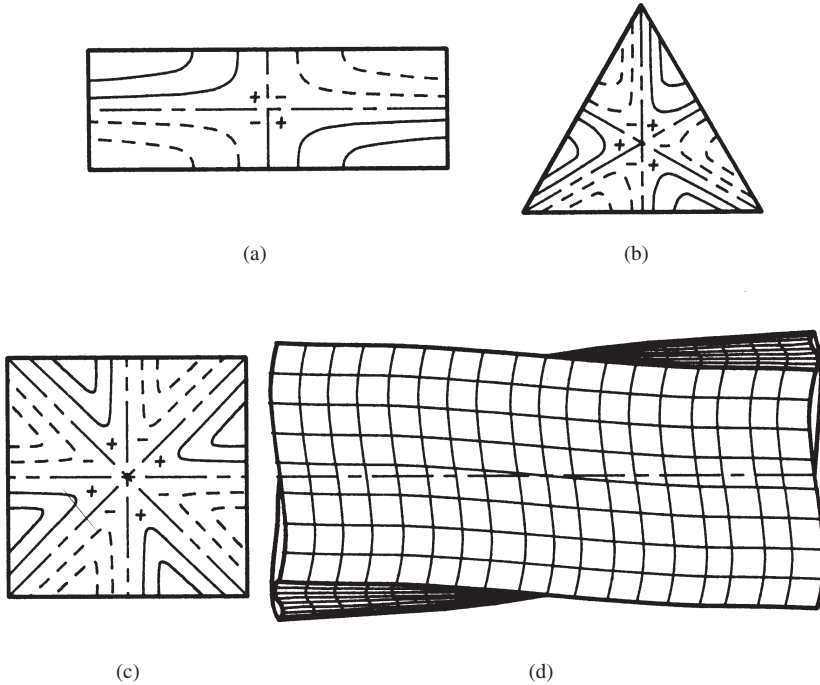


Fig. 2.7 (a–c) Cross-sectional warping distributions. (d) Elevation of square cross-section rod under uniform torsion showing warping displacements

It may also be shown that the relative rotation between the ends of the rod,  $\theta$ , is related to the applied torque by:

$$\theta = \frac{TL}{GJ} \quad (2.2)$$

where  $G$  is the elastic shear modulus and  $L$  is the rod length.

### 2.3.2 Non-circular sections

The deformation of non-circular solid sections is more complicated, due to the presence of warping displacements. The warping displacement distribution over the cross-section is divided into symmetrical and anti-symmetrical regions by zero-warping cross-sectional lines of symmetry, as indicated in Fig. 2.7.

The shear stress distribution is correspondingly more complex, and a general solution may be sought either by a displacement approach in terms of the warping or by a force method utilizing a stress function.

*Displacement, strain and stress relationships*

Taking axes  $x$ ,  $y$  and  $z$  where  $x$  and  $y$  are cross-sectional axes as shown in Fig. 2.8 and  $z$  is the axis of the rod, then the corresponding displacements of a general point, P, are taken to be  $u$ ,  $v$  and  $w$ . The original position of P is defined by the polar coordinates  $(r, \alpha)$  and it displaces to P' due to the rotation, which, at a distance  $z$  along the rod, is  $\theta (= \theta'z)$ , where  $\theta'$  is the (constant) rate of twist. Since the cross-section is assumed rigid,

$$u = -s \sin \alpha = -(r\theta'z) \frac{y}{r} = -y\theta'z, \quad v = s \cos \alpha = (r\theta'z) \frac{x}{r} = x\theta'z \quad (2.3)$$

The displacement components  $u$  and  $v$  may therefore be related to the position of P and the rate of twist,  $\theta'$ , by equations (2.3) but the strain–stress situation must be further explored in order to find a solution for the warping displacement,  $w$ . It is assumed that the warping on each cross-section of the rod is identical, hence

$$\frac{\partial w}{\partial z} = 0 \quad (2.4)$$

Substituting from equations (2.3) and (2.4) in the strain–displacement relationships of general elasticity (equations (1.3) and (1.4)) gives

$$\begin{aligned} \epsilon_x = \frac{\partial u}{\partial x} = 0, \quad \epsilon_y = \frac{\partial v}{\partial y} = 0, \quad \epsilon_z = \frac{\partial w}{\partial z} = 0 \\ \gamma_{xy} = \frac{\partial u}{\partial y} + \frac{\partial v}{\partial x} = 0 \\ \gamma_{yz} = \frac{\partial v}{\partial z} + \frac{\partial w}{\partial y} = \left( x\theta' + \frac{\partial w}{\partial y} \right) \\ \gamma_{zx} = \frac{\partial w}{\partial x} + \frac{\partial u}{\partial z} = \left( -y\theta' + \frac{\partial w}{\partial x} \right) \end{aligned} \quad (2.5)$$

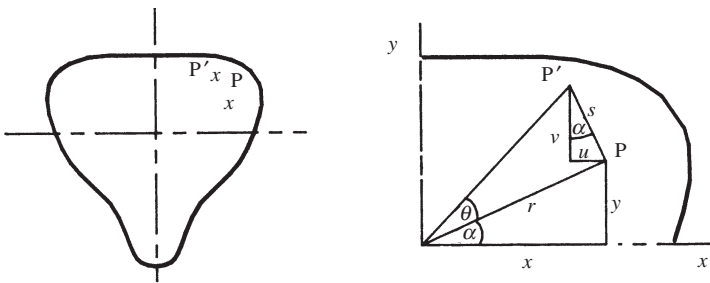


Fig. 2.8 Typical cross-section

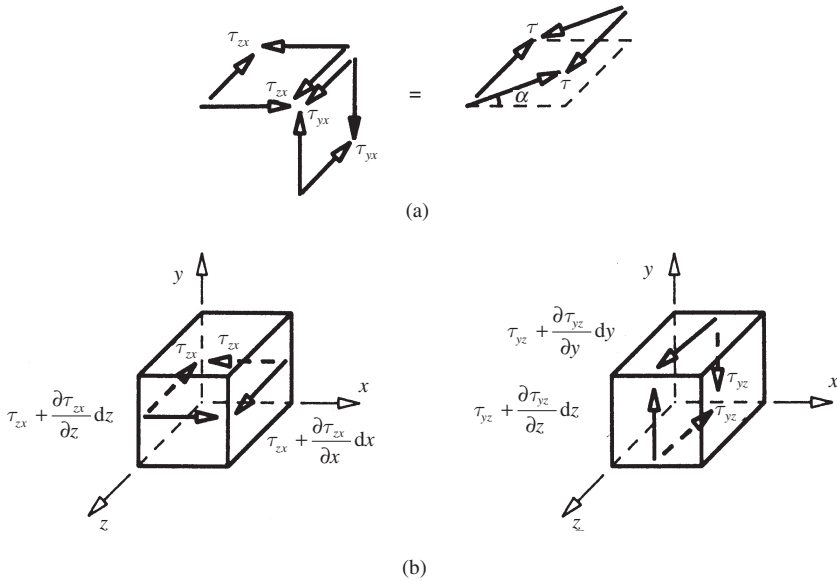


Fig. 2.9 Torsional shear stress components

The stress–strain relationships (equations (1.8)) are now used to determine the stresses as

$$\begin{aligned}
 \sigma_x = \sigma_y = \sigma_z = \tau_{xy} &= 0 \\
 \tau_{yz} = G\gamma_{yz} &= G\left(x\theta' + \frac{\partial w}{\partial y}\right) \\
 \tau_{zx} = G\gamma_{zx} &= G\left(-y\theta' + \frac{\partial w}{\partial x}\right)
 \end{aligned} \tag{2.6}$$

Under Saint–Venant conditions, torsion is therefore resisted by shear stress alone, the direct stress components being zero throughout the bar, and the shear stress may be represented by the two normal components,  $\tau_{yz}$  and  $\tau_{zx}$ . These components both act in planes which are perpendicular to that of the cross-sectional plane of the rod and may be combined to give a resultant shear stress which also acts in a plane perpendicular to that of the cross-section (Fig. 2.9(a)). It should be noted that the zero values of the stress components  $\sigma_x$ ,  $\sigma_y$  and  $\tau_{xy}$  are a direct result of the rigid cross-section assumption, while the zero direct longitudinal stress,  $\sigma_z$ , follows from the unrestrained warping assumption of uniform torsion.

### Equilibrium

In Fig. 2.9(b), the two non-zero sets of shear stress components are shown acting on elementary blocks, having sides  $dx$ ,  $dy$  and  $dz$ . The complementary nature of these stresses ensures satisfaction of moment equilibrium; force equilibrium may be ensured by resolution first in the  $x$ -,  $y$ -directions to give

$$\frac{\partial \tau_{zx}}{\partial z} = \frac{\partial \tau_{yz}}{\partial z} = 0 \quad (2.7)$$

Thus, the shear stresses do not vary with position along the bar so that the shear stress distribution on each cross-section of the bar is identical, just as it was earlier assumed (equation (2.4)) that the warping distribution is independent of cross-section.

Resolving in the  $z$ -direction:

$$\frac{\partial \tau_{zx}}{\partial x} dx(dy dz) + \frac{\partial \tau_{yz}}{\partial y} dy(dx dz) = 0$$

So that

$$\frac{\partial \tau_{zx}}{\partial x} + \frac{\partial \tau_{yz}}{\partial y} = 0 \quad (2.8)$$

Equation (2.8) is the fundamental *equilibrium* equation of torsion.

### Displacement formulation

To obtain a general torsion equation in terms of the warping displacements, the shear stress components of equation (2.6) are substituted into the equilibrium equation (2.8) to give

$$G \frac{\partial}{\partial x} \left( -y\theta' + \frac{\partial w}{\partial x} \right) + G \frac{\partial}{\partial y} \left( x\theta' + \frac{\partial w}{\partial y} \right) = 0$$

Hence

$$\frac{\partial^2 w}{\partial x^2} + \frac{\partial^2 w}{\partial y^2} = 0 \quad (2.9)$$

Since  $w$  is assumed to be a continuous function, compatibility is automatically satisfied, so that a solution to the torsion problem is represented by a function of  $w$  which satisfies equation (2.9) at all points on the section and which also satisfies the boundary conditions. Warping will not be directly subject to boundary restraints in the Saint–Venant case, but there will usually be restrictions on the boundary values of the shear stress components which may be related to differential functions of  $w$  by equations (2.6). The equation of interest, equation (2.9), is of the *Laplace* type which was encountered previously in connection with plane stress analysis (equation

(1.19)). Unfortunately, closed-form solutions to the Laplace equation are not readily derived for practical torsional boundary conditions, and numerical methods are therefore usually employed. Once a warping displacement solution has been obtained, the shear stress components may be calculated from equations (2.6).

### Stress function formulation

This approach aims to utilize a stress function so that the equilibrium equation is automatically satisfied. Such a function may be obtained for the torsion problem by taking the shear stress in a given direction to be the derivative of the stress function in the direction normal to that of the stress. Thus,

$$\tau_{xz} = \frac{\partial\phi}{\partial y}, \quad \tau_{yz} = -\frac{\partial\phi}{\partial x} \quad (2.10)$$

In equation (2.10), the negative sign in the  $\tau_{yz}$  shear stress component arises from the fact that its normal (which is generated by taking a positive (anti-clockwise) rotation from the stress component) is in the negative  $x$ -direction (Fig. 2.10).

By substitution from equations (2.10), it is readily shown that  $\phi$  satisfies the equilibrium equation (2.8). It remains to ensure that the compatibility and material laws are fulfilled. This may be achieved by noting that, at any given point on the section, the two shear strain components,  $\gamma_{yz}$  and  $\gamma_{zx}$ , are related to a single independent displacement,  $w$  (see equation (2.5)). The two shear strain components must therefore be related by a compatibility condition which may be derived, in terms of the shear stress components, by eliminating  $w$  from equations (2.6) to give

$$\frac{\partial\tau_{yz}}{\partial x} - \frac{\partial\tau_{zx}}{\partial y} = 2G\theta' \quad (2.11)$$

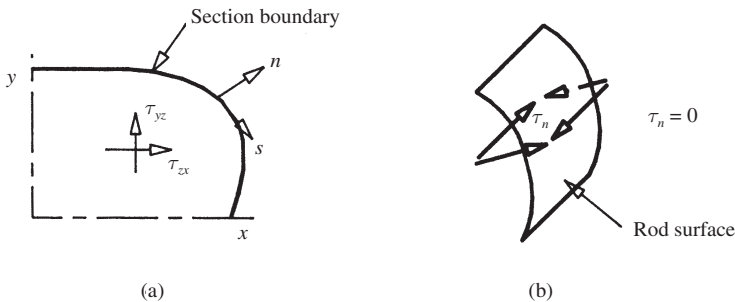


Fig. 2.10 Boundary condition: (a) quarter cross-section; (b) boundary enlargement

Substituting in equation (2.11) for  $\tau_{yz}$  and  $\tau_{zx}$  from equation (2.10) produces the general stress function equation of torsion as

$$\frac{\partial^2 \phi}{\partial x^2} + \frac{\partial^2 \phi}{\partial y^2} = -2G\theta' \quad (2.12)$$

Equation (2.12) is of the *Poisson* type and, to assess the expected difficulty of its solution, it is necessary to explore the nature of the boundary conditions. At a boundary (Fig. 2.10), the stress component normal to the boundary must be zero or a complementary component would exist *on* the exterior surface of the bar which would conflict with the stress-free state of this surface. In stress function terms, this implies that:

At a boundary

$$\tau_n = \frac{\partial \phi}{\partial s} = 0 \quad (2.13)$$

Integration of equation (2.13) shows that the stress function must have constant value around the boundary. The choice of this constant is immaterial, but it is conveniently taken to be zero. The problem therefore requires the solution of equation (2.12) subject to a zero-valued stress function at the boundary. Although this is a relatively simple boundary condition, closed-form solutions have only been derived for regular sections (Timoshenko and Goodier, 1982) and numerical methods are used for more complex shapes. Once a stress function solution has been obtained, the corresponding shear stress components follow from equation (2.10).

### *Torque and torsion constant determination*

The torque required to produce a specified rate of twist,  $\theta'$ , may be calculated from the corresponding stress component solution. The torque,  $dT$ , acting on the element shown in Fig. 2.11, is given by

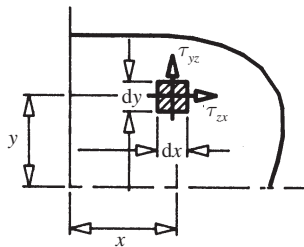


Fig. 2.11 Torque determination

$$dT = -y\tau_{zx} dx dy + x\tau_{yz} dx dy \quad (2.14)$$

And, thus, the total torque,  $T$ , by

$$T = \iint (-y\tau_{zx} + x\tau_{yz}) dx dy \quad (2.15)$$

If a stress function approach is being used, then the torque may be found directly from the stress function by substituting in equation (2.15) from equation (2.10) to give

$$T = \iint \left( -y \frac{d\phi}{dy} - x \frac{d\phi}{dx} \right) dx dy \quad (2.16)$$

Integrating equation (2.16) by parts shows that

$$T = \int \left( [-y\phi]_a^b + \int \phi dy \right) dx + \int \left( [-x\phi]_c^d + \int \phi dx \right) dy \quad (2.17)$$

where a, b, c and d are points on the section boundary.

Making use of the zero  $\phi$  boundary condition results in

$$T = 2 \iint \phi dx dy \quad (2.18)$$

Equation (2.18) allows  $T$  to be calculated from the stress function, and equation (2.17) incidentally demonstrates that the two shear stress components make equal contributions to the total torque. As for the circular section case, a relationship exists between  $T$  and  $\theta'$  of the form (see equation (2.2))

$$T = GJ \frac{\theta}{L} = GJ\theta' \quad (2.19)$$

Equation (2.19) can now be used to obtain the torsion constant,  $J$ , if  $T$  has been calculated for the specified  $\theta'$  as just described (equation (2.15) or (2.18)).

### 2.3.3 Finite difference solutions

The need for a numerical method has been indicated above, and a convenient approach is the finite difference method, which approximates the relevant partial differential equations by sets of simultaneous linear equations. The reader who has not studied this technique previously is referred to Appendix A, where the characteristics of the method and some necessary basic relationships are presented. In this section, the method is first applied to the warping displacement formulation, and second to the stress function formulation, and the results from the use of the two approaches are then compared.

#### *Warping displacement approach*

*Example 2.1 – rectangular section.* The finite difference method will be used to determine the shear stress distribution and the torsion constant for the



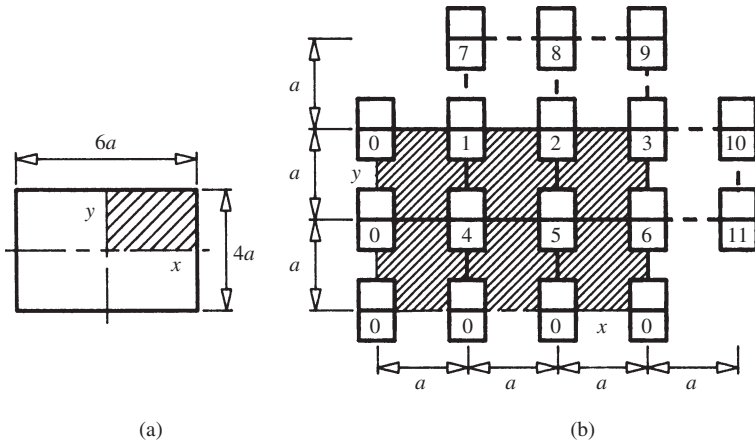


Fig. 2.12 (a) Rectangular section. (b) Finite difference grid

rectangular section of Fig. 2.12(a) when it is subjected to a uniform torque,  $T$ , producing a constant rate of twist,  $\theta'$ . By symmetry, only a quarter of the section need be considered and the  $3 \times 2$  grid to be used is shown in Fig. 2.12(b). To produce a finite difference model of this torsion problem, difference approximations to the general warping displacement equation (2.9) must be created at all relevant grid points and the appropriate boundary conditions must be incorporated. It is first noted that warping does not occur on the two lines of symmetry, so that only six independent points on the section need be considered (Fig. 2.12(b)). However, the shear stress boundary conditions (Fig. 2.10) require that the normal shear stress components along the edges  $x = 3a$  and  $y = 2a$  be zero so that along

$$x = 3a, \quad \tau_{zx} = 0 \quad (2.20a)$$

and along

$$y = 2a, \quad \tau_{yz} = 0 \quad (2.20b)$$

From the shear stress expressions (equations (2.6)), it is seen that these boundary conditions involve first derivatives of the warping displacement. To evaluate the central difference expression (equation (A.5)) for a typical first derivative,  $\partial w / \partial y$ , at point 1, for example, requires a grid position 7 (Fig. 2.12(b)) and points 8–11 are required for the evaluation of the derivatives needed at the remaining boundary points. These fictitious points outside the section have no physical significance but are mathematically legitimate, since there is no reason why the warping displacement function should not extend beyond the confines of the section, provided it obeys the boundary conditions at the section edges.

There are thus 11 independent warping displacements to be calculated. Applying the Laplace operator (Appendix A, Fig. A.5(a)) to points 1–6 will provide six of the necessary equations, while the remaining five result from difference approximations to the stress component boundary conditions (equations (2.6) and (2.20)). The difference approximation to the boundary condition at point 1, for instance, is formed as follows:

$$(\tau_{yz})_1 = G \left( x\theta' + \frac{\partial w}{\partial y} \right)_1 = G \left( a\theta' + \frac{w_7 - w_4}{2a} \right) = 0$$

Hence

$$-w_4 + w_7 = -2a^2\theta'$$

The remaining boundary conditions may be developed in a similar fashion, and the full set of difference equations is presented as

$$\begin{bmatrix} -4 & 1 & 0 & 1 & 0 & 0 & 1 & 0 & 0 & 0 & 0 \\ 1 & -4 & -1 & 0 & 1 & 0 & 0 & 1 & 0 & 0 & 0 \\ 0 & 1 & -4 & 0 & 0 & 1 & 0 & 0 & 1 & 1 & 0 \\ 1 & 0 & 0 & -4 & 1 & 0 & 0 & 0 & 0 & 0 & 0 \\ 0 & 1 & 0 & 1 & -4 & 1 & 0 & 0 & 0 & 0 & 0 \\ 0 & 0 & 1 & 0 & 1 & -4 & 0 & 0 & 0 & 0 & 1 \\ 0 & 0 & 0 & -1 & 0 & 0 & 1 & 0 & 0 & 0 & 0 \\ 0 & 0 & 0 & 0 & -1 & 0 & 0 & 1 & 0 & 0 & 0 \\ 0 & 0 & 0 & 0 & 0 & -1 & 0 & 0 & 1 & 0 & 0 \\ 0 & -1 & 0 & 0 & 0 & 0 & 0 & 0 & 0 & 1 & 0 \\ 0 & 0 & 0 & 0 & -1 & 0 & 0 & 0 & 0 & 0 & 1 \end{bmatrix} \{w\} = \begin{bmatrix} 0 \\ 0 \\ 0 \\ 0 \\ 0 \\ 0 \\ -2 \\ -4 \\ -6 \\ 4 \\ 2 \end{bmatrix} a^2\theta' \quad (2.21)$$

where  $\{w\} = \{w_1, w_2, \dots, w_{11}\}^T$  is the warping vector. The solution to equation (2.21) is

$$\begin{aligned} \{w\} = \{ & -1.275, -2.103, -1.694, -0.499, \\ & -0.722, -0.284, -2.499, -4.722, \\ & -6.284, +1.897, +1.278 \}^T a^2\theta' \end{aligned} \quad (2.22)$$

The shear stress components may be calculated from difference approximations to equations (2.6). For example, at point 5 (Fig. 2.12(b)),

$$\begin{aligned} \tau_{yz} &= G \left( x\theta' + \frac{\partial w}{\partial y} \right) = G \left( 2a\theta' + \frac{w_2 - 0}{2a} \right) = 0.95aG\theta' \\ \tau_{zx} &= G \left( -y\theta' + \frac{\partial w}{\partial x} \right) = G \left( -a\theta' + \frac{w_6 - w_4}{2a} \right) = -0.89aG\theta' \end{aligned} \quad (2.23)$$

Figure 2.13(a) shows the shear stress components and, also, the direction of the shear stress resultants, which may be compared with the expected trajectory diagram of Fig. 2.13(b). It may also be observed from the shear stress solution along the centre-lines that, unlike the circular section, shear stress is not linearly related to distance from the centroid. The maximum shear stress is, in fact, at the centre of the longer side.

The torque needed to produce  $\theta'$  may be determined from the shear stress components by numerical evaluation of the double integral in equation (2.15). The double integration may be accomplished by the familiar (Stroud, 1995) Simpson's rule, namely, for an odd number of stations at equal spacing,  $h$ , the 'one-third rule' is

$$I = \int f \, dx \cong \frac{h}{3} [(f_1 + f_n) + 4(f_2 + \dots + f_{n-2}) + 2(f_3 + \dots + f_{n-1})] \quad (2.24)$$

A similar rule may be developed for an even number of equally spaced stations, in which case the 'three-eighths rule' is

$$I = \int f \, dx \cong \frac{3h}{8} [(f_1 + f_n) + 3(f_2 + \dots + f_{n-1})] \quad (2.25)$$

The ordinate values of the function  $-y\tau_{zx} + x\tau_{yz}$  involved in equation (2.15) are given in Fig. 2.14(a). Applying equation (2.24) for each of the grid-lines in the  $y$ -direction provides the areas under the function along these lines, as given in Fig. 2.14(b). Using equation (2.25) to integrate these areas into a volume for the quarter section gives

$$V = \frac{3}{8} [(4.19 + 11.32 + 3(4.49 + 6.05))] a^4 G\theta' = 17.67 a^4 G\theta'$$

The total torque is therefore

$$T = 4 \times 17.67 a^4 G\theta' = 70.7 a^4 G\theta'$$

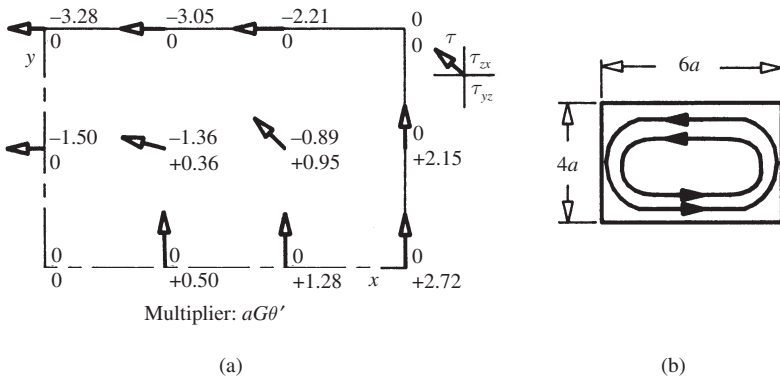
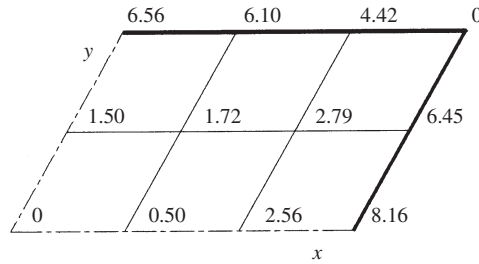
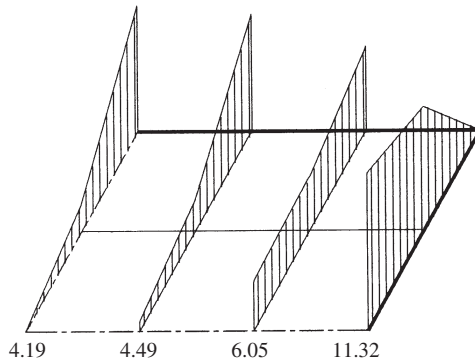


Fig. 2.13 (a) Shear stress solution. (b) Shear stress trajectories



Multiplier:  $a^2 G \theta'$

(a)



Multiplier:  $a^3 G \theta'$

(b)

Fig. 2.14 (a) Ordinates for torque computation. (b) Areas enclosed by ordinates

From equation (2.19), it follows that the torsion constant,  $J = 70.7a^4$ . A closed-form series solution is available for this problem (Timoshenko and Goodier, 1982) and comparative values are given in Table 2.1.

### Stress function approach

*Example 2.2 – rectangular section.* If example 2.1 is tackled using a stress function, then six independent grid positions again need to be considered (Fig. 2.15). However, the six points are now all interior points, since boundary stress function values are known to be zero (see equation (2.13) *et seq.*).

Symmetry requires that the shear stress components along the centre-lines be zero. From the stress function definition (equation (2.10)), this implies that the first derivatives of the stress function normal to the centre-lines must also be zero. Equation (A.5) shows that this type of requirement is met by symmetrical difference points. The points required are shown in Fig. 2.15, and this symmetry of the stress function should be contrasted with the anti-symmetry of the warping displacements.

Using equation (A.11) to model the general stress function equation (2.12) at the six grid points, the difference equations are as presented below:

$$\begin{bmatrix} -4 & 2 & 0 & 2 & 0 & 0 \\ 1 & -4 & 1 & 0 & 2 & 0 \\ 0 & 1 & -4 & 0 & 0 & 2 \\ 1 & 0 & 0 & -4 & 2 & 0 \\ 0 & 1 & 0 & 1 & -4 & 1 \\ 0 & 0 & 1 & 0 & 1 & -4 \end{bmatrix} \{\phi\} = \begin{bmatrix} -1 \\ -1 \\ -1 \\ -1 \\ -1 \\ -1 \end{bmatrix} 2a^2 G\theta' \quad (2.26)$$

where  $\{\phi\} = \{\phi_1, \phi_2, \dots, \phi_6\}^T$  is the stress function vector.

Table 2.1 Rectangular section solution comparison

	Max. $\tau$	$J$
Multiplier	$aG\theta'$	$a^4$
Finite difference	3.28	70.7
Closed form	3.40	75.3

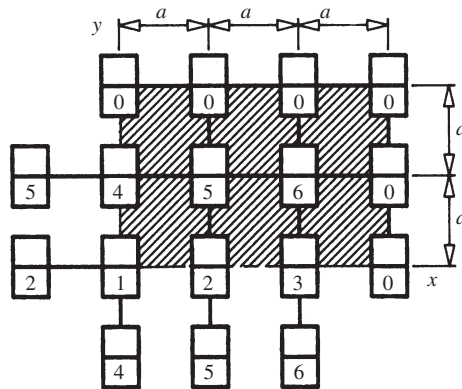
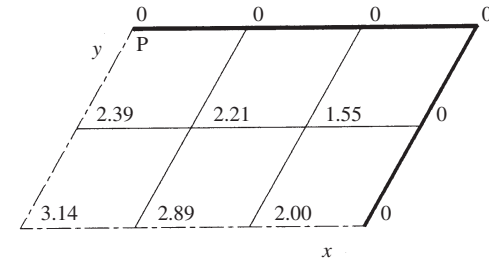
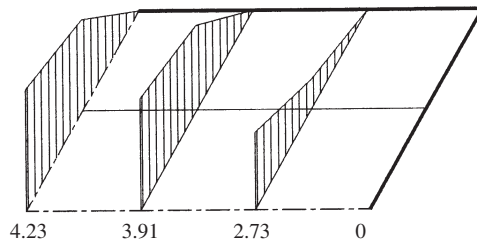


Fig. 2.15 Stress function finite difference grid



Multiplier:  $a^2 G \theta'$

(a)



Multiplier:  $a^3 G \theta'$

(b)

Fig. 2.16 (a) Stress function ordinates. (b) Areas enclosed by ordinates

The solution to equations (2.26) is

$$\{\phi\} = \{3.317, 2.889, 1.997, 2.387, 2.206, 1.551\}^T a^2 G \theta' \quad (2.27)$$

From the stress function solution, the shear stress components may be calculated by difference forms of equations (2.10). At interior points, the required first derivatives may be calculated from central differences but, at boundary points, the absence of exterior points requires the use of backward differences (see Appendix A). Thus, at the point of maximum shear stress, P (Fig. 2.16), by application of equation (A.10), the shear stress is

$$\tau_P = (\tau_{zx})_P = \left( \frac{\partial \phi}{\partial y} \right)_P = \frac{3 \times 0 - 4 \times 2.39 + 3.14}{2a} a^2 G \theta' = -3.21 a G \theta' \quad (2.28)$$

Simpson's rules for numerical integration, equations (2.24) and (2.25), may again be employed to calculate the torque from equation (2.18), using the stress function values of Fig. 2.16(a). Applying equation (2.24) for each of the grid-lines in the  $y$ -direction provides the areas under the stress function along

these lines, as given in Fig. 2.16(b). Using equation (2.25) to integrate these areas into a volume for the quarter section gives

$$V = \frac{3}{8}[(4.23 + 0) + 3(3.91 + 2.73)]a^4 G\theta' = 9.06a^4 G\theta'$$

Whence

$$T = 2 \times 4 \times 9.06a^4 G\theta' = 72.5a^4 G\theta'$$

The torsion constant,  $J$ , then follows from equation (2.19), and the resulting value is compared with other solutions in Table 2.2.

### 2.3.4 Comparison of solution methods

Regular solid sections are generally amenable to classical methods, often resulting in a closed-form series solution (Timoshenko and Goodier, 1982)

Table 2.2 Rectangular section solution comparison

	Max. $\tau$	$J$
Multiplier	$aG\theta'$	$a^4$
Finite difference – displacement method	3.28	70.7
Finite difference – stress method	3.21	72.5
Closed form	3.40	75.3

Table 2.3 Properties of solid sections





Section	Max. $\tau$ multiplier: ( $T/J$ ) or $G\theta'$	$J$	Example
Circle $D = \text{diameter}$	$1.00(D/2)$	$0.098D^4$	
Square $s = \text{side}$	$1.35(s/2)$	$0.141s^4$	
Rectangle $B = \text{breadth}$ $t = \text{thickness}$ For $\alpha, \beta$ see Table 2.4	$\alpha(t/2)$	$\beta Bt^3$	
Equilateral triangle $h = \text{height}$	$1.50(h/3)$	$0.0385h^4$	

Table 2.4 Rectangular section coefficients

$B/t$	1	1.2	1.5	2	2.5	3	4	5	10	$\infty$
$\alpha$	1.35	1.52	1.70	1.86	1.94	1.97	1.99	2.00	2.00	2.00
$\beta$	0.141	0.166	0.196	0.229	0.249	0.263	0.281	0.291	0.312	0.333

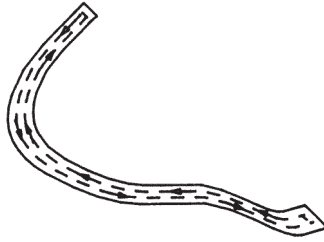


Fig. 2.17 Open thin-walled section

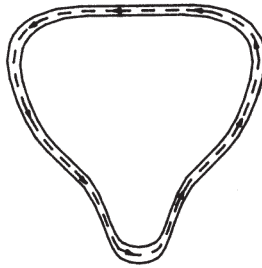


Fig. 2.18 Closed thin-walled section

and results for some common shapes are given in Table 2.3. Irregular sections usually require a numerical approach, which can be based either on finite differences, as used here, or on the finite element method.

If finite elements are used, then either an assumed warping displacement function or an assumed stress function may be employed, although the latter approach (Ross, 1986) is the more usual. If the finite difference method is used, then, for a given grid, the warping displacement approach will provide somewhat superior accuracy (see Table 2.2) in respect of shear stress evaluation, at the expense of generally requiring more equations and having more awkward boundary conditions than the stress function method.

### 2.3.5 Properties of solid sections

For the non-circular sections, the maximal shear stress values given in Table 2.3 all occur at the edge of the section in the middle of a side (the longer one in the case of a rectangle). If the twist for a given torque is required, then equation (2.2) should be used with the appropriate torsion constant,  $J$ .

## 2.4 Thin-walled sections

Thin-walled sections are such that the structural thickness is everywhere small as compared with the overall dimensions of the section. The behaviour of an *open* thin-walled section (Fig. 2.17) is different from that of a *closed* section (Fig. 2.18). In both cases, however, the restricted section thickness



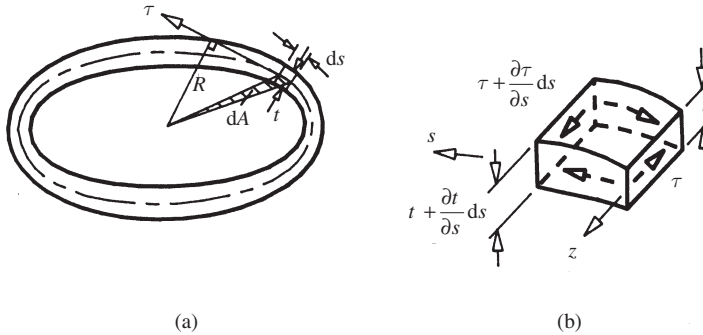


Fig. 2.19 (a) Singly-closed section. (b) Element of the rod

ensures that the direction of the shear stress is generally parallel to the direction of the section *contour* (the mid-thickness line). Under pure torsion, the shear stress trajectories must form closed loops, as otherwise a resultant force would ensue. For the closed section case, a closed stress trajectory is possible following the section contour (Fig. 2.18). In the open case, a closed shear stress trajectory must form within the thickness of the thin section, giving rise to restricted ‘lever-arms’ for the shear stresses and hence low torsional stiffness, as compared with closed sections, which are characterized by their high torsional stiffness. For example, if a thin closed tube is ‘opened’ by the introduction of a narrow longitudinal slit, then the torsional stiffness of the section can be reduced several hundred times.

The treatment of singly closed sections is rather different from that of multiply closed sections. These two forms are therefore described separately, and consideration is then given to open sections. In all cases, although warping will occur, it is possible, and simplest, to calculate the shear stress and twist responses without determining the warping displacements.

### 2.4.1 Singly closed sections

#### *Shear stress response*

For a closed section, a thin wall makes it reasonable to assume that, at any point, the shear stress is constant across the thickness. Taking axes  $s$  and  $z$  in the contour and bar axis directions respectively, the equilibrium of an element (Fig. 2.19(b)) of sides  $ds$  and  $dz$  may be considered as follows:

Resolving in the  $z$ -direction,

$$\left(\tau + \frac{\partial \tau}{\partial s} ds\right) \left(t + \frac{\partial t}{\partial s} ds\right) dz - \tau t dz = 0$$

or (to a first order)

$$\left(\frac{\partial \tau}{\partial s} t + \tau \frac{\partial t}{\partial s}\right) ds dz = \frac{\partial}{\partial s} (\tau t) ds dz = 0$$

Hence

$$\tau t = q = \text{constant} \quad (2.29)$$

Thus the quantity  $\tau t$ , known as the *shear flow*,  $q$ , is constant around the section. The shear flow may be related to the applied torque,  $T$ , by summing the contributions to the torque from elements such as that shown in Fig. 2.19(a).

Thus

$$dT = (\tau t ds) R = qR ds \quad (2.30)$$

and

$$T = \oint qR ds = q \oint R ds$$

since  $q$  is a constant.

But  $R ds = 2 dA$  (Fig. 2.19(a)), hence

$$T = 2q \oint dA = 2qA \quad (2.31)$$

where  $A$  is the area enclosed by the section contour.

Equation (2.31) allows the shear flow and, from equation (2.29), the shear stress to be determined for a given torque. The twist response remains to be examined, and, for this, the displacement of the section must be considered.

### Rotational response

It will again be assumed that the cross-section remains rigid (which may require the provision of transverse diaphragms for these non-solid sections). At a distance,  $z$ , along the rod, the rotation is  $\theta'z$  and, following a similar argument to that employed in the derivation of equations (2.3), the displacement,  $u$ , along the contour is

$$u = Rz\theta' \quad (2.32)$$

The  $z$ -direction (warping) displacement is again taken to be  $w$ , so that the shear strain,  $\gamma$ , by analogy to equation (1.4), is given by

$$\gamma = \frac{\partial u}{\partial z} + \frac{\partial w}{\partial s} \quad (2.33)$$

Using equation (2.32),

$$\gamma = R\theta' + \frac{\partial w}{\partial s} \quad (2.34)$$

So that

$$\tau = G \left( R\theta' + \frac{\partial w}{\partial s} \right) \quad (2.35)$$

Integrating equation (2.35) around the contour:

$$\oint \tau \, ds = \int_0^S G \left( R\theta' + \frac{\partial w}{\partial s} \right) ds = G\theta' \oint R \, ds + [w_S - w_0] \quad (2.36)$$

where  $S$  is the contour length.

However, since the value of  $w$  is identical at the start and finish of the contour,

$$\oint \tau \, ds = G\theta' \oint R \, ds$$

but  $\tau = q/t$  and  $\oint R \, ds = 2A$ , hence

$$\oint \frac{q}{t} \, ds = 2AG\theta' \quad (2.37)$$

Equation (2.37) relates the rate of twist,  $\theta'$ , to the shear flow,  $q$ , rather than to the applied torque,  $T$ . This may be remedied, however, by substituting for  $q$  from equation (2.31) to give

$$\oint \frac{T}{2At} \, ds = 2AG\theta' \quad (2.38)$$

or

$$\theta' = \frac{T}{G \left[ 4A^2 / \left( \oint ds/t \right) \right]} = \frac{T}{GJ} \quad (2.39)$$

where

$$J = \frac{4A^2}{\oint ds/t} \quad (2.40)$$

$$\left( = \frac{4A^2 t}{S} \text{ if } t \text{ is constant} \right)$$

The torsional response of a singly connected closed section therefore presents relatively few difficulties, not least because the problem is statically determinate and, hence, only equilibrium considerations are needed to evaluate the shear flow (equation (2.31)). Multiple connection introduces redundancy, so that geometric as well as statical arguments are required to achieve a stress solution.

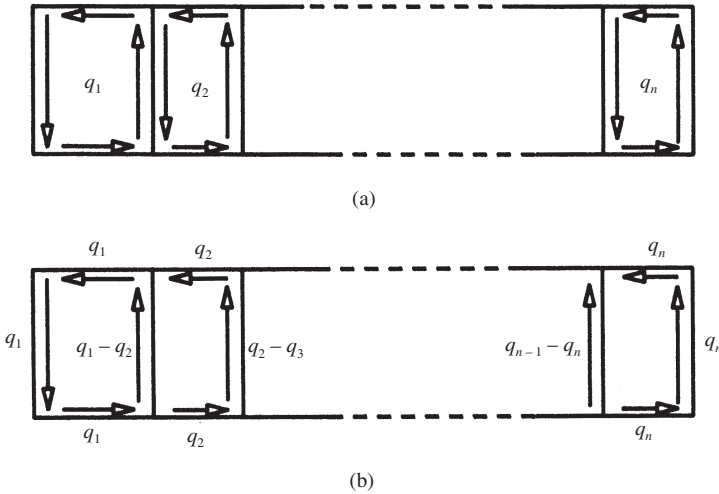


Fig. 2.20 (a)  $n$ -cell box girder. (b) Shear flows in  $n$ -cell girder

### 2.4.2 Multiply closed sections

As mentioned in the introduction to this chapter, a multiply closed section requires the application of torsion theory to determine the distribution of the shear stresses, even if the load passes through the shear centre (Fig. 2.3) and hence does not cause the section to twist. As well as investigating the effects of torsion on multiply connected girders, which is covered in the following section, it is therefore necessary to consider the effects of a bending load, which are subsequently described. Finally, an indication is given of how these two analyses may be combined to determine the effects of a general load, such as  $W$  in Fig. 2.3, which does not pass through the shear centre.

#### Box girder under applied torque

The analysis of a multiply closed section such as the  $n$ -cell box girder shown in Fig. 2.20(a) is based on the following considerations:

- (a) Shear flows exist within each cell due to torque application, as shown in Fig. 2.20(a).
- (b) Flows in common members are the resultant of the shear flows in the adjoining cells (Fig. 2.20(b)), thus justifying, by fluid analogy, the choice of the term shear *flow*. This property of ‘shear flow into a junction equalling shear flow out’ follows from the equilibrium of the shear flows complementary to those shown in Fig. 2.20(b). Thus, for the example junction of Fig. 2.21:

Resolving in the  $z$ -direction,

$$q_1 dz - q_2 dz - q_3 dz = 0$$

or

$$q_1 = q_2 + q_3$$

- (c) The sum of the individual cell torques, which are determined from equation (2.31), equilibrates the applied torque,  $T$ . This provides a single, statical equation.
- (d) The remaining  $(n - 1)$  equations needed for the determination of the  $n$  shear flows are obtained from the geometric observation that, in the absence of section deformation, each cell rotates similarly. Hence, applying equation (2.37) to each cell in turn and eliminating  $\theta'$  from the resulting  $n$  equations produces the required  $(n - 1)$  equations.

*Example 2.3 – box girder under applied torque.* The three-cell box girder of Fig. 2.22(a) is to be analysed for the effects of a clockwise applied torque of 10 000 kN m. The symmetry of the section results in there being only two independent shear flows, which are shown in Fig. 2.22(b).

For this section,

$$A_1 = A_3 = (2 \times 1.5/2) = 1.5 \text{ m}^2$$

and

$$A_2 = (4 \times 1.5) = 6 \text{ m}^2$$

Using equation (2.31) to express the cell torques in terms of the shear flows, the statical equation is

$$2(1.5q_1 + 6.0q_2 + 1.5q_1) = 10\,000$$

or

$$q_1 + 2q_2 = 1667 \quad (2.41)$$

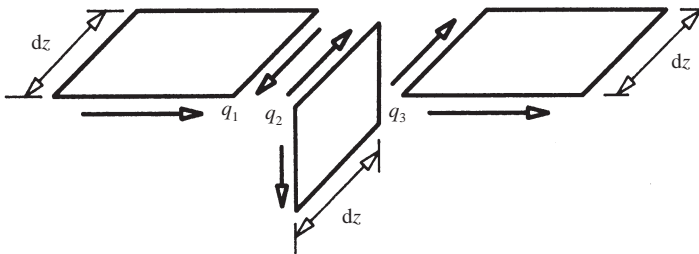


Fig. 2.21 Typical junction

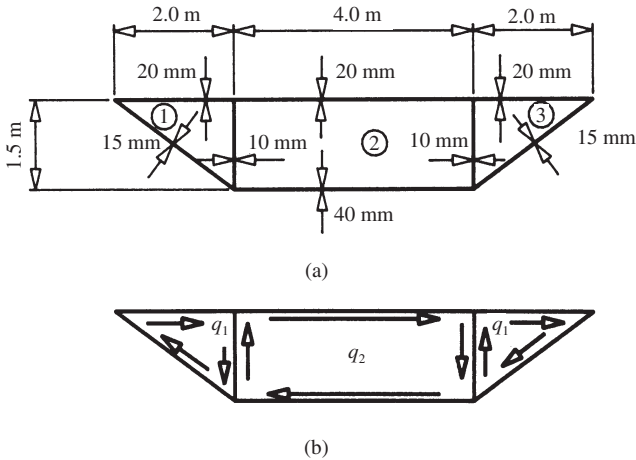


Fig. 2.22 (a) Box girder example. (b) Shear flows (kN/m) in box girder

Applying equation (2.37) to the first two cells in turn, taking due regard to shear flow directions, yields:

For cell 1

$$q_1 \times 2 / (0.02) + (q_1 - q_2) \times 1.5 / (0.01) + q_1 \times 2.5 / (0.015) = 2G(1.5)\theta'$$

or

$$417q_1 - 150q_2 = 3G\theta' \quad (2.42)$$

For cell 2

$$q_2 \times 4 / (0.02) + (q_2 - q_1) \times 1.5 / (0.01) + q_2 \times 4 / (0.04) + (q_2 - q_1) \times 1.5 / (0.01) = 2G(6)\theta'$$

or

$$-300q_1 + 600q_2 = 12G\theta' \quad (2.43)$$

Eliminating  $\theta'$  from equations (2.42) and (2.43) gives

$$1968q_1 - 1200q_2 = 0 \quad (2.44)$$

Solving equations (2.41) and (2.44) provides the solution

$$q_1 = q_3 = 390 \text{ kN/m}$$

$$q_2 = 638 \text{ kN/m}$$

The final shear flows are shown in Fig. 2.23, and the corresponding shear stresses may be obtained by use of the shear flow definition (equation (2.29)). If the rate of twist is needed, then equation (2.42) or (2.43) can be used to give  $\theta'$  as  $0.279 \times 10^{-3}$  rad/m (taking  $G = 80 \times 10^6$  kN/m<sup>2</sup>).

Box girder under shear load

A load applied through the shear centre of a beam is known as a shear load and, as mentioned previously, such a load causes bending without twisting. For singly connected sections, the shear flows due to this type of load may be determined by considering the equilibrium of an elemental beam length. As with torsion, multiply connected sections are not susceptible to a purely statical approach. The method of attack is therefore as follows:

- (a) A 'cut' is introduced in each cell so as to make the section singly connected and hence statically determinate.
- (b) The shear flows in the cut section are calculated by determinate theory (Megson, 1996a) which gives the shear flow as

$$q = \frac{QA\bar{y}}{I} \tag{2.45}$$

where  $Q$  is the applied shear load,  $A$  is the area of the section from the point under consideration to a free surface,  $\bar{y}$  is the lever arm of area  $A$ , and  $I$  is the second moment of area of section. Note: the quantities  $\bar{y}$  and  $I$  are both related to the axis about which bending occurs, which is here assumed to be a *principal* axis.

- (c) Constant, redundant, correction shear flows are additionally assumed to be present in each cell.
- (d) Application of equation (2.37) to each cell in turn, together with the condition of zero rotation for every cell, yields a set of linear equations from which the redundant shear flows may be determined.

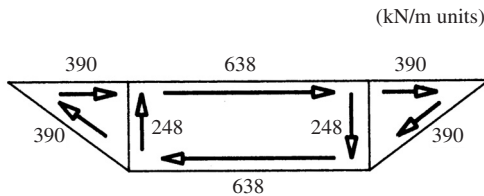


Fig. 2.23 Resultant box girder shear flows

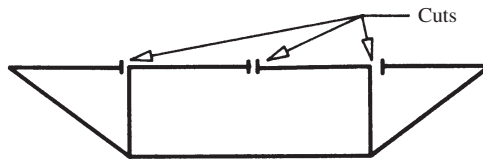


Fig. 2.24 Cuts in three-cell girder

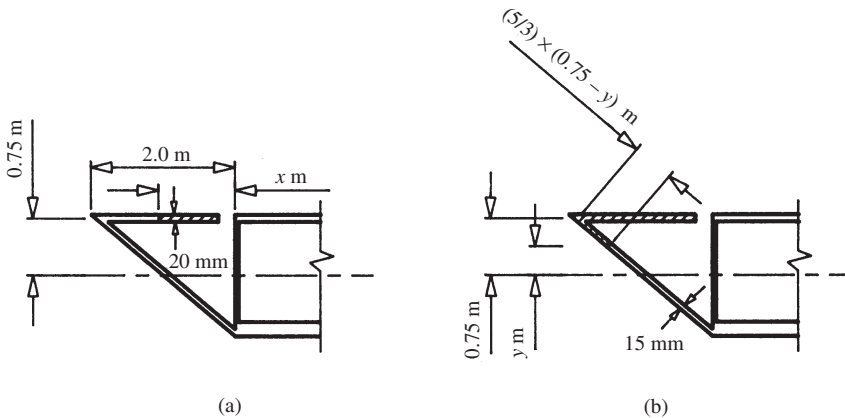


Fig. 2.25 Determinate shear flow calculation. (a) Flange. (b) Web

(e) The resultant shear flows are obtained by summation of the determinate and redundant solutions.

*Example 2.4 – box girder under shear load.* The three-cell box girder of Fig. 2.22(a) is again to be analysed under the action of a downwards shear load of 2000 kN. The section is such that its centroid is at mid-depth and  $I = 0.2 \text{ m}^4$ .

The first step is to introduce the ‘cuts’, which should generally be positioned so as to preserve whatever symmetry the section may possess. There can also be some numerical ‘conditioning’ advantage in siting cuts in places where the shear flow is expected to be small (near the centre of flange sections), since the determinate values should then be a reasonable approximation to the complete solution. Cuts close to junctions result in somewhat simpler calculations, however, so that, in the present case, symmetrical cuts close to the web/flange intersections will be used in the outer cells, while, to preserve symmetry, a central cut is needed in the middle cell (Fig. 2.24).

The determinate shear flows may now be obtained from equation (2.45). In the left-hand cell, for example, with reference to Fig. 2.25:

In the flange

$$q_x = \frac{2 \times 10^3 \times 0.020(x) \times 0.75}{0.2} = 150x \text{ kN/m}$$

In the web

$$q_y = (150 \times 2) + \frac{2 \times 10^3 \times 0.015 \times (5/3) \times (0.75 - y) \times (1/2) \times (0.75 + y)}{0.2} \text{ kN/m}$$



Hence

$$q_y = 300 + 125(0.5625 - y^2) \text{ kN/m}$$

Similar calculations for the central cell enable the full determinate shear flow picture to be assembled as shown in Fig. 2.26. The direction of the flows may be deduced by observing that a downwards shear load will produce downwards flows in the webs. The flange flow directions then follow from the continuous nature of shear flow.

Consideration of the symmetrical shear flows in the central cell shows that these flows satisfy the requirement for zero twist (equation (2.37)). The introduction of a redundant shear flow into this cell would therefore imply a non-existent twist, and it must be concluded that no such redundant flow exists in the central cell. The redundant flows in the outer cells must be numerically equal, so that the problem reduces to the determination of this flow (Fig. 2.27(a)) by application of the zero-twist requirement to an outer cell.

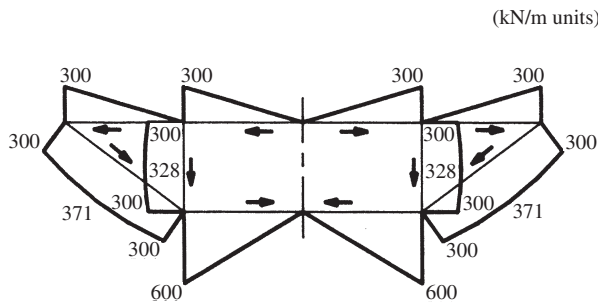


Fig. 2.26 Determinate shear flow

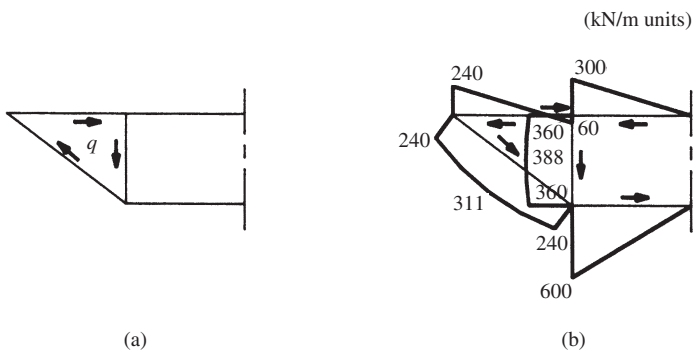


Fig. 2.27 (a) Redundant shear flow (kN/m). (b) Resultant shear flows (kN/m)

Thus, applying equation (2.37) to the left-hand cell in a clockwise sense results in

$$\frac{-(1/2) \times 300 \times 2}{0.02} + \frac{300 \times 1.5}{0.01} + \frac{(2/3) \times (328 - 300) \times 1.5}{0.01} - \frac{300 \times 2.5}{0.015} - \frac{(2/3) \times (371 - 300) \times 2.5}{0.015} + \frac{q \times 2}{0.02} + \frac{q \times 1.5}{0.01} + \frac{q \times 2.5}{0.015} = 0$$

Whence

$$q = 60 \text{ kN/m}$$

Summing the now known redundant flow to the determinate flows of Fig. 2.26 gives the resultant flows shown in Fig. 2.27(b).

### *Box girder under general load*

A load which does not pass through the shear centre may be replaced by a statically equivalent torque and shear load. Thus, the general load  $W$  of Fig. 2.3 may be replaced by a shear load ( $= W$ ) together with a torque ( $= We$ ). The effects due to these statically equivalent loads may then be determined separately by the procedures which have just been described. Superposition of the two solutions gives the resultant values. An alternative, and much speedier, approach (Megson, 1974) is to apply the shear load analysis using a non-zero rate of twist,  $\theta'$ . For an  $n$ -cell girder, eliminating  $\theta'$  from the resulting set of linear equations gives  $(n - 1)$  equations in the  $n$  redundant shear flows. The required additional equation is obtained by equating the moment of the redundant and determinate shear flows about any specified point to the moment of the applied load about the same point. If the position of the shear centre is unknown, then this latter approach must be used, or a modified method may be followed, whereby the position of the shear centre is determined (Megson, 1974).

### 2.4.3 Open sections

It has already been observed that closed shear flow loops must form within open sections subjected to pure torsion (section 2.4). The portions of the loop shown in Fig. 2.28(a) which are parallel to the contour are of constant thickness,  $dy$ , and are at constant distance,  $y$ , from the section contour. If it is assumed that the section contour is free from shear strain, while the *Kirchhoff* assumption of lines normal to the contour remaining normal is also made, then it may be shown that these premises imply that the shear strain (and therefore stress) is constant at constant distance from the section contour. Hence, given the constant thickness,  $dy$ , the shear flow,  $q$ , is also constant, and closed section theory (equation (2.37)) may be used to give

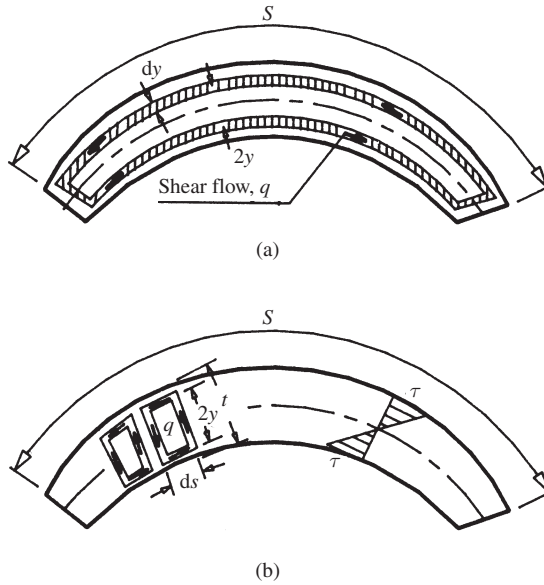


Fig. 2.28 General open section

$$\oint \frac{q}{dy} ds = 2AG\theta' \quad (2.46)$$

If the section is thin, so that  $y$  is negligible in comparison with the contour length,  $S$ , then

$$\oint ds = 2S, \quad A = 2yS \quad (2.47)$$

Also,

$$q = \tau dy \quad (2.48)$$

Hence, from equation (2.46),

$$\tau = \frac{2x2ySG\theta'}{2S} = 2yG\theta' \quad (2.49)$$

Equation (2.49) relates the shear stress to the rate of twist and also shows that the stress is linearly related to  $y$ , the distance from the contour. Thus, the shear stress distribution at any point takes the form shown in Fig. 2.28(b) and the greatest stress is at the section surfaces. This contrasts strongly with the closed section case, where the shear stress at any point is constant across the section thickness. If the variation of shear stress along the length of a section surface

is considered, then it may also be observed from equation (2.49) that the greatest shear stress will occur at the point where  $y$  is largest, that is, where the thickness is greatest. This reverses the singly closed section experience, where, because of the constant shear flow around the section, the greatest shear stress is found at the point of minimum thickness.

In respect of maximal shear stress, it should be mentioned that sections possessing re-entrant corners are subject to considerable *stress concentration* effects which can be minimized, but not eliminated, by suitable fillet design (Timoshenko and Goodier, 1982).

To relate the rate of twist to the applied torque, the torsional resistances provided by shear flows acting on elementary loops (Fig. 2.28(b)) are summed, since the normal shear flows in adjacent elements will cancel, except at the ends, leaving a flow loop as before (Fig. 2.28(a)).

Applying equation (2.31) to an elementary loop:

$$dT_e = 2q(2y ds) \quad (2.50)$$

where  $dT_e$  is the torque resistance of the elementary loop, and  $T_e$  is the torque resistance of length  $ds$  of section.

Or

$$dT_e = 4(\tau dy)y ds \quad (2.51)$$

And, using equation (2.49),

$$dT_e = 8y^2 G\theta' dy ds \quad (2.52)$$

Integrating:

$$T_e = 8G\theta' \int_0^{t/2} y^2 dy ds \quad (2.53)$$

Integrating along the section contour:

$$T = G\theta' \int_0^s \frac{t^3}{3} ds = GJ\theta' \quad (2.54)$$

Hence

$$\theta' = \frac{T}{G \int_0^s (t^3/3) ds} = \frac{T}{GJ} \quad (2.55)$$

where

$$J = \int_0^s (t^3/3) ds \quad (2.56)$$

(=  $St^3/3$  if  $t$  is constant)

Equation (2.55) provides the desired rate of twist–torque relationship and may be used to eliminate  $G\theta'$  from equation (2.49) to produce a surface shear stress–torque relationship as

$$\tau = 2 \frac{t}{J} \frac{T}{J} = \frac{Tt}{J} \quad (2.57)$$

For the maximum surface shear stress in open sections under torsion,

$$\tau_{\max} = \frac{Tt_{\max}}{J} \quad (2.58)$$

Equation (2.56) defines the torsion constant,  $J$ , for a general open, thin-walled section. For a section which ‘branches’, Fig. 2.29(a) for example, the torsion constant may be obtained by summing contributions derived from equation (2.56).

Thus, for the channel of Fig. 2.29(b),

$$J = \sum_{i=1}^3 \frac{B_i t_i^3}{3} \quad (2.59)$$

For some standard, rolled steel sections, torsional constant values have been accurately determined (Owen and Knowles, 1992). For non-standard metal sections, the above type of application of equation (2.56) will give approximate values. For improved accuracy, the constant factor of (1/3) in equation (2.56) may be replaced by the section-dependent factor  $\beta$  of Table 2.4. It may, incidentally, be noted that the  $\beta$ -value given in Table 2.4 for a negligibly thin rectangle is in agreement with the (1/3) derived in this section. Several techniques are available to improve the accuracy even further, by including, for example, the effects of fillets and junctions (Kollbrunner and Basler, 1969).

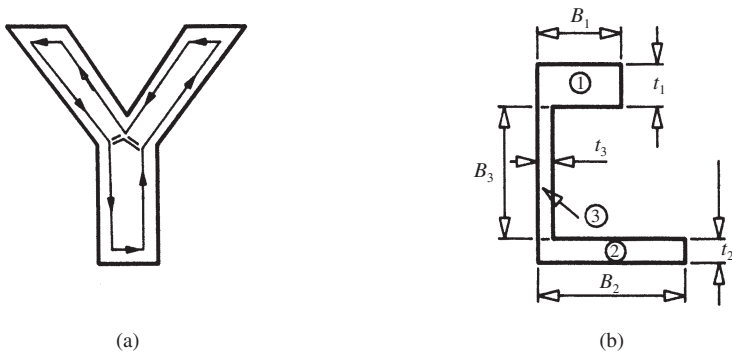
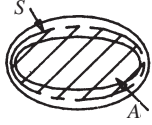
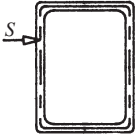
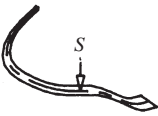
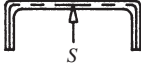
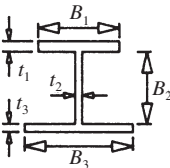


Fig. 2.29 (a) Branched open section. (b) Channel section

Table 2.5 Properties of thin-walled sections

Section	$t_{\max}$	$J$	Example
Closed Variable thickness, $t$ Area enclosed by contour, $A$	$\frac{T}{2At_{\min}}$	$\frac{4A^2t}{\oint(ds/t)}$	
Closed Constant thickness, $t$ Contour perimeter, $S$ Area enclosed by contour, $A$	$\frac{T}{2At}$	$\frac{4A^2t}{S}$	
Unbranched open Variable thickness, $t$ Contour length, $S$	$\frac{Tt_{\max}}{J}$	$\int_0^S \frac{t^3}{3} ds$	
Unbranched open Constant thickness, $t$ Contour length, $S$	$\frac{Tt}{J} = \frac{3T}{St^2}$	$\frac{St^3}{3}$	
Unbranched open Consists of $n$ unbranched, open, constant-thickness sections	$\frac{Tt_{\max}}{J}$	$\frac{1}{3} \sum_{i=1}^n B_i t_i^3$	

#### 2.4.4 Properties of thin-walled sections

The torsional properties of thin-walled sections are summarized in Table 2.5. For closed sections, the maximum shear stress occurs at the thinnest point of the section, but, for open sections, the maximum shear stress is located at the thickest point. If the twist for a given torque is required, then equation (2.2) should be used with the appropriate torsion constant,  $J$ .

### 2.5 Soap-bubble (membrane) analogy

It may be shown (Timoshenko and Goodier, 1982) that the governing partial differential equation for the deformation of a stretched membrane under normal pressure is analogous to that governing the stress function formulation of the torsion problem (equation (2.12)). This *Prandtl* membrane analogy has been used to provide experimental values of torsional properties by measuring the deformation of either inflated soap films or rubber membranes, which are

stretched across cut-outs of the section for which the properties are to be evaluated. Numerical techniques have superseded this practical approach but the analogy can still provide a useful qualitative check on torsional properties.

Figure 2.30 shows the stress function distributions (or inflated membrane shapes) for a rectangular and L-shaped section. Equation (2.10) shows that the torsional shear stress component in any given direction is proportional to the slope of the stress function *in the normal* direction. Thus, for the rectangular section (Fig. 2.30(a)) the shear stress *normal* to the longer sides of the rectangle is essentially zero because the function has no slope (except near the ends) in directions *parallel* to the longer sides. The shear stress component parallel to the longer sides has a maximum value at the edge, where the function has maximal slope *normal* to the edge, and the stress then decreases until the contour is reached where the normal slope is zero. The stress then increases once more, as progress is made to the opposite edge, but the direction of the stress is reversed, since the sign of the function slope changes past the summit. Consideration of the membrane shape therefore supports the torsional shear stress distribution for the section previously established in Section 2.4.3. Equation (2.18) indicates that the torsional constant is proportional to the volume enclosed by the stress function. Clearly, therefore, the broader arm of the L-shape section (Fig. 2.30(b)) provides the majority of the contribution to the torsion constant (resistance) of this particular section.

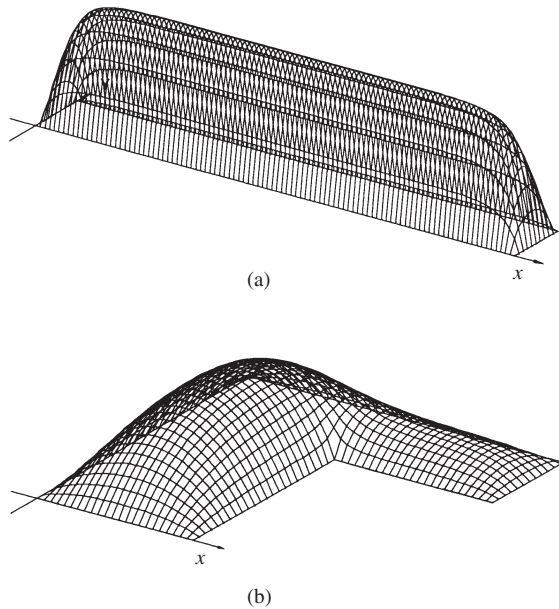


Fig. 2.30 Prandtl membrane for: (a) rectangular section; (b) L-section

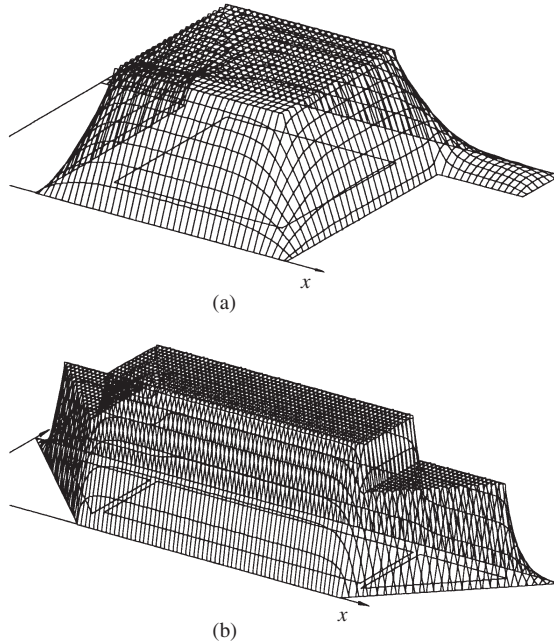


Fig. 2.31 Prandtl membranes for: (a) singly-closed sections; (b) multiply-closed sections

In the case of closed sections, it is necessary to represent the cut-outs of the section by rigid plates which remain in the same plane when the membrane is inflated. Using this concept, the membrane deformation (stress function) distributions for a single and a multiply closed section are shown in Fig. 2.31. From the singly closed section plot (Fig. 2.31(a)), it may be seen that the shear stress parallel to the outline of the cut-out is almost constant and is in a consistent direction, as verified by the approximately constant normal slope of the membrane making the connection to the horizontal rigid surface above the cut-out. From the minimal enclosed volumes, it may also be seen that the ‘open’ cantilever arms make a negligible contribution to the overall torsional resistance of the section.

## 2.6 Non-uniform torsion

If warping displacements are restrained at any point, or if the applied torque is not uniform, then the constant rate of twist assumption, which is central to Saint–Venant’s theory, is no longer valid and the cross-sectional displacements and stresses will vary with position along the structural length. Non-uniform torsion occurs in many situations, including those in which the load eccentricity varies, as in bow girders, or in which the warping is physically



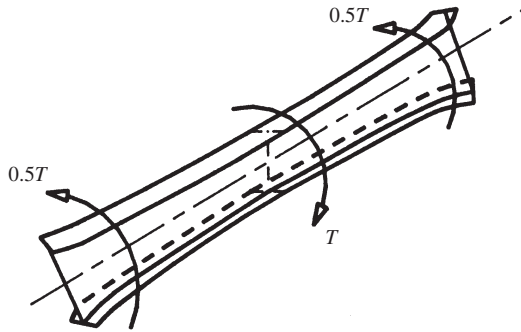


Fig. 2.32 Non-uniform torsion

restrained at a support. A single, central, eccentric load (Fig. 2.32) will also produce non-uniform torsion. This may be viewed either as a case of non-uniform torque, since the torques in the two halves are of opposite sense, or as a case of restrained warping, since, by symmetry, no warping occurs on the central cross-section.

The stress implications of non-uniform torsion are that, in addition to a modified shear stress distribution, direct longitudinal stresses are also developed, as may readily be imagined from the restrained warping feature. The effects of non-uniform torsion are particularly pronounced in the case of open sections, but, even for closed sections, there can be a significant influence over considerable lengths of the structural member, although the greatest impact will be at positions of warping restraint. Non-uniform torsion can thus neither be completely treated by Saint-Venant's torsion theory, nor is his localization principle (Section 1.3.1) valid. For the determination of stresses due to non-uniform torsion, the reader is referred to specialized texts (e.g. Heins, 1975; Megson, 1974; Zbirohowski-Koscia, 1967).

## References and further reading

- American Concrete Institute (1973) *Analysis of Structural Systems for Torsion*. ACI Publication SP-35. ACI, Detroit. Provides examples of torsion in concrete construction.
- Heins, C. P. (1975) *Bending and Torsional Design of Beams*. Heath, Lexington. Uniform and non-uniform torsion is covered with an orientation towards the analysis of bridge girders.
- Horne, M. R. (1977) *Structural Action in Steel Box Girders*. CIRIA, London. Chapter 1 deals with both uniform and non-uniform torsion, while the remainder of the publication covers the buckling and post-buckling behaviour of box girders.
- Hsu, T. T. C. (1984) *Torsion of Reinforced Concrete*. Van Nostrand Reinhold,

- New York. Chapter 1 applies Saint–Venant torsion theory to concrete sections.
- Kollbrunner, C. F. and Basler, K. (1969) *Torsion in Structures*. Springer, Berlin. Chapters 1 and 2 present Saint–Venant torsion theory in terms of the membrane analogy. An appendix deals with the accurate determination of the torsional properties of open thin-walled metal sections.
- Megson, T. H. G. (1974) *Linear Analysis of Thin-walled Beams*. Surrey University Press, Leighton Buzzard. A full description of uniform torsion and an introduction to non-uniform torsion for thin-walled sections.
- Megson, T. H. G. (1996a) *Structural and Stress Analysis*. Arnold, London, Ch. 10.
- Megson, T. H. G. (1996b) *Structural and Stress Analysis*. Arnold, London, Ch. 11.
- Murray, N. W. (1984) *Introduction to the Theory of Thin-walled Structures*. Oxford University Press, Oxford. Chapter 1 covers uniform torsion and includes multiply connected box girder examples – the remainder of this advanced text deals with non-uniform and non-linear analysis.
- Ross, C. T. F. (1996) *Finite Element Programs in Structural Engineering and Continuum Mechanics*. Albion, Chichester. Chapter 17 describes finite element programs for the solution of the torsion problem based on assumed stress functions.
- Owen, G. W. and Knowles, P. R. (eds) (1992) *Steel Designers' Manual*, 5th edn. Blackwell, London, pp. 1106–1149. Provides torsional properties for standard steel sections.
- Stroud, K. A. (1995) *Engineering Mathematics*. Macmillan, Basingstoke. Covers approximate integration, including Simpson's rule.
- Timoshenko, S. P. and Goodier, J. N. (1982) *Theory of Elasticity*, 3rd edn. McGraw-Hill, New York. Chapter 10 gives a classical treatment of the torsion problem.
- Trahair, N. S. (1993) *Flexural–torsional Buckling of Structures*. Spon, London. Extensive theoretical treatment of elastic and inelastic buckling problems, including the effects of uniform and non-uniform torsion.
- Zbirohowski-Koscia, K. (1967) *Thin-walled Beams*. Crosby Lockwood, London. An approachable description of Vlasov's theory of non-uniform torsion as applied to open thin-walled sections.

## Problems

- 2.1 For a square section of side  $a$ , make use of symmetry, and, adopting a net of side  $a/6$ , use the finite difference method to determine the warping displacements due to a uniform rate of twist,  $\theta'$ .
- Hence calculate the shear stress components at each of the net points, in terms of  $a$ ,  $\theta'$  and the shear modulus,  $G$ , and use these components to find the torsion constant for the section.

Repeat the analysis using the stress function approach and compare the values for maximum shear stress and torsion constant with the values obtained by the warping displacement method and with the exact values of Table 2.3.

- 2.2 Use the finite difference method to determine the stress function values at the grid nodes of the L-section shown in Fig. 2.33 if the section is subjected to a constant rate of twist,  $\theta'$ , and the shear modulus is  $G$ .

From the stress function values, determine the maximum shear stress and the torsion constant for the section. Compare these values with corresponding values obtained by application of a thin-walled 'combined rectangles' approximation (equations (2.58) and (2.59)) and discuss how it might be established as to which of the solutions is the more accurate.

- 2.3 For a rectangular grid, spacing  $a$  in the  $x$ -direction and  $b$  in the  $y$ -direction, show that the finite difference module for the Laplace equation is as shown in Fig. 2.34(a), where

$$A = 1/a^2, \quad B = 1/b^2, \quad C = -2(1/a^2 + 1/b^2)$$

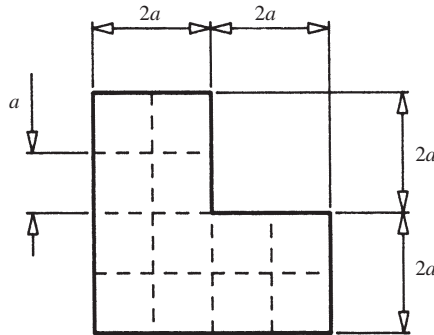


Fig. 2.33

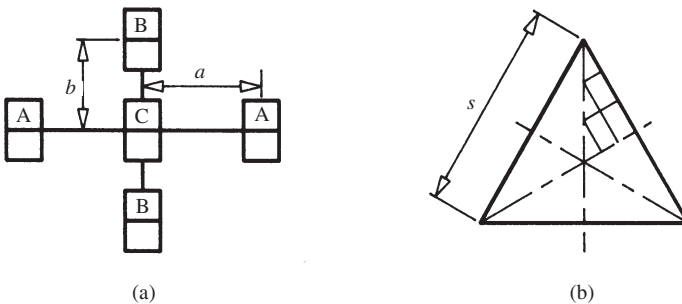


Fig. 2.34

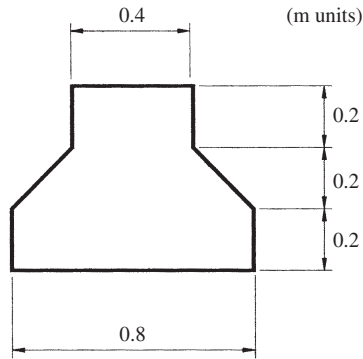


Fig. 2.35

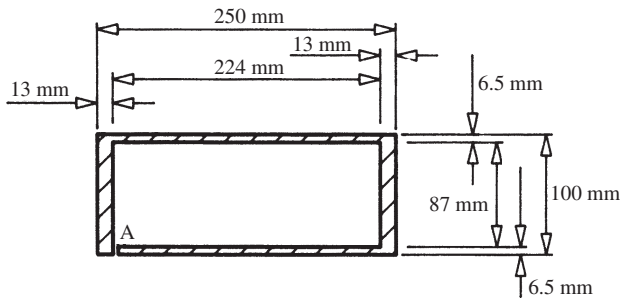


Fig. 2.36

Use the module of Fig. 2.34(a) to determine the warping displacements at the node points of the grid shown in Fig. 2.34(b). The section is an equilateral triangle of side,  $s$ . Hence determine the maximum shear stress and compare your solution with the exact value given in Table 2.3.

- 2.4 For the pre-stressed concrete beam section shown in Fig. 2.35, make use of symmetry, and, adopting a regular net of side 0.2 m, use the finite difference method to determine the stress function values at the net intersection points for a uniform rate of twist,  $\theta'$ . Hence determine an approximation to the torsion constant,  $J$ .

(NTU)

- 2.5 Figure 2.36 shows the cross-section of an aluminium alloy bar. What torque will cause a maximum shear stress of  $60 \text{ N/mm}^2$ ? Calculate, also, the angle of twist (in degrees) in a length of 2 m when this torque is applied if the modulus of rigidity is  $25 \text{ kN/mm}^2$ .

The section is now closed by rigidly sealing the gap at 'A' along the full length of the bar. Determine the new maximum stress and rotation under the same conditions as before and compare the two sets of results.

- 2.6 Figure 2.37 shows two concrete beam sections which have equal cross-sectional areas. Determine the torsional constant for the closed section based on the contour line for the section indicated in Fig. 2.37(a). Determine, also, the torsional constant for the open section using the sub-division indicated in Fig. 2.37(b).
- 2.7 Figure 2.38 shows five rods (A–E) which all have the same cross-sectional area. Sketch the expected stress function distributions for the five rods. Hence, or otherwise, rank the sections according to their expected torsional stiffness, giving reasons for your decisions.

(NTU)

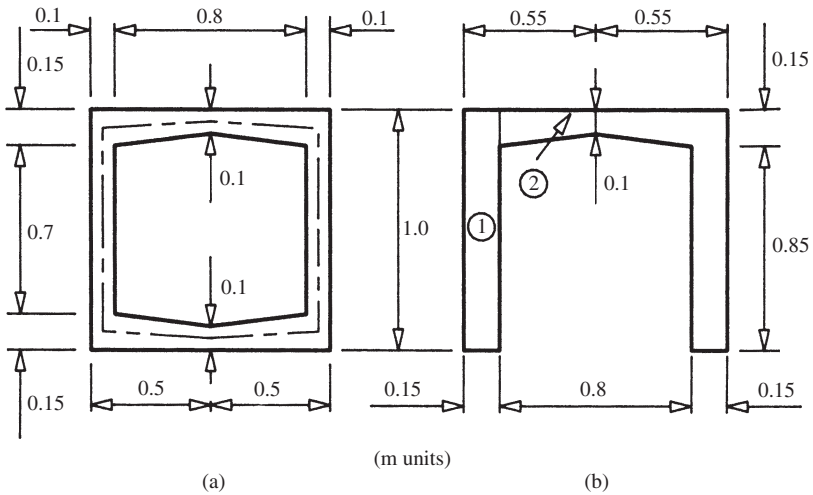


Fig. 2.37

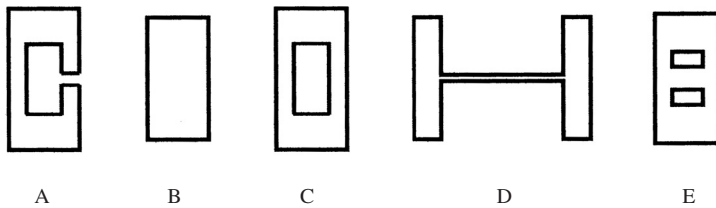


Fig. 2.38

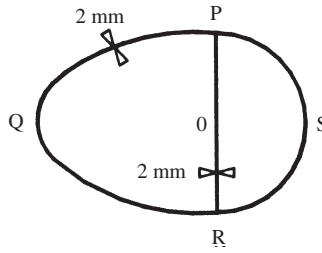


Fig. 2.39

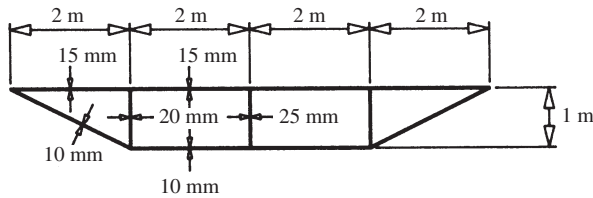


Fig. 2.40

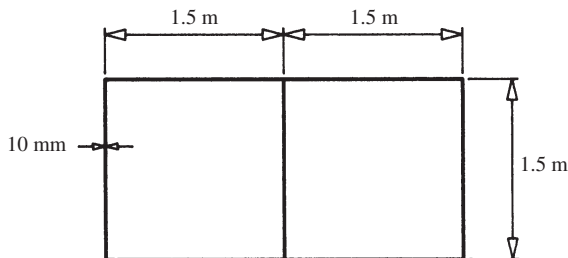


Fig. 2.41

- 2.8 Figure 2.39 shows the cross-section of a long spar formed in an alloy whose modulus of rigidity is  $25 \text{ kN/mm}^2$ . On the right-hand side of the section, the mean line is approximately circular, on the left-hand side it is approximately elliptical, and the areas enclosed by these lines and the mean line of the web are  $4000 \text{ mm}^2$  and  $8000 \text{ mm}^2$  respectively. The thickness of the wall and of the web is  $2 \text{ mm}$ . Given that the lengths of the mean lines are  $PQR = 240 \text{ mm}$ ,  $PSR = 160 \text{ mm}$  and  $POR = 100 \text{ mm}$ , estimate the torsional rigidity ( $= T/\theta'$ ), in ( $\text{kN m}^2/\text{degree}$ ), about an axis perpendicular to the section.

(UCL)

- 2.9 A bridge deck, which may be considered as thin-walled, has the singly symmetric cross-section shown in Fig. 2.40. Determine the torsional stiffness of the section,  $T/\theta'$ , in  $(\text{kN m}^2/\text{degree})$ , if the shear modulus is constant throughout and of value  $70\,000 \text{ N/mm}^2$ .  
(EC)
- 2.10 The two-cell box girder shown in Fig. 2.41 supports a downwards load of  $500 \text{ kN}$  through its centroid. The webs and flanges are both of constant  $10 \text{ mm}$  thickness. Determine the shear flow distribution for the cross-section and comment on the relative magnitudes of the maximum flows sustained by the central and outer webs.

## 3. Plates and slabs

### 3.1 Introduction

The plane stress analysis considered in Chapter 1 was concerned with plate elements which were subjected to in-plane loading only. Plate bending analysis is similarly concerned with planar elements but the loading is now normal to the plane of the element. It is presumed that the plate is free from in-plane loads, the effects of which, if present, may be analysed separately and a resultant solution obtained by superposition.

Plate elements are usually of either metal or concrete construction. In the former case the elements are referred to simply as plates, while the latter are normally referred to as slabs. Both plates and slabs are used as flooring elements and as bridge decks. Other applications of these components are found in retention structures of various forms. The ‘counterfort’ retaining wall shown in Fig. 3.1(a), for example, incorporates vertical and horizontal slabs, both of which are subjected to normal loading. The same is true of the rectangular section hopper shown in Fig. 3.1(b).

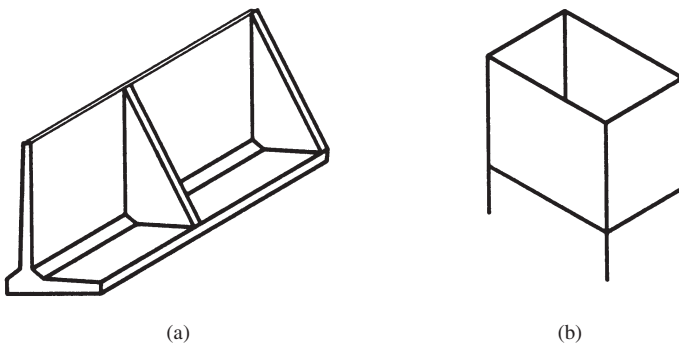


Fig. 3.1 (a) Counterfort retaining wall. (b) Hopper structure



### 3.2 Physical behaviour

#### 3.2.1 Beam analogy

A plate subject to normal loading may be considered as an extension of a beam, in which the width of the beam has become of the same order as the length, while the depth (thickness) remains of a smaller order. The discrete supports applicable to beam analysis may also occur in plate problems but supports along lines in the plane of the plate are commoner. With this relationship between beam and plate elements, some correspondence between their modes of structural behaviour can be expected. This is the case to the extent that a plate element resists normal loading by bending and shearing actions, as does a beam. However, in the case of a plate, the actions are clearly not restricted to the single direction – that along its length, which is available to a beam – but can occur in any direction in the plane of the plate. If rectangular Cartesian coordinates are being used, a closer analogy to plate action is

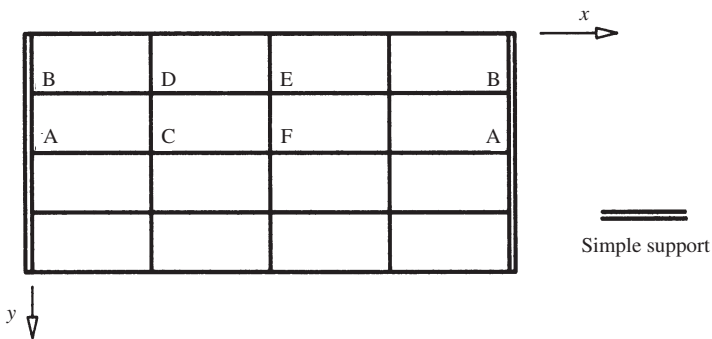


Fig. 3.2 Plan of example grid

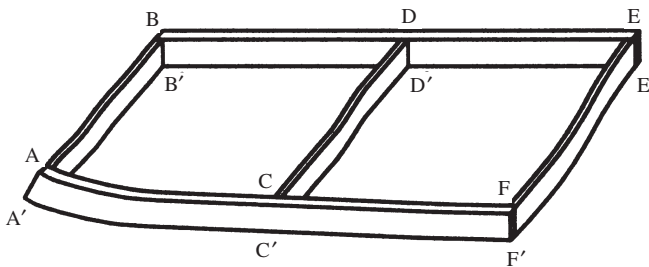


Fig. 3.3 Deformation of part of the grid

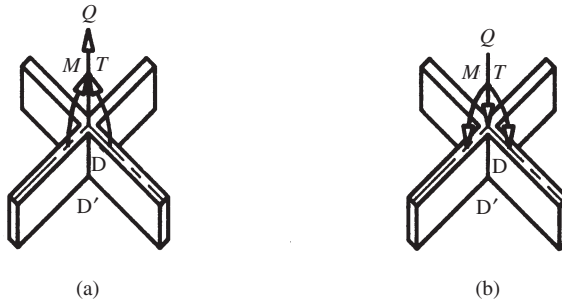


Fig. 3.4 Forces at typical grid node

provided by a grid of rigidly interconnected beam elements set out along the coordinate directions. The behaviour of such a grid (Fig. 3.2) is therefore considered next.

### 3.2.2 Grid analogy

For the grid shown in Fig. 3.2, the edges parallel to the  $y$ -axis are presumed to be continuously ‘simply’ supported (that is, normal displacement is prevented but rotation about the support line is free to occur). The sides parallel to the  $x$ -axis are unsupported (free) and the behaviour of the grid to a concentrated normal load applied to its central point (F) is to be examined. By the nature of the supports, it may be presumed that resistance to the load is principally provided by the structural elements along the line AA. The left-hand half (AF) of AA will be considered to deflect under load as shown in Fig. 3.3, while the remainder of the grid points are assumed undeflected, and the effect of AF’s deflection on the more remote parts of the grid will be investigated. By symmetry, the members along AF will not twist and the line FF’ will remain vertical when deflection takes place. EE’ also remains vertical, since deflection along BE was not permitted, so that no twist is induced in FE by deflection along AF. Bending is, however, induced in FE, since F is now lower than E. Applying similar ideas to AB, it is deduced that there is no bending in this member since there is no twist in AC (and hence no bending rotation applied to AB), while A’ and B’ remain on the same level, that of the support. There is a twist developed in AB because AA’ has rotated from its originally vertical orientation while BB’ has been kept upright. For the more general member, CD, both twisting and bending effects will be present due to the relative rotation of CC’ and DD’ and the relative vertical displacement of C and D.

The reactions required at point D to ensure the assumed rigidity will be as shown in Fig. 3.4(a). The moment  $T$  counteracts the torque in CD, while the

force  $Q$  and the moment  $M$  balance the bending effects of CD. If point D is now allowed to displace, it will be subjected to the effects shown in Fig. 3.4(b), and deformation must occur until the internal stress resultants generated by the deformation equilibrate the 'out-of-balance' force,  $Q$ , and moments  $M$  and  $T$ . Thus,  $Q$  and  $T$  will tend to produce bending in members BD and BE, while  $M$  will tend to twist these elements.

The complete structural action may now be described as follows. Grid members along AA resist the load by bending alone and are stiffened by the transverse grid members, typically CD, which assist by a combination of bending and twisting actions. The transverse members, in turn, invoke resistance from the neighbouring longitudinal members by causing them to bend and twist. This process is repeated, with diminished effect, for the more distant systems of transverse and longitudinal members.

The bending and twisting in the longitudinal and transverse grid members at the general point D offers a model for plate behaviour whereby the bending of the plate, in a rectangular Cartesian coordinate system, may similarly be represented by bending effects along both the coordinate directions accompanied by twisting, also about both directions.

### 3.2.3 Poisson's ratio effect

Although the grid analogy provides a helpful demonstration of how a plate acts, true plate behaviour differs in one important respect due to the effect of Poisson's ratio. In order that an appreciation of this effect may be obtained, the behaviour of a small plate element under the effect of a constant distributed moment applied to two opposite sides may be considered. The grid model would suggest that the effect of such a loading would be to produce a singly curved deformed surface (Fig. 3.5(a)) in which the longitudinal members all have similar deflected shapes and the transverse members are subjected to rigid-body displacements only.

However, if the plate material has a non-zero Poisson's ratio, the deflected shape will not be as in Fig. 3.5(a), since curvature in the  $z$ - $x$  plane will induce curvature in the  $z$ - $y$  plane. This is accomplished as follows: sagging bending of a plate element in the  $z$ - $x$  plane produces compressive stress in the top of the plate and tensile stress in the lower part. It follows from the Poisson's ratio effect (see Section 1.2.3) that tensile strain will therefore be produced transversely in the top of the plate and compressive transverse strain will result in the lower half of the plate. To accommodate this effect, the true deflected surface must be of a doubly curved (*anti-clastic*) form (Fig. 3.5(b)).

The Poisson's ratio effect therefore results in the curvature in a particular direction being no longer solely caused by the bending moment in that direction. For example, there is no bending moment in the  $y$ -direction for the element of Fig. 3.5(b) and yet curvature exists in this direction. The curvature

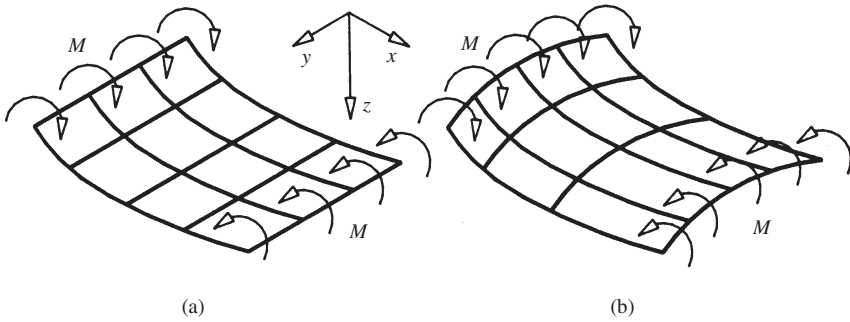


Fig. 3.5 Grid and plate deformed surfaces

in any direction is, in fact, made up of two components, one resulting from bending in the direction considered and one produced by the Poisson's ratio effect. Since concrete has a substantially lower Poisson's ratio than that of metals, the Poisson's ratio effect is sometimes neglected in slab analysis. This assumption makes the grid model exact and grid analogies are widely used in bridge slab analysis. In the analysis of metal plates, however, the Poisson's ratio effect always needs to be considered.

### 3.3 Elastic plate theory

#### 3.3.1 Introduction

Provided that the plate is thin, the three-dimensional plate problem may be reduced to a two-dimensional problem provided that sufficient assumptions are incorporated to allow the deformation at any point in the plate to be readily derived from the deformation of a plane reference surface. The reference surface is taken to be a *middle* surface which is defined by the locus of the mid-thickness points of the plate. The required deformation assumptions are:

- The middle surface does not deform in its own plane, that is, with the notation of chapter 1, the displacement components  $u$  and  $v$  (Fig. 1.4) are zero everywhere on a middle plane which coincides with the  $x$ - $y$  plane.
- The normals to the middle plane in the undeformed state remain straight and normal to the middle surface in the deformed state.

The above assumptions are similar to those used in simple beam theory and reduce the plate problem, when formulated in terms of displacements, to a one independent displacement variable problem. For this reason, it is usual to formulate plate theory in terms of a displacement rather than a stress function, and this approach will be followed here.

The first of the above assumptions results in the displaced shape of the middle surface being completely defined by its normal displacement,  $w$ , at every point, so that  $w$  is the single independent variable. The second assumption then allows the deformation at points other than those on the middle surface to be related to the deformation of the middle surface. The way in which this is done is treated in detail in the next section.

### 3.3.2 Displacements and strains

With the right-hand screw sign convention of Fig. 3.6(a), the rotations (Figs 3.6(b) and 3.6(c)) at a general point on the middle surface (assuming small angles) may be related to the normal displacement variable,  $w$ , by

$$\theta_y = -\frac{\partial w}{\partial x}, \quad \theta_x = \frac{\partial w}{\partial y} \quad (3.1)$$

where the negative sign arises due to the negative slope produced by a positive rotation  $\theta_y$ .

Making use of assumptions (a) and (b) above, the variation of the displacements  $u$  and  $v$  through the thickness of the plate may be related to the normal displacement variable,  $w$ , by (Figs 3.6(b) and 3.6(c))

$$u = z\theta_y = -z\frac{\partial w}{\partial x} \quad (3.2)$$

$$v = -z\theta_x = -z\frac{\partial w}{\partial y} \quad (3.3)$$

where the negative sign in the displacement,  $v$ , arises from the negative sense of  $v$  produced by a positive rotation  $\theta_x$  (Fig. 3.6(c)).

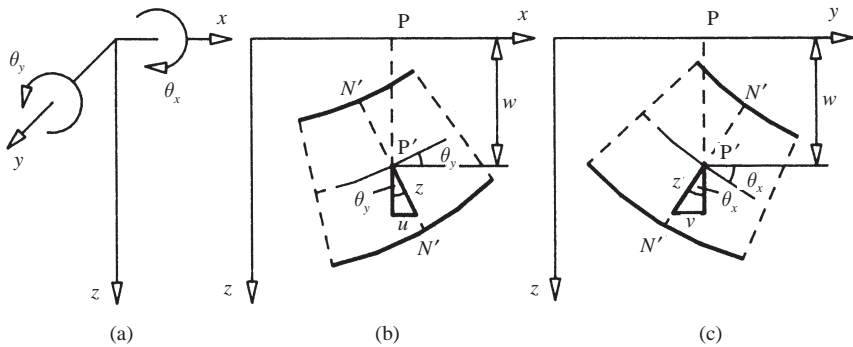


Fig. 3.6 (a) Rotation sign convention. (b) Displacements in  $x$ - $z$  plane. (c) Displacements in  $y$ - $z$  plane

Elasticity theory (equations (1.3) and (1.4)) may now be invoked to relate the strains to the above displacements by

$$\varepsilon_x = \frac{\partial u}{\partial x} = -z \frac{\partial^2 w}{\partial x^2}, \quad \varepsilon_y = \frac{\partial v}{\partial y} = -z \frac{\partial^2 w}{\partial y^2}, \quad \varepsilon_z = \frac{\partial w}{\partial z},$$

$$\gamma_{xy} = \frac{\partial u}{\partial y} + \frac{\partial v}{\partial x} = -2z \frac{\partial^2 w}{\partial x \partial y}, \quad \gamma_{yz} = \frac{\partial v}{\partial z} + \frac{\partial w}{\partial y}$$

From equation (3.3)

$$\frac{\partial v}{\partial z} = -\frac{\partial w}{\partial y}$$

since  $\partial w / \partial y$  ( $= \theta_x$ ) is constant due to the straight normal assumption. Therefore,

$$\gamma_{yz} = -\frac{\partial w}{\partial y} + \frac{\partial w}{\partial y} = 0$$

Similarly,

$$\gamma_{zx} = \frac{\partial w}{\partial x} + \frac{\partial u}{\partial z} = \frac{\partial w}{\partial x} - \frac{\partial w}{\partial x} = 0 \quad (3.4)$$

### 3.3.3 Strains, stresses and stress resultants

A further assumption is now made, namely that the normal stress,  $\sigma_z$ , is everywhere zero. Clearly this assumption cannot be strictly fulfilled in the vicinity of applied loads or reactions but, provided that the plate is thin, the normal stresses will be of a lower order than the in-plane stresses and may therefore be neglected. Adding this further assumption to equations (3.4), the only non-zero stresses at any given level in the plate are seen to be those of plane stress, that is,  $\sigma_x$ ,  $\sigma_y$  and  $\gamma_{xy}$ . Assuming an isotropic material, the stresses may therefore be related to the corresponding strains by the relevant plane stress equations (1.16), which, making use of equations (3.4) and (1.7), gives

$$\sigma_x = \frac{E}{1-\nu^2} (\varepsilon_x + \nu \varepsilon_y) = \frac{-Ez}{1-\nu^2} \left( \frac{\partial^2 w}{\partial x^2} + \nu \frac{\partial^2 w}{\partial y^2} \right)$$

$$\sigma_y = \frac{E}{1-\nu^2} (\nu \varepsilon_x + \varepsilon_y) = \frac{-Ez}{1-\nu^2} \left( \nu \frac{\partial^2 w}{\partial x^2} + \frac{\partial^2 w}{\partial y^2} \right) \quad (3.5)$$

$$\tau_{xy} = G \gamma_{xy} = \frac{-Ez}{1+\nu} \frac{\partial^2 w}{\partial x \partial y}$$

By summing the effects of these stresses through the thickness of the plate, stress resultants may be obtained which are, in fact, the moments

corresponding to the bending in the coordinate directions and the twisting about both these directions which were discussed earlier in relation to the physical behaviour of plates.

If the stress component sign convention used in Chapter 1 is adopted, then, for a positive  $z$ -coordinate, the stress components will act positively as shown in Fig. 3.7. The sign convention for the moments will be taken to be as shown in Fig. 3.8, where the equality of magnitude but opposing sense of the twisting moments arises from the complementary nature of the shear stresses shown in Fig. 3.7(c). The moments will all be considered to be moments *per unit length* of the plate in the direction about which the moment acts. The units of the moments will therefore be, typically, kilonewton metres per metre (kN m/m) and, if the element shown in Fig. 3.8 is of size  $dx$ ,  $dy$ , then the total bending moment in the  $x$ -direction will be given by  $M_x dy$ , in view of the per unit length nature of the moment. The moment stress resultants may be related to their tributary stresses, from Figs 3.7 and 3.8, by

$$\begin{aligned}
 M_x dy &= \int_{-t/2}^{t/2} z(\sigma_x dy dz) \\
 M_y dx &= \int_{-t/2}^{t/2} z(\sigma_y dx dz) \\
 M_{xy} dy &= - \int_{-t/2}^{t/2} z(\tau_{xy} dy dz)
 \end{aligned}
 \tag{3.6}$$

where the negative sign in  $M_{xy}$  arises from the resultant moment due to the stresses  $\tau_{xy}$  being in the negative sense of  $M_{xy}$ .

By use of equations (3.5), the moments may be related to the normal displacement function,  $w$ , by

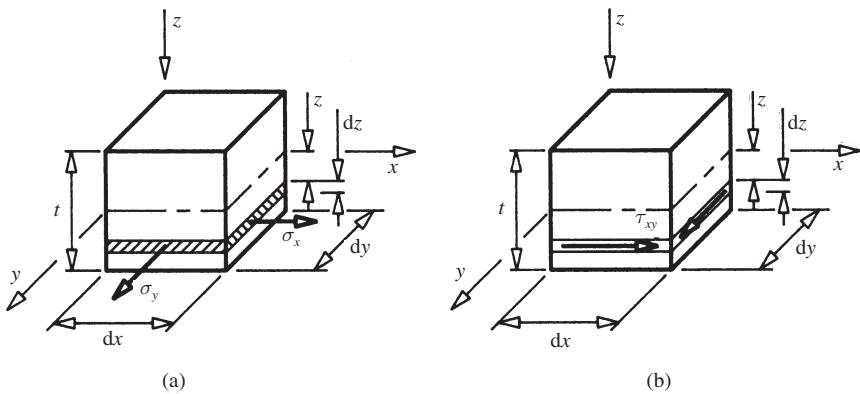


Fig. 3.7 Stress sign conventions

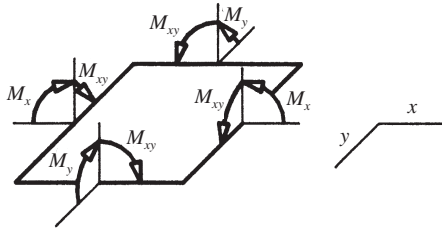


Fig. 3.8 Moment sign conventions

$$\begin{aligned}
 M_x &= \int_{-t/2}^{t/2} z \sigma_x dz = \frac{-E}{1-\nu^2} \left( \frac{\partial^2 w}{\partial x^2} + \nu \frac{\partial^2 w}{\partial y^2} \right) \int_{-t/2}^{t/2} z^2 dz = -D \left( \frac{\partial^2 w}{\partial x^2} + \nu \frac{\partial^2 w}{\partial y^2} \right) \\
 M_y &= \int_{-t/2}^{t/2} z \sigma_y dz = \frac{-E}{1-\nu^2} \left( \nu \frac{\partial^2 w}{\partial x^2} + \frac{\partial^2 w}{\partial y^2} \right) \int_{-t/2}^{t/2} z^2 dz = -D \left( \nu \frac{\partial^2 w}{\partial x^2} + \frac{\partial^2 w}{\partial y^2} \right) \\
 M_{xy} &= - \int_{-t/2}^{t/2} z \tau_{xy} dz = \frac{E}{1+\nu} \frac{\partial^2 w}{\partial x \partial y} \int_{-t/2}^{t/2} z^2 dz = D(1-\nu) \frac{\partial^2 w}{\partial x \partial y} \quad (3.7)
 \end{aligned}$$

where  $D = Et^3/12(1 - \nu^2)$  is the *flexural rigidity* of the plate.

### 3.3.4 Moments, curvatures and stresses

Before proceeding further, it is convenient to establish the relationships which relate the plate curvatures and stresses to the associated moments. For small slopes, the curvatures in the coordinate directions may be obtained as follows.

From equation (3.7)

$$M_x - \nu M_y = -D(1-\nu^2) \frac{\partial^2 w}{\partial x^2} = -\frac{Et^3}{12} \frac{\partial^2 w}{\partial x^2}$$

Hence

$$\chi_x = \frac{\partial^2 w / \partial x^2}{[1 + (\partial w / \partial x)^2]^{3/2}} \approx \frac{\partial^2 w}{\partial x^2} = -\frac{1}{Et^3/12} (M_x - \nu M_y)$$

Similarly,

$$\begin{aligned}
 \chi_y &= \frac{\partial^2 w}{\partial y^2} = -\frac{1}{Et^3/12} (M_y - \nu M_x) \\
 \chi_{xy} &= \frac{\partial^2 w}{\partial x \partial y} = \frac{\partial}{\partial x} (\theta_x) = \theta' = \frac{M_{xy}}{D(1-\nu)} = \frac{M_{xy}}{Et^3/12(1+\nu)} = \frac{M_{xy}}{Gt^3/6} \quad (3.8)
 \end{aligned}$$



The first two expressions of equations (3.8) show that, under small-slope assumptions, the second derivatives  $\partial^2 w / \partial x^2$  and  $\partial^2 w / \partial y^2$  represent the curvatures in the respective coordinate directions. The two equations also confirm the earlier discussion that curvature in a given direction is dependent on both the moment in the specified direction, and also, due to the Poisson's ratio effect, on the moment in the direction normal to the one specified. The last of equations (3.8) shows that the second derivative  $\partial^2 w / \partial x \partial y$  may be geometrically interpreted as a rate of change of twist,  $\theta'$ , about either of the axes, and  $\theta'$  can hence be related to the twisting moment.

To obtain the stresses due to specified moments, substitution from equations (3.8) into equations (3.5) gives, for the maximum stresses (which occur at the top and bottom surfaces),

$$\begin{aligned}\sigma_{x \max} &= \pm \frac{Et}{2(1-\nu^2)} \frac{1-\nu^2}{Et^3/12} M_x = \pm \frac{1}{t^2/6} M_x \\ \sigma_{y \max} &= \pm \frac{1}{t^2/6} M_y \\ \tau_{xy \max} &= \pm \frac{Et}{2(1+\nu)} \frac{12(1-\nu^2)}{Et^3(1-\nu)} M_{xy} = \pm \frac{1}{t^2/6} M_{xy}\end{aligned}\quad (3.9)$$

Equations (3.9) show that the maximum stresses are directly proportional to the corresponding moments. It therefore follows that the concept of principal values, discussed in Chapter 1 as applied to stresses (see Section 1.3.2), will also apply to the set of moments  $M_x$ ,  $M_y$ , and  $M_{xy}$ . The orientation of the principal directions, in which the twisting moments are zero, may therefore be obtained from a moment version of equation (1.9) and the values of the principal moments from an equivalent to equation (1.10).

It may also be noted that the direct bending stresses given by the first two of equations (3.9) have the same form as the corresponding stresses given by simple beam theory, if beams of unit width are considered in each of the coordinate directions.

### 3.3.5 Equilibrium

A solution to the plate problem is to be established in terms of the displacement function  $w$ . If this function is presumed to be continuous, then an explicit compatibility equation is not required. Equations (3.7) relate plate moments to the displacement function and these equations make use of the assumed stress-strain relationships for the plate material. For a complete solution, it therefore remains to establish the equilibrium equations for a plate element in terms of the plate moments. An amalgamation of these equilibrium conditions with equations (3.7) will then represent a full solution to the plate problem.

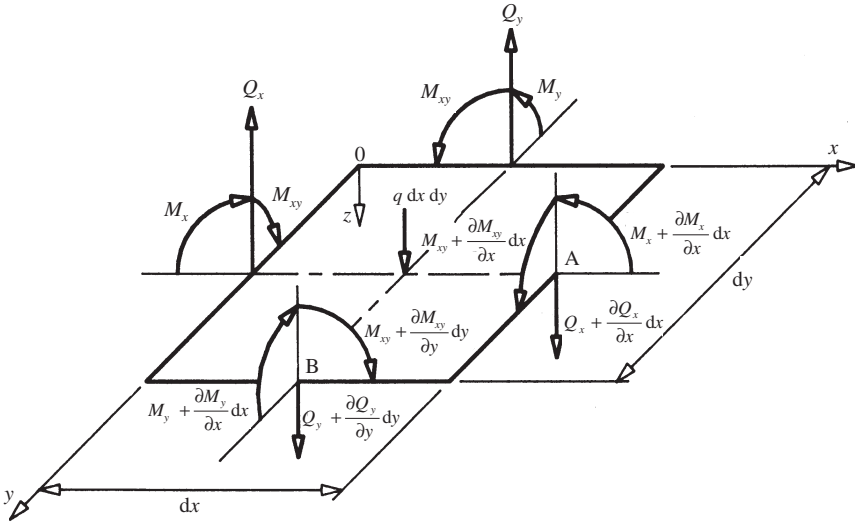


Fig. 3.9 Plate element

Displacements due to vertical shearing effects have been ignored above, since, for thin plates, these displacements are of a smaller order than the bending and twisting deformations. If the equilibrium of the plate is to be correctly represented, it is, however, necessary to include the vertical shear forces which, as with the moments, are measured per unit length of plate and are shown acting in their positive directions in Fig. 3.9.

The element of the plate middle surface shown in Fig. 3.9 is also presumed to be subjected to a normal loading of local intensity,  $q$ /unit area. The equilibrium equations for the plate element may be determined by

- (a) Taking moments about a line parallel to  $0y$  at A,

$$\begin{aligned} (Q_x \, dy) dx - (q \, dx \, dy) \frac{dx}{2} - \left( \frac{\partial M_x}{\partial x} dx \right) dy + \\ \left( \frac{\partial M_{xy}}{\partial y} dy \, dx \right) - \left( \frac{\partial Q_y}{\partial y} dy \, dx \right) \frac{dx}{2} = 0 \end{aligned}$$

or, neglecting lower-order terms and dividing by  $dx \, dy$ ,

$$Q_x = \frac{\partial M_x}{\partial x} - \frac{\partial M_{xy}}{\partial y} \quad (3.10)$$

- (b) Similarly, taking moments about a line parallel to  $0x$  at B,

$$Q_y = \frac{\partial M_y}{\partial x} - \frac{\partial M_{xy}}{\partial x} \quad (3.11)$$

(c) Resolving vertically,

$$(q \, dx \, dy) + \left( \frac{\partial Q_y}{\partial y} \, dy \right) dx + \left( \frac{\partial Q_x}{\partial x} \, dx \right) dy = 0$$

Whence

$$\frac{\partial Q_x}{\partial x} + \frac{\partial Q_y}{\partial y} = -q \quad (3.12)$$

To obtain the general equilibrium equation in terms of the plate moments, the vertical shear forces may be eliminated by substituting in equation (3.12) from equations (3.10) and (3.11) to give

$$\frac{\partial^2 M_x}{\partial x^2} - 2 \frac{\partial^2 M_{xy}}{\partial x \partial y} + \frac{\partial^2 M_y}{\partial y^2} = -q \quad (3.13)$$

### 3.3.6 General elastic plate equation

By substituting for the moments  $M_x$ ,  $M_y$  and  $M_{xy}$  from equations (3.7) in the equilibrium equation (3.13), the general elastic plate equation in terms of the displacement function  $w$  may be obtained as

$$-D \frac{\partial^4 w}{\partial x^4} - D\nu \frac{\partial^4 w}{\partial x^2 \partial y^2} - 2D(1-\nu) \frac{\partial^4 w}{\partial x^2 \partial y^2} - D \frac{\partial^4 w}{\partial y^4} - D\nu \frac{\partial^4 w}{\partial y^2 \partial x^2} = -q$$

or

$$\frac{\partial^4 w}{\partial x^4} + 2 \frac{\partial^4 w}{\partial x^2 \partial y^2} + \frac{\partial^4 w}{\partial y^4} = \frac{q}{D} \quad (3.14)$$

where  $D = Et^3/12(1 - \nu^2)$ . Equation (3.14) is of the *biharmonic* form, as was the stress function formulation of the plane stress problem (equation (1.22)). If a solution for the normal displacement function  $w$  can be found which satisfies both equation (3.14) and the relevant boundary conditions, then the stress resultants may be obtained from this displacement solution. The moments follow from equations (3.7), while the shear forces may be obtained from the moments by equations (3.10) and (3.11). Alternatively, the shear forces may be obtained directly from the displacement solution by substituting into equations (3.10) and (3.11) from equations (3.7) to give

$$Q_x = -D \left( \frac{\partial^3 w}{\partial x^3} + \frac{\partial^3 w}{\partial x \partial y^2} \right), \quad Q_y = -D \left( \frac{\partial^3 w}{\partial y^3} + \frac{\partial^3 w}{\partial x^2 \partial y} \right) \quad (3.15)$$

The stresses corresponding to the moment stress resultants may then be obtained from equations (3.9), while the vertical shear stresses due to the shear force stress resultants may be obtained by application of simple beam shear stress theory (Megson, 1996) as applied to a rectangular section of unit width. For a complete solution, it remains to obtain the reactions at the boundaries and, in the next section, the determination of the reactions is considered, together with consideration of the appropriate boundary conditions for various types of edge support.

### 3.3.7 Boundary conditions

The boundary conditions appropriate to three common forms of line support will be established below. For convenience, the support will be presumed, in each case, to lie along a line parallel to the  $y$ -axis but similar conditions may readily be derived for supports parallel to the  $x$ -axis and, by suitable resolution, for oblique axes (Ghali and Neville, 1997).

#### *Fixed (encastré) edge*

It is here presumed that there is no deflection at any point along the edge and nor is there any rotation of the plate about the support line. Thus, for a fixed edge parallel to the  $y$ -axis (Fig. 3.10), the two geometric boundary conditions may be expressed as

$$w = 0, \quad \frac{\partial w}{\partial x} = 0 \quad (3.16)$$

along the edge.

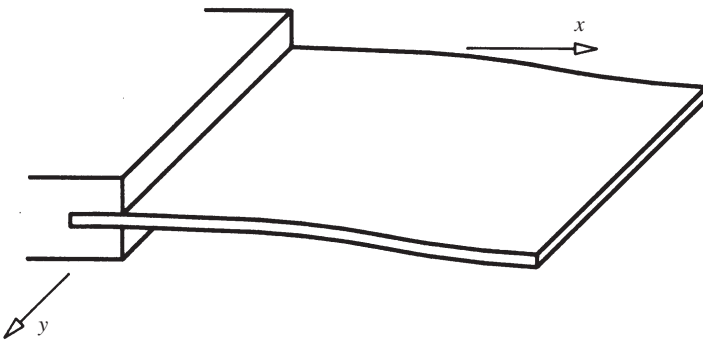


Fig. 3.10 Fixed-edge support

It may also be noted that  $w = 0$  along the support implies that

$$\frac{\partial w}{\partial y} = \frac{\partial^2 w}{\partial y^2} = 0$$

along the edge.

Also,  $\partial w / \partial x = 0$  at all boundary points implies that  $\partial^2 w / \partial x \partial y = 0$  along the edge.

The reactions provided by an edge along the  $y$ -axis would, in general, be required to balance  $M_x$ ,  $M_{xy}$  and  $Q_x$  along the edge. In the case of a fixed edge, the above geometric considerations result in

$$M_{xy} = D(1-\nu) \frac{\partial^2 w}{\partial x \partial y} = 0$$

Thus, the reactions required are

$$V_x = Q_x = -D \left[ \frac{\partial^3 w}{\partial x^3} + \frac{\partial}{\partial y} \left( \frac{\partial^2 w}{\partial x \partial y} \right) \right] = -D \frac{\partial^3 w}{\partial x^3} \quad (3.17)$$

where  $V_x$  is the force reaction (upwards positive) per unit length of support, and

$$R_x = M_x = -D \left( \frac{\partial^2 w}{\partial x^2} + \nu \frac{\partial^2 w}{\partial y^2} \right) = -D \frac{\partial^2 w}{\partial x^2} \quad (3.18)$$

where  $R_x$  is the moment reaction (signs as for  $M_x$ ) per unit length of support.

### Simply supported edge

Along such a support there is prevention of deflection but complete freedom of rotation about an axis along the support, which implies zero bending moment in a direction normal to the edge. Thus, for a simply supported edge along the  $y$ -axis (Fig. 3.11), the two boundary conditions are

$$w = 0, \quad M_x = 0 \quad (3.19)$$

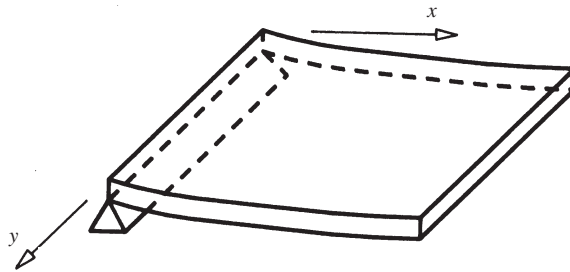


Fig. 3.11 Simply supported edge

As in the fixed-support case, the zero-displacement condition along the edge results in

$$\frac{\partial w}{\partial y} = \frac{\partial^2 w}{\partial y^2} = 0 \quad (3.20)$$

along the edge.

Also, the zero bending moment condition requires that

$$M_x = -D \left( \frac{\partial^2 w}{\partial x^2} + \nu \frac{\partial^2 w}{\partial y^2} \right) = 0 \quad \text{hence} \quad \frac{\partial^2 w}{\partial x^2} = 0 \quad (3.21)$$

and

$$M_y = -D \left( \nu \frac{\partial^2 w}{\partial x^2} + \frac{\partial^2 w}{\partial y^2} \right) = 0 \quad (3.22)$$

The twisting moment will not, in general, be zero along a simply supported boundary, since it is possible for the normal slope to vary along the boundary, so that, from equations (3.7) and (3.1),

$$M_{xy} = D(1-\nu) \frac{\partial^2 w}{\partial x \partial y} = D(1-\nu) \frac{\partial}{\partial y} (-\theta_x) \neq 0$$

Thus, the only non-zero stress resultants along the edge are  $Q_x$  and  $M_{xy}$  and these two effects must be equilibrated by a force reaction, since this is the only

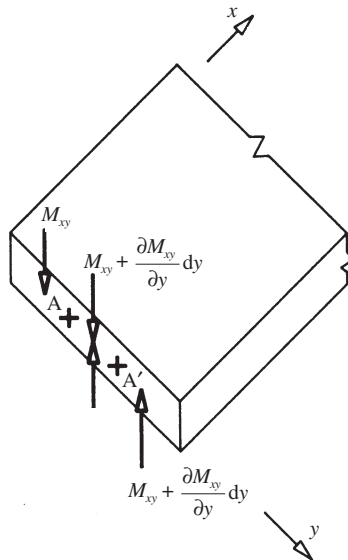


Fig. 3.12 Reaction due to twisting moment

type of reaction which can be provided by a simple support. The action of  $Q_x$  is straightforward, contributing directly to the support reaction. The effect of  $M_{xy}$  needs more careful consideration and may be assessed by considering two neighbouring boundary points, A and A' (Fig. 3.12), which are separated by a distance  $dy$ . The twisting moments at A and A' are taken to be, respectively,

$$M_{xy}, \quad M_{xy} + \frac{\partial M_{xy}}{\partial y} dy$$

These twisting moments may be represented by pairs of vertical forces as shown in Fig. 3.12, since, if the separation of the forces is also taken to be  $dy$ : due to forces  $M_{xy}$ ,

$$\text{twisting moment/unit length} = \frac{M_{xy} dy}{dy} = M_{xy}$$

Resolving vertically, it follows from Fig. 3.12 that the contribution to the reaction over the length AA' is  $-(\partial M_{xy}/\partial y)dy$  or, in terms of reaction/unit length,  $-(\partial M_{xy}/\partial y)$ . Thus, the distributed force reaction along the edge is given by

$$V_x = Q_x - \frac{\partial M_{xy}}{\partial y} \tag{3.23}$$

or, in terms of the displacement function, from equations (3.15) and (3.7),

$$\begin{aligned} V_x &= -D \left( \frac{\partial^3 w}{\partial x^3} + \frac{\partial^3 w}{\partial x \partial y^2} \right) - \frac{\partial}{\partial y} \left( D(1-\nu) \frac{\partial^2 w}{\partial x \partial y} \right) \\ &= -D \left( \frac{\partial^3 w}{\partial x^3} + (2-\nu) \frac{\partial^3 w}{\partial x \partial y^2} \right) \end{aligned} \tag{3.24}$$

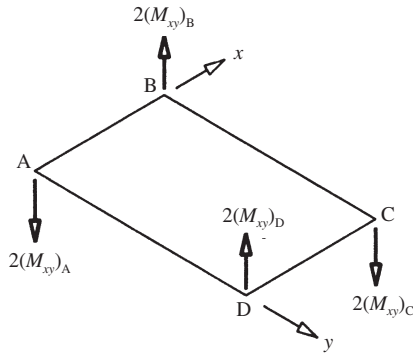


Fig. 3.13 Point reactions due to twisting moments

The distributed reaction given by equation (3.23) will correctly represent the reaction at all points along the edge except at its ends. At these points, the statically equivalent force representation of the twisting moment (Fig. 3.12) results in a single point force, which needs to be equilibrated by a point reaction at the end of the boundary. For twisting moments taken in the positive directions of Fig. 3.8, the corner reactions for a plate which is simply supported along all four edges will therefore be as shown in Fig. 3.13. For such a plate, the corner twisting moments, under symmetric downward load, would, in fact, be positive at corners A and C but negative at B and D. This leads to downward point reactions being required at each corner and substantiates the observed tendency of simply supported plates to curl upwards at corners which are not tied down.

### *Free edge*

An unsupported edge can provide neither a force reaction nor a moment reaction normal to the edge. For a free edge parallel to the  $y$ -axis, the two boundary conditions are, therefore,

$$V_x = 0, \quad M_x = 0$$

By using equations (3.24) and (3.7), the boundary conditions may be expressed geometrically as

$$\begin{aligned} \left( \frac{\partial^3 w}{\partial x^3} + (2 - \nu) \frac{\partial^3 w}{\partial x \partial y^2} \right) &= 0 \\ \left( \frac{\partial^2 w}{\partial x^2} + \nu \frac{\partial^2 w}{\partial y^2} \right) &= 0 \end{aligned} \tag{3.25}$$

### **3.3.8 Classical solutions to the plate problem**

As already noted in Chapter 1, the biharmonic form of partial differential equation is only soluble by the methods of classical calculus in reasonably regular cases. Solutions to the general plate equation (Timoshenko and Woinowsky-Krieger, 1981; Szilard, 1974) are hence only readily available for regular plate shapes (circular or rectangular) subjected to reasonably simple loadings and support conditions. For more complex loadings, use may be made of influence surfaces (Pucher, 1964) but such cases, and irregular plates generally, normally require the use of a numerical method. Both of the numerical approaches described in Chapters 1 and 2 (the finite element and finite difference methods) may be applied to the analysis of plates. Also, the analogy between slab and grid behaviour described above may be used to convert slab problems to grillage analyses. These three approaches are described below and an indication of their relative merits is given.



## 3.4 Finite difference method

### 3.4.1 Introduction

Using a square net of the form described in Appendix A, the requirements of the general plate equation (3.14) may be approximately fulfilled by the use of the biharmonic difference operator (Appendix A, Fig. A.5(c)). The intensity of loading ( $q$ ) which occurs on the right-hand side of the plate equation will be the actual intensity in the case of uniformly distributed loading or a statically equivalent intensity in other cases. Thus, for a point load  $Q$ , situated at 0 (Fig. A.3), the load intensity at 0 is taken to be  $Q/h^2$ . Application of the biharmonic difference operator to each uniquely numbered, non-zero grid point results in a set of equations equal in number to the number of unknown displacements. Before proceeding to the solution of these equations, however, the appropriate boundary conditions must be incorporated.

### 3.4.2 Boundary conditions

#### *Fixed boundary*

The required conditions (equations (3.16)) for fixity along a line parallel to the  $y$ -axis are

$$w = 0, \quad \frac{\partial w}{\partial x} = 0$$

along the edge.

The zero-deflection condition is easily satisfied, since it provides a solution for the unknown boundary displacement, and hence this zero value is assumed and the biharmonic difference operator is not applied to points along a fixed boundary. The zero-slope condition may be satisfied by extending the net one spacing beyond the edge to produce a set of 'fictitious' net points (Fig. 3.14), as already encountered in Section 2.3.2. The zero-slope requirement at a typical net point, say 2, may be expressed in finite difference form as

$$\left(\frac{\partial w}{\partial x}\right)_2 = \frac{w_6 - w_{6'}}{2h} = 0 \quad (3.26)$$

whence  $w_6 = w_{6'}$ . Thus, if the additional points are provided and their displacements are made equal to the displacements of their mirror image points in the boundary, the zero-slope condition will be satisfied.

#### *Simply supported boundary*

In this case the conditions to be enforced along an edge parallel to the  $y$ -axis may be expressed geometrically, from equations (3.19) and (3.21), as

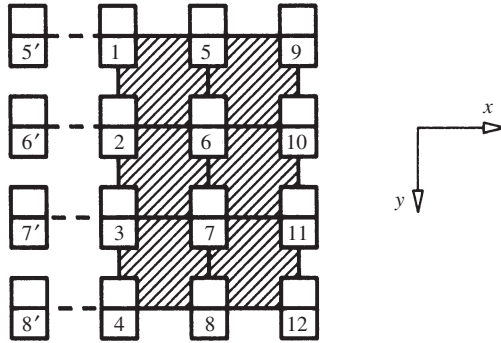


Fig. 3.14 Net at plate boundary

$$w = 0, \quad \chi_x = \frac{\partial^2 w}{\partial x^2} = 0 \quad (3.27)$$

along the edge.

The zero displacement condition is again treated by the assumption of zero boundary displacements, as in the fixed case. The curvature condition at, for example, point 2 (see Fig. 3.14), may be expressed in finite difference form, using equation (A.6), as

$$\left( \frac{\partial^2 w}{\partial x^2} \right)_2 = \frac{w_6 - 2w_2 + w_{6'}}{h^2} = 0 \quad (3.28)$$

whence  $w_6 = -w_{6'}$  since  $w_2 = 0$ .

Thus zero normal curvature is assured by making the displacement of an additional point equal in magnitude but opposite in direction to the displacement of its mirror image point.

### Free edge

Equations (3.25) provide the relevant geometric boundary conditions for a free edge parallel to the  $y$ -axis. In order to express the first of these equations in finite difference terms, it will be necessary to employ two additional points opposite each boundary point (see Fig. 3.17). Since the boundary is free to deflect, the biharmonic operator must be applied to the boundary points in this case. The additional points add two extra unknown displacements for each boundary point but this is compensated for by the fact that two boundary equations are also available.

### 3.4.3 Evaluation of moments and shear forces

Once the difference equations have been formed, they may be readily solved by computer to yield the displacements at the net points. The displacements so obtained may then be utilized to determine the moments and, if desired, the shears at the net points from equations (3.7) and (3.15). The differential expressions occurring in these equations are evaluated by applying the appropriate difference operators to the known set of displacements.

### 3.4.4 Examples

#### Example 3.1 – simply supported slab

The slab to be considered (Fig. 3.15) is square, of side  $L$ , supports a uniform load of intensity  $q$  over a central square of side  $L/2$ , and is simply supported along all four edges. The flexural rigidity is taken to be a constant,  $D$ , while Poisson's ratio is presumed to be zero. The net used is of side  $L/4$  and advantage of symmetry may be taken to reduce the number of unknown displacements to three (Fig. 3.15). Following the conventions of Section A.2, the boundary points are given the reference number zero to indicate their zero displacement, while the additional points outside the edges are given reference numbers opposite in sign to that of their mirror image points to signify the

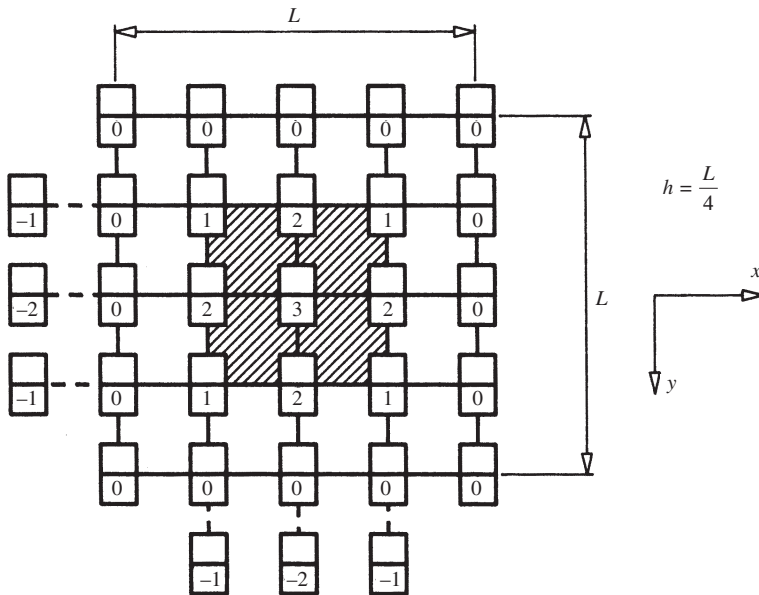


Fig. 3.15 Simply supported slab example

presence of the curvature boundary condition (equation (3.28)). The load intensity appropriate to point 3 is clearly  $q$ , that for point 2 must be taken as  $q/2$ , while that for 1 should be  $q/4$  if the total load on a square of side  $h$ , about the point considered, is to equal the load applied to such a square. Application of the biharmonic difference operator (Fig. A.5(c)) to the points 1, 2 and 3 yields the following simultaneous equations:

$$\frac{1}{h^4} \begin{bmatrix} 20 & -16 & 2 \\ -16 & 24 & -8 \\ 8 & -32 & 20 \end{bmatrix} \begin{Bmatrix} w_1 \\ w_2 \\ w_3 \end{Bmatrix} = \begin{Bmatrix} 0.25 \\ 0.50 \\ 1.00 \end{Bmatrix} \frac{q}{D} \quad (3.29)$$

Solving equations (3.29) gives

$$\{w\}^T = \{w_1, w_2, w_3\} = \{0.00101, 0.00146, 0.00214\} \frac{qL^4}{D} \quad (3.30)$$

Moments, shears and reactions may now be evaluated at the net points. For example, with reference to Fig. 3.15:

At point 2, using the difference approximation of equation (A.6): since  $\nu = 0$ ,

$$\begin{aligned} M_{x2} &= -D \left( \frac{\partial^2 w}{\partial x^2} \right)_2 = -D \frac{w_3 - 2w_2}{h^2} \\ &= -(0.00214 - 2 \times 0.00146) 16qL^2 = 0.013qL^2 \end{aligned}$$

At the lower left-hand point 1, using the difference operator of Fig. A.5(b): since  $\nu = 0$ ,

$$M_{xy1} = D \left( \frac{\partial^2 w}{\partial x \partial y} \right)_1 = D \frac{-w_3}{4h^2} = -0.0086qL^2$$

An exact solution is available for this particular example, and the results of the finite difference solution are compared with the exact values in Fig. 3.16. It may be seen that the agreement is good except in respect of twisting moments and shear forces. Displacements and moments in the slab follow the expected pattern, being greatest at the centre and small at points close to the boundary. In contrast, the twisting moment distribution shows that maximum twist occurs at the corners of the slab, while the centre-lines have zero twist. The zero twist along the centre-lines arises from these being lines of symmetry, in the present case, along which there is zero transverse slope and, hence, no rate of change of this slope which would represent a twisting effect (equation (3.8)). Along a boundary line such as AA (Fig. 3.16), however, the transverse slope varies from zero at the slab corner to a maximum at the slab centre-line, the greatest rate of change being at the corner. This distribution of twisting moments explains why codes of practice normally require corner torsional reinforcement in simply supported slabs.

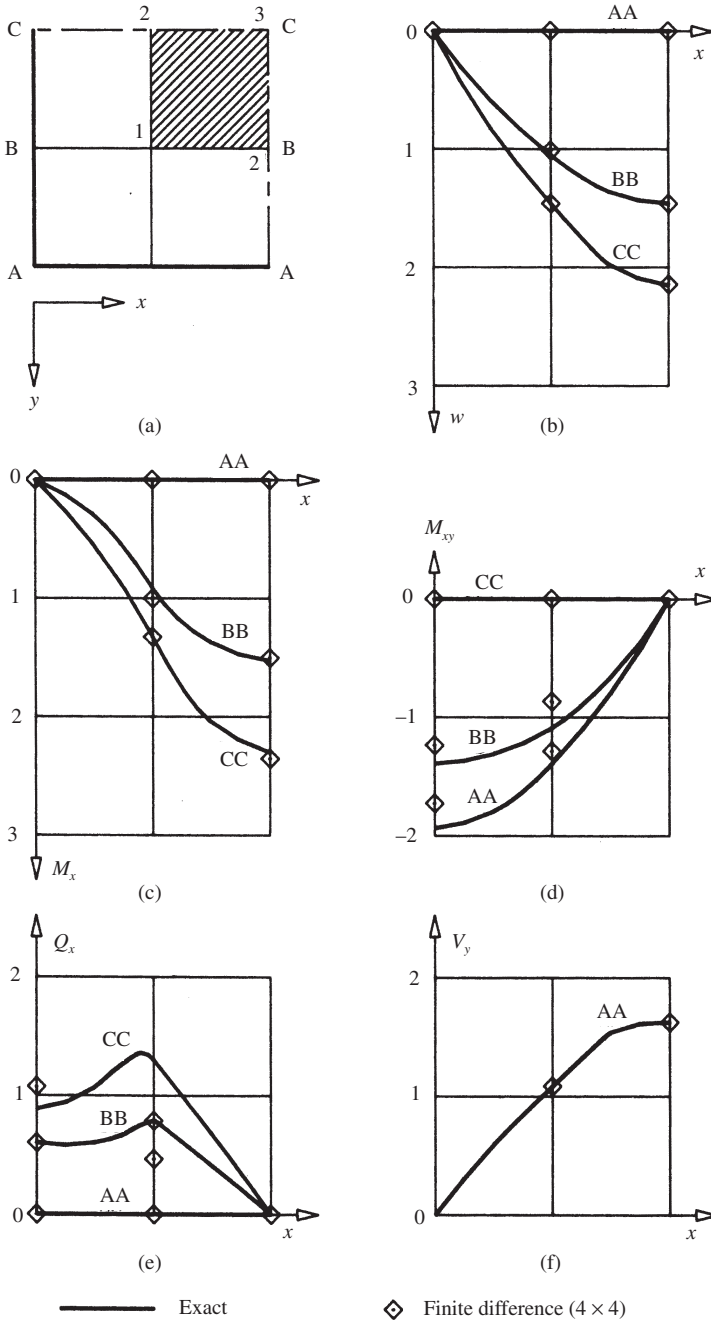


Fig. 3.16 Simply supported slab analysis: (a) reference plan of quarter slab; (b)  $w$  ( $\times 10^{-3}qL^4/D$ ); (c)  $M_x$  ( $\times 10^{-2}qL^2$ ); (d)  $M_{xy}$  ( $\times 10^{-2}qL^2$ ); (e)  $Q_x$  ( $\times 10^{-1}qL$ ); (f)  $V_y$  ( $\times 10^{-1}qL$ )

Shear forces are not usually of importance in slab design but have been included in Fig. 3.16 for completeness. The distribution approximates to that which experience of beam behaviour might suggest, namely that the shear is reasonably constant over the unloaded region of the slab and then decreases uniformly over the loaded region. One interesting feature of the exact distribution is that the maximum shear force does not occur at the boundary. The explanation for this is that the high torsional effects in the vicinity of the boundary result in a rather reduced rate of increase in bending moment in these areas, with consequently somewhat reduced shear forces. The rate of moment increase (Fig. 3.16(c)) then accelerates somewhat around the slab quarter points, giving rise to maximal shear forces at these locations. The reaction distribution (Fig. 3.16(f)) shows that the majority of the load is supported by the central region of the slab, while the corner twisting moments require the downward corner point reactions mentioned earlier if the slab corners are not to rise under load.

### Example 3.2 – fixed-edge slab

The same slab is now considered with fixed edges. The only alteration required to Fig. 3.15 is to change the signs of the additional net points in order that the new boundary condition (equation (3.26)) be observed. If this is done, then application of the biharmonic operator (Fig. A.5(c)) to points 1, 2 and 3 results in the equations

$$\frac{1}{h^4} \begin{bmatrix} 24 & -16 & 2 \\ -16 & 26 & -8 \\ 8 & -32 & 20 \end{bmatrix} \begin{Bmatrix} w_1 \\ w_2 \\ w_3 \end{Bmatrix} = \begin{Bmatrix} 0.25 \\ 0.50 \\ 1.00 \end{Bmatrix} \frac{q}{D} \quad (3.31)$$

The solution to equations (3.31) is

$$\{w\}^T = \{w_1, w_2, w_3\} = \{0.00037, 0.00063, 0.00105\} \frac{qL^4}{D}$$

Table 3.1 Comparative displacement solutions

	$w (\times 10^{-5} qL^4/D)$			
	Fixed		Simple	
Net point	$4 \times 4$	$8 \times 8$	$4 \times 4$	$8 \times 8$
1	37	29	101	101
2	63	52	146	147
3	105	91	214	213

An exact solution is not so easily obtained in the case of clamped edges. In such cases, numerical solutions are normally verified by proceeding to a finer net, the solution being presumed converged if the coarser and finer solutions are in agreement. The results of the above  $4 \times 4$  net are therefore compared with those from an  $8 \times 8$  net in Table 3.1.

Clearly, the solution obtained above is not close to the converged solution in the fixed-edge case. The comparison values presented for the simply supported case indicate that the converged position has essentially been obtained in the  $4 \times 4$  case, as indeed has already been established by correlation with the exact solution. In its present form then, the finite difference solution does not represent fixed edges accurately. Two remedies are available, either to insist on fine nets whenever fixed edges are treated, or to utilize more accurate difference operators (Cope and Clark, 1984) in such cases.

*Example 3.3 – slab with free edges*

The same slab will now be treated with the sides parallel to the  $y$ -axis being unsupported, while those parallel to the  $x$ -axis are simply supported. The net

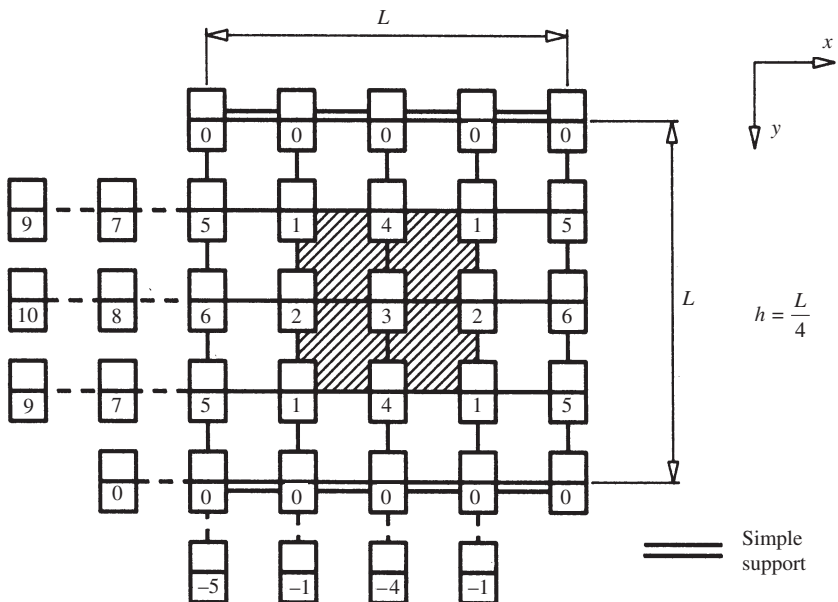


Fig. 3.17 Slab with free edges

for a  $4 \times 4$  solution then becomes as shown in Fig. 3.17, and the required difference equations are given as

$$\begin{bmatrix} 21 & -8 & 2 & -8 & -8 & 2 & 1 & 0 & 0 & 0 \\ -16 & 21 & -8 & 4 & 4 & -8 & 0 & 1 & 0 & 0 \\ 8 & -16 & 20 & -16 & 0 & 2 & 0 & 0 & 0 & 0 \\ -16 & 4 & -8 & 20 & 2 & 0 & 0 & 0 & 0 & 0 \\ -8 & 2 & 0 & 1 & 20 & -8 & -8 & 2 & 1 & 0 \\ 4 & -8 & 1 & 0 & -16 & 20 & 4 & -8 & 0 & 1 \\ 1 & 0 & 0 & 0 & -2 & 0 & 1 & 0 & 0 & 0 \\ 0 & 1 & 0 & 0 & 0 & -2 & 0 & 1 & 0 & 0 \\ -6 & 2 & 0 & 1 & 0 & 0 & 6 & -2 & -1 & 0 \\ 4 & -6 & 1 & 0 & 0 & 0 & -4 & 6 & 0 & -1 \end{bmatrix} \{w\} = \begin{bmatrix} 0.25 \\ 0.50 \\ 1.00 \\ 0.50 \\ 0 \\ 0 \\ 0 \\ 0 \\ 0 \\ 0 \end{bmatrix} \frac{qh^4}{D} \quad (3.32)$$

The first six of equations (3.32) represent the application of the biharmonic difference operator to slab points 1–6. The seventh and eighth equations represent the zero bending moment condition at the free edge points 5 and 6 and are based on a difference approximation to the second of equations (3.25) using the stipulated zero value of Poisson's ratio. The final two equations occur due to the zero force boundary condition (the first of equations (3.25)) and are formed, in the zero Poisson's ratio case, by the application of the operator of Fig. A.6(a) at points 5 and 6. A computer solution to equations (3.32) provides the displacements:

$$\{w\}^T = \{345, 493, 524, 366, 311, 443, 278, 393, 160, 194\} \times 10^{-5} \frac{qL^4}{D}$$

On proceeding to a finer net, the comparable results are as shown in Table 3.2. As in the simply supported case, the  $4 \times 4$  and  $8 \times 8$  solutions are in good agreement and it may be concluded that a fixed-edge support presents the greatest difficulty for a finite difference solution.

Table 3.2 Comparative displacements

$w (\times 10^{-5} qL^4/D)$	Net point					
	1	2	3	4	5	6
$4 \times 4$	345	493	524	366	311	443
$8 \times 8$	332	474	503	353	298	422



### 3.4.5 Extensions and refinements

Orthotropic plates, for which the stiffness is different in two perpendicular directions, may be investigated by use of the appropriate differential equation (Timoshenko and Woinowsky-Krieger, 1981). More complex boundary conditions than the ones covered above are encountered at curved boundaries and at free internal or external corners (Wood, 1961). Oblique or triangular nets (Fig. A.2) are particularly convenient in the case of skew slabs (Morley, 1963). Incorporation of the interaction of slabs with other structural elements, edge beams for example, is not particularly straightforward but has been considered in fairly simple cases (Wood, 1961).

## 3.5 Grid representation method

Grillages are readily analysed elastically by the stiffness method (Ghali and Neville, 1997) and most structural computer packages, based on this approach, possess sub-systems which can analyse grids of essentially any size or complexity. The similarity of grid and plate behaviour has already been utilized in describing general plate response (see Section 3.2) and it is reasonable to enquire as to whether plates may be analysed by standard grillage computer programs. In fact, such a representation is particularly easy to formulate in the case of a slab (zero Poisson's ratio), and the presentation given here will be restricted to such a case.

### 3.5.1 Grid properties

It will be assumed that the slab is to be represented by a rectangular grid of members, which are shown with uniform spacings,  $a$  and  $b$ , in Fig. 3.18, although this is not essential. It has been emphasized above that slab action is

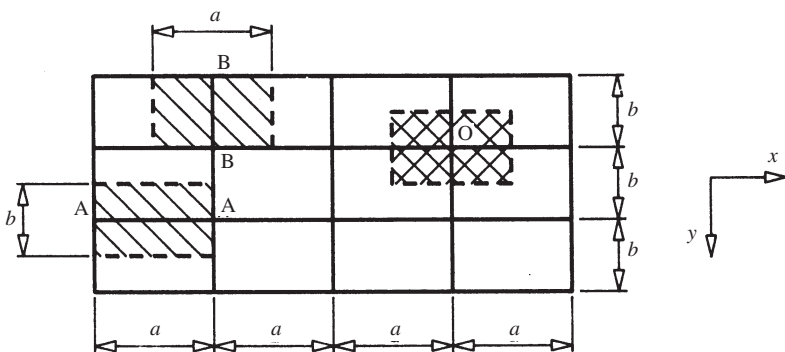


Fig. 3.18 Grid representations

characterized by bending in the  $x$ - and  $y$ -directions, accompanied by twisting about both of these directions. The object of a grid representation is to make the grid members simulate the bending and twisting action of their surrounding slab strips in either the  $x$ - or the  $y$ -direction, as appropriate. Thus, member AA (Fig. 3.18), for example, must represent the  $x$ -direction bending and twisting for the shaded part of the slab, while BB will perform the same function in the  $y$ -direction for its shaded part. The relevant differential equations for slab bending and twisting in the  $x$ -direction may be obtained by setting Poisson's ratio to zero in the first and third of equations (3.7) to give

$$M_x = -D \frac{\partial^2 w}{\partial x^2} = -\frac{Et^3}{12} \frac{\partial^2 w}{\partial x^2} \quad (3.33)$$

$$M_{xy} = D \frac{\partial^2 w}{\partial x \partial y} = \frac{Gt^3}{6} \frac{\partial^2 w}{\partial x \partial y} \quad (3.34)$$

where  $G = E/2$  for  $\nu = 0$  (equation (1.7)).

Since  $M_x$  and  $M_{xy}$  are moments/unit width, the total moments sustained by the shaded strip, AA, of Fig. 3.18 are

$$M'_x = bM_x = -\frac{Ebt^3}{12} \frac{\partial^2 w}{\partial x^2} \quad (3.35)$$

$$M'_{xy} = bM_{xy} = \frac{Gbt^3}{6} \frac{\partial^2 w}{\partial x \partial y} \quad (3.36)$$

The differential equations relating to the behaviour of a grid member in the  $x$ -direction are those of beam bending (Megson, 1996) and elastic torsion (equation (2.2)):

$$M'_x = -EI \frac{\partial^2 w}{\partial x^2} \quad (3.37)$$

$$M'_{xy} = GJ\theta' = GJ \frac{\partial}{\partial x} (\theta_x) = GJ \frac{\partial^2 w}{\partial x \partial y} \quad (3.38)$$

If equations (3.37) and (3.38) are to correctly represent equations (3.35) and (3.36), then

$$I = \frac{bt^3}{12}, \quad J = \frac{bt^3}{6} \quad (3.39)$$

The bending constant,  $I$ , given by equation (3.39) will be recognized as that appropriate to a rectangular section of width  $b$  and depth  $t$ . The suggested torsion constant,  $J$ , is not so readily interpreted, since a rectangular section of width  $b$  and depth  $t$  (small in comparison to  $b$ ) has already been shown (Table 2.5) to be twice the value given by equation (3.39). This factor of two arises due to the different twist responses of an isolated rectangular section



Fig. 3.19 Torsional shear flows

and a rectangular section which forms part of a continuous slab. In the isolated case, the shear flow due to torsion is continuous around the section (Fig. 3.19(a)), while, as shown above (see Section 3.3.3), the shear stresses due to twisting within a slab are parallel to the slab middle surface (Fig. 3.19(b)). It has already been shown (equation (2.17) *et seq.*) that the vertical shear stresses in the isolated section case contribute one half of the total torsion resistance, which accounts for the reduced torsional stiffness of the slab element.

On the basis of equations (3.39), the required properties of all the members involved in the grid representation of Fig. 3.18 may now be readily established as:

For interior  $x$ -direction members:

$$I = \frac{bt^3}{12}, \quad J = \frac{bt^3}{6} \quad (3.40a)$$

For edge  $x$ -direction members:

$$I = \frac{bt^3}{24}, \quad J = \frac{bt^3}{12} \quad (3.40b)$$

For interior  $y$ -direction members:

$$I = \frac{at^3}{12}, \quad J = \frac{at^3}{6} \quad (3.40c)$$

For edge  $y$ -direction members:

$$I = \frac{at^3}{24}, \quad J = \frac{at^3}{12} \quad (3.40d)$$

### 3.5.2 Boundary conditions

Boundary conditions present little difficulty with this approach. Joints along a free edge are simply left unrestrained. Joints along a fixed edge are fully restrained against  $z$ -direction translation and against rotation about both the  $x$ - and  $y$ -axes. This treatment results in the edge members becoming inoperative, and they may be omitted from the analysis if so desired.

Simply supported edges require a little more care. Clearly, joint displacements along a simply supported edge must be prevented and there must be no restraint against rotation about the line of support. The difficulty concerns rotation about an axis perpendicular to the edge. Geometrically, there should be no rotation about such an axis and yet, if rotation is prevented, there are no bending moments in the edge members and hence no shear forces. The absence of shear forces in the edge members results in the inability of the grid to accurately represent the reaction distribution along the support. Thus, geometry requires no rotation about an axis perpendicular to the edge, and yet a satisfactory reaction distribution may only be obtained if such rotations are allowed. These conflicting requirements may be compromised by allowing the rotation but giving the edge members a high bending stiffness and so ensuring that the rotations incurred are small. No alteration should be made to the torsional stiffness of the edge members.

### 3.5.3 Load representation

Loads may be allocated to either the grid members, or to the joints, or to a combination of both members and joints. The allocation of the load is usually based on simple statical principles. In the examples treated below, the loading is allocated to the joints only, and, for comparison with the finite difference method, the apportionment is based on the principles which were used in connection with that method. Thus, for a given joint O (Fig. 3.18), any loads acting within the surrounding shaded rectangle of dimensions  $axb$  are allocated to O. If the shaded area were subjected to a uniformly distributed load of intensity,  $q$ , for example, then an equivalent point load of  $(qab)$  would be applied to O.

### 3.5.4 Evaluation of moments and shear forces

Once the grid has been analysed, slab moments and shears may be evaluated directly from the computer analysis. The results presented will consist of joint displacements and rotations, member shears, bending moments and torques, and joint reactions. The member forces will not be in terms of force/unit length but will be a total force appropriate to the corresponding slab strip. This being the case, it is desirable to express all moments and forces in unit width terms before proceeding further. The reduction to unit length terms is readily achieved by relationships such as

$$M_x = \frac{M'_x}{b}, \quad M_y = \frac{M'_y}{a} \quad (3.41)$$

where the prime signifies a value from the computer analysis.

The slab internal forces may then be obtained by averaging the appropriate reduced forces at the joint considered. For example, at O in Fig. 3.18, two values of  $M_x$  will be available, one from the grid member to the left of O and one from that to the right. The average of these two values will represent the slab value of  $M_x$  at O. Similarly, the values of  $M_y$ ,  $Q_x$  and  $Q_y$  at O may be established. There is only one value of slab twisting moment at O, since the twisting moments in the  $x$ - and  $y$ -directions are complementary; thus  $M_{xy}$  is obtained as the mean of the torques in all the four members meeting at O. This averaging process is of considerable importance, as the individual values may be a poor approximation, but the means will generally give a good representation of the slab behaviour.

### 3.5.5 Evaluation of reactions

Reactions at the boundary points may be obtained from the computed joint reactions by reducing these values to unit length terms. Some difficulty is experienced in the case of a corner force reaction, since the analysis value will incorporate any point corner reaction with a contribution from the distributed reaction over a length  $(a + b)/2$  (presuming that support is provided in both the  $x$ - and  $y$ -directions). These two constituents may be separated by evaluating the corner twisting moment, as described in the previous section, which then provides the value of the point reaction (Fig. 3.13). The point reaction is then subtracted from the analysis reaction to leave the distributed reaction component.

### 3.5.6 Examples

#### Example 3.4 – fixed-edge slab

The slab considered previously (example 3.2) is now analysed by the grid representation method. Due to symmetry, only a quarter of the slab need be analysed, and the member arrangement for a  $4 \times 4$  analysis is as shown in Fig. 3.20. The required member properties are:

For 3–6, 6–9, 7–8, 8–9:

$$I = \frac{L}{8} \frac{t^3}{12} = \frac{Lt^3}{96}, \quad J = \frac{L}{8} \frac{t^3}{6} = \frac{Lt^3}{48}$$

For 4–5, 5–6, 2–5, 5–8:

$$I = \frac{L}{4} \frac{t^3}{12} = \frac{Lt^3}{48}, \quad J = \frac{L}{4} \frac{t^3}{6} = \frac{Lt^3}{24}$$

Members 1–2, 2–3, 1–4, 4–7 are not needed, and  $G = 0.5E$  for all members.

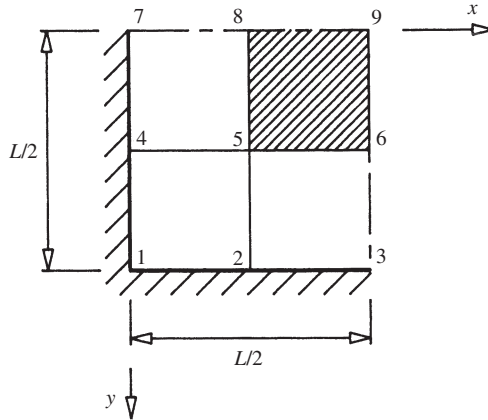


Fig. 3.20 Fixed-edge slab

It should be noted in the above that the use of symmetry results in a halving of the tributary slab areas applicable to the members along the slab centre-lines, and hence a halving of their member properties. To completely model the symmetry condition, it is also necessary to enforce the requirement that the slope normal to any line of symmetry be zero. If these restraint requirements are combined with the restraints due to the fixed edges, the full set of joint restraints becomes:

At 1, 2, 3, 4, 7: no  $z$ -displacement; no rotation about  $x$ - or  $y$ -axis (fixed-edge condition)

At 8: no rotation about  $x$ -axis (symmetry condition)

At 6: no rotation about  $y$ -axis (symmetry condition)

At 9: no rotation about  $x$ - or  $y$ -axis (symmetry conditions).

Using the load allocation procedure described above, the required joint loads at 5, 6, 8 and 9 are equal point loads of  $qL^2/64$ . These equal loads contrast with the dissimilar load intensities applied in the finite difference analysis (equations (3.31)). The reason for this lies in the differing treatments of symmetry employed by the two methods. The grid representation essentially discards three-quarters of the slab, together with the loading applied to this part of the structure. The effect of this discarded portion on the quarter that is analysed is then represented by the enforcement of the symmetry restraints which were detailed above. In the finite difference approach, however, the complete slab is considered (Fig. 3.15) but the selected system of nodal numbering reflects the symmetrical displacement of the slab and thereby reduces the size of the analysis. The results of a computer analysis based on the above grid representation are given in Fig. 3.21, where they are compared with an  $8 \times 8$  analysis

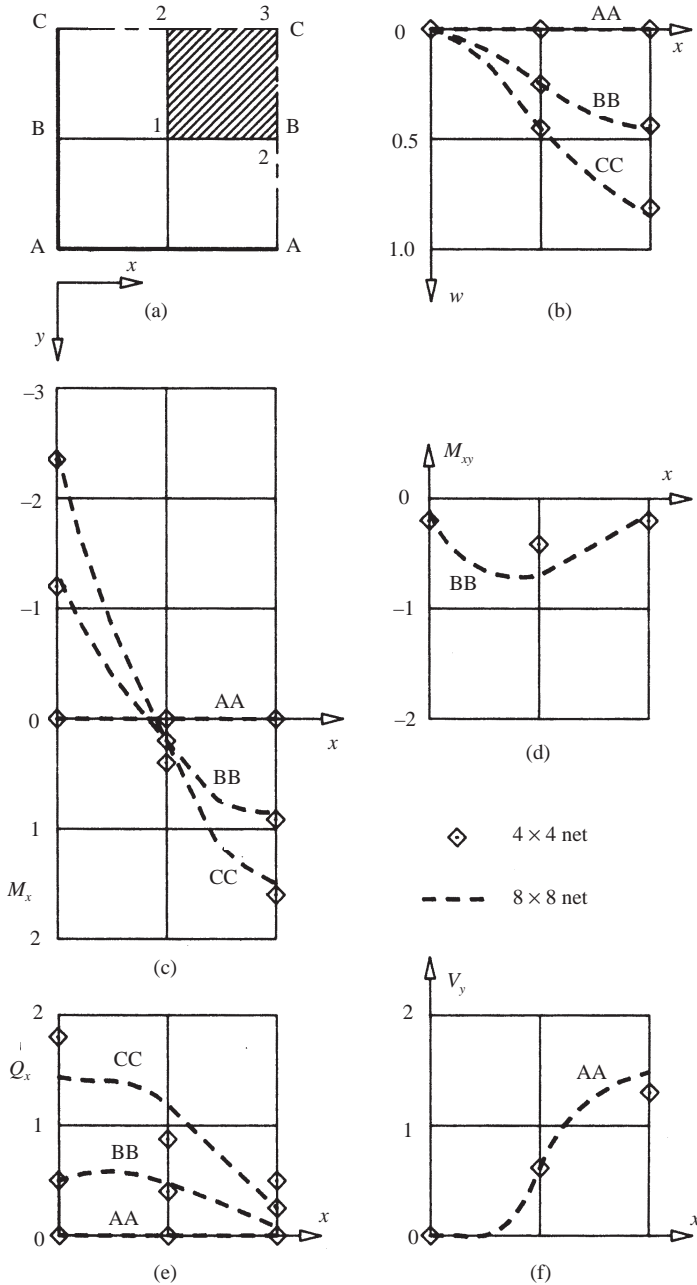


Fig. 3.21 Fixed-edge slab: (a) reference plan of quarter slab; (b)  $w$  ( $\times 10^{-3}qL^4/D$ ); (c)  $M_x$  ( $\times 10^{-2}qL^2$ ); (d)  $M_{xy}$  ( $\times 10^{-2}qL^2$ ); (e)  $Q_x$  ( $\times 10^{-1}qL$ ); (f)  $V_y$  ( $\times 10^{-1}qL$ )

by the same method. It may be observed that the agreement is good in respect of displacements and bending moments, but is much less satisfactory in respect of twisting moments, shear forces and reactions. The latter variables are, in fact, the most difficult to model by any numerical method. It may also be noted that there should be zero shear force (Fig. 3.21) along the line of symmetry CA (Fig. 3.21(a)) but this condition is rather poorly represented by the analyses, particularly the coarser one.

The displacement and moment distributions, as would be anticipated, show maximum hogging curvature and moment at the fixed supports and maximum sagging curvature and moment at the centre of the slab. The distributions also indicate that the central slab strips sustain most of the load, there being little bending towards the corners of the slab.

The twisting moment distribution (Fig. 3.21(d)) is rather different from the simply supported slab example (Fig. 3.16(d)), with which it may be contrasted. No twisting moment can exist along the lines of symmetry, CA and CC, or along the fixed edges, since there is no change of transverse slope along such lines. The analyses do not represent these conditions particularly well (Fig. 3.21(d)) but do show that the maximum twisting moment occurs around the slab quarter point, with smaller twisting moments in the regions of the centre-lines and the supports. It may be noted that the magnitude of the maximum twisting moment occurring in the fixed case is only about one-third that of the simply supported maximum; thus, twisting moments are of less concern in continuous slabs than in simply supported ones.

The shear force and reaction distributions are somewhat similar in form to those encountered in the simply supported case. No corner point reactions are present in the fixed case, however, due to the absence of boundary twisting moments. The reaction distribution confirms the earlier suggestion that the majority of the load is carried by the central slab strips.

### *Example 3.5 – slab with free edges*

The same slab will be analysed with the edges parallel to the  $y$ -axis being unsupported (Fig. 3.22) while those parallel to the  $x$ -axis are simply supported. Making use of symmetry, as before, the required member properties are:

For 1–4, 4–7, 3–6, 6–9, 7–8, 8–9:

$$I = \frac{L}{8} \frac{t^3}{12} = \frac{Lt^3}{96}, \quad J = \frac{L}{8} \frac{t^3}{6} = \frac{Lt^3}{48}$$

For 4–5, 5–6, 2–5, 5–8:

$$I = \frac{L}{4} \frac{t^3}{12} = \frac{Lt^3}{48}, \quad J = \frac{L}{4} \frac{t^3}{6} = \frac{Lt^3}{24}$$

For 1–2, 2–3:



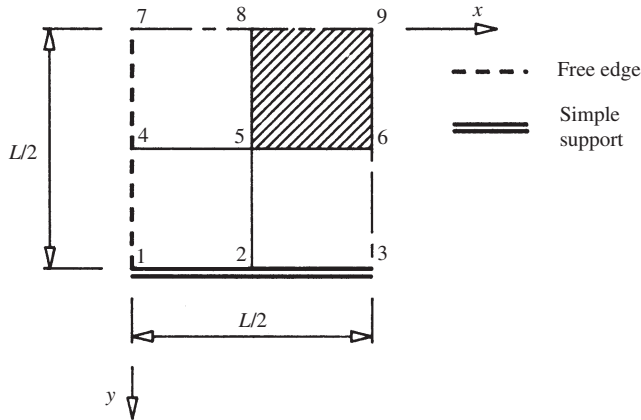


Fig. 3.22 Slab with free edges

$$I = 100 \frac{L t^3}{8 \cdot 12} = \frac{100}{96} L t^3, \quad J = \frac{L t^3}{8 \cdot 6} = \frac{L t^3}{48}$$

The  $I$  values of the members along the simple support have been increased by a nominal multiple of 100 (Section 3.5.2) and  $G = 0.5E$  for all members.

The required joint restraints are:

- At 1, 2: no  $z$ -displacement
- At 3: no  $z$ -displacement, no rotation about  $y$ -axis (symmetry condition)
- At 6: no rotation about  $y$ -axis (symmetry condition)
- At 7, 8: no rotation about  $x$ -axis (symmetry condition)
- At 9: no rotation about  $x$ - or  $y$ -axis (symmetry conditions).

The loading arrangements remain the same as in the previous example, namely vertical point loads of magnitude  $qL^2/64$  will be applied to joints 5, 6, 8 and 9. Computer results from a  $4 \times 4$  analysis based on the above representation are compared with values from an  $8 \times 8$  grid analysis in Fig. 3.23 and show satisfactory agreement. The bending moment and deflection distributions indicate that essentially ‘one-way’ bending occurs. The slab behaviour approximates to that of a simply supported beam having the same width and depth as the slab and loaded with a uniformly distributed load of intensity  $(qL/2)$ /unit length over its central half-length. Such an approximation would result in a maximum bending moment of  $0.047qL^2$ , which may be compared with the value of  $0.051qL^2$  given by the  $8 \times 8$  grid representation.

The beam-type behaviour results in the twisting and transverse moments being small in comparison with the longitudinal moments. In respect of transverse moments, it may be noted that the analyses indicate small hogging moments close to the free edges where the unloaded longitudinal strips give considerable support to the transverse strips.

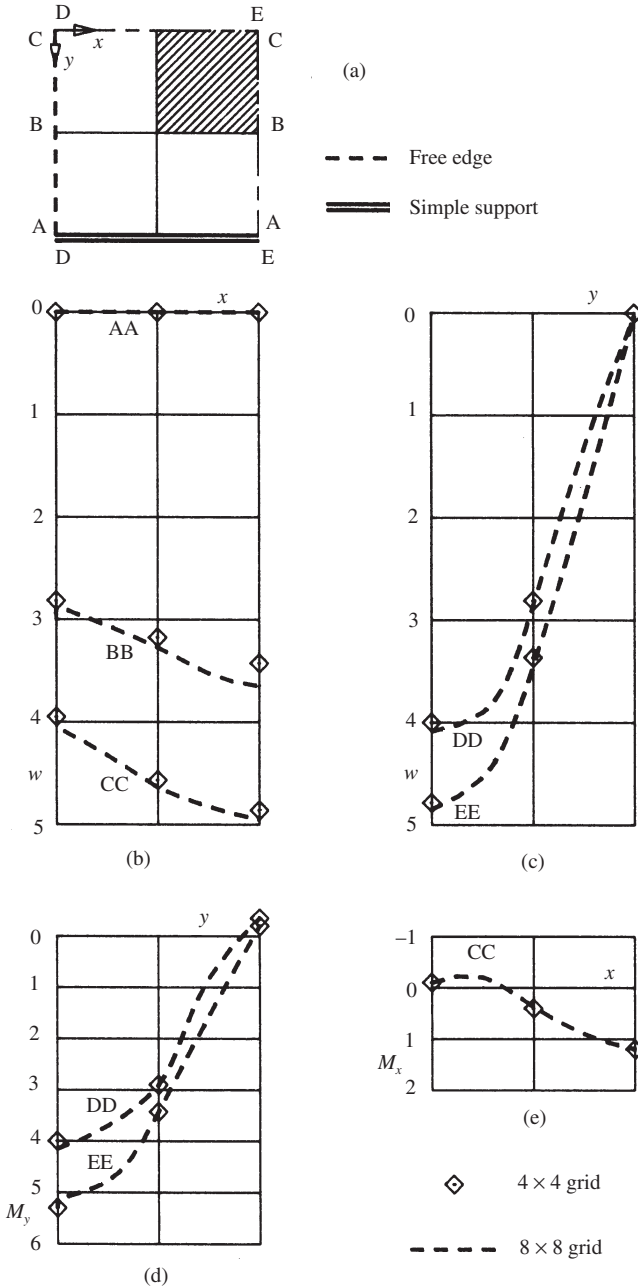


Fig. 3.23 Slab with free edges: (a) reference plan for quarter slab; (b)  $w$  ( $\times 10^{-3} qL^4/D$ ); (c)  $w$  ( $\times 10^{-3} qL^4/D$ ); (d)  $M_y$  ( $\times 10^{-2} qL^2$ ); (e)  $M_x$  ( $\times 10^{-2} qL^2$ )

### 3.5.7 Extensions and refinements

Non-zero Poisson's ratio causes some difficulty with this approach, since, as discussed already, grids do not naturally model the Poisson's ratio effect. Thus, although suitable grid models have been suggested for plate analysis with non-zero Poisson's ratio, the finite difference or finite element methods are generally more convenient. Variation in slab thickness causes no real problems, since suitable adjustments to the member properties may be readily effected. Orthotropy may, similarly, be treated by adjustment of the member properties, and one of the main applications of this method has been to orthotropic bridge decks (Hambly, 1998).

Non-linear boundaries are not readily modelled on the basis presented here and, again, although triangular grid models have been proposed, other methods are usually to be preferred, except in the case of curved-bridge decks, where curved-beam theory can be effectively employed. Interaction effects with beams, stiffeners, columns and similar line elements are easily catered for by simply incorporating these members in the analysis. If columns are introduced, then a space frame rather than a grid analysis program will, of course, be required.

## 3.6 Finite element method

### 3.6.1 Rectangular element theory

For plate bending, the finite element method is most readily formulated for a rectangular element (Fig. 3.24(a)). Although the deformation of a plate may be uniquely represented in terms of the normal displacement variable,  $w$ , alone, a more effective representation is achieved if the dependent  $x$ - and  $y$ -axis rotations are also included in the formulation, so that the displacement of a general point, P, will be given by

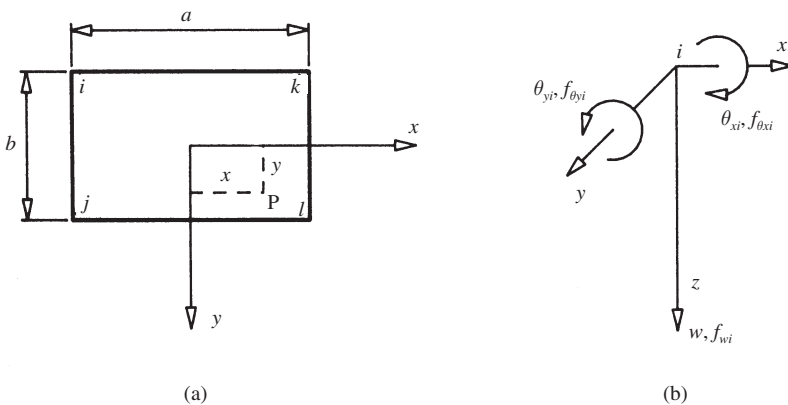


Fig. 3.24 (a) Rectangular plate bending element. (b) Nodal displacements and forces

$$\{\delta\} = \begin{Bmatrix} w \\ \theta_x \\ \theta_y \end{Bmatrix} = \begin{Bmatrix} w \\ \frac{\partial w}{\partial y} \\ -\frac{\partial w}{\partial x} \end{Bmatrix} \quad (3.42)$$

There are thus three displacement ‘components’ to be considered at each point of the element and, in particular, since there are four nodes, a total of 12 nodal displacements will be involved. It follows that the polynomial displacement function should have a total of 12 terms. Unlike the triangular plane stress element, the displacement components are not independent of each other and it will therefore be sufficient for the normal displacement variable alone to be represented by the polynomial function, since the rotational displacements may then be determined from the final two of equations (3.42). A suitable polynomial representation for the normal displacement variable is

$$w = \alpha_1 + \alpha_2 x + \alpha_3 y + \alpha_4 x^2 + \alpha_5 xy + \alpha_6 y^2 + \alpha_7 x^2 + \alpha_8 x^2 y + \alpha_9 xy^2 + \alpha_{10} y^3 + \alpha_{11} x^3 y + \alpha_{12} xy^3 \quad (3.43)$$

The polynomial representation of equation (3.43) includes a full cubic function which comprises ten terms, so only two fourth-order terms may be incorporated. The chosen two terms are selected on the basis of preserving a symmetric representation in  $x$ ,  $y$  and of keeping the order of the individual variables  $x$  and  $y$  as low as possible.

From equations (3.43) and (3.42), the complete displacement vector is given by

$$\{\delta\} = \begin{Bmatrix} w \\ \frac{\partial w}{\partial y} \\ -\frac{\partial w}{\partial x} \end{Bmatrix} = \begin{bmatrix} 1 & x & y & x^2 & xy & y^2 & x^3 & x^2 y & xy^2 & y^3 & x^3 y & xy^3 \\ 0 & 0 & 1 & 0 & x & 2y & 0 & x^2 & 2xy & 3y^2 & x^3 & 3xy^2 \\ 0 & -1 & 0 & -2x & -y & 0 & -3x^2 & -2xy & -y^2 & 0 & -3x^2 y & -y^3 \end{bmatrix} \{\alpha\} = [C]\{\alpha\} \quad (3.44)$$

In the following, the detailed treatment will be restricted, for simplicity, to a square slab bending element (Fig. 3.25). The same general theory may, however, be applied to rectangular isotropic or orthotropic plate bending elements. If the general point, P (Fig. 3.25), is taken to be the nodes  $i, j, k$  and  $l$  in turn, then substituting successively in equation (3.44) allows the 12 nodal

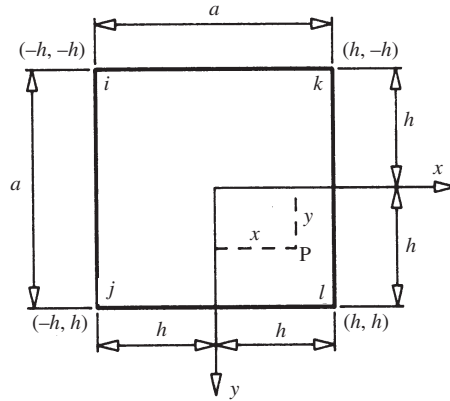


Fig 3.25 Square slab bending element

displacements to be related to the 12 undetermined coefficients by equations (3.45). It may be shown that  $[C^e]$  is non-singular, as well as square, so that the undetermined polynomial coefficients may be related to the nodal displacements by equation (3.46), in which the inversion of  $[C^e]$  for the square slab element has been achieved by computer:

$$\{\delta^e\} = \begin{Bmatrix} \delta_i \\ \delta_j \\ \delta_k \\ \delta_l \end{Bmatrix} = \begin{bmatrix} C_i \\ C_j \\ C_k \\ C_l \end{bmatrix} \{\alpha\}$$

$$= \begin{bmatrix} 1 & -h & -h & h^2 & h^2 & h^2 & -h^3 & -h^3 & -h^3 & -h^3 & h^4 & h^4 \\ 0 & 0 & 1 & 0 & -h & -2h & 0 & h^2 & 2h^2 & 3h^2 & -h^3 & -3h^3 \\ 0 & -1 & 0 & 2h & h & 0 & -3h^2 & -2h^2 & -h^2 & 0 & 3h^3 & h^3 \\ 1 & -h & h & h^2 & -h^2 & h^2 & -h^3 & h^3 & -h^3 & h^3 & -h^4 & -h^4 \\ 0 & 0 & 1 & 0 & -h & 2h & 0 & h^2 & -2h^2 & 3h^2 & -h^3 & -3h^3 \\ 0 & -1 & 0 & 2h & -h & 0 & -3h^2 & 2h^2 & -h^2 & 0 & -3h^3 & -h^3 \\ 1 & h & -h & h^2 & -h^2 & h^2 & h^3 & -h^3 & h^3 & -h^3 & -h^4 & -h^4 \\ 0 & 0 & 1 & 0 & h & -2h & 0 & h^2 & -2h^2 & 3h^2 & h^3 & 3h^3 \\ 0 & -1 & 0 & -2h & h & 0 & -3h^2 & 2h^2 & -h^2 & 0 & 3h^3 & h^3 \\ 1 & h & h & h^2 & h^2 & h^2 & h^3 & h^3 & h^3 & h^3 & h^4 & h^4 \\ 0 & 0 & 1 & 0 & h & 2h & 0 & h^2 & 2h^2 & 3h^2 & h^3 & 3h^3 \\ 0 & -1 & 0 & -2h & -h & 0 & -3h^2 & -2h^2 & -h^2 & 0 & -3h^3 & -h^3 \end{bmatrix} \{\alpha\} \quad (3.45)$$

$$\{\alpha\} = [C^e]^{-1} \{\delta^e\}$$

$$= \frac{1}{8h^4} \begin{bmatrix} 2h^4 & h^5 & -h^5 & 2h^4 & -h^5 & -h^5 & 2h^4 & h^5 & h^5 & 2h^4 & -h^5 & h^5 \\ -3h^3 & -h^4 & h^4 & -3h^3 & h^4 & h^4 & 3h^3 & h^4 & h^4 & 3h^3 & -h^4 & h^4 \\ -3h^3 & -h^4 & h^4 & 3h^3 & -h^4 & -h^4 & -3h^3 & -h^4 & -h^4 & 3h^3 & -h^4 & h^4 \\ 0 & 0 & h^3 & 0 & 0 & h^3 & 0 & 0 & -h^3 & 0 & 0 & -h^3 \\ 4h^2 & h^3 & -h^3 & -4h^2 & h^3 & h^3 & -4h^2 & -h^3 & -h^3 & 4h^2 & -h^3 & h^3 \\ 0 & -h^3 & 0 & 0 & h^3 & 0 & 0 & -h^3 & 0 & 0 & h^3 & 0 \\ h & 0 & -h^2 & h & 0 & -h^2 & -h & 0 & -h^2 & -h & 0 & -h^2 \\ 0 & 0 & -h^2 & 0 & 0 & h^2 & 0 & 0 & h^2 & 0 & 0 & -h^2 \\ 0 & h^2 & 0 & 0 & -h^2 & 0 & 0 & -h^2 & 0 & 0 & h^2 & 0 \\ h & h^2 & 0 & -h & h^2 & 0 & h & h^2 & 0 & -h & h^2 & 0 \\ -1 & 0 & h & 1 & 0 & -h & 1 & 0 & h & -1 & 0 & -h \\ -1 & -h & 0 & 1 & -h & 0 & 1 & h & 0 & -1 & h & 0 \end{bmatrix} \{\delta^e\}$$

(3.46)

The finite element method next requires that suitable ‘strains’ be defined, which may be related to the nodal displacement variables and to appropriately defined ‘stress’ variables by strain and elasticity relationships respectively. In the case of plate bending, ‘stresses’ are perhaps more readily defined than ‘strains’, since the general theory given above suggests that the ‘stress’ at P may be suitably represented by the moment stress resultants as

$$\{\sigma\} = \begin{Bmatrix} M_x \\ M_y \\ M_{xy} \end{Bmatrix} \quad (3.47)$$

Equations (3.8) then suggest that the ‘strains’ are appropriately defined in terms of curvatures so that

$$\{\varepsilon\} = \begin{Bmatrix} -\frac{\partial^2 w}{\partial x^2} \\ -\frac{\partial^2 w}{\partial y^2} \\ 2\frac{\partial^2 w}{\partial x \partial y} \end{Bmatrix} = \begin{Bmatrix} -\chi_x \\ -\chi_y \\ 2\chi_{xy} \end{Bmatrix} \quad (3.48)$$

The factor of two which occurs in the definition of the torsional strain arises due to the requirement that  $\{\varepsilon\}^T \{\sigma\}$  represent a quantity of work. It may, in fact, be shown that  $-\chi_x M_x$ ,  $-\chi_y M_y$ , and  $-\chi_{xy} M_{xy}$  all represent work/unit area of

plate and, since the torsional moment occurs in both coordinate directions, the total work it produces is  $2\chi_{xy}M_{xy}$ . The strains may now be related to the undetermined coefficients by substitution from equation (3.43) into equation (3.48) to give

$$\{\varepsilon\} = \begin{bmatrix} 0 & 0 & 0 & -2 & 0 & 0 & -6x & -2y & 0 & 0 & -6xy & 0 \\ 0 & 0 & 0 & 0 & 0 & -2 & 0 & 0 & -2x & -6y & 0 & -6xy \\ 0 & 0 & 0 & 0 & 2 & 0 & 0 & 4x & 4y & 0 & 6x^2 & 6y^2 \end{bmatrix} \{\alpha\}$$

$$= [Q]\{\alpha\} \quad (3.49)$$

The strain matrix then follows in the normal manner by substituting for the undetermined coefficients in equation (3.49) from equation (3.46). Hence

$$\{\varepsilon\} = [Q][C^e]^{-1}\{\delta^e\} = [B]\{\delta^e\} \quad (3.50)$$

The strain matrix for the square slab element, obtained by substituting in equation (3.50) for  $[Q]$  and  $[C^e]^{-1}$  from equations (3.49) and (3.46), respectively, is

$$[B] = \frac{1}{4h^4} \begin{bmatrix} -3x(h-y) & 0 & -h(h-y)(h-3x) \\ -3y(h-x) & h(h-x)(h-3y) & 0 \\ 4h^2 - 3(x^2 + y^2) & h(h-y)(h+3y) & -h(h-x)(h+3x) \\ -3x(h+y) & 0 & -h(h+y)(h-3x) \\ 3y(h-x) & -h(h-x)(h+3y) & 0 \\ -4h^2 + 3(x^2 + y^2) & h(h+y)(h-3y) & h(h-x)(h+3x) \\ 3x(h-y) & 0 & h(h-y)(h+3x) \\ -3y(h+x) & h(h+x)(h-3y) & 0 \\ -4h^2 + 3(x^2 + y^2) & -h(h-y)(h+3y) & -h(h+x)(h-3x) \\ 3x(h+y) & 0 & h(h+y)(h+3x) \\ 3y(h+x) & -h(h+x)(h+3y) & 0 \\ 4h^2 - 3(x^2 + y^2) & -h(h+y)(h-3y) & h(h+x)(h-3x) \end{bmatrix} \quad (3.51)$$

It should be noted that the strain matrix  $[B]$ , unlike its triangular plane stress element counterpart, is a variable matrix, since, although matrix  $[C^e]$  is constant, depending only on the known element size, the matrix  $[Q]$  depends upon the variable coordinates  $x$  and  $y$  of the general point, P. It follows that the strains, and hence stresses, vary with position for this type of element. The relationship between the chosen stresses and strains may be obtained by recasting equations (3.7) in matrix form to produce the elasticity relationships:

$$\{\sigma\} = \begin{Bmatrix} M_x \\ M_y \\ M_{xy} \end{Bmatrix} = \frac{Et^3}{12(1-\nu^2)} \begin{bmatrix} 1 & \nu & 0 \\ \nu & 1 & 0 \\ 0 & 0 & \frac{1-\nu}{2} \end{bmatrix} \begin{Bmatrix} -\frac{\partial^2 w}{\partial x^2} \\ -\frac{\partial^2 w}{\partial y^2} \\ 2\frac{\partial^2 w}{\partial x \partial y} \end{Bmatrix} = [D]\{\varepsilon\} \quad (3.52)$$

The stresses may now be related to the element nodal displacements in the normal way by eliminating the strains from equations (3.52) and (3.50) to give

$$\{\sigma\} = [D][B]\{\delta^e\} = [H]\{\delta^e\} \quad (3.53)$$

For the particular case of the square slab element, the elasticity matrix is obtained by setting Poisson's ratio to zero in equation (3.52) to produce

$$[D] = \frac{Et^3}{12} \begin{bmatrix} 1 & 0 & 0 \\ 0 & 1 & 0 \\ 0 & 0 & \frac{1}{2} \end{bmatrix} \quad (3.54)$$

Substituting in equation (3.53) for  $[D]$  and  $[B]$  from equations (3.54) and (3.51), respectively, produces the stress matrix for the square slab element:

$$[H] = \frac{Et^3}{12} \frac{1}{4h^4} \begin{bmatrix} -3x(h-y) & 0 & -h(h-y)(h-3x) \\ -3y(h-x) & h(h-x)(h-3y) & 0 \\ 2h^2 - \frac{3}{2}(x^2 + y^2) & \frac{h}{2}(h-y)(h+3y) & -\frac{h}{2}(h-x)(h+3x) \\ -3x(h+y) & 0 & -h(h+y)(h-3x) \\ 3y(h-x) & -h(h-x)(h+3y) & 0 \\ -2h^2 + \frac{3}{2}(x^2 + y^2) & \frac{h}{2}(h+y)(h-3y) & \frac{h}{2}(h-x)(h+3x) \\ 3x(h-y) & 0 & h(h-y)(h+3x) \\ -3y(h+x) & h(h+x)(h-3y) & 0 \\ -2h^2 + \frac{3}{2}(x^2 + y^2) & -\frac{h}{2}(h-y)(h+3y) & -\frac{h}{2}(h+x)(h-3x) \\ 3x(h+y) & 0 & h(h+y)(h+3x) \\ 3y(h+x) & -h(h+x)(h+3y) & 0 \\ 2h^2 - \frac{3}{2}(x^2 + y^2) & -\frac{h}{2}(h+y)(h-3y) & \frac{h}{2}(h+x)(h-3x) \end{bmatrix} \quad (3.55)$$



Since  $[B]$  depends on the position of P, the stresses calculated from equation (3.53) will vary and may be determined at any given point in the element by substitution of the relevant coordinates  $x$  and  $y$ . It is, in fact, usual to determine the moments at the four nodes of each element by substituting successively in equation (3.53) for the coordinates of the nodes  $i, j, k$  and  $l$  to produce the element stress matrix

$$\{\sigma^e\} = \begin{Bmatrix} \sigma_i \\ \sigma_j \\ \sigma_k \\ \sigma_l \end{Bmatrix} = \begin{bmatrix} H_i \\ H_j \\ H_k \\ H_l \end{bmatrix} \{\delta^e\} = [H^e] \{\delta^e\} \quad (3.56)$$

The stress matrix  $[H^e]$  for a square slab element may be obtained by following the same procedure of successive coordinate substitution, in this case in equation (3.55), and the resulting element stress matrix is given in Fig. 3.26.

Since the strain and elasticity matrices are now available from equations (3.50) and (3.52), general finite element theory (see Appendix B) may be invoked to obtain the element stiffness matrix as

$$[k] = \int_{\text{area}} [B]^T [D] [B] da \quad (3.57)$$

In equation (3.57), it should be noticed that the integral is taken over the area of the rectangular element since, as noted earlier, the product  $\{\varepsilon\}^T \{\sigma\}$  represents a quantity of work/unit area in this case. Also, unlike the triangular plane stress element, the integrand is not constant, due to the variable nature of the strain matrix. Nevertheless, the indicated integration may be evaluated to give the element stiffness matrix and this will be exemplified by consideration of the square slab element. First, the integration is simplified by substituting for  $[B]$  in equation (3.57) from equation (3.50) since  $[C^e]^{-1}$  is a constant matrix, hence

$$\begin{aligned} [k] &= \int_{-h}^{+h} \int_{-h}^{+h} ([Q][C^e]^{-1})^T [D] [Q][C^e]^{-1} dx dy \\ &= ([C^e]^{-1})^T \left( \int_{-h}^{+h} \int_{-h}^{+h} [Q]^T [D] [Q] dx dy \right) [C^e]^{-1} \end{aligned}$$

So that

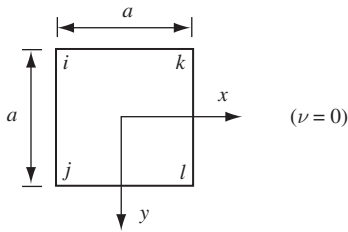
$$[k] = ([C^e]^{-1})^T [S] [C^e]^{-1} \quad (3.58)$$

where

$$[S] = \int_{-h}^{+h} \int_{-h}^{+h} [Q]^T [D] [Q] dx dy$$

$$[H^e] = \frac{Et^3}{12} \left( \frac{1}{a^2} \right) \begin{array}{c} \\ i \\ j \\ k \\ l \end{array} \begin{array}{cccc|cccc|cccc} & i & & j & & k & & l & & & & \\ \hline & 6 & 0 & -4a & 0 & 0 & 0 & -6 & 0 & -2a & 0 & 0 & 0 \\ & 6 & 4a & 0 & -6 & 2a & 0 & 0 & 0 & 0 & 0 & 0 & 0 \\ & -1 & -a & a & 1 & 0 & -a & 1 & a & 0 & -1 & 0 & 0 \\ \hline & 0 & 0 & 0 & 6 & 0 & -4a & 0 & 0 & 0 & -6 & 0 & -2a \\ & -6 & -2a & 0 & 6 & -4a & 0 & 0 & 0 & 0 & 0 & 0 & 0 \\ & -1 & 0 & a & 1 & -a & -a & 1 & 0 & 0 & -1 & a & 0 \\ \hline & -6 & 0 & 2a & 0 & 0 & 0 & 6 & 0 & 4a & 0 & 0 & 0 \\ & 0 & 0 & 0 & 0 & 0 & 0 & 6 & 4a & 0 & -6 & 2a & 0 \\ & -1 & -a & 0 & 1 & 0 & 0 & 1 & a & a & -1 & 0 & -a \\ \hline & 0 & 0 & 0 & -6 & 0 & 2a & 0 & 0 & 0 & 6 & 0 & 4a \\ & 0 & 0 & 0 & 0 & 0 & 0 & -6 & -2a & 0 & 6 & -4a & 0 \\ & -1 & 0 & 0 & 1 & -a & 0 & 1 & 0 & a & -1 & a & -a \end{array}$$

(a)



$$[k] = \frac{Et^3}{12} \left( \frac{1}{15a^2} \right) \times \begin{array}{c} \\ i \\ j \\ k \\ l \end{array} \begin{array}{cccc|cccc|cccc} & i & & j & & k & & l & & & & \\ \hline & 162 & 33a & -33a & -72 & 33a & -12a & -72 & 12a & -33a & -18 & 12a & -12a \\ & 33a & 24a^2 & 0 & -33a & 9a^2 & 0 & 12a & 6a^2 & 0 & -12a & 6a^2 & 0 \\ & -33a & 0 & 24a^2 & -12a & 0 & 6a^2 & 33a & 0 & 9a^2 & 12a & 0 & 6a^2 \\ \hline & -72 & -33a & -12a & 162 & -33a & -33a & -18 & -12a & -12a & -72 & -12a & -33a \\ & 33a & 9a^2 & 0 & -33a & 24a^2 & 0 & 12a & 6a^2 & 0 & -12a & 6a^2 & 0 \\ & -12a & 0 & 6a^2 & -33a & 0 & 24a^2 & 12a & 0 & 6a^2 & 33a & 0 & 9a^2 \\ \hline & -72 & 12a & 33a & -18 & 12a & 12a & 162 & 33a & 33a & -72 & 33a & 12a \\ & 12a & 6a^2 & 0 & -12a & 6a^2 & 0 & 33a & 24a^2 & 0 & -33a & 9a^2 & 0 \\ & -33a & 0 & 9a^2 & -12a & 0 & 6a^2 & 33a & 0 & 24a^2 & 12a & 0 & 6a^2 \\ \hline & -18 & -12a & 12a & -72 & -12a & 33a & -72 & -33a & 12a & 162 & -33a & 33a \\ & 12a & 6a^2 & 0 & -12a & 6a^2 & 0 & 33a & 9a^2 & 0 & -33a & 24a^2 & 0 \\ & -12a & 0 & 6a^2 & -33a & 0 & 9a^2 & 12a & 0 & 6a^2 & 33a & 0 & 24a^2 \end{array}$$

(b)

Fig. 3.26 Square slab bending element matrices. (a) Element stress matrix. (b) Element stiffness matrix

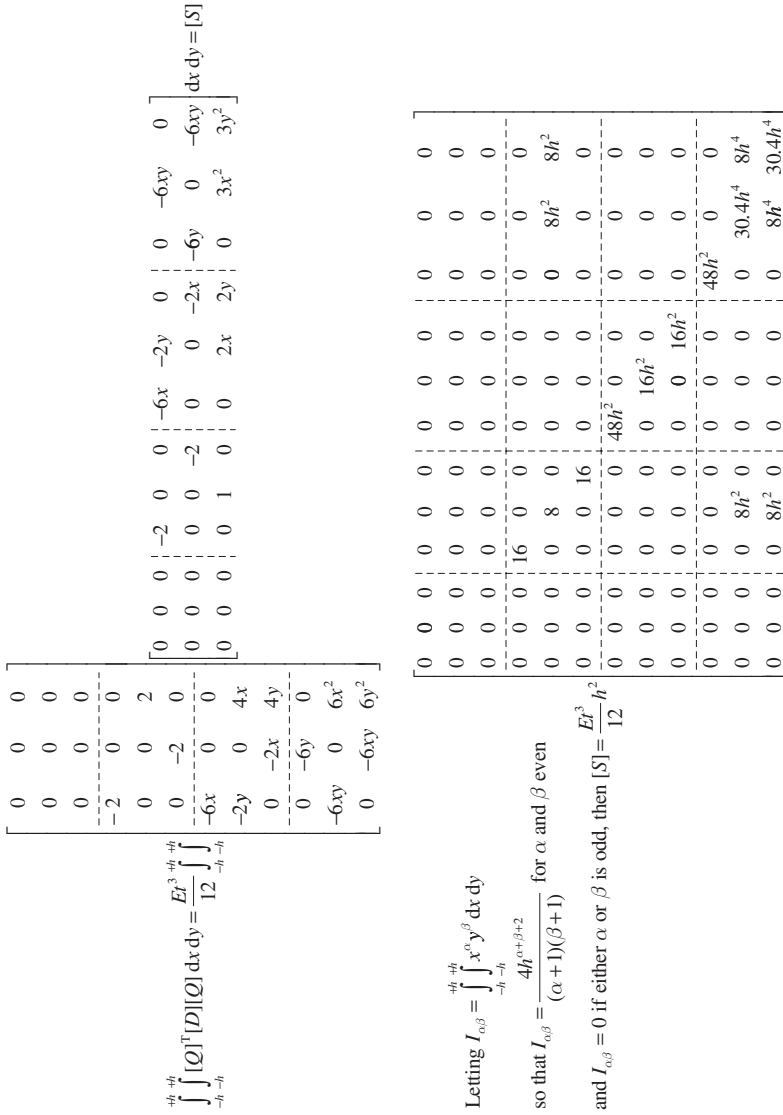


Fig. 3.27 Integrand evaluation for slab element

The evaluation of the integrand is now relatively straightforward due to the form of the elasticity matrix (equation (3.54)) and the fact that the origin of the coordinate system was located at the centre of the element (Fig. 3.25). The details of the integrand evaluation are given in Fig. 3.27, and the element stiffness matrix, derived by subsequent substitution in equation (3.58) for  $[C^e]^{-1}$  from equation (3.46) and  $[S]$  from Fig. 3.27, is presented in Fig. 3.26.

Plate analysis by the finite element method therefore consists of assembling a set of structure stiffness equations based on the element stiffness matrices derived from equation (3.57). Following the enforcement of the boundary conditions, the solution to the stiffness equations provides the plate displacements, which may be employed to obtain element stress solutions by use of equation (3.56). The application of these processes is illustrated in the example given below.

### 3.6.2 Example

#### Example 3.6 – fixed-edge slab

The example slab considered previously will be analysed by the finite element method under the fixed-edge condition, using the element sub-division and numbering systems shown in Fig. 3.28. Since the boundary conditions require that all the displacement components be zero at nodes 5, 6, 7, 8 and 9 the conditions may be enforced by not forming stiffness equations at these nodes, where the displacements are known, and the structure stiffness matrix will take the general form

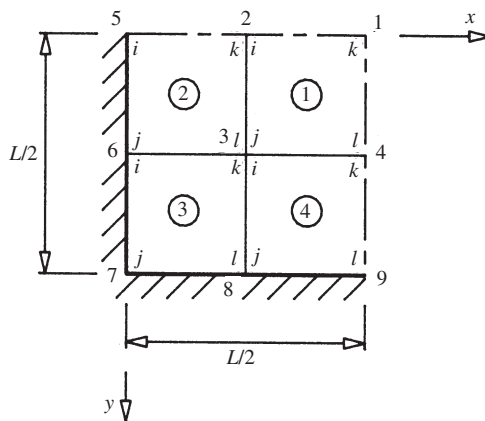


Fig. 3.28 Fixed-edge slab

$$\begin{Bmatrix} F_1 \\ \vdots \\ F_4 \end{Bmatrix} = [K] \begin{Bmatrix} \delta_1 \\ \vdots \\ \delta_4 \end{Bmatrix} \quad (3.59)$$

where

$$F_1 = \begin{Bmatrix} F_{w1} \\ F_{x1} \\ F_{y1} \end{Bmatrix}$$

the total ‘force’ components at node 1.

### Displacement solution

From Fig. 3.26, the element stiffness equations for the square slab element may be written, in sub-matrix form, as

$$\begin{Bmatrix} f_i \\ f_j \\ f_k \\ f_l \end{Bmatrix} = \begin{bmatrix} k_{ii} & k_{ij} & k_{ik} & k_{il} \\ k_{ji} & k_{jj} & k_{jk} & k_{jl} \\ k_{ki} & k_{kj} & k_{kk} & k_{kl} \\ k_{li} & k_{lj} & k_{lk} & k_{ll} \end{bmatrix} \begin{Bmatrix} \delta_i \\ \delta_j \\ \delta_k \\ \delta_l \end{Bmatrix} \quad (3.60)$$

To accord with general finite element theory, the nodal ‘forces’ involved in equation (3.60) must be such that  $\{\delta_i\}^T \{f_i\}$  represents a work quantity. With the chosen ‘displacement’ components (equation (3.42)), this will be so if the ‘forces’ are taken to be a force in the  $w$ -direction together with moments about the  $x$ - and  $y$ -axes in the positive directions shown in Fig. 3.24(b).

The structure stiffness matrix will be formed, as in example 1.1, by considering each of the nodes 1–4 in turn, and summing the force contributions from the elements which each node interconnects. Taking node 1 first (Fig. 3.28), the only element involved is element 1. Since the  $i, j, k$  and  $l$  designation of element 1 is 2, 3, 1 and 4, its element stiffness equations, from equation (3.60), take the form

$$\begin{Bmatrix} f_2 \\ f_3 \\ f_1 \\ f_4 \end{Bmatrix} = \begin{bmatrix} k_{ii} & k_{ij} & k_{ik} & k_{il} \\ k_{ji} & k_{jj} & k_{jk} & k_{jl} \\ k_{ki} & k_{kj} & k_{kk} & k_{kl} \\ k_{li} & k_{lj} & k_{lk} & k_{ll} \end{bmatrix} \begin{Bmatrix} \delta_2 \\ \delta_3 \\ \delta_1 \\ \delta_4 \end{Bmatrix} \quad (3.61)$$

The third of equations (3.61) relates to node 1, and, since only element 1 is involved, this provides the first structure stiffness equation as

$$\{F_1\} = [k_{kk}^1 : k_{ki}^1 : k_{kj}^1 : k_{kl}^1] \{\Delta\} \quad (3.62)$$

where  $\{\Delta\} = \{\delta_1, \dots, \delta_4\}^T$  and  $^1$  indicates evaluation for element 1.

Node 2 interconnects elements 1 and 2, so that the force contributions from these two elements need to be summed to produce the second structure stiffness equation. In the case of element 1, the forces at node 2 are given by the first of equations (3.61). Element 2 has node 2 as its 'k' node and it will therefore be the third of equations (3.60) which represents the node 2 forces for this element. When expanded, the relevant equation becomes

$$\begin{aligned}\{f_2^2\} &= [k_{ki}^2]\{\delta_5\} + [k_{kj}^2]\{\delta_6\} + [k_{kk}^2]\{\delta_2\} + [k_{kl}^2]\{\delta_3\} \\ &= [k_{kk}^2]\{\delta_2\} + [k_{kl}^2]\{\delta_3\}\end{aligned}\quad (3.63)$$

since  $\{\delta_5\} = \{\delta_6\} = \{0, 0, 0\}^T$  (boundary conditions).

Combining the contributions from the two elements together results in the second structure stiffness equation:

$$\{F_2\} = \{f_2^1\} + \{f_2^2\} = [k_{ik}^1 : k_{ii}^1 + k_{kk}^2 : k_{ij}^1 + k_{kl}^2 : k_{il}^1]\{\Delta\}\quad (3.64)$$

Similar consideration of nodes 3 and 4 enables the complete structure stiffness matrix to be assembled, in sub-matrix form, as

$$[k] = \begin{array}{c} \begin{array}{cccc} 1 & 2 & 3 & 4 \\ \left[ \begin{array}{cccc} k_{kk}^1 & k_{ki}^1 & k_{kj}^1 & k_{kl}^1 \\ k_{ik}^1 & k_{ii}^1 + k_{kk}^2 & k_{ij}^1 + k_{kl}^2 & k_{il}^1 \\ k_{jk}^1 & k_{ji}^1 + k_{lk}^2 & k_{jj}^1 + k_{ll}^2 + k_{kk}^3 + k_{ii}^4 & k_{jl}^1 + k_{ik}^4 \\ k_{lk}^1 & k_{li}^1 & k_{lj}^1 + k_{ki}^4 & k_{ll}^1 + k_{kk}^4 \end{array} \right] \end{array} \end{array}\quad (3.65)$$

Since, in this example, all the elements are similar, the complete stiffness equations may be obtained by direct substitution for the sub-matrices of equation (3.65) from Fig. 3.26(b). Such a substitution would normally be made numerically, but, for comparison with earlier solutions, algebraic geometric representations will be used. Also, the same form of load allocation will be employed as in the grid representation, that is, equal point loads of  $q(L/2)^2/4$  at each of nodes 1, 2, 3 and 4. When formed in this way, the structure stiffness equations are as given in Fig. 3.29(a).

Although the equations of Fig. 3.29(a) incorporate the boundary conditions due to the fixed edge (by omission of nodes 5–9), there are additional restraints due to the use of symmetry. No rotation can occur about lines of symmetry, since this would produce non-symmetric twists, and the additional restraints required to model these conditions are, with reference to Fig. 3.28:

Along 5–2–1:  $\theta_x = 0$

Along 9–4–1:  $\theta_y = 0$

It should be noted that, on lines of symmetry, rotation about lines normal to the symmetry lines is acceptable and will, in general, occur due to the bending

$$\frac{D}{15a^2} \begin{bmatrix} 162 & * & * & -72 & * & 33a & -18 & 12a & 12a & -72 & 33a & * \\ * & 24a^2 & 0 & 12a & 6a^2 & 0 & -12a & 6a^2 & 0 & -33a & 9a^2 & 0 \\ * & 24a^2 & -33a & 0 & 9a^2 & -12a & 0 & 6a^2 & 12a & 0 & 6a^2 & \\ \hline & & 324 & 66a & 0 & -144 & 66a & 0 & -18 & 12a & -12a & \\ & & & * & 48a^2 & 0 & -66a & 18a^2 & 0 & -12a & 6a^2 & 0 \\ & & & & 48a^2 & 0 & 0 & 0 & 12a^2 & 12a & 0 & 6a^2 \\ \hline & & & & & 648 & 0 & 0 & -144 & 0 & -66a & \\ & & & & & & 96a^2 & 0 & 0 & 12a^2 & 0 & \\ & & & & & & & 96a^2 & 66a & 0 & 18a^2 & \\ \hline & & & & & & & & 324 & 0 & 66a & \\ & & & & & & & & & 48a^2 & 0 & \\ & & & & & & & & & & * & 48a^2 \end{bmatrix} \begin{Bmatrix} w_1 \\ \theta_{x1} \\ \theta_{y1} \\ w_2 \\ \theta_{x2} \\ \theta_{y2} \\ w_3 \\ \theta_{x3} \\ \theta_{y3} \\ w_4 \\ \theta_{x4} \\ \theta_{y4} \end{Bmatrix} = \begin{Bmatrix} 1 \\ R_{\theta_{x1}} \\ R_{\theta_{y1}} \\ 1 \\ R_{\theta_{x2}} \\ 0 \\ 1 \\ 0 \\ 0 \\ 1 \\ 0 \\ R_{\theta_{y4}} \end{Bmatrix} \frac{qa^2}{4}$$

symmetric ( $a = L/4, D = Et^3/12$ )  
\* = restraint

(a)

$$\frac{D}{15a^2} \begin{bmatrix} 162 & -72 & 33a & -18 & 12a & 12a & -72 & 33a \\ & 324 & 0 & -144 & 66a & 0 & -18 & 12a \\ & & 48a & 0 & 0 & 12a & 12 & 0 \\ & & & 648 & 0 & 0 & -144 & 0 \\ & & & & 96a & 0 & 0 & 12a \\ & & & & & 96a & 66 & 0 \\ & & & & & & 324 & 0 \\ & & & & & & & 48a \end{bmatrix} \begin{Bmatrix} w_1 \\ w_2 \\ \theta_{y2} \\ w_3 \\ \theta_{x3} \\ \theta_{y3} \\ w_4 \\ \theta_{x4} \end{Bmatrix} = \begin{Bmatrix} 1 \\ 1 \\ 0 \\ 1 \\ 0 \\ 0 \\ 1 \\ 0 \end{Bmatrix} \frac{qa^2}{4}$$

symmetric

(b)

$$\frac{D}{15a^2} \begin{bmatrix} 162 & -72 & 33 & -18 & 12 & 12 & -72 & 33 \\ & 324 & 0 & -144 & 66 & 0 & -18 & 12 \\ & & 48 & 0 & 0 & 12 & 12 & 0 \\ & & & 648 & 0 & 0 & -144 & 0 \\ & & & & 96 & 0 & 0 & 12 \\ & & & & & 96 & 66 & 0 \\ & & & & & & 324 & 0 \\ & & & & & & & 48 \end{bmatrix} \begin{Bmatrix} w_1 \\ w_2 \\ a\theta_{y2} \\ w_3 \\ a\theta_{x3} \\ a\theta_{y3} \\ w_4 \\ a\theta_{x4} \end{Bmatrix} = \begin{Bmatrix} 1 \\ 1 \\ 0 \\ 1 \\ 0 \\ 0 \\ 1 \\ 0 \end{Bmatrix} \frac{qa^2}{4}$$

symmetric

(c)

Fig. 3.29 Example slab stiffness equations. (a) Unrestrained equations. (b) Restrained equations. (c) Restrained equations (modified variables)

of the slab. At the centre point, 1, however, the slope in all directions will be zero and hence both rotation components must be restrained.

The symmetry restraints are reflected in the equations of Fig. 3.29(a) by the specification of restraint moments,  $R$ . These moments arise due to interaction with the quarters of the slab which are not considered in the analysis. If the known zero-rotation values due to symmetry are introduced into the equations

of Fig. 3.29(a), then the columns of the stiffness matrix corresponding to these components become null and may be deleted. The equations corresponding to the restrained rotations are also discarded to give the stiffness equations for the restrained slab which are shown in Fig. 3.29(b), where equations relating to moment equilibrium have, for convenience, been divided by  $a$ . To facilitate the numerical solution of the equations, it is convenient to change the rotational variables,  $\theta$ , to  $a\theta$ , in which case the restrained stiffness equations become as given in Fig. 3.29(c). A computer solution to these equations follows:

$$\begin{Bmatrix} w_1 \\ w_2 \\ a\theta_{y2} \\ w_3 \\ a\theta_{x3} \\ a\theta_{y3} \\ w_4 \\ a\theta_{x4} \end{Bmatrix} = \begin{Bmatrix} 53.94 \\ 30.07 \\ -38.97 \\ 16.41 \\ -22.55 \\ -22.55 \\ 30.07 \\ -38.97 \end{Bmatrix} \times 10^{-3} \frac{15qa^4}{4D} = \begin{Bmatrix} 79.02 \\ 44.05 \\ -57.08 \\ 24.03 \\ -33.03 \\ -33.03 \\ 44.05 \\ -57.08 \end{Bmatrix} \times 10^{-5} \frac{qL^4}{4D} \quad (3.66)$$

The displacement solution of equation (3.66) exhibits further symmetry properties of the slab, namely the equal displacement and rotation components at nodes 2 and 4 and the equal rotation components at node 3. It would, in fact, have been possible to take advantage of these relationships to reduce the number of stiffness equations to be solved (see problem 3.10).

### Stress solution

To exemplify the stress solution, the moments at node 2 will be determined. These moments can be derived from either element 1 or element 2 (Fig. 3.28), so that the normal practice of deriving the moments from both elements and then averaging will be followed. In the case of element 1, node 2 is node  $i$  and, from equation (3.55), the moments at the node are given by

$$\{\sigma_2\} = \begin{Bmatrix} M_{x2} \\ M_{y2} \\ M_{xy2} \end{Bmatrix} = [H_i]\{\delta^e\} = [H_i] \begin{Bmatrix} \delta_2 \\ \delta_3 \\ \delta_1 \\ \delta_4 \end{Bmatrix} \quad (3.67)$$

By substituting in equation (3.67) for the stress sub-matrix from Fig. 3.26 and for the nodal displacements from equation (3.66), the moments at node 2 may be determined by









$$\begin{aligned}
 \begin{Bmatrix} M_{x2} \\ M_{y2} \\ M_{xy2} \end{Bmatrix} &= \frac{D}{a^2} \left( \begin{bmatrix} 6 & 0 & -4 \\ 6 & 4 & 0 \\ -1 & -1 & 1 \end{bmatrix} \begin{Bmatrix} w_2 \\ a\theta_{x2} \\ a\theta_{y2} \end{Bmatrix} + \begin{bmatrix} 0 & 0 & 0 \\ -6 & 2 & 0 \\ 1 & 0 & -1 \end{bmatrix} \begin{Bmatrix} w_3 \\ a\theta_{x3} \\ a\theta_{y3} \end{Bmatrix} + \right. \\
 &\quad \left. \begin{bmatrix} -6 & 0 & -2 \\ 0 & 0 & 0 \\ 1 & 1 & 0 \end{bmatrix} \begin{Bmatrix} w_1 \\ a\theta_{x1} \\ a\theta_{y1} \end{Bmatrix} + \begin{bmatrix} 0 & 0 & 0 \\ 0 & 0 & 0 \\ -1 & 0 & 0 \end{bmatrix} \begin{Bmatrix} w_4 \\ a\theta_{x4} \\ a\theta_{y4} \end{Bmatrix} \right) \\
 &= \frac{D}{(L/4)^2} \left( \begin{bmatrix} 6 & 0 & -4 \\ 6 & 4 & 0 \\ -1 & -1 & 1 \end{bmatrix} \begin{Bmatrix} 44.05 \\ 0 \\ -57.08 \end{Bmatrix} + \begin{bmatrix} 0 & 0 & 0 \\ -6 & 2 & 0 \\ 1 & 0 & -1 \end{bmatrix} \begin{Bmatrix} 24.03 \\ -33.03 \\ -33.03 \end{Bmatrix} + \right. \\
 &\quad \left. \begin{bmatrix} -6 & 0 & -2 \\ 0 & 0 & 0 \\ 1 & 1 & 0 \end{bmatrix} \begin{Bmatrix} 79.02 \\ 0 \\ 0 \end{Bmatrix} + \begin{bmatrix} 0 & 0 & 0 \\ 0 & 0 & 0 \\ -1 & 0 & 0 \end{bmatrix} \begin{Bmatrix} 44.05 \\ -57.08 \\ 0 \end{Bmatrix} \right) \times 10^{-5} \frac{qL^4}{D} \\
 &= \begin{Bmatrix} 29.6 \\ 86.5 \\ -14.6 \end{Bmatrix} \times 10^{-4} qL^2 \tag{3.68}
 \end{aligned}$$

Following a similar procedure for element 2, node 2 becomes node 'k' and the moments are calculated as shown:

$$\begin{aligned}
 \{\sigma_2\} &= \begin{Bmatrix} M_{x2} \\ M_{y2} \\ M_{xy2} \end{Bmatrix} = [H_k] \{\delta^e\} = [H_k] \begin{Bmatrix} \delta_5 \\ \delta_6 \\ \delta_2 \\ \delta_3 \end{Bmatrix} = [H_k] \begin{Bmatrix} 0 \\ 0 \\ \delta_2 \\ \delta_3 \end{Bmatrix} \\
 &= \frac{D}{(L/4)^2} \left( \begin{bmatrix} 6 & 0 & 4 \\ 6 & 4 & 0 \\ 1 & 1 & 1 \end{bmatrix} \begin{Bmatrix} 44.05 \\ 0 \\ -57.08 \end{Bmatrix} + \right. \\
 &\quad \left. \begin{bmatrix} 0 & 0 & 0 \\ -6 & 2 & 0 \\ 1 & 0 & -1 \end{bmatrix} \begin{Bmatrix} 24.03 \\ -33.03 \\ -33.03 \end{Bmatrix} \right) \times 10^{-5} \frac{qL^4}{D} \\
 &= \begin{Bmatrix} 57.6 \\ 86.5 \\ -6.4 \end{Bmatrix} \times 10^{-4} qL^2 \tag{3.69}
 \end{aligned}$$

Table 3.3 Comparative results from slab analyses

Analysis	Net	Central deflection			Maximum bending moment		
		S	E	F	S	E	F
Finite difference	4 × 4	214	105	524	220	-200	507
	8 × 8	213	91	504	223	-238	507
Grid representation	4 × 4	201	78	472	248	-243	519
	8 × 8	210	82	491	232	-256	511
Finite element	4 × 4	201	79	471	231	-240	511
	8 × 8	210	83	490	227	-252	507
Multiplier		$10^{-5} qL^4/D$			$10^{-4} qL^2$		
Support types:		S		E		F	
 Simple							
 Encastré							
 Free							

Comparing equations (3.68) and (3.69) shows that only the  $y$ -direction moments are in agreement, there being marked differences between the other two pairs of moments. In addition, zero twisting moment would be expected at node 2 but this symmetry condition is not well represented by the analysis. More representative moments are obtained by averaging the two sets of moments obtained already,

$$\begin{Bmatrix} M_{x2} \\ M_{y2} \\ M_{xy2} \end{Bmatrix} \begin{Bmatrix} 43.6 \\ 86.5 \\ -10.5 \end{Bmatrix} \times 10^{-4} qL^2 \quad (3.70)$$

but the twisting moment is still significantly different from zero, although its magnitude is small compared with the size of the maximum moments in the slab (Table 3.3).

### 3.6.3 Extensions and refinements

Non-zero Poisson's ratio and orthotropy (Zienkiewicz and Taylor, 1991) may both be treated by use of appropriate elasticity matrices in place of the slab relationships (equation (3.54)) used here. Beam elements may be used in conjunction with slab elements, and the inclusion of slab elements in complete structure analysis presents little theoretical difficulty. A more 'consistent' system of load allocation is possible, while non-rectangular plates and slabs require triangular, oblique or isoparametric elements, for all of which aspects the reader is referred to Zienkiewicz and Taylor (1991). It should be noted, however, that many of these more versatile elements are based on *Mindlin*

plate theory, rather than the *Kirchhoff* thin plate theory. Mindlin's formulation is a thick plate theory, which incorporates shear deformations. In using such elements, it is therefore necessary that realistic plate thicknesses be employed if reliable results are to be obtained.

### 3.7 Comparison of analyses

Results for the analysis of the slab used as an example in this chapter are presented in Table 3.3. The results have been obtained by each of the three numerical methods considered, for each of the three types of edge support condition. In Table 3.3, the finite element and grid representation methods may be observed to give a good indication of structural behaviour in all cases, as judged by the correspondence between results from the finer and coarser nets. The grid representation results correlate closely with the finite element values, which might have been anticipated, since, in the forms presented above, the methods are closely related. Both approaches form three equilibrium equations at each node of the net, and it may also be shown that both methods assume that the displacement between adjacent nodes may be represented by a cubic polynomial.

As noted previously, the finite difference solution performs well in the simply supported and free-edge cases but is considerably less satisfactory when fixed edges are treated. The feature of the fixed support which creates the difficulty is the presence of curvature reversal in this case, which can be less effectively modelled by the quadratic displacement representation of the difference approach (equation (A.1)) than by the cubic representation of the two other methods. This deficiency may, however, be overcome by using finer difference nets in regions of expected curvature reversal, and it is the availability of large-scale standard computer packages and their enhanced flexibility which explain the general preference for grid representation or finite element methods for plate bending analysis.

### 3.8 Design moments

#### 3.8.1 Introduction

Whichever method is used to determine the moment distribution in a slab or plate, the next problem confronted is normally that of how to ensure that the strength of the plate is adequate to resist the calculated moments. This problem may be viewed as one of knowing how to design, in particular, for the twisting moments,  $M_{xy}$ . If a metal plate is being designed, it is usual to convert the moments into stresses using equations (3.9) and then to employ an appropriate failure criterion, often that due to von Mises (Megson, 1996), to ensure the adequacy of the plate.

In the case of a reinforced concrete slab, which is reinforced by an orthogonal system of bars placed in the  $x$ - and  $y$ -directions, the problem is to determine the *design moments*  $M_x^*$ ,  $M_y^*$  the reinforcement should be designed for if adequate strength is to be available in *all* directions. Once  $M_x^*$ ,  $M_y^*$  have been found, the reinforcement may be designed to resist these moments by the normal analysis of a section in bending. The design moments are commonly referred to as *Wood–Armer* (Wood, 1968) moments, and the following recommendations follow Wood’s suggestions.

### 3.8.2 Recommendations

#### Bottom reinforcement

Generally

$$M_x^* = M_x + |M_{xy}|, \quad M_y^* = M_y + |M_{xy}| \quad (3.71)$$

If either  $M_x^*$  or  $M_y^*$  in equations (3.71) is found to be negative, it is changed to zero, as follows: either

$$M_x^* = M_x + \left| \frac{M_{xy}^2}{M_y} \right| \quad \text{with} \quad M_y^* = 0 \quad (3.72)$$

or

$$M_y^* = M_y + \left| \frac{M_{xy}^2}{M_x} \right| \quad \text{with} \quad M_x^* = 0 \quad (3.73)$$

If, in these changed formulae, the wrong algebraic sign results for  $M_x^*$  or  $M_y^*$ , then no such reinforcement is required.

If *both*  $M_x^*$  and  $M_y^*$  are negative, then no bottom reinforcement is required.

#### Top reinforcement

Generally

$$M_x^* = M_x - |M_{xy}|, \quad M_y^* = M_y - |M_{xy}| \quad (3.74)$$

If either  $M_x^*$  or  $M_y^*$  in equations (3.74) is found to be positive, then change to either

$$M_x^* = M_x - \left| \frac{M_{xy}^2}{M_y} \right| \quad \text{with} \quad M_y^* = 0 \quad (3.75)$$

or

$$M_y^* = M_y - \left| \frac{M_{xy}^2}{M_x} \right| \quad \text{with} \quad M_x^* = 0 \quad (3.76)$$

If, in these changed formulae, the wrong algebraic sign results for  $M_x^*$  or  $M_y^*$ , then no such reinforcement is required.

If both  $M_x^*$  and  $M_y^*$  are negative then no top reinforcement is required.

### 3.8.3 Example 3.7 – simply supported slab design moments

Referring to Fig. 3.16, the design moments at various points of the simply supported slab considered previously may be evaluated as follows:

At centre (C):  $M_x = M_y = +0.023qL^2$ ,  $M_{xy} = 0$

Bottom reinforcement:  $M_x^* = M_y^* = +0.023qL^2$

Top reinforcement:  $M_x^* = M_y^* = 0$

At quarter point (1):  $M_x = M_y = +0.009qL^2$ ,  $M_{xy} = -0.011qL$

Bottom reinforcement:  $M_x^* = M_y^* = +0.020qL^2$

Top reinforcement:  $M_x^* = M_y^* = -0.002qL^2$

At corner (A):  $M_x = M_y = 0$ ,  $M_{xy} = -0.019qL^2$

Bottom reinforcement:  $M_x^* = M_y^* = +0.019qL^2$

Top reinforcement:  $M_x^* = M_y^* = -0.019qL^2$

From the above, it may be seen that top (torsional) reinforcement is only required close to the corners, as would be expected, and that the bottom reinforcement requirements at the centre and corners are rather similar. Naturally, much less bottom steel is needed close to the centre point of an edge.

### 3.8.4 Example 3.8 – fixed-edge slab design moments

With reference to Fig. 3.21, the design moments will be calculated at point D, not because this is a particularly critical slab location, but simply to illustrate the application of the design moment computations:

At point D:  $M_x = -0.008qL^2$ ;  $M_y = +0.002qL^2$ ;  $M_{xy} = -0.005qL^2$

Bottom reinforcement:  $M_x^* = -0.003qL^2$ ;  $M_y^* = +0.007qL^2$

So take equation (3):  $M_x^* = 0$ ;  $M_y^* = (+0.002 + 0.005^2/0.008)qL^2 = +0.005qL^2$

Note that the subsidiary calculation results in some moment reduction but that this will be small if the design moment with the offending sign was also small.

Top reinforcement:  $M_x^* = -0.013qL^2$ ;  $M_y^* = -0.003qL^2$ .

## References and further reading

Brown, D. K. (1990) *An Introduction to the Finite Element Method using Basic Programming*, 2nd edn. Chapman and Hall, London. Chapter 5

- describes a program for plate analysis based on the rectangular element use above.
- Cope, R. J. and Clark, L. A. (1984) *Concrete Slabs – Analysis and Design*. Elsevier, London. Higher order finite difference expressions used to improve accuracy.
- Ghali, A. and Neville, A. M. (1997) *Structural Analysis*, 4th edn. Spon, London. Chapter 16 covers the application of the finite difference method to plate bending using rectangular nets and includes modified biharmonic difference operators which allow free-edge conditions to be automatically incorporated rather than explicitly stated as in the above (example 3.3). Chapter 4 describes the displacement method, including its application to grillages.
- Hambly, E. C. (1991) *Bridge Deck Behaviour*, 2nd edn. Chapman and Hall, London. A detailed description of the application of the grid representation method to many different types of concrete bridge deck is given.
- Hrennikoff, A. (1941) Solutions of problems of elasticity by the framework method. *Journal of Applied Mechanics of the ASME* **63**, A-169–A-175. One of the most comprehensive papers on gridwork representations for stress analysis. The representation proposed for plate bending (A-172) is more complex than the one described above but can treat all values of Poisson's ratio.
- Megson, T. H. G. (1996) *Structural and Stress Analysis*. Arnold, London. Chapters 9 and 10 cover the stress analysis of bending and shear, respectively, in simple beams. A discussion of yield criteria can be found in Chapter 14.
- Morley, L. S. D. (1963) *Skew Plates and Structures*. Pergamon, Oxford, pp. 75–84.
- Pucher, A. (1964) *Influence Surfaces of Elastic Plates*. Springer, Vienna.
- Szilard, R. (1974) *Theory and Analysis of Plates*. Prentice Hall, New Jersey. A comprehensive text treating both classical and numerical methods.
- Timoshenko, S. P. and Woinowsky-Krieger, S. (1981) *Theory of Plates and Shells*, 2nd edn. McGraw-Hill, New York. A standard reference work on classical plate theory; Chapter 11 describes orthotropic plate theory.
- Wood, R. H. (1961) *Plastic and Elastic Design of Slabs and Plates*. Thames and Hudson, London. See Chapter VIII.
- Wood, R. H. (1968) The reinforcement of slabs in accordance with a pre-determined field of moments. *Concrete* **2**, No. 2, 69–76.
- Zienkiewicz, O. Z. and Taylor, R. L. (1991) *The Finite Element Method*, 4th edn, Vol. 2. *Solid and Fluid Mechanics Dynamics and Non-linearity*. London: McGraw-Hill. Chapters 1 and 2 treat plate bending and include a full discussion of the problems involved in attempting to ensure displacement compatibility along element boundaries.

## Problems

- 3.1 A square, isotropic slab of side 5 m is such that two opposite sides may be presumed simply supported, while the other two sides are encastré. The slab supports a central point load of 200 kN. Using a net of side 1.25 m, employ the finite difference method to determine the displacements at the net nodal points.

Hence determine the bending moment distributions in the direction of, and along, both centre-lines and relate these distributions to the expected behaviour of the slab. ( $E = 20 \text{ kN/mm}^2$ ,  $\nu = 0$ ,  $t = 100 \text{ mm}$ )

- 3.2 A reinforced concrete foundation raft is used to resist axial loads  $P$  from regularly spaced concrete columns by developing uniform bearing stresses. A typical internal panel is shown in Fig. 3.30. Taking into account all possible symmetry conditions, determine expressions for the normal displacements of the panel at points 1 and 2.

Describe briefly how you would use the results from this type of analysis to obtain the distribution of bending moments.

(UCL)

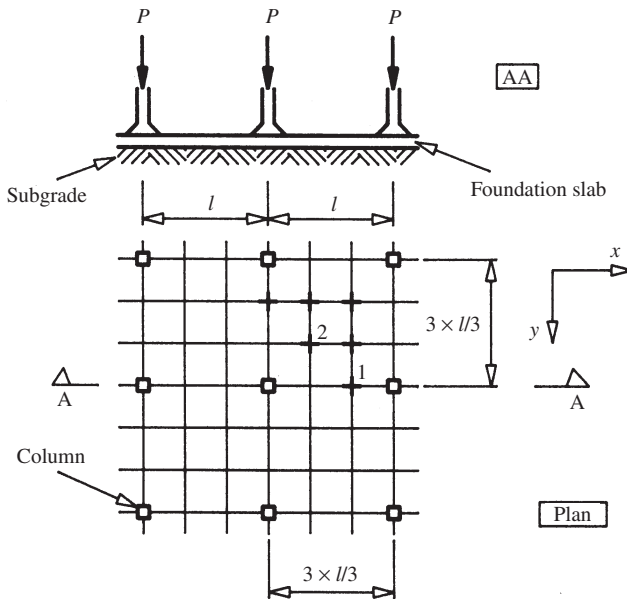


Fig. 3.30

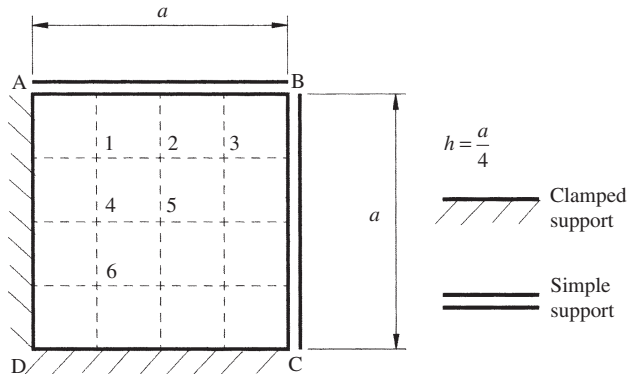


Fig. 3.31

3.3 The square plate ABCD, of side  $a$ , shown in Fig. 3.31 is clamped along AD, DC and simply supported along AB, BC. The plate is isotropic with flexural rigidity  $D$ .

- (a) Establish a set of equations for the solution of the plate when subjected to transverse loading using finite difference approximations, with a mesh size  $a/4$  as shown, when the load is:
  - (i) uniformly distributed,  $q$  per unit area;
  - (ii) a central point load,  $P$ .
- (b) Discuss the principal sources of error in the proposed finite difference idealization and the means by which the accuracy could be improved.
- (c) Describe the main differences in the solution if the edge AD were free, the other support conditions being unchanged.

(CITY)

3.4 For a rectangular difference net such that the net spacing in the  $x$ -direction is  $3h$ , while that in the  $y$ -direction is  $h$ , show that the biharmonic difference operator takes the form shown in Fig. 3.32(a).

The rectangular metal plate shown in Fig 3.32(b) has length  $3L$  and breadth  $L$ , and its edges may be assumed to be simply supported. The plate has flexural rigidity  $D$ , may be presumed isotropic, and is subjected to a uniformly distributed pressure load of intensity  $q$ .

Using the net shown, and making use of symmetry, calculate the normal displacements at the net points 1, 2, 3 and 4 by the finite difference method. Hence determine the bending moments along and in the direction of sections AA and BB. Plot these bending moment distributions and compare the results with those that might be expected from a similar plate in which the length is infinitely greater than the breadth. ( $\nu = 0.3$ ).



3.5 The square slab shown in Fig. 3.33 carries a load of uniform intensity,  $q$ , over a centrally positioned square of side,  $L/4$ . The slab is simply supported on two opposite edges. The other pair of edges are supported by central columns which may be assumed to provide rotationally free point supports. The slab has bending rigidity,  $D$ , and Poisson's ratio,  $\nu$ , may be assumed zero.

Analyse the slab by the finite difference method, using a grid of side  $L/4$ , and compare your results with the values given in Table 3.4, which were obtained by a finite difference analysis using a grid of side  $L/8$ . Plot distributions of  $w$ ,  $M_x$ ,  $M_y$  along the grid lines and relate the distributions to the expected structural response of the slab.

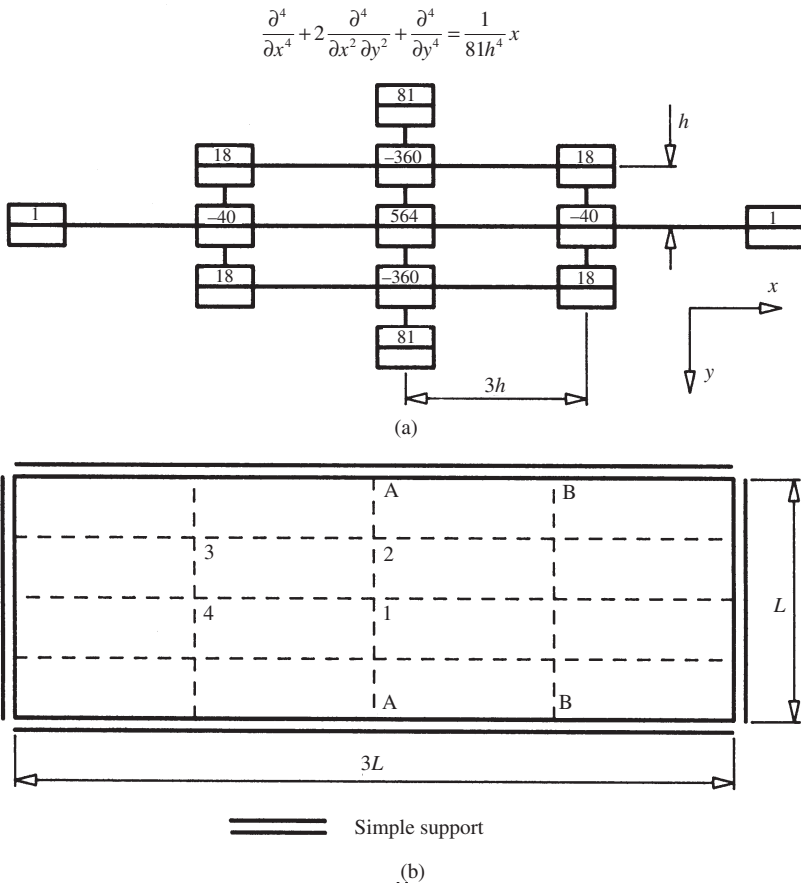


Fig. 3.32

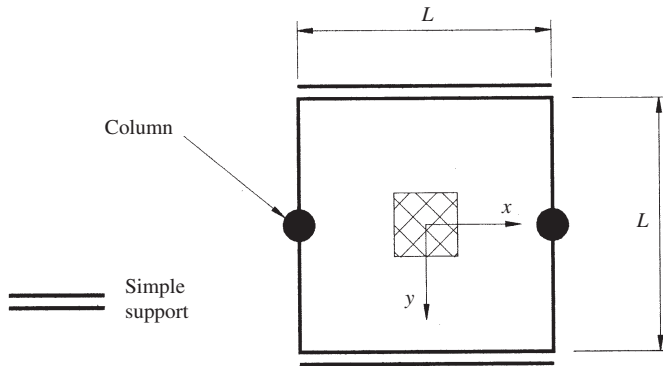


Fig. 3.33

Table 3.4  $L/8$  grid finite difference analysis results

Position	$w (\times 10^{-5} qL^4/D)$	$M_x (\times 10^{-4} qL^2)$	$M_y (\times 10^{-4} qL^2)$
Centre	69	89	90
Column	0	0	-77

- 3.6 A reinforced concrete water tank is to be 10 m square and 3 m high. The tank is open at the top and has walls which vary in thickness from 0.10 m at the top to 0.25 m at the base. By making use of symmetry, it is intended to analyse one half of a wall slab for the effects of water pressure when the tank is full. A grid analogy approach is to be used for the analysis. Young's modulus for concrete may be taken as  $15 \text{ N/mm}^2$  and Poisson's ratio may be assumed to be zero.

Using no more than 25 joints, sketch and number a suitable layout for the analogous grid members and specify:

- the section properties of the grid members;
- the loads to be applied to the grid;
- the restraints to be applied to the grid.

(UEL)

- 3.7 Figure 3.34 shows the plan view of a reinforced concrete water tank. The roof comprises a flat slab which is supported by the tank walls at its edges and by columns at 4 m centres internally, and carries a uniformly distributed load over its complete area. The column head detail is as shown in the figure. It is proposed to analyse the slab by the use of rectangular finite elements, no more than 36 in number. By making use of appropriate symmetry assumptions, the analysis is to be applied to the quarter panel shown hatched in the figure.

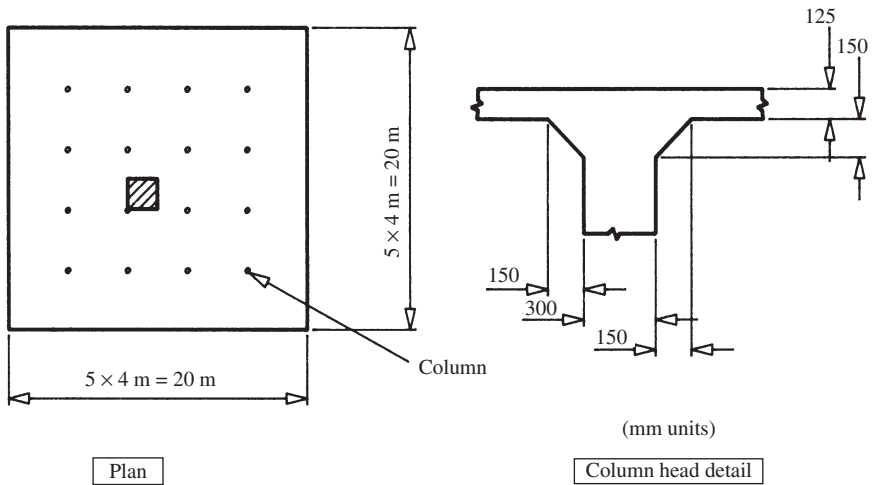


Fig. 3.34

Sketch a suggested element sub-division and state the type of element properties and nodal restraints which would be needed for the analysis. Justify the choice of element sub-division made.

(UEL)

- 3.8 An isoparametric finite element mesh for a skew bridge slab analysis is shown in Fig. 3.35(a). The slab is subjected to a uniformly distributed load and is simply supported on opposite sides, as shown in the figure, the other two sides, being unsupported. Figures 3.35(b) and 3.35(c) show output results in the form of contours of *absolute* maximum principal moment values and principal moment vectors, respectively. Figure 3.35(d) shows the reaction distribution along the edge AB.

Discuss the structural response of the slab to the applied load. Sketch distributions which are equivalent to Figs 3.35(b)–3.35(d), if the bridge deck was constructed of parallel beam strips (as shown in Fig. 3.35(e)) which are structurally independent. Compare and contrast the structural behaviour of the two types of deck construction.

- 3.9 Analyse the slab of problem 3.1 using rectangular plate bending finite elements, adopting square elements of side 1.25 m.

Compare the displacement and bending moment results with those obtained by use of the finite difference method, and state, with reasons, which results would be expected to be the more accurate.

- 3.10 One quarter of a square, encastré slab is to be analysed by the finite element method using the sub-division into equal, square elements

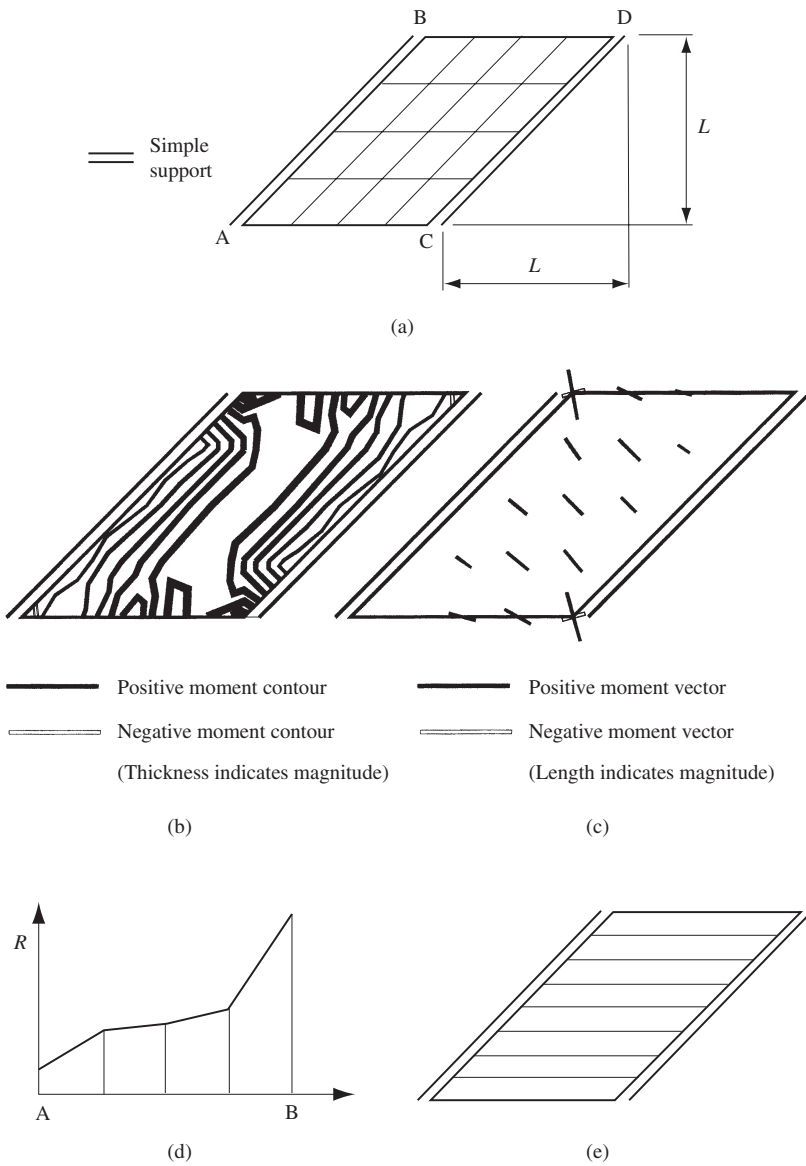
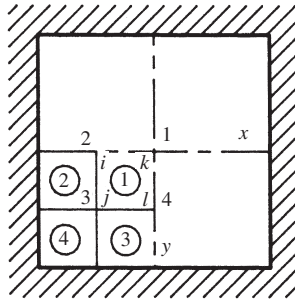
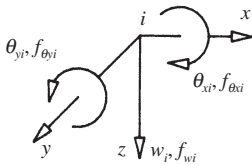


Fig. 3.35



(a)



(b)

$$\begin{Bmatrix} w_1 \\ w_2 \\ \theta_{y2} \\ w_3 \\ \theta_{x3} \end{Bmatrix} = \begin{Bmatrix} 0.02558 \\ 0.01131 \\ -0.01824 \\ 0.00574 \\ -0.00869 \end{Bmatrix} \begin{matrix} \text{m} \\ \text{rad} \\ \text{m} \\ \text{rad} \\ \text{m} \end{matrix}$$

(c)

$$\begin{Bmatrix} 100 \\ 0 \\ 0 \\ 0 \\ 0 \\ 0 \\ 0 \\ 0 \end{Bmatrix} = 100 \begin{bmatrix} 162 & -72 & 33 & -18 & 12 & 12 & -72 & 33 \\ -72 & 324 & 0 & -144 & 66 & 0 & -18 & 12 \\ 33 & 0 & 48 & 0 & 0 & 12 & 12 & 0 \\ -18 & -144 & 0 & 648 & 0 & 0 & -144 & 0 \\ 12 & 66 & 0 & 0 & 96 & 0 & 0 & 12 \\ 12 & 0 & 12 & 0 & 0 & 96 & 66 & 0 \\ -72 & -18 & 12 & -144 & 0 & 66 & 324 & 0 \\ 33 & 12 & 0 & 0 & 12 & 0 & 0 & 48 \end{bmatrix} \begin{Bmatrix} w_1 \\ w_2 \\ \theta_{y2} \\ w_3 \\ \theta_{x3} \\ \theta_{y3} \\ w_4 \\ \theta_{x4} \end{Bmatrix}$$

(d)

$$\begin{Bmatrix} M_x \\ M_y \\ M_{xy} \end{Bmatrix}_k = 1500 \begin{bmatrix} -6 & 0 & 2 & 0 & 0 & 0 & 6 & 0 & 4 & 0 & 0 & 0 \\ 0 & 0 & 0 & 0 & 0 & 0 & 6 & 4 & 0 & -6 & 2 & 0 \\ -1 & -1 & 0 & 1 & 0 & 0 & 1 & 1 & 1 & -1 & 0 & -1 \end{bmatrix} \begin{Bmatrix} \partial_i \\ \partial_j \\ \partial_k \\ \partial_l \end{Bmatrix} \text{ kN m/m}$$

$$\text{where } \{\partial\} = \begin{Bmatrix} w \\ \theta_x \\ \theta_y \end{Bmatrix} \begin{matrix} \text{m} \\ \text{rad} \\ \text{rad} \end{matrix}$$

(e)

Fig. 3.36

---

shown in Fig. 3.36(a), with the displacement sign convention of Fig. 3.36(b). The slab is subjected to a central, vertical, downwards point load of 400 kN.

The stiffness equations for the quarter slab may be shown to be as given by Fig. 3.36(d). Use symmetry to eliminate  $\theta_{y3}$ ,  $w_4$  and  $\theta_{x4}$  from the stiffness equations and hence produce a reduced set of five equations in the displacement variables and  $w_1$ ,  $w_2$ ,  $\theta_{y2}$ ,  $w_3$  and  $\theta_{x3}$ .

The solution to the reduced set of equations is given in Fig. 3.36(c). Use this solution to determine the moments at node 1 if the part stress equations for the element used are as given in Fig. 3.36(e).

(UEL)

## 4. Thin shells

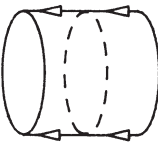
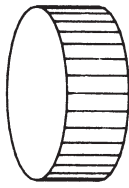
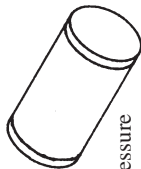


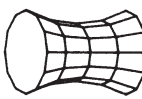

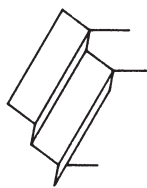
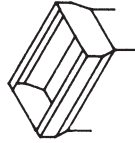
### 4.1 Introduction

#### 4.1.1 Generation, classification and application

A thin shell may be defined as comprising the material contained between two closely separated three-dimensional surfaces. As with plates, provided the two generating surfaces are sufficiently close, the deformation of the single surface formed by the mid-thickness points will be sufficient to describe the deformation of the complete shell. Only the behaviour of a single, *middle surface* will therefore be considered in the following theory, and sufficient assumptions will be made to enable the deformation of any point in the shell to be determined from the deformation of such a middle surface.

Since general three-dimensional surfaces are of interest, the range of possible shell geometries is enormous. Some classification scheme is therefore essential so that advantage may be taken of whatever similarities various shell forms may possess. Relevant strategies may then be adopted so that the potential analytical complexities are minimized by the use of appropriate coordinate systems and similar tactics. The most convenient primary classification is one based on shell geometry, and examples of the simplest geometric types are shown in Table 4.1. The forms included in Table 4.1 do cover many of the commonest types used in practice, but shells with other geometric regularity features are also employed as, indeed, are shells of irregular geometry. As will be seen from Table 4.1, shells find a wide range of application as storage and pressure vessels on land and also on sea and in the air when employed as ship or aeroplane hull structures. In civil engineering, the routine use of shell roofs has been curtailed by increased labour costs, and shell roofing (Cronowicz, 1968) tends to be restricted to structures which are of special architectural significance, such as the Sydney Opera House in Australia. Major applications of shells remain, however, in the construction of cooling towers and water storage and retention structures (mainly circular tanks, cylindrical or conical towers, and arch dams). Shell theory may also be used for the analysis of box girders (see Fig. 2.1) and of core-supported buildings (see Fig. 2.2), so that the fields of application are almost as diverse as the possible geometric forms.

Table 4.1 Classification of shells

Type	Mode of generation	Examples
Closed cylindrical	Translation of a closed curve in its normal direction	   Pressure vessels
Open cylindrical	Translation of an open curve in its normal direction	  Roofs
Axisymmetric (shell of rotation)	Rotation of a plane curve about an axis in its own plane	 Cooling towers
		 Domes
Folded plates	Intrconnection of non-co-planar plates along their edges	  Roofs and storage bunkers



### 4.1.2 Structural behaviour

In general, shells resist loads by a combination of bending and in-plane actions. In the case of shells, in-plane action is characterized by the plane stress system of direct and shear stresses (see Fig. 1.9) and is normally referred to as *membrane* action. This terminology derives from the inability of membrane materials, such as fabrics, to resist any bending whatsoever, and their consequent total reliance on in-plane action. Examples of membrane shells are sails, tents, balloons and inflated structures, each of which can only resist in-plane actions and must therefore adopt a shape which allows the imposed loading to be resisted in this manner. Such structures do not therefore have a unique non-loaded geometry, as their rigid counterparts do, and determining the form of such structures under their initial prestressing and/or self-weight effects becomes a problem in its own right (Firt, 1983).

Plates represent a special case of shell and may be considered to be the antithesis of membranes in the sense that, when normally loaded, no membrane stresses exist (see Chapter 3) and resistance is provided by bending alone. Membrane resistance may be given to a thin plate by folding it, and the effect of the folding is to dramatically increase the stiffness. Thus, if the flexible thin sheet of Fig. 4.1(a) is converted into the folded-plate type of shell shown in Fig. 4.1(b), then the sheet is able to sustain quite substantial loads, whereas it previously exhibited gross deformation under a much more modest load. Closed shells, in particular, exhibit high strength and stiffness, as evidenced by the familiar example of the 'nut which is hard to crack', or, in relation to its thickness, even an egg-shell. The high stiffness is primarily due to membrane action, bending often being of secondary or localized significance.

The influence of bending effects on shell behaviour depends on the type of restraints and loading which are involved as well as the shape of the shell. In respect of shell shape, however, bending will always need to be considered in the cases of folded plates and open cylindrical sections (see Table 4.1). For axisymmetric shells, bending effects will tend to be localized, but the rate of decay of these effects will depend upon the nature of the principal radii of

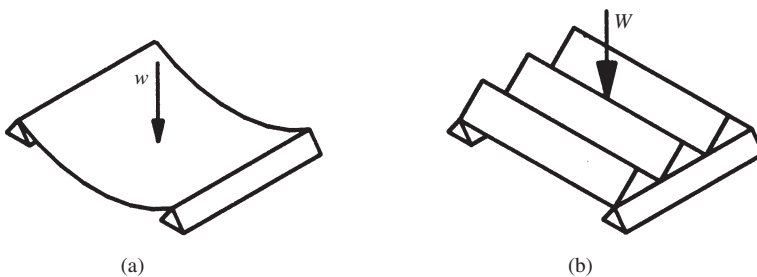


Fig. 4.1 Flat and folded plate

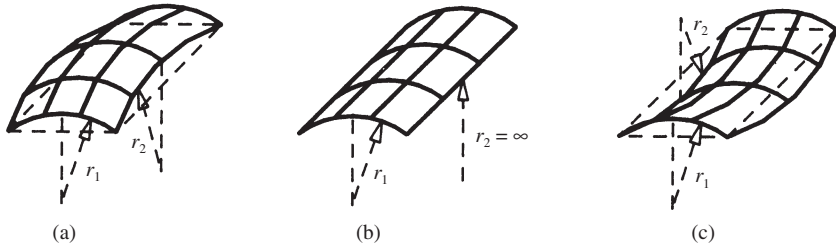


Fig. 4.2 Gaussian curvature of surfaces: (a) positive; (b) zero; (c) negative

curvature which describe the shape of the shell. The product of the two principal curvatures of a surface is known as the *Gaussian curvature* of the surface, so that

$$\text{Gaussian curvature} = \chi_1 \chi_2 = \frac{1}{r_1} \frac{1}{r_2} \quad (4.1)$$

where  $\chi_1, \chi_2$  are the principal curvatures, and  $r_1, r_2$  are the principal radii of curvature.

If the two principal radii are of the same sign (Fig. 4.2(a)), as in a dome, then the surface has positive Gaussian curvature, and bending effects will tend to decay rather rapidly. If one of the principal radii is infinitely large, as in the case of a cylindrical shell (Fig. 4.2(b)), then the surface has zero Gaussian curvature and bending influence will persist over a greater region. Radii of curvature of opposing signs, as in the cooling tower of Table 4.1, produce negative Gaussian curvature (Fig. 4.2(c)), which is also susceptible to bending. Axisymmetric shells are therefore conveniently sub-divided into positive, zero, and negative Gaussian curvature types, it being anticipated that bending influence will be greater for zero or negative Gaussian curvature forms than for shells of positive curvature.

### 4.1.3 Scope of the chapter

As just described, membrane shells resist loads by in-plane forces alone, and membrane effects are also generally predominant in closed axisymmetric shells. The neglect of bending considerably simplifies shell analysis, and the initial treatment will therefore be based on such an assumption. In addition, for reasons of geometric simplicity, only axisymmetric shells will be considered. This restriction excludes the open cylindrical and folded-plate varieties of Table 4.1, which has some consistency with the neglect of bending effects, since bending is of greater significance in these cases.

Further simplification of the analysis is produced if the loads are presumed to be axisymmetric, as well as the shell shape. This further assumption will therefore be made and will have the practical effect of restricting the discussion to dead, snow, over-pressure, and similar loads which may be presumed axisymmetric. Wind and other non-axisymmetric loads will have to be excluded. An analysis derived on the above basis is termed a membrane analysis for thin elastic shells under axisymmetric loading.

A membrane analysis can be helpful even when significant bending occurs, since, as described, the bending effects will sometimes be localized and a membrane solution will then represent the shell behaviour at regions distant from the areas of localized bending. Even when bending is significant throughout the shell, use can be made of a membrane analysis as a 'primary' solution to which 'corrections' are made to allow for the bending effects (Baker *et al.*, 1979; Billington, 1982; Zingoni, 1997). Shell analysis incorporating bending tends to be complex, whether tackled in the way just mentioned or by any other analytic closed-form approach. A numerical technique is therefore often preferred, and the finite element method generally offers the most flexible approach. As an example of the application of the finite element method to shell analysis, the method is therefore applied to the analysis of circular cylindrical shells in the later sections of this chapter. Such an analysis is usually known as a linear thin shell bending analysis.

## 4.2 Membrane theory for axisymmetric shells

### 4.2.1 Basic properties

#### *Geometric preliminaries*

An axisymmetric surface is generated by revolving a curve about an *axis* in its own plane (Fig. 4.3). The generating curve and all curves formed by the intersection of the surface and planes containing the axis are then known as *meridians*. The intersections of the surface with planes which are normal to

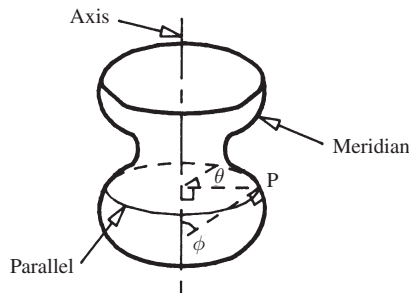
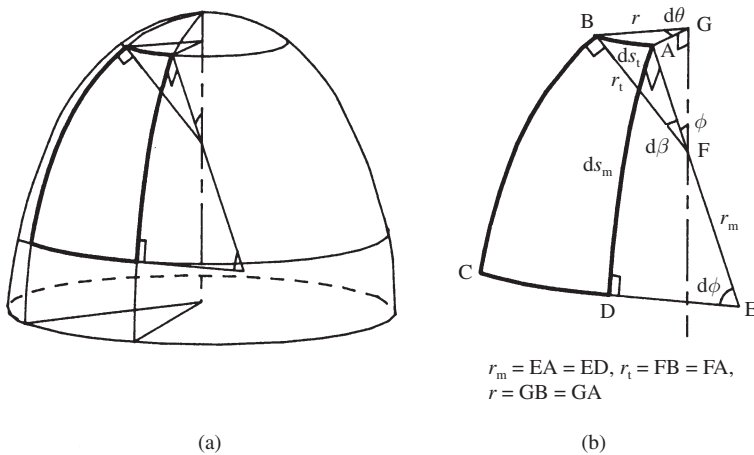


Fig. 4.3 Axisymmetric surface geometry

the axis will be a set of circles which are termed *parallels*. If, for convenience, the axis is taken in the vertical direction, then, for a general point P on the surface, the angle  $\theta$  may be defined as the angle in a horizontal plane between an arbitrary fixed line and the perpendicular from P to the axis. An angle  $\phi$  may also be defined as the angle in a vertical plane between the normal to the surface at P and the axis. If the surface is such that its Gaussian curvature is of constant sign it will then be possible to uniquely define the position of P by the parameters  $\theta$  and  $\phi$ . An example of such a system of position definition is the use of lines of longitude and latitude on the surface of the earth.

'Lines' of curvature on a three-dimensional surface are defined to be curves which have the property that the normals to the surface at adjacent points on a line of curvature are co-planar. Since the normals are co-planar, they will, in general, intersect. A principal *radius of curvature* is then defined as the distance from the surface to such an intersection point. The lines of curvature at any point on the surface may further be shown to be mutually perpendicular (Wang, 1953).

A differential element of an axisymmetric surface is now considered which is bounded by a pair of adjacent meridians and a pair of adjacent parallels (Fig. 4.4(a)). The normal at the point A (Fig. 4.4(b)) will intersect the normal at an adjacent point D on the meridian through A, because, by axisymmetry, both the normals to the surface lie in the vertical plane containing the axis and the meridian. The meridians are therefore lines of curvature for an axisymmetric surface. The normal to the surface at a point B, which is adjacent to A and lies on the parallel through A, will, by axisymmetry, intersect with the normal at A at a point on the axis. The parallels of an axisymmetric surface are therefore also lines of curvature, and the meridians and parallels do possess the orthogonal property of lines of curvature referred to previously.



$$r_m = EA = ED, r_t = FB = FA, \\ r = GB = GA$$

Fig. 4.4 (a) Element of an axisymmetric surface. (b) Enlargement of the element

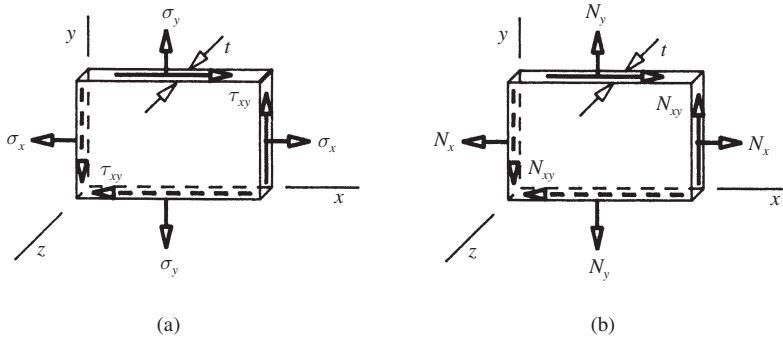


Fig. 4.5 (a) In-plane stresses. (b) In-plane resultants

With reference to Fig. 4.4(b), the following geometric relationships should be noted for future use:

$$ds_m = r_m d\phi \quad (4.2)$$

$$ds_t = r d\theta = r_t d\beta \quad (\text{for small angles}) \quad (4.3)$$

So that

$$d\phi = \frac{ds_m}{r_m}, \quad d\beta = \frac{ds_t}{r_t} \quad (4.4)$$

### Stress resultant preliminaries

As with plates (see Chapter 3), it is convenient, and usual in shell theory, to work in terms of stress resultants rather than in terms of the stresses themselves. The stress resultants are taken to be the resultant forces and moments acting on a normal section which is of unit length. Since only in-plane stresses are considered in membrane theory, the stresses on a plane shell element in Cartesian coordinates will be the plane stress components considered in Chapter 1 (Fig. 4.5(a)). The corresponding stress resultants are illustrated in Fig. 4.5(b), and, since these resultants are taken to act on unit lengths, the stresses are related to the corresponding stress resultants by equations of the form

$$\sigma = \frac{N}{1 \times t} = \frac{N}{t} \quad (4.5)$$

For axisymmetric shells, it is convenient to employ a *curvilinear* set of coordinates based on the meridian and parallel directions. In this case, the direct stress resultants are referred to as the *meridional* and *tangential* stress

resultants; the tangential stress resultant being sometimes alternatively termed the *parallel*, *circumferential*, or *hoop* stress resultant. If the loading is axisymmetric as well as the shell geometry, as assumed here, then, by symmetry, the tangential stress resultant must be constant along any given parallel. It also follows that the shear stress resultants, which would produce non-symmetric deformations, must be everywhere zero. The stress resultants therefore take the form illustrated in Fig. 4.6(a) where the tangential component has been assumed constant but the variation of the meridional component has been differentially included. There is a geometric parallel to this stress resultant situation in that the distance along any meridian between adjacent parallels will be constant but the distance along parallels between adjacent meridians will vary. Again, this is reflected in the figure.

### Equilibrium

Since only two stress resultants need to be determined at any point, a solution may be obtained by statics alone. Equilibrium must be ensured in the parallel, meridional and normal coordinate directions. The constancy of the tangential stress resultant fulfils the equilibrium condition in the parallel direction, and the appropriate conditions in the remaining two directions are then sufficient for the determination of the two unknown stress resultants.

Equilibrium in the normal direction is considered first, and the component of the external load in this direction is taken to be a pressure,  $p$  (Fig. 4.6(a)), which is measured per unit area of shell surface. To determine the components of the two stress resultants in the normal direction, it is helpful to consider the

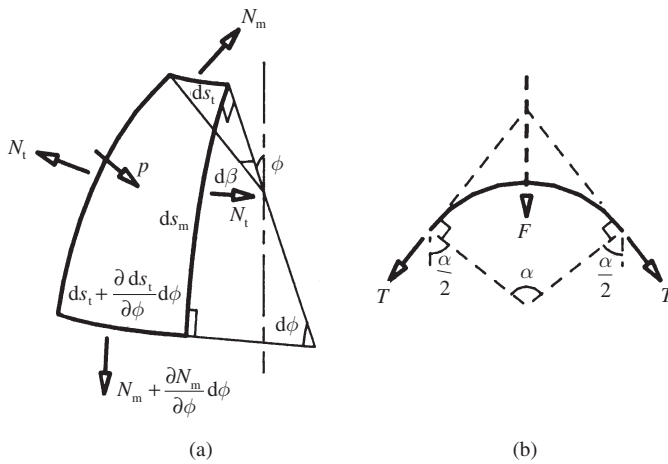


Fig. 4.6 (a) Element of shell. (b) Circular arc tension

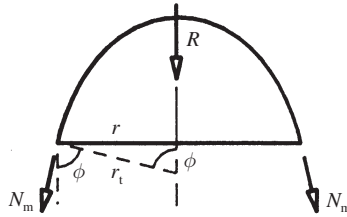


Fig. 4.7 Shell frustum

resultant of a constant tension,  $T$ , acting around a circular arc (Fig. 4.6(b)). In this case, the radial resultant,  $F$ , is given by

$$F = 2T \sin \frac{\alpha}{2} = T\alpha \quad (\text{for small } \alpha) \quad (4.6)$$

Using this result to calculate the components of the stress resultants in the normal direction, the relevant equilibrium equation is established as

$$(N_t ds_m) d\beta + (N_m ds_t) d\phi + p ds_m ds_t = 0 \quad (4.7)$$

where increments of  $N_m$  and  $ds_t$  have been neglected as second-order quantities.

Substituting from equations (4.4) gives

$$N_t ds_m \frac{ds_t}{r_t} + N_m ds_t \frac{ds_m}{r_m} + p ds_m ds_t = 0$$

Whence

$$\frac{N_t}{r_t} + \frac{N_m}{r_m} + p = 0 \quad (4.8)$$

Equation (4.8) is the final form of the first equilibrium equation. As indicated above, the second equilibrium equation could be obtained by resolution in the meridional direction. It is, however, more convenient to consider the vertical equilibrium of a frustum of the shell above an arbitrary parallel (Fig. 4.7).

The advantage gained in using such a frustum of the shell is that, by taking the section along a parallel, only the meridional stress resultant is sectioned (Fig. 4.8) and the vertical equilibrium equation is therefore independent of the tangential stress resultant. Thus, resolving vertically for the frustum,

$$(2\pi r)N_m \sin \phi + R = 0 \quad (4.9)$$

where  $R$  is the total vertical component of the applied load on the frustum.

For any given problem, therefore, the meridional stress resultant may be determined directly from equation (4.9) and substitution in equation (4.8) then

provides the tangential stress component. The total vertical component of the applied loading,  $R$ , is in general obtained by suitable integration over the surface of the frustum, but, for the particular cases of a constant normal pressure or a fluid pressure,  $R$  may be obtained more simply from results (Feodosyev, 1968) which are described in the next section. Examples of the application of membrane theory to the analysis of a variety of thin axisymmetric shells and loading conditions are then given.

*Vertical load due to uniform normal pressure*

An elementary portion of the shell surface is considered which is bounded by the parallels defined by angles  $\phi'$  and  $d\phi'$  (Fig. 4.8(a)). The vertical force component,  $dR$ , due to the uniform normal pressure,  $p$ , acting on this surface is then given by

$$dR = (p dA') \cos \phi' = p (dA' \cos \phi') \tag{4.10}$$

The quantity in brackets in equation (4.10) can, however, be shown to be the projected area of  $dA'$  on a horizontal plane at the base of the frustum, that is the annular area,  $dA$  (Fig. 4.8(a)). This follows from the area projection rule which states that areas (Fig. 4.8(b)) project according to

$$dA = dA' \cos \phi' \tag{4.11}$$

Hence

$$R = \int_0^\phi dR = \int_0^\phi p (dA' \cos \phi') = \int_0^\phi p dA = pA = \pi r^2 p \tag{4.12}$$

where  $A$  is the projected area of the shell frustum on a horizontal plane.

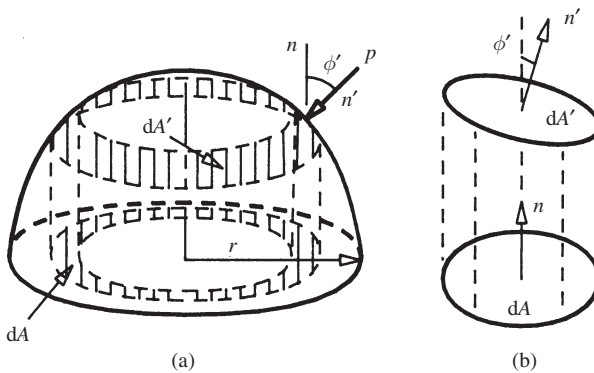


Fig. 4.8 (a) Shell frustum. (b) Area projection



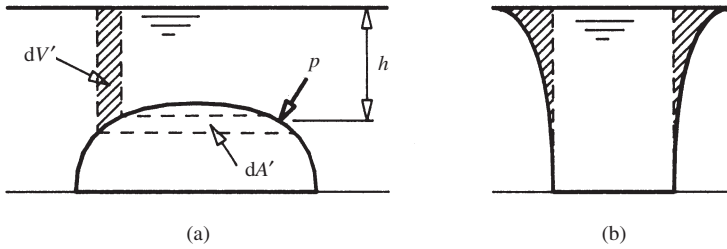


Fig. 4.9 Shell frustums under fluid pressure

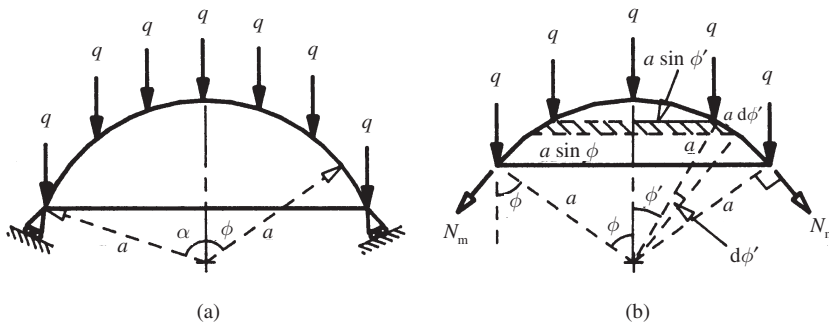


Fig. 4.10 (a) Spherical dome example. (b) Frustum of the dome

Equation (4.12) provides the required expression for the vertical component of load due to a normal pressure acting on a shell frustum, and use of this expression is made in example 4.2 below.

#### Vertical load due to fluid pressure

If a shell frustum is now considered under hydrostatic pressure (Fig. 4.9(a)), then the vertical force due to the normal hydrostatic pressure acting on an elementary area,  $dA'$ , will be given, by the previous theorem, as

$$dR = p dA = \rho g h dA = \rho g dV \quad (4.13)$$

where  $\rho$  is the mass density of the fluid,  $dA$  is the area  $dA'$  when projected onto a horizontal plane, and  $dV$  is the tubular volume generated by rotation of the hatched area in Fig. 4.9(a).

Equation (4.13) therefore shows that the total vertical force,  $R$ , will be equal to the weight of the fluid *supported by* the shell surface. Care is needed in identifying the appropriate weight of supported fluid in cases such as that

illustrated in Fig. 4.9(b), where it is the weight of the hatched volume that is supported by the sides of the frustum shown, *not* the weight of the total contained volume of fluid. This feature is illustrated in example 4.3 below.

#### 4.2.2 Example 4.1 – spherical dome under dead load

The membrane theory of thin shells will be used to determine the membrane forces due to a constant self-weight load,  $q$ /unit area, for a spherical dome of radius  $a$ , which is simply supported and has a half-angle  $\alpha$  (Fig. 4.10(a)).

Following the theory described above, the vertical equilibrium of a frustum of the dome (Fig. 4.10(b)) is considered first. The vertical load acting on an element of the frustum is given by

$$dR = q(2\pi a \sin \phi')(ad\phi')$$

Hence

$$R = 2\pi a^2 q \int_0^\phi \sin \phi' d\phi' = 2\pi a^2 q [-\cos \phi']_0^\phi = 2\pi a^2 q(1 - \cos \phi)$$

Thus, for vertical equilibrium, either resolving directly or by substitution in equation (4.9),

$$(2\pi a \sin \phi)N_m \sin \phi + 2\pi a^2 q(1 - \cos \phi) = 0$$

Whence

$$N_m = \frac{-aq(1 - \cos \phi)}{\sin^2 \phi} = \frac{-aq(1 - \cos \phi)}{1 - \cos^2 \phi} = \frac{-aq}{1 + \cos \phi} \quad (4.14)$$

Equation (4.14) shows that the meridional membrane force is compressive at all points on the dome and that its magnitude increases with increasing  $\phi$ , being bounded by

$$-\frac{aq}{2} \geq N_m \geq -aq \quad (4.15)$$

where the smallest compression occurs at the summit of the dome and the greatest occurs at the base of a hemispherical dome (Fig. 4.11).

Equation (4.8) may now be used to find the tangential membrane force. The geometry of a sphere is particularly simple since the normals at every point on the sphere surface have the same length, namely the sphere radius,  $a$ . Thus, the meridional and tangential radii of curvature are equal and are of length  $a$ , so that substitution in equation (4.8) gives

$$\frac{N_t}{a} + \frac{N_m}{a} + q \cos \phi = 0$$

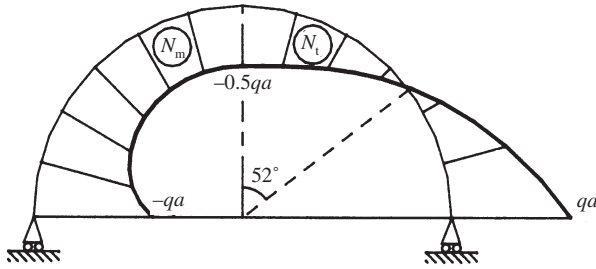


Fig. 4.11 Membrane forces in a hemispherical dome

Whence, substituting for  $N_m$  from equation (4.14) gives

$$N_t = \frac{aq}{1 + \cos \phi} - aq \cos \phi = aq \left[ \frac{1}{1 + \cos \phi} - \cos \phi \right] \quad (4.16)$$

Equation (4.16) shows that the tangential membrane force is also compressive at the dome summit but can become tensile if  $\phi$  is sufficiently large, since the limits for the magnitude of the tangential membrane force are given by

$$-\frac{aq}{2} \leq N_t \leq aq \quad (4.17)$$

where the maximum compression occurs at the dome summit and the maximum tension occurs at the base of a hemispherical dome (Fig. 4.11).

Comparison of equations (4.15) and (4.16) shows that the tangential and meridional membrane forces are equal at the dome summit, a result which is, in fact, true for all axisymmetric domes under axisymmetric loading, since, at the summit, the tangential direction to any given meridian is itself in a meridional direction. The transition from a compressive to a tensile tangential membrane force will take place when, from equation (4.16),

$$\frac{1}{1 + \cos \phi} = \cos \phi$$

or

$$\cos^2 \phi + \cos \phi - 1 = 0$$

whence  $\phi = 52^\circ$ .

Thus, if the dome half-angle is greater than  $52^\circ$ , the tangential stress will become tensile towards the base of the dome, reflecting the action of the tangential fibres in restraining the tendency of the meridional fibres to 'bulge' outwards.

### 4.2.3 Limitations of membrane theory

It will be noticed that the ‘simple supports’ (Fig. 4.10(a)) referred to in example 4.1 consist of roller supports which are tangential to the meridian at the base of the dome, so that the equivalent form of support based on rods would be as shown in Fig. 4.12(a). This type of support is sometimes used in practice, but more frequently the support provides a vertical reaction only (Fig. 4.12(b)). In this case, the reaction cannot be equilibrated by the meridional force at the base, and a shear force (Fig. 4.12(b)), and hence bending, must exist if equilibrium is to be ensured. One effect of vertical supports is therefore to produce bending in the edge region but they will also substantially modify the membrane forces in this area, since these forces, particularly in the tangential (parallel) direction, must now provide the horizontal component of restraint which was previously given by the support. The result is that very substantial tangential tensile forces are developed towards the rim of the dome (problem 4.1). To accommodate these tensile forces, it is normal to provide a ring beam at the support (Fig. 4.12(c)), which will absorb the tangential tension by providing a horizontal restraint. Bending will, however, still be produced in the neighbourhood of the connection of the ring to the shell, since the strains in the ring and the base of the shell, as determined by membrane theory, may be shown to be incompatible.

Non-meridional and (for obvious reasons) moment-resistant supports therefore result in shell bending but these are by no means the only features to have this effect. Bending will always exist close to *lines of distortion* on the shell middle surface (Gol’denveizer, 1961). These lines of distortion occur at points of discontinuity and, for axisymmetric shells, will take the form of parallel circles. Lines of distortion are created by:

- (a) shell edges along which either no, or other than tangential, support is provided;
- (b) discontinuities in the applied loading;

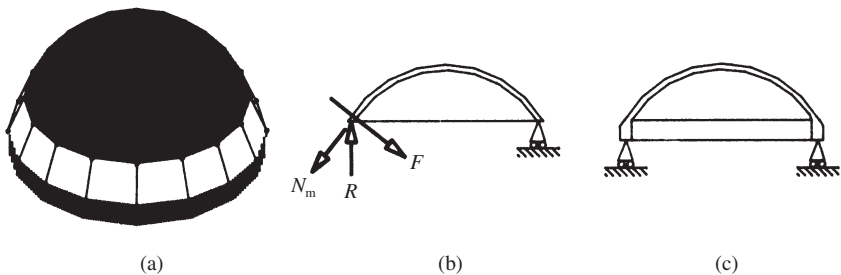


Fig. 4.12 (a) Meridionally (simply) supported dome. (b) Vertically supported dome. (c) Dome with ring beam

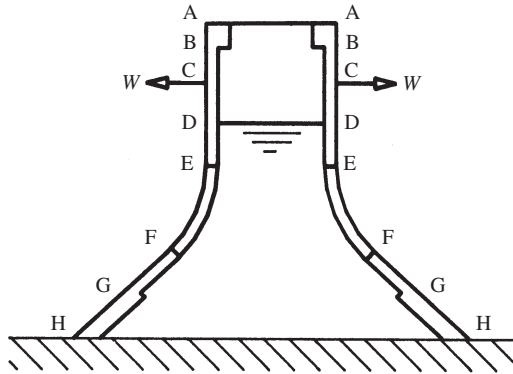


Fig. 4.13 Lines of distortion example shell

- (c) curvature discontinuities;
- (d) abrupt changes in the elastic properties or thickness of the shell material.

The fluid container example shown in Fig. 4.13 will be used to illustrate the various types of lines of distortion which will exist at the lettered sections: at AA due to the free edge, at BB due to the change in thickness at the end of the rim stiffener, at CC due to the ring point load, at DD due to the discontinuity in changing from an unloaded state to a fluid pressure load, at EE due to the change from a straight to a curved generator, at FF also due to the abrupt change in curvature, at GG due to the thickness change, and at HH due to the non-tangential, in fact encasté, support.

If no lines of distortion exist, then membrane theory can be expected to provide an accurate solution for all points on the shell, except in the case of 'shallow' shells, the behaviour of which resembles that of plates and hence involves bending. When lines of distortion do exist, then the question arises as to whether the consequent bending will be restricted to an area local to the line of distortion or not. If the bending is localized, then a membrane solution will be valid for all parts of the shell remote from the lines of distortion, in the region of which a separate investigation will be needed. Clearly, no localization of bending will take place if the lines of distortion are close together as in the example of Fig. 4.13. Gol'denveizer (1961) shows that the spread of the bending effects will be considerable whenever a line of distortion touches a line of zero curvature on the shell. This concept explains the localized nature of bending effects in shells of positive curvature referred to earlier (see Section 4.1.2), since such forms do not possess lines of zero curvature. On the other hand, shells of zero or negative curvature (see Fig. 4.2) will both exhibit lines of zero curvature and hence be susceptible to widespread bending if a zero-curvature line touches a line of distortion.

### 4.2.4 Example 4.2 – paraboloid dome under internal pressure

The membrane forces in a paraboloid dome under a uniform internal pressure,  $p$ /unit area, will be determined. The dome is presumed to be ‘simply supported’ (Fig. 4.14(a)) so that membrane theory will be applicable to the complete shell surface. Uniform internal pressure loads are encountered in practice either when shells are used for the storage of gases or when flexible inflated structures are subjected to their initial, prestressing over-pressure.

It is assumed that the shell is generated from a parabolic curve of the form

$$2ay = x^2 \tag{4.18}$$

where  $a$  is a constant.

Since it is convenient to work in terms of the parametric coordinate,  $\phi$ , the Cartesian coordinates,  $x$  and  $y$ , and the principal radii of curvature must first be expressed in terms of  $\phi$ .

Thus, from Fig. 4.14(a) and equation (4.18),

$$\frac{dy}{dx} = \tan \phi = \frac{1}{2a} 2x = \frac{x}{a} \tag{4.19}$$

Hence

$$x = a \tan \phi \tag{4.20a}$$

and, from equation (4.18),

$$y = \frac{a}{2} \tan^2 \phi \tag{4.20b}$$

Then, from Fig. 4.14(a),

$$r = x = a \tan \phi \tag{4.21}$$

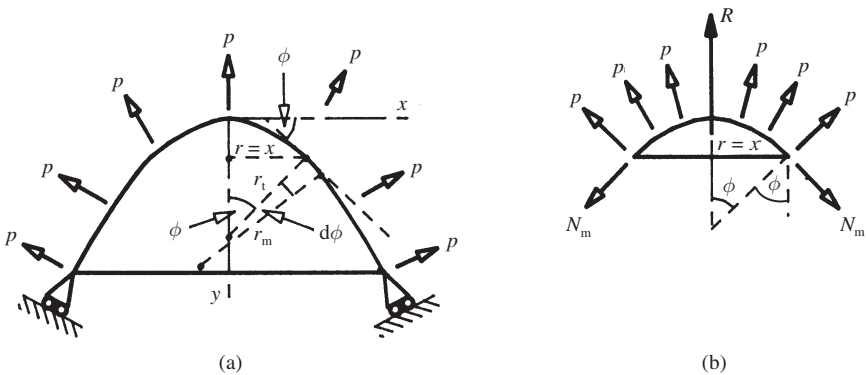


Fig. 4.14 (a) Paraboloid dome example. (b) Frustum of the dome

and

$$r_i = \frac{x}{\sin \phi} = \frac{a}{\cos \phi} \quad (4.22)$$

Now

$$r_m = \frac{[1 + (dy/dx)^2]^{3/2}}{d^2y/dx^2} \quad (4.23)$$

and, from equation (4.19),

$$\frac{dy}{dx} = \tan \phi \quad (4.24)$$

Also,

$$\frac{d^2y}{dx^2} = \frac{d}{dx} \left( \frac{dy}{dx} \right) = \frac{d}{dx} \left( \frac{x}{a} \right) = \frac{1}{a} \quad (4.25)$$

Substituting from equations (4.24) and (4.25) in equation (4.23) gives

$$r_m = \frac{(1 + \tan^2 \phi)^{3/2}}{1/a} = \frac{a}{\cos^3 \phi} \quad (4.26)$$

With the aid of these geometric relationships, the membrane forces may be determined in a similar fashion to that employed previously. Since a uniform normal pressure is involved, equation (4.12) may be used to determine the resultant vertical component of the load on a frustum of the shell (Fig. 4.14(b)). Thus, using equation (4.12) and subsequently substituting from equation (4.21),

$$R = -\pi r^2 p = -\pi a^2 \tan^2 \phi p \quad (4.27)$$

where the negative sign indicates the upward direction of  $R$ .

Then, resolving vertically for the shell frustum,

$$2\pi r N_m \sin \phi - \pi a^2 \tan^2 \phi p = 0$$

Whence

$$N_m = \frac{ap}{2 \cos \phi} \quad (4.28)$$

Substitution in equation (4.8) for  $N_m$ ,  $r_m$  and  $r_i$  from equations (4.28), (4.23) and (4.22), respectively, gives

$$\frac{ap \cos^3 \phi}{2 \cos \phi a} + \frac{N_i \cos \phi}{a} - p = 0$$

where the negative sign indicates the outward direction of  $p$ . Whence

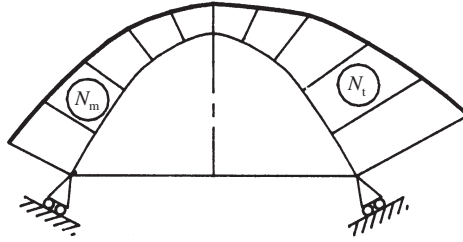


Fig. 4.15 Paraboloid dome membrane force distributions

$$N_t = \frac{ap}{\cos \phi} \left( 1 - \frac{\cos^2 \phi}{2} \right) = \frac{ap}{2 \cos \phi} (1 + \sin^2 \phi) \quad (4.29)$$

Equation (4.28) shows that, as expected for an internal pressure, the meridional membrane force is tensile throughout and increases with increasing  $\phi$ . The tangential membrane force (equation (4.29)) is also tensile everywhere and also increases with increasing  $\phi$ , but does so at a faster rate than the meridional force. Typical distributions of the two membrane forces over the surface of a paraboloid shell are shown in Fig. 4.15, where the equality of the forces at the dome summit, mentioned in the spherical case, should be noted.

#### 4.2.5 Example 4.3 – conical shell under fluid pressure

The conical tank shown in Fig. 4.16(a) is presumed to be full of fluid, and it is required to determine the distribution of the membrane forces in the tank walls due to the fluid pressure.

Following the normal procedure, the total vertical component of the applied load acting on a frustum of the shell (Fig. 4.16(b)) will be determined first. Thus, for an element of the frustum (Fig. 4.16(b)),

$$dR = (2\pi x') p ds' \cos \alpha \quad (4.30)$$

The tank walls are generated from a straight line given by

$$y = \tan \alpha x \quad (4.31)$$

Hence

$$x' = \frac{y'}{\tan \alpha} \quad (4.32)$$

Also, from Fig. 4.16(b),

$$ds' = \frac{dy}{\sin \alpha} \quad (4.33)$$



While the fluid pressure,  $p$ , is given by

$$p = \rho g(H - y') \quad (4.34)$$

where  $\rho$  is the mass density of the liquid. Thus

$$dR = 2p \frac{y'}{\tan \alpha} \rho g(H - y') \frac{dy'}{\sin \alpha} \cos \alpha$$

or

$$dR = \frac{2\pi\rho g}{\tan^2 \alpha} y'(H - y') dy'$$

The total vertical component of the applied load acting on the frustum is therefore given by

$$R = \frac{2\pi\rho g}{\tan^2 \alpha} \int_y^H y'(H - y') dy' \quad (4.35)$$

Hence

$$R = \frac{2\pi\rho g}{\tan^2 \alpha} \left[ \frac{Hy'^2}{2} - \frac{y'^3}{3} \right]_y^H \quad (4.36)$$

and

$$R = \frac{2\pi\rho g}{\tan^2 \alpha} \left[ \frac{H^3}{6} - \frac{Hy^2}{2} + \frac{y^3}{3} \right] \quad (4.37)$$

Alternatively, and more simply, the vertical load acting on the frustum may be obtained by application of the theorem of supported fluid weight described above. In this case, the weight of the fluid supported by the walls of the

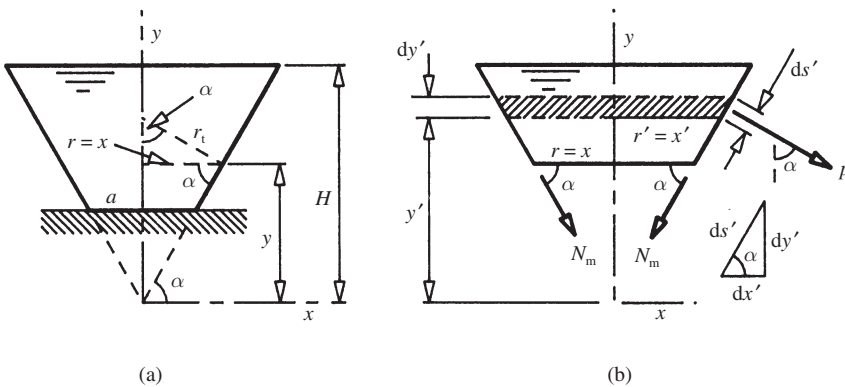


Fig. 4.16 (a) Conical tank example. (b) Frustum of the tank

frustum is the weight of fluid contained in the volume swept out by rotation of the hatched area in Fig. 4.17. Thus, with reference to Fig. 4.17,

$$dR = \rho g dV = \rho g 2\pi x'(H - y') dx' = \rho g 2\pi \frac{y'}{\tan \alpha} (H - y') \frac{dy'}{\tan \alpha}$$

So that

$$R = \frac{2\pi\rho g}{\tan^2 \alpha} \int_y^H y'(H - y') dy'$$

Whence, as before,

$$R = \frac{2\pi\rho g}{\tan^2 \alpha} \left[ \frac{H^3}{6} - \frac{Hy^2}{2} + \frac{y^3}{3} \right]$$

Thus, resolving vertically for the frustum gives,

$$(2\pi x) N_m \sin \alpha + \frac{2\pi\rho g}{\tan^2 \alpha} \left[ \frac{H^3}{6} - \frac{Hy^2}{2} + \frac{y^3}{3} \right] = 0$$

or

$$\frac{y}{\tan \alpha} N_m \sin \alpha + \frac{\rho g}{\tan^2 \alpha} \left[ \frac{H^3}{6} - \frac{Hy^2}{2} + \frac{y^3}{3} \right] = 0$$

Whence

$$N_m = -\frac{\rho g}{y \sin \alpha \tan \alpha} \left[ \frac{H^3}{6} - \frac{Hy^2}{2} + \frac{y^3}{3} \right] \quad (4.38)$$

To obtain the tangential membrane force, equation (4.8) is used once more. Since the meridians of a cone are straight lines:

$$r_m = \infty$$

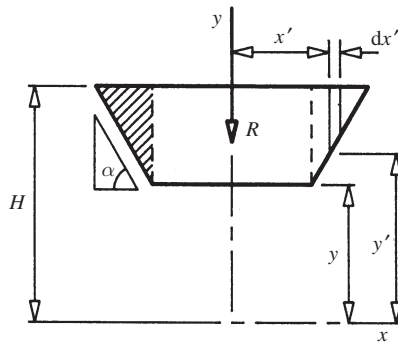


Fig. 4.17 Vertical load on conical frustum

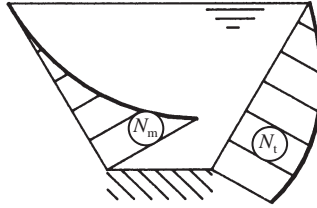


Fig. 4.18 Membrane forces in a conical tank

Also, from Fig. 4.17(a),

$$r_t = \frac{x}{\sin \alpha}$$

Thus, from equation (4.8),

$$\frac{\sin \alpha N_t}{x} - p = 0$$

where the negative sign occurs due to the outward direction of  $p$ . Hence

$$N_t = \frac{px}{\sin \alpha} = \frac{\rho g(H-y)x}{\sin \alpha} = \frac{\rho g(H-y)y}{\sin \alpha \tan \alpha} \quad (4.39)$$

Equations (4.38) and (4.39) show that the meridional and tangential membrane forces are compressive and tensile respectively throughout the shell. Differentiation of the two equations further shows that the maximum meridional force occurs at the base of the tank but that the maximum tangential force occurs when  $y = H/2$ .

The distribution of the membrane forces therefore takes the form illustrated in Fig. 4.18 for a typical tank. It will be noted from Fig. 4.18 that the meridional membrane force becomes large towards the base of the tank and, indeed, equation (4.38) predicts that this force becomes infinite at the apex of a cone. Such infinite forces do not of course exist physically, since the membrane force distribution in the neighbourhood of a cone apex is substantially modified due to the bending effects which must exist in this region due to the abrupt geometric change at the apex. Also, if the base of the tank is provided with an encasté support as indicated in this example, then bending effects will again be present in the lower regions of the tank. The moment resistance provided by such a support will obviously induce bending moments but the membrane force distributions will also be significantly modified. For example, the tangential force distribution predicted by membrane theory includes a substantial force at the tank base (Fig. 4.18). If horizontal movement is prevented at the base, however, the tangential strain at the base will be zero and, hence (for zero Poisson's ratio), the tangential stress and membrane force will also be zero.

### 4.3 Bending of circular cylindrical shells

The inclusion of bending in classical shell theory considerably increases the complexity of the problem. Nevertheless, solutions for a wide range of shell geometries and loading conditions have been obtained (Gibson, 1980; Timoshenko and Woinowsky-Krieger, 1981; Flügge, 1960). However, features such as varying thickness, complex loading or irregular shell shapes can all render solutions by classical methods, at best, difficult and, at worst, intractable. These situations therefore generally require the use of a numerical approach, and a variety of methods is available. The relevant differential equations may be numerically integrated directly (Kraus, 1967) or through a finite difference approximation (Ghali, 1979; Soare, 1967). The finite element method is, however, currently the generally preferred technique and, as an example of a numerical approach, the application of the finite element method will be described, as applied to the bending analysis of closed, circular cylindrical shells under axisymmetric, radial loading. The chosen shell geometry and loading are thus the simplest possible but the concepts established may be extended to more general shells and loads.

#### 4.3.1 Finite element method

Since, under axisymmetric conditions, the behaviour of a segment of a cylindrical shell is the same as that of any other segment of the same arc length, a segment of unit arc length (Fig. 4.19(a)) will be considered for convenience. Also, the meridians of a cylindrical shell are parallel to its axis, and it is convenient to use the axial coordinate,  $y$ , as the single independent position variable. For a circular cylinder of given radius,  $r$ , the distance  $y$  then locates a unique

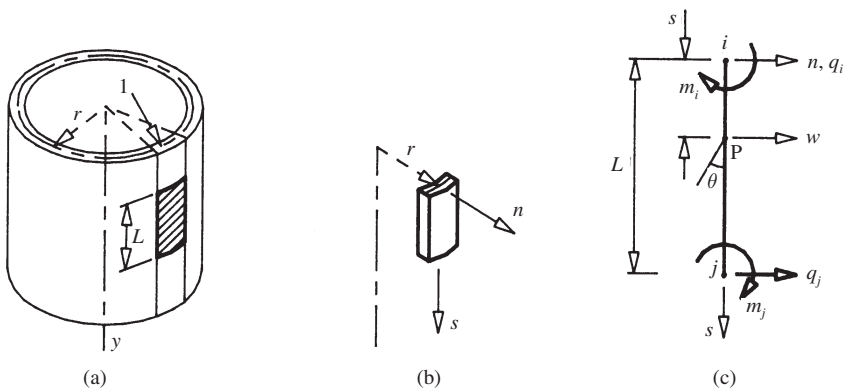


Fig. 4.19 (a) Circular cylindrical shell. (b) Finite element. (c) Finite element (diagrammatic)

parallel, the position along which is immaterial in view of the axisymmetry. A length,  $L$ , of the segment of unit arc length will be taken as the basic finite element (Fig. 4.19(b)), and the displacement variables at a general point P will be the radial displacement,  $w$ , and the rotation about a tangential axis,  $\theta$ . These displacements are shown related to a local set of meridional ( $s$ ) and radial ( $n$ ) axes in Fig. 4.19(c). As with plates, the chosen displacement components are not independent of each other, since (Fig. 4.19(c))

$$\theta = -\frac{dw}{ds} \quad (4.40)$$

The element has two nodes and, hence, four nodal displacement variables. Also, there is only one independent displacement variable, say  $w$ , so that the relationship to be assumed between  $w$  and the position coordinate,  $s$ , must contain four undetermined coefficients. Thus, using the simplest polynomial with four undetermined coefficients,

$$w = \alpha_1 + \alpha_2 s + \alpha_3 s^2 + \alpha_4 s^3 \quad (4.41)$$

Hence, from equation (4.40),

$$\theta = -\frac{dw}{ds} = -\alpha_2 - 2\alpha_3 s - 3\alpha_4 s^2 \quad (4.42)$$

Applying equations (4.41) and (4.42) to the nodes,  $i$  and  $j$ , the nodal displacement variables may be related to the unknown coefficients by

$$\{\delta^e\} = \begin{Bmatrix} w_i \\ \theta_i \\ w_j \\ \theta_j \end{Bmatrix} = \begin{bmatrix} 1 & 0 & 0 & 0 \\ 0 & -1 & 0 & 0 \\ 1 & L & L^2 & L^3 \\ 0 & -1 & -2L & -3L^2 \end{bmatrix} \{\alpha\} = [C^e] \{\alpha\} \quad (4.43)$$

Then, solving the linear equations represented by equation (4.43), the unknown coefficients may be related to the nodal displacements by

$$\{\alpha\} = \begin{bmatrix} 1 & 0 & 0 & 0 \\ 0 & -1 & 0 & 0 \\ -\frac{3}{L^2} & \frac{2}{L} & \frac{3}{L^2} & \frac{1}{L} \\ \frac{2}{L^3} & -\frac{1}{L^2} & -\frac{2}{L^3} & -\frac{1}{L^2} \end{bmatrix} \{\delta^e\} = [C^e]^{-1} \{\delta^e\} \quad (4.44)$$

The next step in the general finite element formulation technique (see Appendix B) requires the strain vector at P to be related to the displacement variables at that point. To establish a suitable strain vector for the present element, it is helpful to consider initially the stress resultants which will act at

a point on the element. In Fig. 4.20(a), the bending moment in the tangential direction,  $M_t$ , is constant due to axisymmetry and hence there is no shear force in this direction. For similar reasons, there are no twisting moments, but the bending moment in the meridional direction,  $M_m$ , will vary and therefore be accompanied by a shear force,  $Q_m$ . As with plates, all the stress resultants will be measured per unit length of the shell element.

For the conditions considered, the meridional direct force may be readily shown to be zero, since, with radial loading only (Fig. 4.21), vertical resolution for a frustum of the cylinder gives

$$2\pi r N_m = 0 \tag{4.45}$$

The cylinder is therefore subject to uni-axial direct force in the tangential direction, so that

$$N_m = \sigma_t(1 \times t) = Et\varepsilon_t \tag{4.46}$$

Also, due to the uni-axial direct stress,

$$\varepsilon_m = -\nu\varepsilon_t \tag{4.47}$$

It follows from equation (4.47) that there is only one independent direct strain which may conveniently be taken to be the tangential one. The tangential strain may be related to the independent displacement variable,  $w$ , by consideration of Fig. 4.20(b), as follows:

$$\varepsilon_t = \frac{2\pi[(r+w) - r]}{2\pi r} = \frac{w}{r} \tag{4.48}$$

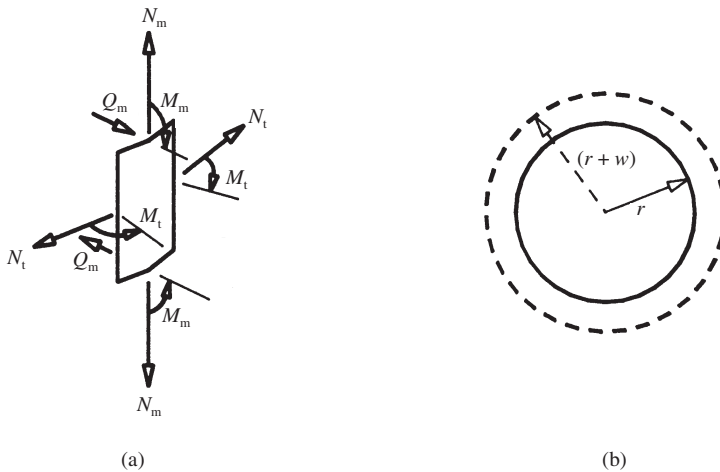


Fig. 4.20 (a) Element stress resultants. (b) Radial displacement

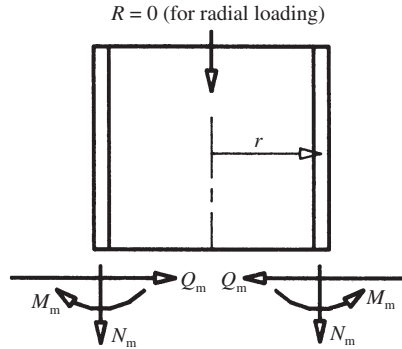


Fig. 4.21 Cylindrical shell frustum

To relate the bending moments to the corresponding curvatures the first two of equations (3.7) may be employed, provided that the negative signs in the equations are made positive to reflect the opposing relative orientations of the normal axis and the moments in Figs 3.7 and 3.8 and Figs 4.19(b) and 4.20(a). Thus,

$$M_m = D(\chi_m + \nu\chi_t), \quad M_t = D(\nu\chi_m + \chi_t) \quad (4.49)$$

where  $D = Et^3/12(1 - \nu^2)$ . The meridional curvature may be related to the radial displacement,  $w$ , by the normal small-slope relationship of

$$\chi_m = \frac{d^2w}{ds^2} \quad (4.50)$$

The change in tangential curvature may be established from Fig. 4.20(b) as

$$\chi_t = \frac{1}{r+w} - \frac{1}{r} = \frac{r - (r+w)}{r(r+w)} \approx -\frac{w}{r^2} \quad (4.51)$$

This curvature change is an order smaller than the tangential direct strain (equation (4.48)), and therefore, to a first order,

$$\chi_t = 0 \quad (4.52)$$

Hence, there is only one independent curvature, that in the meridional direction, and equations (4.49) become

$$M_m = D\chi_m = \frac{Et^3}{12(1 - \nu^2)} \chi_m \quad (4.53a)$$

and

$$M_t = \nu D\chi_m = \nu M_m \quad (4.53b)$$

On the basis of the above, the independent ‘stress’ and ‘strain’ variables, which may be shown to satisfy the internal virtual work requirement of Appendix B if a unit *length* of element is considered, will be taken to be

$$\{\sigma\} = \begin{Bmatrix} N_t \\ M_m \end{Bmatrix}, \quad \{\varepsilon\} = \begin{Bmatrix} \varepsilon_t \\ \chi_m \end{Bmatrix} \quad (4.54)$$

Also, using the strain–displacement relationships of equations (4.48) and (4.50), in conjunction with equation (4.41), the strains may be related to the undetermined coefficients by

$$\{\varepsilon\} = \begin{Bmatrix} \frac{w}{r} \\ \frac{d^2w}{ds^2} \end{Bmatrix} = \begin{bmatrix} \frac{1}{r} & \frac{s}{r} & \frac{s^2}{r} & \frac{s^3}{r} \\ 0 & 0 & 2 & 6s \end{bmatrix} \{\alpha\} \quad (4.55)$$

So that, using equation (4.44),

$$\{\varepsilon\} = \begin{bmatrix} \frac{1}{r} & \frac{s}{r} & \frac{s^2}{r} & \frac{s^3}{r} \\ 0 & 0 & 2 & 6s \end{bmatrix} \begin{bmatrix} 1 & 0 & 0 & 0 \\ 0 & -1 & 0 & 0 \\ -\frac{3}{L^2} & \frac{2}{L} & \frac{3}{L^2} & \frac{1}{L} \\ \frac{2}{L^3} & -\frac{1}{L^2} & -\frac{2}{L^3} & -\frac{1}{L^2} \end{bmatrix} \{\delta^e\} = [B]\{\delta^e\} \quad (4.56)$$

The strain matrix  $[B]$  is therefore given, by expansion of equation (4.56), as

$$[B] = \begin{bmatrix} \frac{1-3p^2+2p^3}{r} & \frac{L(-p+2p^2-p^3)}{r} & \frac{3p^2-2p^3}{r} & \frac{L(p^2-p^3)}{r} \\ \frac{-6+12p}{L} & \frac{4-6p}{L} & \frac{6-12p}{L^2} & \frac{2-6p}{L} \end{bmatrix} \quad (4.57)$$

where  $p = s/L$ . The elasticity relationships are obtained by combining equations (4.46) and (4.53a) to give

$$\{\sigma\} = \begin{Bmatrix} N_t \\ M_m \end{Bmatrix} = \begin{bmatrix} Et & 0 \\ 0 & \frac{Et^3}{12(1-\nu^2)} \end{bmatrix} \begin{Bmatrix} \varepsilon_t \\ \chi_m \end{Bmatrix} = [D]\{\varepsilon\} \quad (4.58)$$

The stresses at the general point P (Fig. 4.19(c)) may now be related to the element nodal displacements by substituting in equation (4.58) from equation (4.56) to give the standard equation

$$\{\sigma\} = [D][B]\{\delta^e\} = [H]\{\delta^e\} \quad (4.59)$$



Since the strain matrix,  $[B]$ , varies with the position of  $P$ , the stresses will also vary along the member. The practice of evaluating the stresses at the element nodes will therefore be adopted, as was done in the case of the slab element of Chapter 3. In this instance, the element (Fig. 4.19(c)) has two nodes, so that substituting for nodes  $i$  ( $p = 0$ ) and  $j$  ( $p = 1$ ), in turn, in an expanded form of equation (4.59), produces the desired relationship between element nodal stresses and element nodal displacements as

$$\{\sigma^e\} = \begin{Bmatrix} N_{ti} \\ M_{mi} \\ N_{tj} \\ M_{mj} \end{Bmatrix} = \begin{bmatrix} \mu & 0 & 0 & 0 \\ -6\beta & 4\beta & 6\beta & 2\beta \\ L & L & L & L \\ 0 & 0 & \mu & 0 \\ \beta & -2\beta & -6\beta & -4\beta \\ L & L & L & L \end{bmatrix} \{\delta^e\} = [H^e] \{\delta^e\} \quad (4.60)$$

where

$$\mu = \frac{Et}{r}, \quad \beta = \frac{Et^3}{12(1-\nu^2)L}$$

General finite element theory (equation (B.11)) may now be invoked to determine the element stiffness matrix. It should be recalled, however, that equation (B.11) presupposes the definition of element nodal force variables such that  $\{\delta^e\}^T \{f^e\}$  represents a quantity of work. It may be shown that this requirement is satisfied if the nodal force variables (Fig. 4.19(c)) are as defined below:

$$\{f^e\} = \begin{Bmatrix} f_i \\ f_j \end{Bmatrix} \quad (4.61)$$

where

$$\{f_i\} = \begin{Bmatrix} q_i \\ m_i \end{Bmatrix}$$

It should also be recalled, from the above, that the chosen element stress and strain variables are such that  $\{\varepsilon\}^T \{\sigma\}$  represents an amount of work per unit *length* of element so that the integral of equation (B.11) is taken along the length of the element and the element stiffness matrix is given by

$$[k] = \int_0^L [B]^T [D] [B] ds = \int_0^1 [B]^T [D] [B] L dp \quad (4.62)$$

The expanded form of the element stiffness matrix may be derived by substituting in equation (4.62) from equations (4.57) and (4.58) and then evaluating the integral. As an example of this process, one term ( $k_{11}$ ) of the element stiffness matrix will now be derived. Thus,

$$[B]^T[D][B]=$$

$$\begin{bmatrix} \frac{1-3p^2+2p^3}{r} & \frac{-6+12p}{L^2} \\ \vdots & \vdots \end{bmatrix} \begin{bmatrix} Et & 0 \\ 0 & \frac{Et^3}{12(1-\nu^2)} \end{bmatrix} \begin{bmatrix} \frac{1-3p^2+2p^3}{r} & \dots \\ \frac{-6+12p}{L^2} & \dots \end{bmatrix}$$

So that

$$\begin{aligned} k_{11} &= \frac{Et}{r^2} \int_0^1 (1-3p^2+2p^3)^2 L dp + \frac{Et^3}{12(1-\nu^2)} \int_0^1 \frac{(-6+12p)^2}{L^4} L dp \\ &= \alpha \int_0^1 (1-6p^2+4p^3+9p^4-12p^5+4p^6) dp + \frac{\beta}{L^2} \int_0^1 36(1-4p+4p^2) dp \end{aligned}$$

where

$$\alpha = \frac{EtL}{r^2} \quad \text{and} \quad \beta = \frac{Et^3}{12(1-\nu^2)L}$$

Hence

$$\begin{aligned} k_{11} &= \alpha \left[ p - 2p^3 + p^4 + \frac{9p^5}{5} - 2p^6 + \frac{4p^7}{7} \right]_0^1 + \frac{36\beta}{L^2} \left[ p - 2p^2 + \frac{4p^3}{3} \right]_0^1 \\ &= \frac{13\alpha}{35} + \frac{12\beta}{L^2} \end{aligned}$$

The remaining terms may be determined in a similar fashion, and the resulting element stiffness matrix is

$$[k] = \begin{bmatrix} k1 & k2 & k3 & k4 \\ & k5 & -k4 & k6 \\ \text{---} & \text{---} & k1 & -k2 \\ \text{sym.} & & & k5 \end{bmatrix} \quad (4.63)$$

where

$$\begin{aligned} k1 &= \frac{13\alpha}{35} + \frac{12\beta}{L^2}, \quad k2 = -\frac{11\alpha L}{210} - \frac{6\beta}{L}, \quad k3 = \frac{9\alpha}{70} - \frac{12\beta}{L^2} \\ k4 &= \frac{13\alpha L}{420} - \frac{6\beta}{L}, \quad k5 = \frac{\alpha L^2}{105} + 4\beta, \quad k6 = -\frac{\alpha L^2}{140} + 2\beta \end{aligned}$$

and

$$\alpha = \frac{EtL}{r^2}, \quad \beta = \frac{Et^3}{12(1-\nu^2)L}$$

The  $\beta$ -coefficients in equation (4.63) may be observed to have the same form as the element stiffness coefficients for a beam element, a property which results from the adoption of a cubic displacement function in both instances.

As when the finite element method was considered previously, a numerical example will be provided to reinforce the theoretical description just given. For the example considered below, it is possible to obtain a solution of acceptable accuracy by 'hand'. It should, however, again be emphasized that this will, in general, not be the case and the use of fully automated computer packages is normally essential.

### 4.3.2 Example 4.4 – circular tank of uniform thickness

The circular cylindrical tank of Fig. 4.22(a) is monolithically connected to a base slab which is sufficiently rigid for encastré support conditions to be assumed at the base of the tank.

The tank is to be analysed for the effects of a ring moment of 10 kN m/m applied to its rim. Such a moment could in practice arise from the effect of a roof cover which is eccentrically supported by the tank walls. Since an isolated bending load of this form can be expected to result in a localized response, the element sub-division should coarsen with distance from the rim. Accordingly, the sub-division shown in Fig. 4.22(b) is selected for analysis, which results in four different types of element being involved, of lengths 0.5, 1, 2 and 4 m.

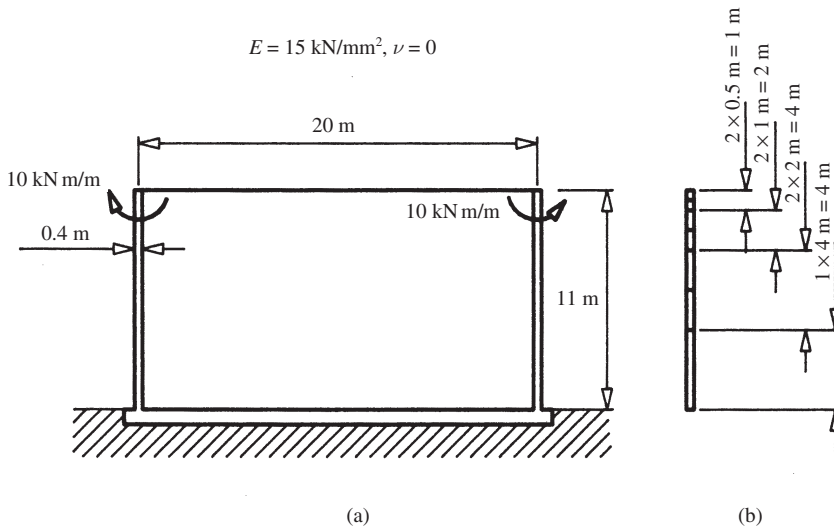


Fig. 4.22 (a) Uniform circular tank example. (b) Element sub-division

*Displacement solution*

The element stiffness matrices for the four types of element may be obtained by suitable substitution in equation (4.63). Thus, using the data of Fig. 4.22(a) for an element of length 0.5 m, then, in kilonewton and metre units,

$$\alpha = \frac{15 \times 10^6 \times 0.4 \times 0.5}{10^2} = 30\,000$$

$$\beta = \frac{15 \times 10^6 \times 0.4^3}{12 \times 0.5} = 160\,000$$

So that

$$[k]_{0.5} = 10^3 \begin{bmatrix} 7691.1 & -1920.8 & -7676.1 & -1919.5 \\ & 640.1 & 1919.5 & 319.5 \\ & \text{sym.} & 7691.1 & 1920.8 \\ & & & 640.1 \end{bmatrix} \quad (4.64)$$

In a similar fashion, the remaining three element stiffness matrices may be shown to be

$$[k]_1 = 10^3 \begin{bmatrix} 982.3 & -483.1 & -952.3 & -478.1 \\ & 320.6 & 478.1 & 159.6 \\ & \text{sym.} & 982.3 & 483.1 \\ & & & 320.6 \end{bmatrix}$$

$$[k]_2 = 10^3 \begin{bmatrix} 164.6 & -132.6 & -104.6 & -112.6 \\ & 164.6 & 112.6 & 76.6 \\ & \text{sym.} & 164.6 & 132.6 \\ & & & 164.6 \end{bmatrix} \quad (4.65)$$

$$[k]_4 = 10^3 \begin{bmatrix} 104.1 & -80.3 & 15.9 & -0.3 \\ & 116.6 & 0.3 & 12.6 \\ & \text{sym.} & 104.1 & 80.3 \\ & & & 116.6 \end{bmatrix}$$

The structure stiffness matrix is relatively straightforward to assemble in the present case, due to the nature of the element interconnections. If the nodes are numbered sequentially, starting with node 1 at the rim (Fig. 4.23(a)), then it is first noted that the final node, 8, is fully restrained on account of the assumed encastré base conditions. Accordingly, the displacements at node 8 are both zero, and this node need not be included in the stiffness equations, since its displacements are prescribed. The structure stiffness matrix, in sub-

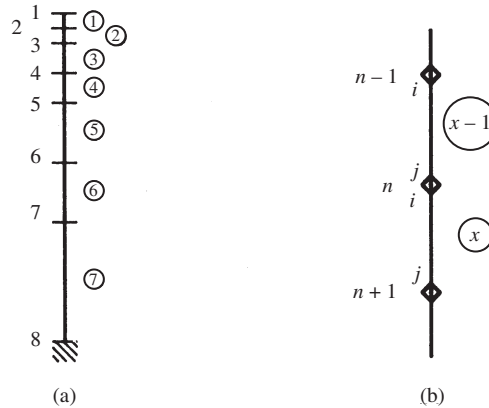


Fig. 4.23 (a) Element and node numbering. (b) Typical element interconnection

matrix form, will therefore relate the total forces acting at the seven unrestrained nodes to the displacement components at these same seven nodes, and will, hence, be  $7 \times 7$  in size.

The element stiffness equations (equation (B.11)) for a two-noded element take the form

$$\{f^e\} = \begin{Bmatrix} f_i \\ f_j \end{Bmatrix} = [k]\{\delta^e\} = \begin{bmatrix} k_{ii} & k_{ij} \\ k_{ji} & k_{jj} \end{bmatrix} \begin{Bmatrix} \delta_i \\ \delta_j \end{Bmatrix} \quad (4.66)$$

If a typical node,  $n$ , is considered (Fig. 4.23(b)), then node  $n$  is only connected to members  $x-1$  and  $x$ . Thus, the total force at node  $n$  is obtained by summing the force contributions at this node from members  $x-1$  and  $x$ . In the case of member  $x-1$ , its  $i, j$  designation is  $n-1, n$ . It is therefore the second of equations (4.66) which relates to the forces which this member produces at node  $n$ , and the equation may be expressed, in expanded form, as

$$\{f_n^{x-1}\} = [k_{ji}^{x-1}]\{\delta_{n-1}\} + [k_{jj}^{x-1}]\{\delta_n\} \quad (4.67)$$

For member  $x$ , its  $i, j$  designation is  $n, n+1$ , and hence the first of equations (4.66) is relevant in this case. Adding the contribution of element  $x$  to that of element  $x-1$  (equation (4.67)) produces the stiffness equation at node  $n$  as follows:

$$\{f_n^{x-1}\} + \{f_n^x\} = [k_{ji}^{x-1}]\{\delta_{n-1}\} + [k_{jj}^{x-1} + k_{ii}^x]\{\delta_n\} + [k_{ij}^x]\{\delta_{n+1}\} \quad (4.68)$$

Node  $n$  is typical of all the nodes (Fig. 4.23(a)) except the first and last, so that equation (4.68) shows that the structure stiffness matrix is tri-diagonal in this case and will take the form

$$\left[ \begin{array}{ccccccc} k_{ii}^1 & k_{ij}^1 & 0 & & & & \\ k_{ji}^1 & k_{jj}^1 + k_{ii}^2 & k_{ij}^2 & 0 & & & \\ 0 & k_{ji}^2 & k_{jj}^2 + k_{ii}^3 & k_{ij}^3 & 0 & & \\ & & \ddots & \ddots & \ddots & \ddots & \\ & & & & & & k_{ji}^6 & k_{jj}^6 + k_{ii}^7 \end{array} \right] \quad (4.69)$$

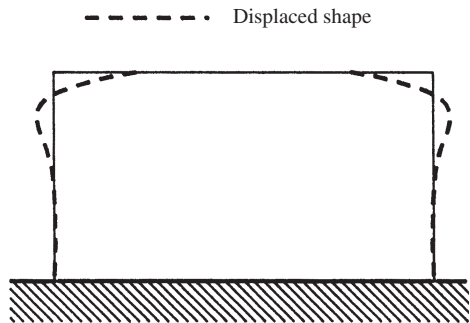
Substitution into equation (4.69) from equations (4.64) or (4.65), as appropriate, produces the structure stiffness equation, in numeric form, as given by equation (4.70) (page 197). The load vector corresponding to the specified rim moment at node 1 is given as equation (4.71), and a computer solution of the resulting stiffness equations is presented in Fig. 4.24.

$$\{W\} = \{0, -10, 0, 0, 0, 0, 0, 0, 0, 0, 0, 0, 0, 0\}^T \quad (4.71)$$

Figure 4.24 also shows a sketch of the displacement solution, from which it may be observed that, as expected, the effect of the applied moment is greatest in the vicinity of the tank rim and decays rapidly in the lower regions of the tank, there being no significant displacement in the lower half of the tank. To confirm that this behaviour also extends to the stress resultants, it is necessary to use equation (4.60) to determine the bending moments and direct forces in the tank, which is done in the next section.

$$\left\{ \begin{array}{l} w_1 \\ \theta_1 \\ w_2 \\ \theta_2 \\ w_3 \\ \theta_3 \\ w_4 \\ \theta_4 \\ w_5 \\ \theta_5 \\ w_6 \\ \theta_6 \\ w_7 \\ \theta_7 \end{array} \right\} = \left\{ \begin{array}{l} -0.1443 \\ -0.1899 \\ -0.0647 \\ -0.1293 \\ -0.0134 \\ -0.0778 \\ 0.0276 \\ -0.0128 \\ 0.0262 \\ 0.0104 \\ 0.0044 \\ 0.0069 \\ -0.0012 \\ 0.0001 \end{array} \right\} \begin{array}{l} \\ \\ \\ \\ \\ \\ \times 10^{-3} \text{ m} \\ \text{or} \\ \times 10^{-3} \text{ rad} \\ \\ \\ \\ \\ \end{array}$$

(a)



(b)

Fig. 4.24 Circular tank displacement solution

$$[K] = 10^3 \begin{bmatrix}
 7691 & -1921 & -7676 & -1920 & 0 & 0 & 0 & 0 & 0 & 0 & 0 & 0 & 0 & 0 & 0 & 0 & 0 & 0 & 0 & 0 & 0 \\
 640 & 1920 & 320 & 0 & 0 & 0 & 0 & 0 & 0 & 0 & 0 & 0 & 0 & 0 & 0 & 0 & 0 & 0 & 0 & 0 & 0 \\
 15382 & 0 & -7676 & -1920 & 0 & 0 & 0 & 0 & 0 & 0 & 0 & 0 & 0 & 0 & 0 & 0 & 0 & 0 & 0 & 0 & 0 \\
 1280 & 1920 & 320 & 0 & 0 & 0 & 0 & 0 & 0 & 0 & 0 & 0 & 0 & 0 & 0 & 0 & 0 & 0 & 0 & 0 & 0 \\
 8673 & 1437 & -952 & -478 & 0 & 0 & 0 & 0 & 0 & 0 & 0 & 0 & 0 & 0 & 0 & 0 & 0 & 0 & 0 & 0 & 0 \\
 961 & 478 & 159 & 0 & 0 & 0 & 0 & 0 & 0 & 0 & 0 & 0 & 0 & 0 & 0 & 0 & 0 & 0 & 0 & 0 & 0 \\
 1965 & 0 & -952 & -478 & 0 & 0 & 0 & 0 & 0 & 0 & 0 & 0 & 0 & 0 & 0 & 0 & 0 & 0 & 0 & 0 & 0 \\
 641 & 478 & 160 & 0 & 0 & 0 & 0 & 0 & 0 & 0 & 0 & 0 & 0 & 0 & 0 & 0 & 0 & 0 & 0 & 0 & 0 \\
 1147 & 351 & -105 & -113 & 0 & 0 & 0 & 0 & 0 & 0 & 0 & 0 & 0 & 0 & 0 & 0 & 0 & 0 & 0 & 0 & 0 \\
 485 & 113 & 77 & 0 & 0 & 0 & 0 & 0 & 0 & 0 & 0 & 0 & 0 & 0 & 0 & 0 & 0 & 0 & 0 & 0 & 0 \\
 329 & 0 & -105 & -113 & 0 & 0 & 0 & 0 & 0 & 0 & 0 & 0 & 0 & 0 & 0 & 0 & 0 & 0 & 0 & 0 & 0 \\
 329 & 113 & 77 & 0 & 0 & 0 & 0 & 0 & 0 & 0 & 0 & 0 & 0 & 0 & 0 & 0 & 0 & 0 & 0 & 0 & 0 \\
 269 & 269 & 52 & 281 & 281 & 281 & 281 & 281 & 281 & 281 & 281 & 281 & 281 & 281 & 281 & 281 & 281 & 281 & 281 & 281 & 281 \\
 281 & 281
 \end{bmatrix}$$

(4.70)

Stress resultant solution

As an example of the element stress resultant calculation, element 1 will be considered. For this element, from Fig. 4.24,

$$\{\delta^1\} = \begin{Bmatrix} \delta_1 \\ \delta_2 \end{Bmatrix} = \begin{Bmatrix} -0.1443 \\ -0.1899 \\ -0.0647 \\ -0.1293 \end{Bmatrix} \times 10^{-3} \begin{matrix} \text{m} \\ \text{rad} \\ \text{m} \\ \text{rad} \end{matrix} \quad (4.72)$$

Thus, from equation (4.60) (using the properties of the element 1 from Fig. 4.22) in kilonewton and metre units,

$$\mu = \frac{Et}{r} = \frac{15 \times 10^6 \times 0.4}{10} = 600\,000$$

$$\beta = \frac{Et^3}{12(1-\nu^2)L} = \frac{15 \times 10^6 \times 0.4^3}{12 \times 0.5} = 160\,000$$

Whence

$$\{\sigma^1\} = \begin{Bmatrix} N_{t1} \\ M_{m1} \\ N_{t2} \\ M_{m2} \end{Bmatrix} = 10^3 \begin{bmatrix} 600 & 0 & 0 & 0 \\ -1920 & 640 & 1920 & 320 \\ 0 & 0 & 600 & 0 \\ 1920 & -320 & -1920 & -640 \end{bmatrix} \begin{Bmatrix} -0.1443 \\ -0.1899 \\ -0.0647 \\ -0.1293 \end{Bmatrix} \times 10^{-3}$$

So that

$$\{\sigma^1\} = \begin{Bmatrix} N_{t1} \\ M_{m1} \\ N_{t2} \\ M_{m2} \end{Bmatrix} = \begin{Bmatrix} -86.6 \\ -10.1 \\ -38.8 \\ -9.3 \end{Bmatrix} \begin{Bmatrix} \text{kN/m} \\ \text{kN m/m} \\ \text{kN/m} \\ \text{kN m/m} \end{Bmatrix} \quad (4.73)$$

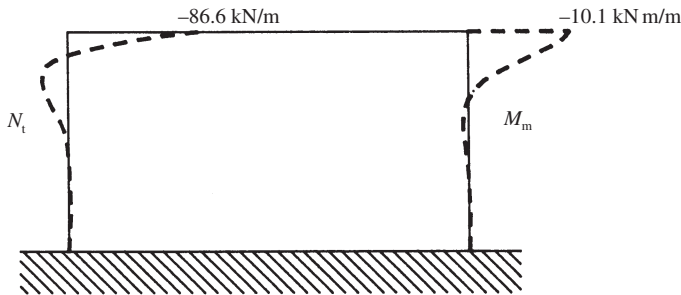


Fig. 4.25 Stress resultant solution



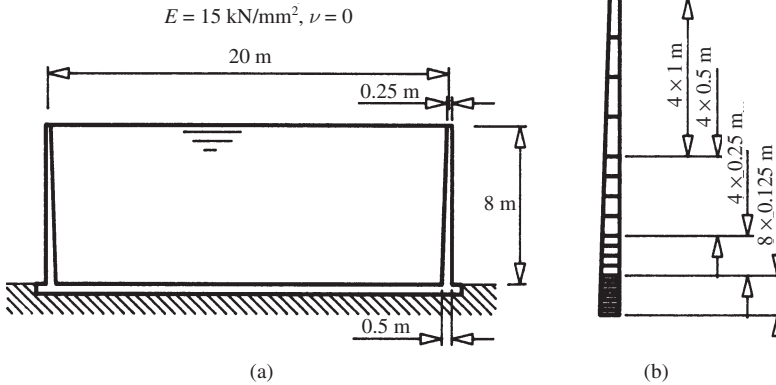


Fig. 4.26 (a) Non-uniform circular tank example. (b) Element sub-division (enlarged scale)

Proceeding in the same way for the rest of the elements gives the complete stress resultant solution. The nature of the formulation ensures that the tangential forces will be continuous from element to element, provided that all the elements have the same thickness. There will, however, be a discrepancy in the meridional moment values as computed from adjacent elements. In the present example these discrepancies are small and are not therefore indicated on Fig. 4.25, which shows sketches of the stress resultant solution and is based on nodal average values. It should be noted that the distribution of the tangential direct force is similar to that of the radial displacement solution (Fig. 4.24). This feature follows from the linear relationship between the force and radial displacement (equations (4.46) and (4.48)) adopted in this formulation. The meridional bending moment is linearly related to the meridional curvature (equation (4.53a)) rather than the radial displacement, but still decays with distance from the tank rim, although at a slightly reduced rate (Fig. 4.25).

### 4.3.3. Example 4.5 – circular tank of non-uniform thickness

The circular tank shown in Fig. 4.26(a) has walls of linearly varying thickness. To obtain bounds on the effect of the varying degrees of rotational restraint which might be provided by the base slab, full restraint will be assumed initially and the analysis will then be repeated under a condition of zero rotational base restraint. The tank is to be analysed for water pressure effects, it being assumed that the tank is filled to its rim. The loading is severest at the base of the tank and, certainly in the fully restrained base case, the bending moment will tend to have its greatest rate of change at the bottom of the tank. The finite elements should therefore be smallest towards the tank base and, to meet this requirement, the element sub-division shown in Fig. 4.26(b) is to be

adopted. There are thus four types of element lengths to be considered, namely 1, 0.5, 0.25 and 0.125 m and there are 20 elements in total.

The varying wall thickness is accommodated by using the constant-thickness element derived above, with the thickness of each element being the average wall thickness over its length. The thicknesses to be used for the elements, using successive element numbering from the rim, are then as given in Table 4.2. The varying thickness could alternatively (Ross, 1998) be incorporated within the finite element formulation and a rather more powerful element thereby derived.

The loading effects of the water pressure will be represented by statically equivalent, radial, nodal loads, although a more rigorous treatment of distributed loading would be to use equivalent nodal forces and moments, which are derived in a manner which is *consistent* with the element formulation (Zienkiewicz and Taylor, 1991). If a typical element is considered (Fig. 4.27), then the statically equivalent nodal loads for the element may be determined as indicated on the figure. Summing the loads produced by adjoining elements gives the total nodal loads given in Table 4.2.

### Finite element analysis

In this case, the analysis has been undertaken using a program based on the finite element theory given above. The input data comprised the geometric

Table 4.2 Element thicknesses and nodal loads

Element or node	Element thickness (m)	Nodal load (kN/m)
1	0.266	1.64
2	0.297	9.81
3	0.328	19.63
4	0.359	29.43
5	0.383	28.21
6	0.398	22.08
7	0.414	24.52
8	0.430	26.98
9	0.441	21.77
10	0.449	15.33
11	0.457	15.94
12	0.465	16.56
13	0.471	12.80
14	0.475	8.73
15	0.479	8.89
16	0.482	9.04
17	0.486	9.19
18	0.490	9.35
19	0.494	9.51
20	0.498	9.65

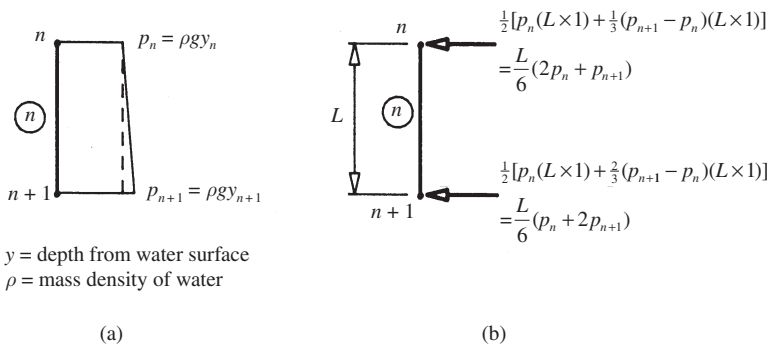


Fig. 4.27 (a) Pressure distribution on a typical element. (b) Statically equivalent load determination

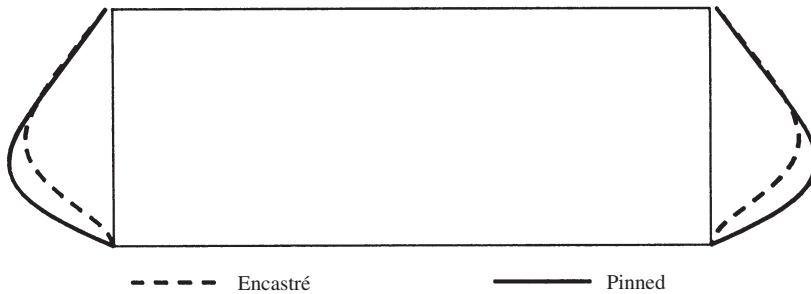


Fig. 4.28 Displacement solutions

and load data of Fig. 4.26 and Table 4.2 from which the program determined the displacement and stress resultant solutions for the two assumed base conditions. For the full rotational (encastré) support condition, the stiffness equations at the node at the base of the tank would be deleted in view of the prescribed zero displacements. In the zero rotational support (pinned) base condition, the radial force stiffness equation would be deleted, since radial displacement is still prevented, but the moment stiffness equation at the base would be retained in view of the non-zero rotation under these conditions.

The displacement solutions obtained from the two analyses are sketched in Fig. 4.28, and the corresponding stress resultant solutions are given in Fig. 4.29. The displacement solutions show the generally more flexible response under the pinned-base condition, but also indicate that the solutions tend to be independent of the base condition in, approximately, the upper half of the tank.

The stress resultant solutions (Fig. 4.29) again demonstrate the similarity of the tangential force and displacement distributions. The pinned support may be seen to result in rather larger tangential forces, and both solutions show that bending effects become most pronounced towards the base, especially in the encasté case, where a substantial restraining moment is developed. It may readily be shown that this restraining moment is significant in stress terms by comparing the bending stress due to the moment with the stress due to the maximum tangential force of 433 kN/m (Fig. 4.29). Thus, assuming a homogeneous structural material,

$$\max. \sigma_{\text{dir.}} = \frac{\max. N_t}{1 \times t_{4.5}} = \frac{433 \times 10^3}{250[1 + (4.5/8)] \times 10^3} = 1.1 \text{ N/mm}^2$$

and

$$\max. \sigma_{\text{bend.}} = \frac{\max. M_m}{(1 \times t_9^2)/6} = \frac{92.6 \times 10^6}{(10^3 \times 500^2)/6} = 2.2 \text{ N/mm}^2$$

For this example, therefore, the maximum bending stress, under the encasté base condition, considerably exceeds the maximum direct stress.

### Membrane analysis comparison

To fulfil the conditions for a membrane solution to be exactly applicable to the present example, the supports would have to provide a reaction only in the meridional tangent (vertical) direction at the base (see Section 4.2.3), that is, roller (free-sliding) supports are needed (Fig. 4.30).

Roller supports do not involve a horizontal reaction component at the base, which is present in both the pinned and encasté supports. For these latter

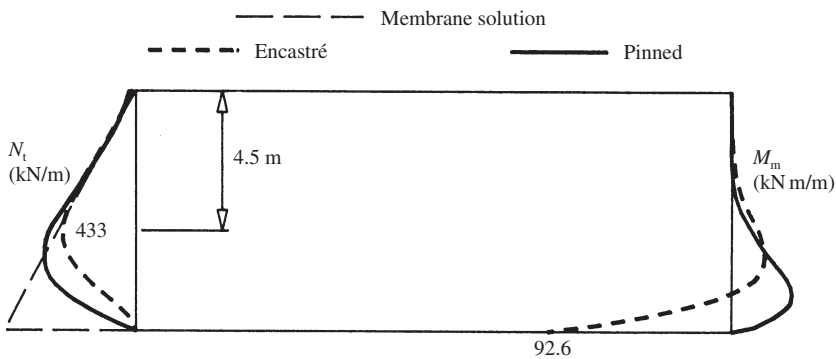


Fig. 4.29 Stress resultant distributions

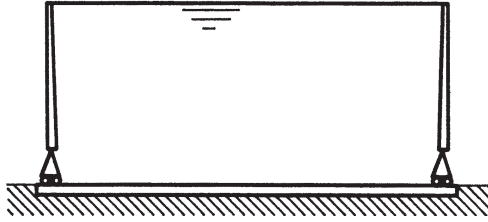


Fig. 4.30 Membrane analysis supports

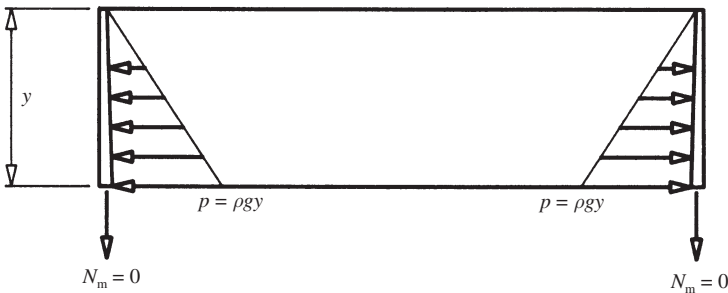


Fig. 4.31 Circular tank membrane analysis

supports, the tangential direct force is zero at the base, since radial displacement is prevented, so that the horizontal reaction component can only be provided by a shear force which implies significant bending in the base region, as already encountered above. The impact of this bending on the tangential direct force may be investigated by comparison with a membrane solution, which is readily obtained for the present example.

Since the meridional radius of curvature is infinite (equation (4.4)), the tangential direct force, under membrane conditions, may be obtained directly from the first membrane equilibrium equation (4.8). Thus, with reference to the portion of the tank shown in Fig. 4.31 and noting the outward direction of the pressure,  $p$ ,

$$\frac{N_t}{r} - \rho gy = 0$$

Whence

$$N_t = \rho gry \quad (4.74)$$

The tangential force solution provided by equation (4.74) is shown in Fig. 4.29 and it may be seen that the high tangential direct force, required by the membrane solution to resist the radial base pressure, is absent in the other

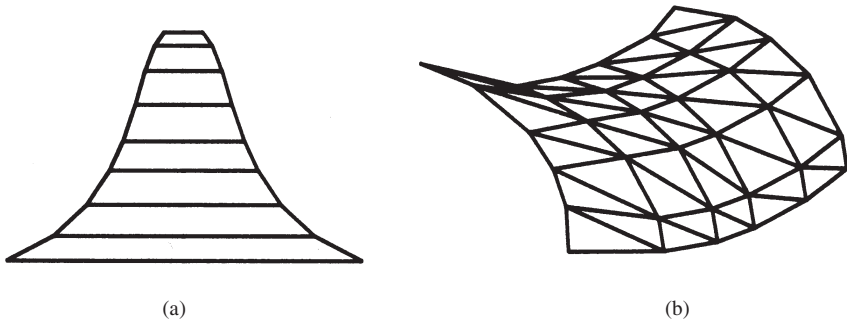


Fig. 4.32 Finite element shell representations: (a) axisymmetric shell; (b) general shell

two solutions, where this horizontal thrust can, and must, be sustained by shear forces. It may also be observed, however, that the pinned and encastré solutions both tend to the membrane result in the upper half of the tank, where the moment solution confirms the absence of significant bending in this region. The height to which bending is of importance does, in fact, depend upon the tank proportions (Manning, 1967). The walls of an encastré-supported tank which is wide and shallow will essentially act as a vertical cantilever, and bending effects will be significant over almost the full height. In a narrow, deep tank, on the other hand, membrane effects will predominate in the upper portions of the wall, and bending will only be significant in a limited region close to the base.

#### 4.4 Finite elements for non-cylindrical shells

The element employed above for a circular cylindrical shell may also be derived from a more general element (Ross, 1998) which models an axisymmetric shell problem by a sequence of elements (Fig. 4.32(a)), each of which has flat, sloping sides. Radially unsymmetric loading can be treated without having recourse to a different element by a technique in which the loading distribution is replaced by an approximating Fourier series (Zienkiewicz and Taylor, 1991).

For more general shells, a wide variety of finite elements is available (Zienkiewicz and Taylor, 1991). Perhaps the simplest in concept is to take the triangular plane stress element of Chapter 1, add a plate bending representation to the element, and so obtain a shell element which will model general shell surfaces by planar triangular regions (Fig. 4.32(b)). The discontinuities inherent in this *facet* approach can lead to significant inaccuracy, however, and curved elements (Gould, 1998) are generally to be preferred.

---

## References and further reading

- Baker, E. H., Kovalevsky, L. and Rish, F. L. (1972) *Structural Analysis of Shells*. McGraw-Hill, London. Many standard results and detailed advice on correction treatments for bending effects.
- Billington, D. P. (1982) *Thin Shell Concrete Structures*, 2nd edn. McGraw-Hill, New York. An outline of general shell theory accompanied by a wide variety of analyses of concrete shells.
- Cronowicz, A. (1968) *The Design of Shells*, 3rd edn. Crosby Lockwood, London. Includes many approximate methods for the analysis of shells and a collection of plates illustrating concrete shell roof forms.
- Feodosyev, V. (1968) *Strength of Materials*. Mir, Moscow. Chapter X gives a brief but convincing account of membrane theory.
- Firt, V. (1983) *Statics, Formfinding and Dynamics of Air-supported Membrane Structures*. Martinus Nijhoff, The Hague. Includes membrane theory for axisymmetric shells generated from conic sections.
- Flügge, W. (1960) *Stresses in Shells*. Springer, Berlin. Perhaps the most accessible, analytical shell theory text.
- Ghali, A. (1979) *Circular Storage Tanks and Silos*. Spon, London. An exact stiffness matrix is given for a circular cylindrical tank element of uniform thickness; this matrix may be used in place of the approximate element derived above. Tank walls of non-uniform thickness are analysed by the finite difference method.
- Gibson, J. E. (1980) *Thin Shells – Computing and Theory*. Pergamon Press, Oxford. An introductory text on both classical and numerical methods of shell analysis; Chapter 9 describes the analysis of cylindrical shells by the finite element method, including meridional displacement variables which are omitted in the formulation given above.
- Gol'denveizer, A. L. (1961) *Theory of Thin Elastic Shells*. Pergamon Press, Oxford. An advanced, general treatment of classical shell theory which includes (pp. 474–484) a particularly thorough discussion on the limitations of membrane theory.
- Gould, P. L. (1998) *Analysis of Shells and Plates*. Prentice Hall, New York. Includes finite element formulations for curved shell analysis.
- Kraus, H. (1967) *Thin Elastic Shells*. Wiley, New York. Part IV deals with numerical methods and includes several examples of complex practical analyses undertaken by these techniques.
- Manning, G. P. (1967) *Reservoirs and Tanks*. Concrete Publications, London. Chapter 3 deals with the effects of circular tank proportions and support conditions on the membrane and bending behaviour of the tank.
- Novozhilov, V. V. (1964) *Thin Shell Theory*. Noordhoff, Groningen. Classical shell theory.
- Pflüger, A. (1961) *Elementary Statics of Shells*. Dodge, New York. Basic theory and extensive tabulation of membrane shell solutions.

- Ross, C. T. F. (1998) *Advanced Applied Finite Element Methods*. Horwood, Chichester. Chapter 12 describes the analysis of axisymmetric shells using a finite element of tapered thickness and flat, sloping sides.
- Soare, M. (1967) *Application of Finite Difference Equations to Shell Analysis*. Pergamon Press, Oxford. An extensive treatment of the application of the finite difference method to the membrane and bending analysis of practical shell structures.
- Timoshenko, S. P. and Woinowsky-Krieger, S. (1981) *Theory of Plates and Shells*, 2nd edn. McGraw-Hill, New York. A standard reference work on classical shell theory.
- Wang, C. (1953) *Applied Elasticity*. McGraw-Hill, New York. Chapter 12 provides a summary of the geometry of surfaces and descriptions of membrane theory and the classical bending theory of circular cylindrical shells.
- Zienkiewicz, O. Z. and Taylor, R. L. (1991) *The Finite Element Method*, 4th edn, Vol. 2. *Solid and Fluid Mechanics Dynamics and Non-linearity*. McGraw-Hill, London. Chapters 3–6 deal with the application of the finite element method to shell analysis.
- Zingoni, A. (1997) *Shell Structures in Civil and Mechanical Engineering*. Thomas Telford, London. Clear description of the limitations of membrane theory and of the application of approximating bending theory to the analysis of axisymmetric and circular cylindrical shells.

## Problems

- 4.1 Use membrane thin shell theory to determine expressions for the distributions of the meridional and tangential membrane forces in the spherical dome shown in Fig. 4.33(a). For a spherical dome having  $a = 1430$  mm,  $t = 60$  mm,  $p = 2$  N/mm<sup>2</sup> and  $\alpha = 39^\circ$ , supported as shown in Fig. 4.33(b), a bending theory predicts the membrane stresses to vary as shown in Fig. 4.33(c). Compare membrane theory results with those of Fig. 4.33(c) and comment on any discrepancies.
- 4.2 The spherical, constant-thickness dome shown in Fig. 4.34(a) is open for  $0 \leq \phi \leq \alpha_1$  and is supported vertically at  $\phi = \alpha_2$ . The dome carries a rim load of  $P$ /unit length in addition to its self-weight of  $q$ /unit area. Show that, by membrane theory, the meridional and tangential direct stress resultants are given by

$$N_m = -\frac{qa(\cos \alpha_1 - \cos \phi) + P \sin \alpha_1}{\sin^2 \phi}$$

$$N_t = qa \left( \frac{\cos \alpha_1 - \cos \phi}{\sin^2 \phi} - \cos \phi \right) + \frac{P \sin \alpha_1}{\sin^2 \phi}$$



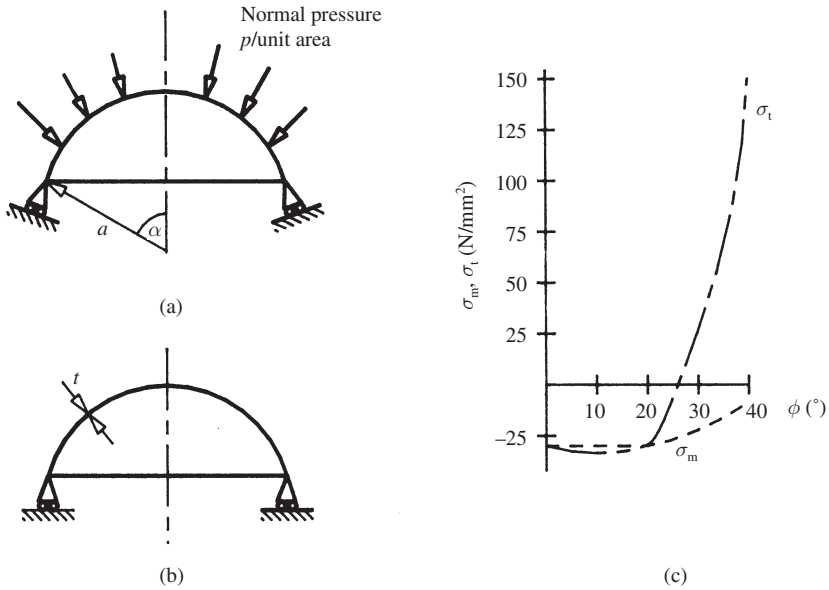


Fig. 4.33

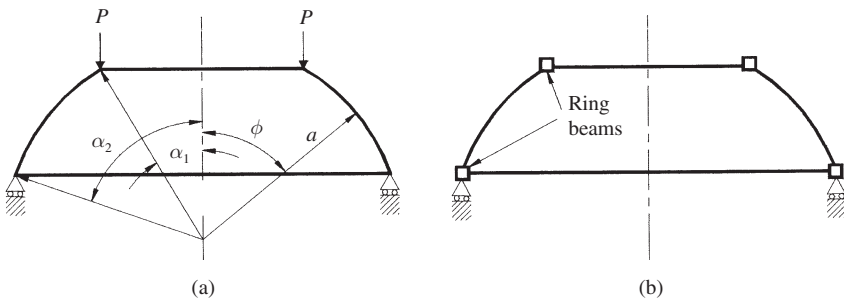


Fig. 4.34

Why will this solution not be valid in regions close to  $\phi = \alpha_1$  and  $\phi = \alpha_2$ ? If ring beams were provided as shown in Fig. 4.34(b), state, with reasons, whether each ring would be in tension or compression under the specified loading.

(UEL)

- 4.3 The general axisymmetric dome shown in Fig. 4.35 is subjected to an internal, uniform over-pressure,  $p$  per unit area. Show that the direct stresses, as predicted by membrane thin shell theory, are given by

$$\sigma_m = \frac{pr}{2t \sin \phi}, \quad \sigma_t = \sigma_m \left( 2 - \frac{r}{r_m \sin \phi} \right)$$

- 4.4 The paraboloid dome shown in Fig. 4.36 is generated by rotating a portion of the parabola  $2ay = x^2$  (where  $a$  is a constant) about the  $y$ -axis. The dome is subjected to a snow load which may be approximated as a vertical load of variable intensity  $q$  per unit area, where  $q = q' \cos^2 \phi$  and  $q'$  is constant. Show that the direct forces due to this load, as given by thin shell membrane theory, are

$$N_m = \frac{-q'a}{1 + \cos \phi}, \quad N_t = \frac{-q'a \cos^3 \phi}{1 + \cos \phi}$$

Sketch and comment on the distributions of these membrane forces.

- 4.5 A conical umbrella-shaped roof of uniform thickness is supported by a central column as shown in Fig. 4.37.
- Determine general expressions for the membrane stress resultants due to self-weight,  $q$ , per unit surface area and find the force in the column.
  - Sketch the variation of the membrane stress resultants, showing their significant values. Calculate values for  $p = 0, 0.1, 0.5$  and  $1.0$ .
  - Interpret and discuss the results critically.

(UCL)

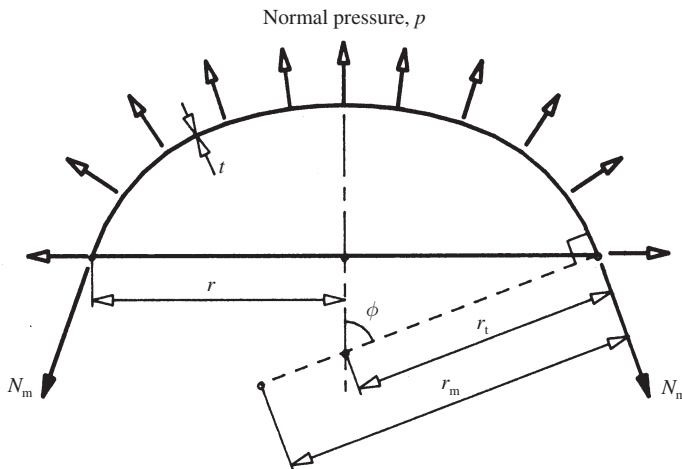


Fig. 4.35

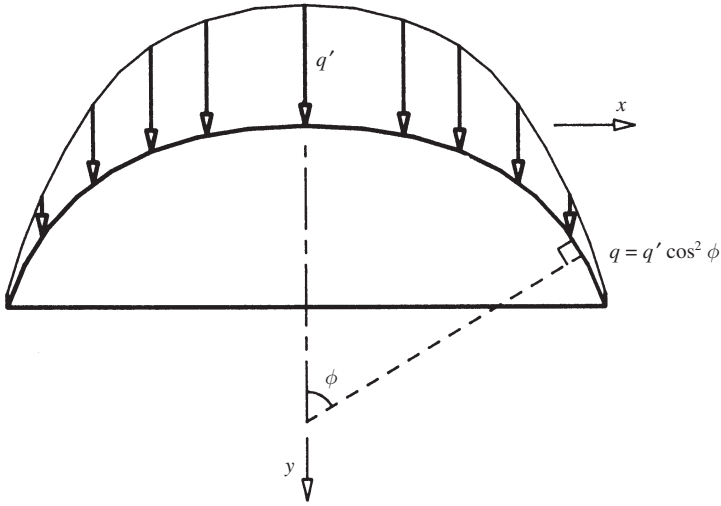


Fig. 4.36

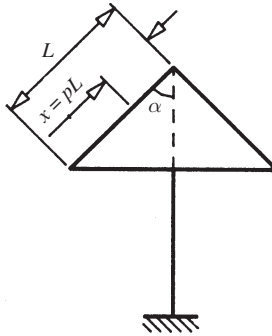


Fig. 4.37

- 4.6 A fluid container (Fig. 4.38(a)) is generated by rotating a portion of the hyperbola  $b^2x^2 - a^2y^2 = a^2b^2$  about the  $y$ -axis. When the container is filled with a fluid of mass density,  $\rho$ , show that the resultant vertical force,  $R$ , due to the pressure of the fluid on the sides of a frustum of the shell (Fig. 4.38(b)) is given by

$$R = 2\pi\rho g \left(\frac{a}{b}\right)^2 \left[ \frac{H^3}{6} - \frac{Hy^2}{2} + \frac{y^3}{3} \right]$$

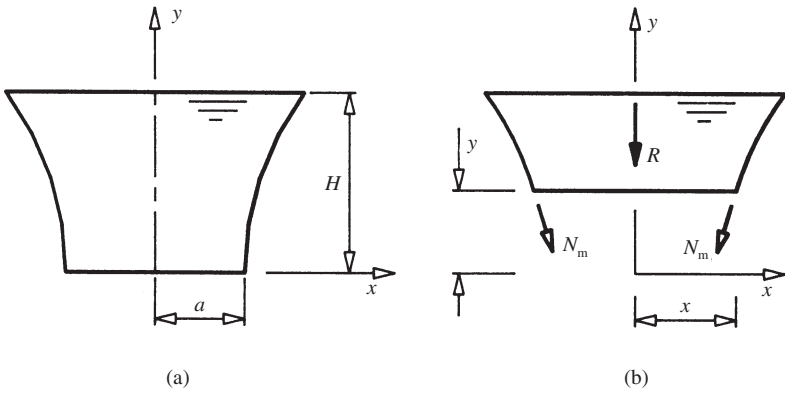


Fig. 4.38

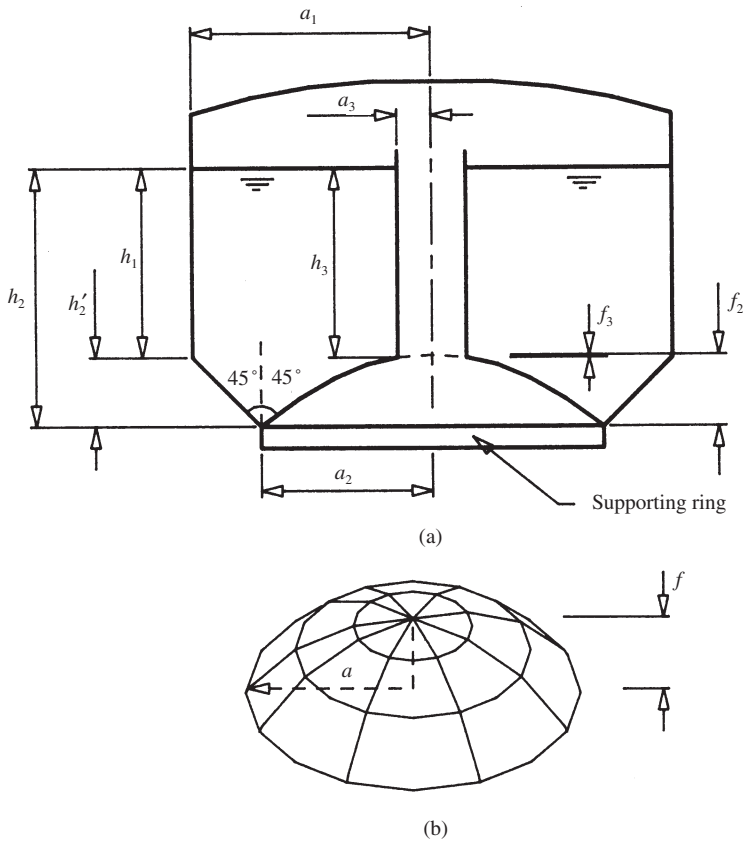


Fig. 4.39

Also, by considering the vertical equilibrium of the frustum, show that

$$N_m = -\frac{a^2 \rho g (a^4 y^2 + b^4 x^2)^{1/2}}{b^4 x^2} \left[ \frac{H^3}{6} - \frac{Hy^2}{2} + \frac{y^3}{3} \right]$$

Hence determine the meridional force at the base of the container.

(UEL)

4.7 Consider the Intze-type fluid container generated by the rotation of the cross-section shown in Fig. 4.39(a) about its central axis.

- (a) Establish the criterion that the supporting ring should be loaded by vertical forces only. (Neglect the self-weight of the structure.)
- (b) Check if this criterion is satisfied (with reasonable approximation) for the dimensions (in metres):

$$a_1 = 7.00, h_1 = 5.50, h'_2 = 2.00$$

$$a_2 = 5.00, h_2 = 7.50, f_2 = 2.07$$

$$a_3 = 1.00, h_3 = 5.50, f_3 = 0.07$$

- (c) Explain briefly why and where a bending correction would be necessary.

Note that for a shell cap (Fig. 4.39(b)):

$$V = \frac{\pi f}{6} (3a^2 + f^2)$$

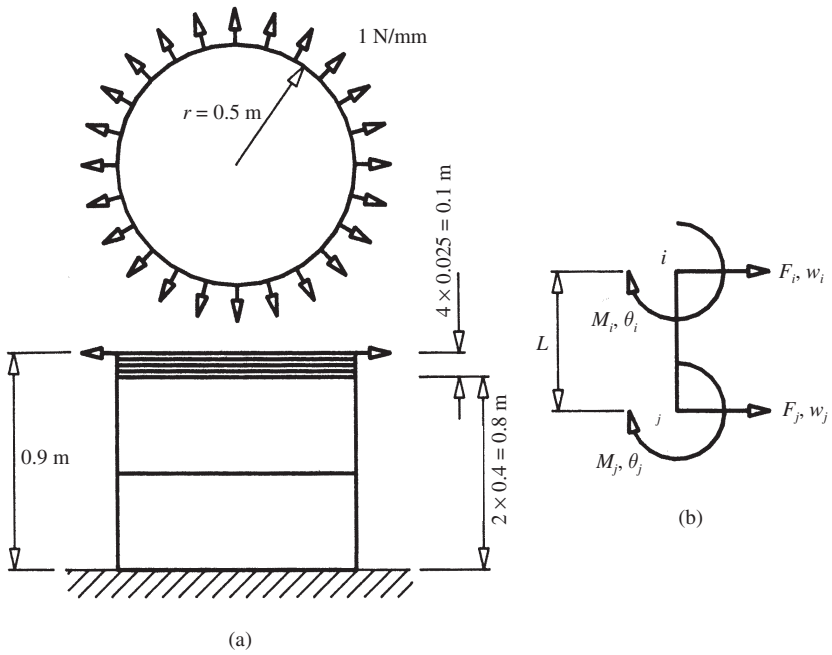
(UCL)

4.8 The circular cylindrical shell shown in Fig. 4.40(a) is to be analysed by the finite element method using the element sub-division indicated in the figure. The shell is subjected to a radial rim load of 1 N/mm and is fully fixed at the base. The element stiffness equations (in kilonewton and metre units) for circular cylindrical shell elements of axial lengths 25 and 400 mm and 1 mm arc length are given in Fig. 4.40(c), where the sign convention of Fig. 4.40(b) has been used. Form, but do not solve, the overall stiffness equations for the finite element analysis.

(UEL)

4.9 The cylindrical metal tank shown in Fig. 4.41(a) is filled with liquid of weight density 9 kN/m<sup>3</sup>. A finite element analysis of the tank has been undertaken, and displacement results for the region of the tank adjacent to the change in wall thickness are given in Fig. 4.41(b). Use the stress matrix of Fig. 4.41(c) to determine the averaged stress resultants at nodes 7, 8 and 9 using elements 7 and 8 only. Hence calculate the maximum bending and membrane stresses in this region. Are bending effects significant in this region? ( $E = 200 \text{ kN/mm}^2$ ,  $\nu = 0$ ).

(UEL)



For 25 mm element:

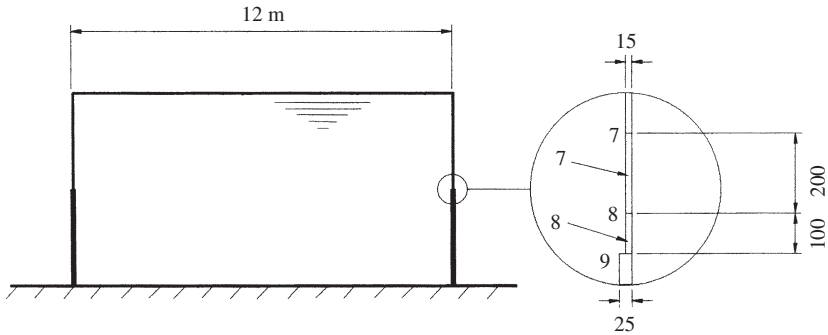
$$\begin{bmatrix} F_i \\ M_i \\ F_j \\ M_j \end{bmatrix} = \begin{bmatrix} 0.14 & -1.72 & -0.13 & -1.68 \\ & 28.41 & 1.68 & 14.05 \\ \text{sym.} & & 0.14 & 1.72 \\ & & & 28.41 \end{bmatrix} \begin{bmatrix} w_i \\ \theta_i \\ w_j \\ \theta_j \end{bmatrix}$$

For 400 mm element:

$$\begin{bmatrix} F_i \\ M_i \\ F_j \\ M_j \end{bmatrix} = \begin{bmatrix} 0.12 & -7.05 & 0.04 & 4.15 \\ & 513.77 & -4.15 & -383.12 \\ \text{sym.} & & 0.12 & 7.05 \\ & & & 513.77 \end{bmatrix} \begin{bmatrix} w_i \\ \theta_i \\ w_j \\ \theta_j \end{bmatrix}$$

(c)

Fig. 4.40



(a)

Node	$w$ (mm)	$\theta$ ( $\times 10^{-3}$ rad)
7	0.3068	0.0683
8	0.2627	0.3441
9	0.2206	0.4789

(b)

$$\{\sigma^e\} = \begin{Bmatrix} N_{vi} \\ M_{mi} \\ N_{vj} \\ M_{mj} \end{Bmatrix} = \begin{bmatrix} \mu & 0 & 0 & 0 \\ -\frac{6\beta}{L} & 4\beta & \frac{6\beta}{L} & 2\beta \\ 0 & 0 & \mu & 0 \\ \frac{6\beta}{L} & -2\beta & -\frac{6\beta}{L} & -4\beta \end{bmatrix} \{\delta^e\} = [H^e] \{\delta^e\}$$

$$\text{where } \mu = \frac{Et}{r} \text{ and } \beta = \frac{Et^3}{12(1-\nu^2)L}$$

(c)

Fig. 4.41

4.10 The circular cylindrical pressure vessel shown in Fig. 4.42(a) has ends which are sufficiently rigid to prevent rotation or radial displacement at the vessel wall/end junction. One half of the vessel has been analysed by the finite element method for the effects of a uniform internal radial pressure of  $3000 \text{ kN/m}^2$ . The finite element mesh used was as shown in Fig. 4.42(b) and displacement results from the analysis are given, in part, in Fig. 4.42(c).

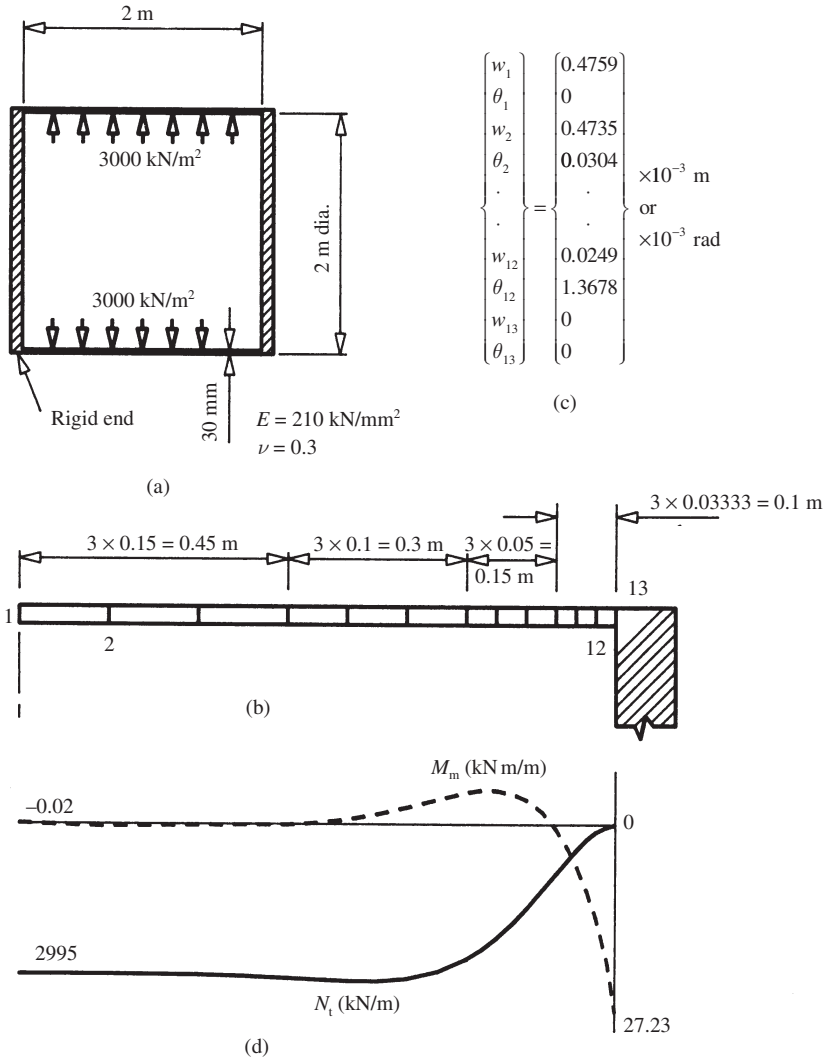


Fig. 4.42

- Comment on the element sub-division choice.
- Use the element 'stress' matrix (equation (4.60)) to determine the stress resultants at nodes 1 and 13.
- Determine the stress resultants as given by membrane theory and compare the finite element results with this membrane solution and with the analytical solution given in Fig. 4.42(d).



- (d) Discuss the relationship of the available solutions to the expected physical behaviour of the vessel.
- (e) What modifications would need to be made to the stress resultant solution if it were required to incorporate the effects of the pressure on the vessel ends, presuming that longitudinal movement is unrestrained?

(UEL)

## 5. *Structural dynamics*

### 5.1 Introduction

In the previous chapters it has been assumed that the applied loads do not vary with time and the analysis has therefore been undertaken on a *static* basis. If the loading is *dynamic*, in the sense that it becomes time-dependent, then it may be still be possible to use a static analysis, for design purposes, if statically equivalent loads are used to model the dynamic effects. In many cases, however, either the effects of winds, waves, blasts, earthquakes and other dynamic disturbances cannot be accurately represented by statically equivalent loading, or the importance of the structure may be such that a consideration of its dynamic behaviour is warranted.

A dynamic analysis can reveal the possibility of a serviceability failure which it would be impossible to predict by a purely static treatment. There have been cases, for example, of oil-rigs having to be abandoned in quite mild seas due to the onset of oscillations which were intolerable to the crews. Electric transmission lines have been known to develop dynamic ‘galloping’ of such severity that the lines touched, which did not necessarily result in structural distress, but which certainly represented a serviceability failure as far as the electricity supply consumers were concerned. Structures under construction are often particularly prone to dynamic effects, and temporary damping, for example, was needed for the towers of the Forth Road Bridge in Scotland to minimize dynamic effects prior to the main cables being spun.

Even on pure strength grounds, dynamic analysis may be required if fatigue is likely to be a determining feature. In such cases, it is necessary to be able to predict not only the magnitude of the stresses within the structure but also the frequency of occurrence of different stress levels, since a regularly sustained low stress can have severer fatigue effects than an occasionally experienced higher stress.

The aims of this chapter are therefore to describe the types of vibration which may be experienced by engineering structures and to give an introduction to the analytical techniques which may be used both to predict the likelihood of excessive oscillation and also to determine the dynamic

displacements and stresses which are produced during the course of acceptable vibration.

## 5.2 Types of vibration

### 5.2.1 Free, undamped vibration

Although dynamic behaviour has been introduced in terms of the structural effects of time-dependent loading, it is most helpful to begin with an account of the vibration of simple structures which are not subject to dynamic loads. This form of vibration is termed *free* vibration and occurs whenever a structure is disturbed from its position of static equilibrium. Free vibrations are initiated either by impulses, such as a collision impact or a blast, or by an abrupt support movement. In experimental work, free vibrations may be obtained by applying a constant disturbing force which is suddenly released, leaving the structure free to vibrate naturally.

If, in addition to the absence of time-dependent forces, energy is not dissipated from the vibrating system, then the motion is both free and *undamped*. Energy losses occur due to friction, air-resistance and similar effects, so that undamped vibration, rather impractically, assumes the absence of these features, but is, nevertheless, a very helpful theoretical concept.

As a simple example of free, undamped vibration, the cantilever beam of Fig. 5.1(a) will be considered. The beam will be assumed to be effectively massless itself but capable of supporting a constant (time-independent) point load at its free end, which will subsequently be referred to as a mass to permit a distinction from 'loads', which will be presumed to be dynamic (time-dependent). If the beam is displaced laterally from its static position and then released, vibration will ensue, and it is possible to obtain the instantaneous shape of the beam from a single parameter, often termed a *coordinate*, which is conveniently taken to be the lateral displacement of the mass from its position of static equilibrium. In the present example, therefore, there is just one coordinate and the structure is said to possess one *degree of freedom* since its displaced shape is uniquely determined by a single coordinate.

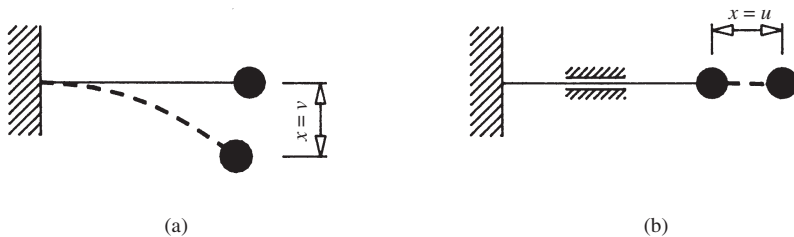


Fig. 5.1 Cantilever beam example

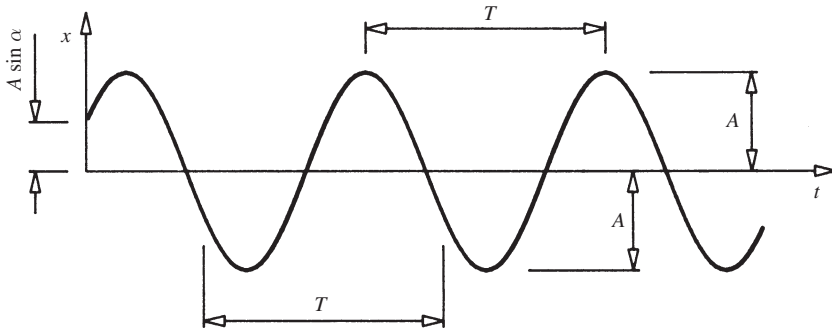


Fig. 5.2 Free undamped vibration

If the variation of the displacement,  $x$ , with time,  $t$ , is plotted (Fig. 5.2), then, in the absence of damping, the vibration may be shown to be of a sinusoidal (harmonic) form and may be described mathematically by

$$x = A \sin(\omega t + \alpha) \quad (5.1)$$

where  $A$ , the *amplitude*, is the maximum displacement from the undisturbed position,  $T$ , the *period*, is the time required for one complete cycle of vibration (s),  $\omega (= 2\pi/T)$  is the *circular natural frequency* (rad/s),  $f (= 1/T)$  is the *natural frequency* (cycles/s = Hz), and  $\alpha$  is the *phase angle* (rad).

In equation (5.1), the amplitude and phase angle constants may be determined from the conditions under which the motion commenced. These conditions may be represented by the initial displacement and velocity, and an expression for the latter parameter can be obtained by differentiation of equation (5.1) with respect to time. The units suggested in equation (5.1) are those which are most convenient and usual in the SI system. In particular, it should be noted that the standard terminology for the frequency unit is hertz (Hz), which replaces its more expressive equivalent of cycles per second.

Figure (5.2) shows that the beam vibrates from side to side such that the amplitude and period (and hence frequency) remain constant. The magnitude of the amplitude, however, is dependent on the initial conditions, as well as on the physical properties of the beam and mass, while the frequency depends solely on these two latter parameters. Natural frequencies, in fact, may be shown, quite generally, to increase with structural stiffness and decrease with mass. Thus, increasing the bending stiffness of the beam of Fig. 5.1(a) would result in a higher frequency; but increasing the point mass would produce a lower-frequency vibration.

So far it has been presumed that the manner, or *mode*, of vibration is prescribed. The mode of vibration is, however, dependent on the nature of the initiating disturbance. Had the beam, for example, been subjected to an initial

elongation and then released (fig 5.1(b)), the subsequent free vibrations would have been in an axial mode, in contrast to the bending (or flexural) mode described earlier. The system still possesses one degree of freedom, since, in a purely axial mode, the motion may be described by a single coordinate,  $u$ , the longitudinal displacement of the mass. In practice it would be necessary to provide a sleeve guide (Fig. 5.1(b)) to prevent the accidental simultaneous development of the bending mode and so ensure that pure axial vibration occurred. With the help of the sleeve, yet another mode could be investigated by giving the mass an initial twist and thereby producing a torsional mode of vibration.

Different modes of structural action therefore result in differing modes of vibration, each with its own natural frequency. The position becomes even more complicated if multiple degrees of freedom are involved for a single form of structural action. This type of situation may be explored by adding a second mass to the cantilever beam, as shown in Fig. 5.3(a). In free, undamped vibration, the cantilever beam will still oscillate from side to side following a lateral disturbance, but observations show that the vibration does not necessarily possess constant frequency and mode shape. These features can, in fact, only be consistently maintained if the initial disturbance is such as to displace the beam exactly in one of the two shapes illustrated in Fig. 5.3. In either of these *principal* (or natural) modes, both the masses will vibrate harmonically at a similar *natural* frequency, which is different for the two modes. In addition, the mode shape will be maintained throughout the motion such that the ratio of the displacements of the two masses remains constant at a value which is characteristic of the mode.

At first sight, principal modes may appear to be of little interest, since it is highly unlikely that a disturbance would produce one or other of the principal mode shapes exactly. Clearly, the mode of Fig. 5.3(b) resembles the effect of the release of a normal end-force. However, even in this case, it may be shown that the displaced shape produced by an end force does not correspond *exactly* to the principal mode of vibration. The importance of principal modes and natural frequencies lies, then, not in their common occurrence, but in the facts that it is possible to express *any* vibration as a linear combination of the principal modes and that the natural frequencies characterize the way in which the

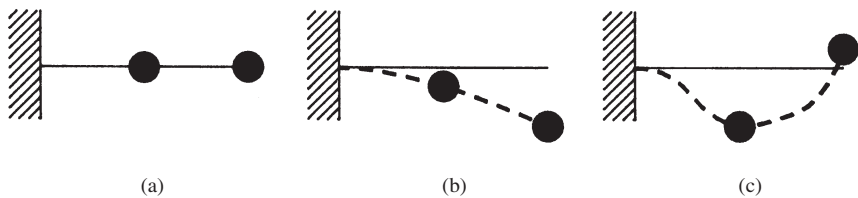


Fig. 5.3 Cantilever beam with two masses

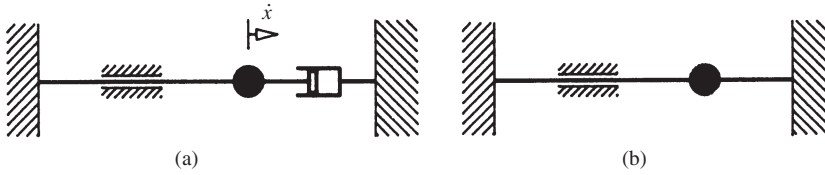


Fig. 5.4 (a) Damped cantilever beam. (b) Stiffened cantilever beam

structure responds to dynamic loading, features which will be explored in some detail later in this chapter.

### 5.2.2 Free, damped vibration

Damping occurs due to a loss of energy during the vibration, the energy lost being either dissipated as heat or transported from the structure by radiation (sound, for example). Energy losses occur partly due to internal friction in structural materials and partly due to friction at structural joints, losses due to air-resistance normally being secondary. The damping provided by internal material friction varies considerably, being particularly high for a material such as rubber, a property which can be utilized when rubber bearings are specified. Other structural materials have lower intrinsic damping, with composite materials such as reinforced concrete being rather better damping agents than metals. In metal structures there is clearly more friction at bolted joints than at welded ones, and bolted structures therefore exhibit higher damping.

It is customary to represent damping effects by a ‘dashpot’ system, which might be incorporated into the cantilever system of Fig. 5.1(b) as shown in Fig. 5.4(a). The dashpot can consist of a plunger inside a tube, and the energy loss then arises from the flow of air through the small gap between the plunger and the tube walls. This type of arrangement results in the creation of a damping force which is of opposite sense to the velocity of the plunger, at any instant, but which is proportional to the speed of the plunger. Thus, assuming a rigid connection between the mass and the plunger of Fig. 5.4(a),

$$\text{damping force} = -c\dot{x} \quad (5.2)$$

where  $c$  is the *coefficient of viscous damping*,  $\dot{\phantom{x}}$  indicates differentiation with respect to time, and the negative sign indicates that the damping force and  $\dot{x}$  act in opposite directions.

Practical structures do not necessarily conform to the physical laws of dashpot (or *viscous*) damping. However, since the dashpot model is mathematically convenient to handle, it is usual to derive equivalent dashpot parameters so that the relative simplicity of this model may be utilized.

If the system of Fig. 5.4(a) is disturbed axially and then allowed to vibrate freely, the motion will be attenuated due to the damping and will gradually die out. The rate of decay will depend on the severity of the damping, and, if the damping is large enough, it is possible that the vibration does not occur at all, in which case the system simply gradually returns to its undisturbed position without oscillation. The value of damping at which this phenomenon is first observed is known as *critical damping*. Practical structures do not possess this degree of damping and are therefore *underdamped*, it being convenient to express the degree of damping as a proportion of the critical damping, thus

$$\zeta = \frac{c}{c_{cr}} \quad (5.3)$$

where  $\zeta$  is the damping ratio, and  $c_{cr}$  is the critical damping coefficient.

Structural damping ratios are generally towards the lower end of the range 0.5–20% (Blevins, 1977). The axial vibration of the mass in Fig. 5.4(a), for example, will be as shown by Fig. 5.5, in which two representative values of damping ratio have been used. The characteristic decay of the vibration under damping may be noted in Fig. 5.5, which also illustrates two further points of particular importance. First it will be seen that, although damping produces a significant progressive reduction in the amplitude of the vibration, the frequency remains virtually unaffected. The analytical significance of this is that the simpler free-vibration model may be used to determine natural frequencies which will be equally applicable to the damped system. The second feature is that, since damping effects are progressive, a lightly damped model is close to an undamped one in the early stages of the motion, again a property which can lead to analytical simplification.

Before leaving the topic of damping, it is worth emphasizing the difference between damping and stiffness in respect of dynamic behaviour. The introduction of damping to the cantilever beam example (Fig. 5.4(a)) has been seen to lead to a characteristic attenuation of free vibration with little frequency change, effects which arise due to loss of energy through the damper. If the

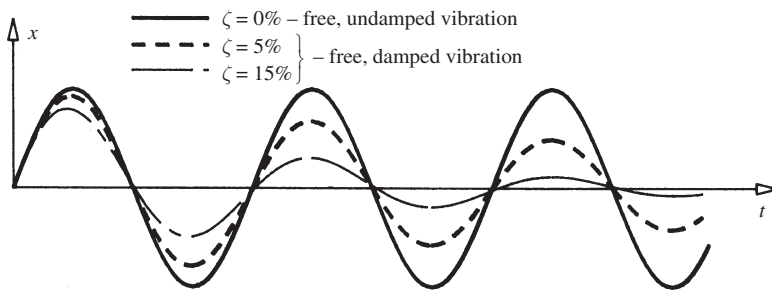


Fig. 5.5 Damped and undamped free vibration

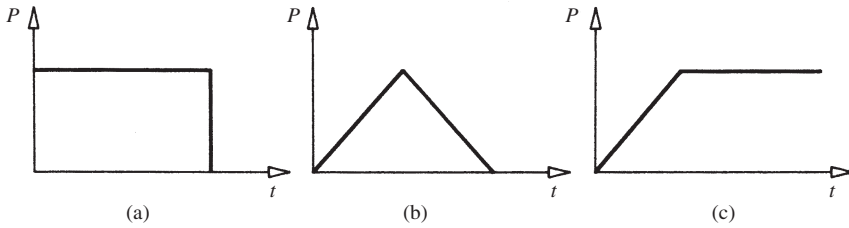


Fig. 5.6 Forcing functions

beam is alternatively stiffened by the addition of a further elastic rod (Fig. 5.4(b)), then longitudinal free-vibration oscillations would not diminish with time but the frequency of the vibration would certainly be increased due to the increased stiffness. In energy terms, stiffness (or *spring*) elements are storers rather than dissipators of energy – energy is continuously being stored as elastic strain energy and subsequently released as kinetic energy.

### 5.2.3 Forced, damped vibration

If the structure is subject to sustained time-dependent loads or support disturbances, then the resulting motion is said to be *forced* and the time-dependent forcing effect is referred to as an *excitation*. The nature of a forced vibration depends on the form of the excitation, and the effects of some common types of excitation are described in this section.

#### *Transient excitation*

If the forcing effect is sustained for a finite period of time, then the excitation is said to be *transient*. The effects of an isolated wave, wind gust or earthquake could all be treated as transient excitations, and simple representations of transient *forcing* functions are shown in Fig. 5.6.

The severity of the dynamic response to a transient excitation depends upon the rate at which the excitation changes in relation to the natural periods of the structure. Should the time taken to develop the maximum forcing load in Fig. 5.6(c), for example, be extremely brief, so that the load is ‘suddenly’ applied, then the maximum dynamic displacements and stresses are likely to be approximately double the values which would be obtained if the maximum load acted statically, a result which is commonly used in the specification of safety factors for abrupt loading. If, on the other hand, the time taken to apply the dynamic load is more than about three times the longest natural period of the structure, then there will be little difference between the dynamic and static responses. If impact loading is considered a special case, then the most



significant types of transient loading will be cases where the excitation occurs over a length of time which is of the same order as the natural period of the mode which is of interest. The severest dynamic effects due to such transient excitation will be experienced either during the application of the excitation or shortly afterwards, when the motion becomes damped, free vibration, with, as has been shown, a gradually diminishing response intensity. The time of most interest is therefore of the same order as the natural period and occurs at the start of the motion. Under these circumstances, light damping will not have developed a significant effect (Fig. 5.5) and an undamped assumption will usually yield acceptable results.

*Periodic excitation*

A periodic forcing function is such that the excitation takes the form of a function which is continuously repeated at a fixed frequency (Fig. 5.7(a)). Should the forcing function be sinusoidal, then the excitation is *harmonic*

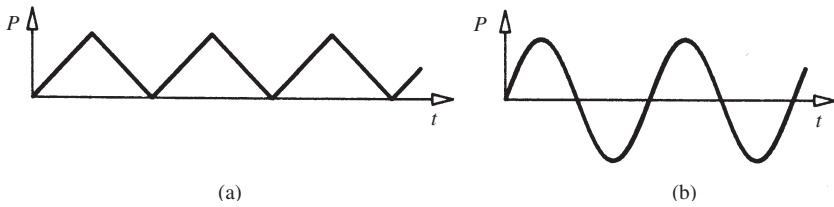


Fig. 5.7 (a) Periodic forcing function. (b) Harmonic forcing function

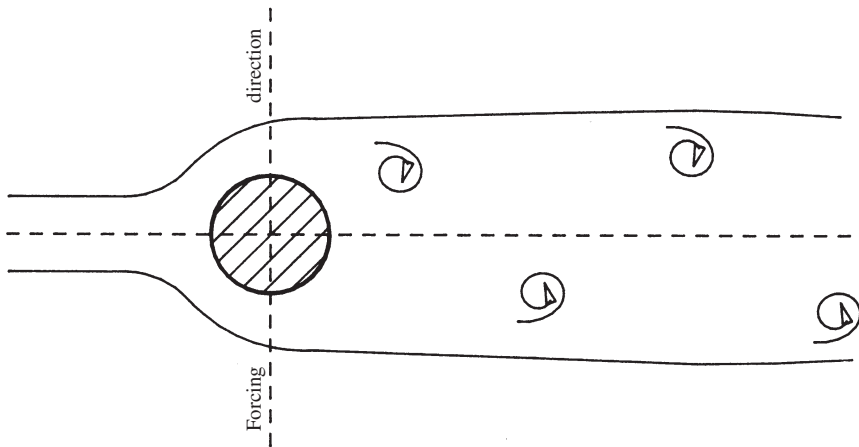


Fig. 5.8 Harmonic forcing due to vortex shedding

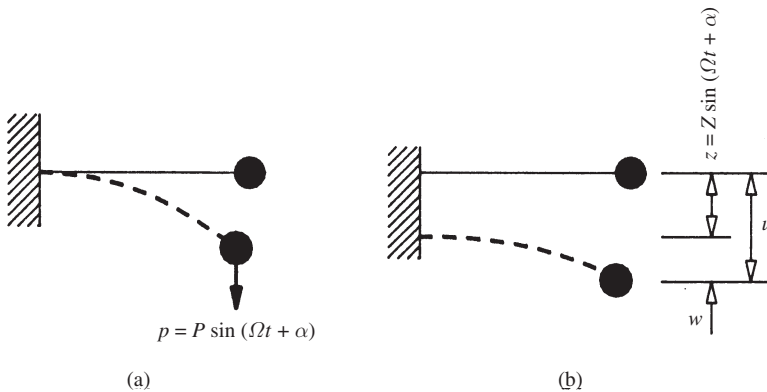


Fig. 5.9 (a) Harmonic force excitation of cantilever. (b) Harmonic support displacement excitation

(Fig. 5.7(b)). Harmonic excitation is of special importance for a variety of reasons. First, several practical excitation sources do produce harmonic forcing effects. This is the case for rotating machinery such as turbines, fans and motors and also arises when a chimney or cable is in a *steady* air-stream or an immersed tube is in a steady flow of fluid. The excitation in these two latter instances arises from vortex shedding on alternate sides of the circular section (Fig. 5.8), which leads to the generation of a harmonic forcing effect normal to the flow direction.

Harmonic forcing is also of importance for the investigation of the phenomenon of *resonance*, which will be pursued further below, and because Fourier series analysis allows *any* forcing function to be expressed as a series of harmonic functions (Craig, 1987). General forcing effects need not therefore be considered separately, since they may be represented as the sum of a set of harmonic analyses. The single degree of freedom cantilever beam will now be considered under the action of a harmonically varying lateral load applied to the end mass (Fig. 5.9(a)). Such an excitation could be produced in practice by attaching a small motor to the end of the beam and arranging for the motor to cause a small eccentric mass to rotate. The dynamic motion of the beam will be found to possess the following characteristics:

- (a) Following a transient response at the commencement of the excitation, the vibration settles down to a *steady-state* response in which its motion is harmonic and is of the same frequency as that of the excitation.
- (b) The beam's response is not in phase with the excitation, that is, the mass does not reach its displacement amplitude at the same time as the forcing effect acquires its maximum value, there being a constant *phase* difference between these two events.

If the frequency of the excitatory force is now gradually increased, the amplitude of the beam's steady-state motion will be observed to increase to a maximum and subsequently to subside as the forcing frequency is increased further. This behaviour may be conveniently examined in terms of a non-dimensional *dynamic magnification factor*, which is defined as the ratio of the beam's steady-state amplitude to the displacement which would be caused by the force amplitude of the excitation,  $P$ , acting statically. Figure 5.10(a) shows the variation of the dynamic magnification factor with the ratio of the forcing frequency to the natural frequency of the beam, and the following aspects of the behaviour are of particular importance:

- (a) Damping only significantly affects the dynamic magnification factor if the forcing frequency is in the vicinity of the natural frequency.
- (b) The dynamic magnification factor increases rapidly as the forcing frequency approaches the natural frequency and peaks when the two frequencies are equal (strictly, approximately so). The equal forcing and natural frequency condition is referred to as *resonance*, and it will be noticed from Fig. 5.10(a) that the effects of resonance are greatly ameliorated by increased damping. Under light damping conditions, resonance produces greatly enhanced displacements, which can result in structural distress.
- (c) Low frequency ratios result in an essentially 'static' response.
- (d) The response at high frequency ratios is considerably diminished in relation to the static response.

Figure 5.10(b) shows the variation in phase angle between the forcing and response functions for a range of frequency ratios. Under low damping

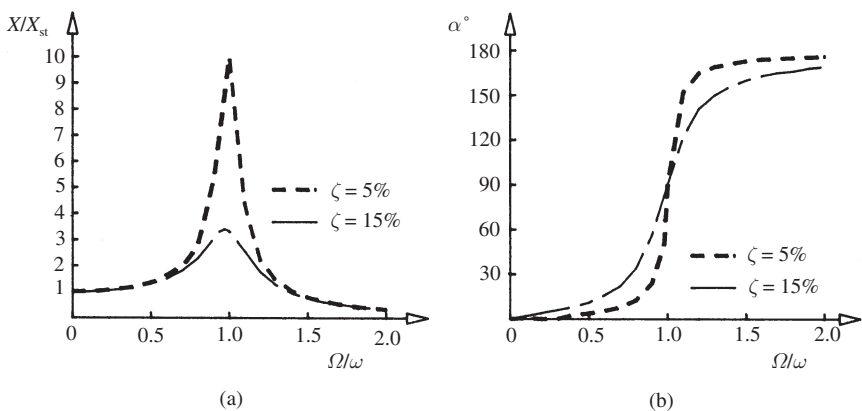


Fig. 5.10 Single degree of freedom—harmonic force excitation: (a) magnification factor against frequency ratio; (b) phase angle against frequency ratio

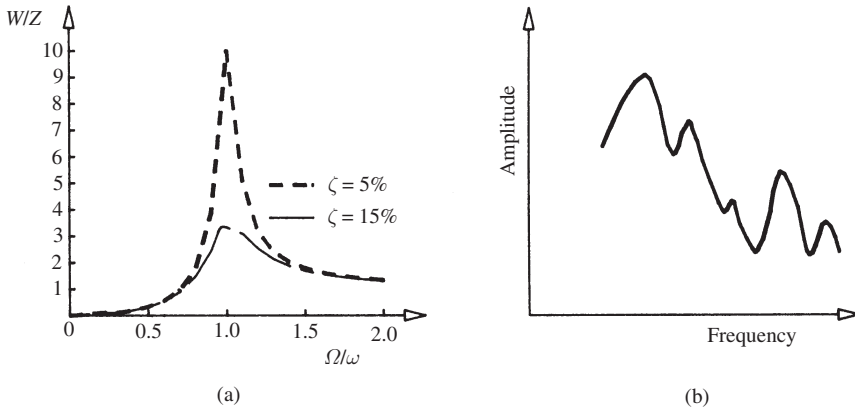


Fig. 5.11 (a) One degree of freedom—harmonic support excitation. Ratio of relative displacement amplitude to support disturbance amplitude against frequency ratio. (b) Multiple degree of freedom system. Typical amplitude against harmonic forcing frequency

conditions, it may be observed that the forcing function and the response are in phase or  $180^\circ$  out of phase, except in the resonance region, where the phase angle changes rapidly and is  $90^\circ$  at resonance. At resonance, therefore, the forcing function attains its maximum value when the system is at its undisturbed position, and has zero value when the system is at its amplitude.

Figure 5.11(a) shows a plot for forced motion of the beam in which the excitation is provided by a harmonic support movement (Fig. 5.9(b)). In this case, the response is most conveniently measured in terms of the relative displacement,  $w$ , between the mass and the support, and the figure shows the variation of the ratio of the amplitude of  $w$ ,  $W$ , to the support movement amplitude,  $Z$ , against frequency ratio. The presence of resonance at the natural frequency may again be observed, and it will also be seen that low-frequency support movements produce no relative displacement, so that the mass follows the support displacement. High-frequency support excitation, however, tends to produce a relative displacement equal in magnitude to the support movement.

### Random excitation

Many natural forcing effects (winds, waves and earthquakes, for example) fall into this category and, while a simplified treatment may be possible on the basis of a periodic forcing assumption, a complete analysis requires a statistical treatment (Gould and Abu-sitta, 1980) which is beyond the scope of the present text.

### Natural frequencies and forced vibration

If a multiple degree of freedom system is considered, for example the two-mass cantilever of Fig. 5.3(a), then, under harmonic forcing, it will resonate in both the mode of Fig. 5.3(b) at its first natural frequency and also in the mode of Fig. 5.3(c) at its second natural frequency. If a general multiple degree of freedom system is subjected to harmonic forcing, then its response may be illustrated diagrammatically by Fig. 5.11(b), where the amplitude of a typical displacement is plotted against forcing frequency. The peaks correspond to the system's natural frequencies, and there is general trend towards lower resonance magnification at higher natural frequencies.

Since resonance involves magnified displacements and, hence, stresses, it is usually of particular concern that the forcing frequencies at which resonance occurs, especially the lower ones, are identified, and it has been seen that these frequencies are the natural frequencies of the structure. In addition to identifying resonant states under harmonic forcing, however, natural frequencies and modes can also be used to investigate more general vibrations of a free, transient or periodic nature, so that the establishment of the natural frequencies of a structure is of paramount importance and will be considered in the next section.

## 5.3 Determination of natural frequencies and modes

### 5.3.1 Modelling

In the following, it will be assumed that the structure may be modelled by a finite number of discrete masses (Fig 5.12) which are interconnected by linear elastic structural elements. The structural elements may be one-dimensional elements in the case of skeletal structures or higher-dimensional finite elements in the case of continua. It will be further assumed that the masses are concentrated into 'point' masses so that their mass moments of inertia are negligibly small, a model which is usually termed a *lumped-mass* approximation.

### 5.3.2 Theory

A lumped-mass model will be assumed to be undergoing free vibration, and its displaced shape, at any instant, will be defined by a set of coordinates,  $\{x\}$ , relative to its position of static equilibrium. In the static equilibrium position, internal forces are developed in the structure which just balance the gravitational forces on the point masses. The dynamic displacements,  $\{x\}$ , therefore represent a disturbance from the static equilibrium position and will result in a set of additional internal forces which will tend to restore the structure to its equilibrium state. The additional internal forces may be related to the dynamic displacements by the usual stiffness relationship as

$$\{F\} = [K]\{x\} \quad (5.4)$$

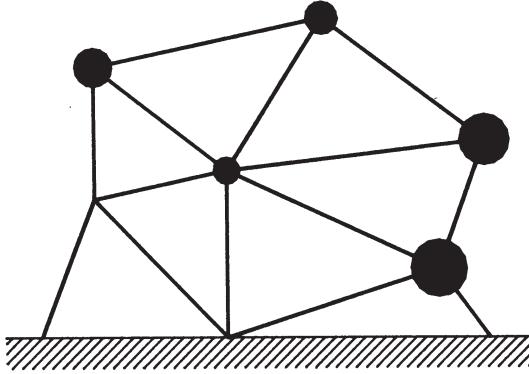


Fig. 5.12 General dynamic model

By virtue of the equality of damped and undamped free-vibration frequencies, natural frequencies may be determined on the simpler undamped model, so that the forces,  $\{F\}$ , are the only *unbalanced* forces acting on the structure. These forces therefore produce a set of accelerations,  $\{\ddot{x}\}$ , to which they may be related by Newton's second law of motion as

$$\begin{aligned}
 F_1 &= -m_1 \ddot{x}_1 \\
 \dots & \\
 F_r &= -m_r \ddot{x}_r \\
 \dots & \\
 F_n &= -m_n \ddot{x}_n
 \end{aligned}
 \tag{5.5}$$

where the negative signs arise since the restoring forces  $\{F\}$  act in the opposite direction to  $\{\ddot{x}\}$ . Or, in matrix terms,

$$\{F\} = -[M]\{\ddot{x}\} \tag{5.6}$$

where  $[M]$  is the diagonal *mass matrix* given by

$$[M] = \begin{bmatrix} m_1 & & & \\ & \cdot & & 0 \\ & & m_r & \\ & 0 & & \cdot \\ & & & & m_n \end{bmatrix} \tag{5.7}$$

However, *if* the structure is undergoing vibration in a *principal* mode, then each displacement component executes harmonic motion *with the same natural frequency*. Hence

$$x_r = A_r \sin(\omega t + \alpha) \tag{5.8}$$

So that

$$\ddot{x}_r = -\omega^2 A_r \sin(\omega t + \alpha) = -\omega^2 x_r \quad (5.9)$$

and

$$\{\ddot{x}\} = -\omega^2 \{x\} \quad (5.10)$$

Hence, by eliminating the unbalanced forces and accelerations from equations (5.4), (5.6) and (5.10),

$$[K]\{x\} = -[M]\{x\} = \omega^2 [M]\{x\} \quad (5.11)$$

or

$$[K - \omega^2 M]\{x\} = \{0\} \quad (5.12)$$

An alternative form of equation (5.12) may be obtained by pre-multiplying equation (5.11) by  $[K]^{-1}$  to give

$$[I]\{x\} = \omega^2 [K]^{-1} [M]\{x\} \quad (5.13)$$

where  $[K]^{-1}[M]$  is known as the *dynamic matrix*.

Upon re-arrangement,

$$\left[ K^{-1}M - \frac{1}{\omega^2} I \right] \{x\} = \{0\} \quad (5.14)$$

Equation (5.14) represents a standard *eigenvalue* problem, as it takes the form

$$[A - \lambda I]\{x\} = \{0\} \quad (5.15)$$

By applying standard solution techniques (Prentis and Leckie, 1963; Jennings, 1977) to either equation (5.12) or (5.14) the eigenvalues and hence the natural frequencies, may be determined. For each eigenvalue, it will be possible to determine an associated principal mode of vibration by solving equations (5.12) for the displacement vector,  $\{x\}$ , which, mathematically, is termed an *eigenvector*. It is, in fact, only possible to determine relative displacements in this way, as will be apparent from the time-dependent nature of the displacements. Any principal mode solution may therefore be multiplied by an arbitrary constant to produce another solution. It is usual and convenient to choose the arbitrary constant such that the principal mode is *normalized*, which may be done in several different ways:

- (a) A *specific* displacement component may be allocated a particular value, normally unity.
- (b) The *largest* displacement component may be allocated a particular value, again normally unity.
- (c) The mode may be normalized such that the *modal* mass defined by

$$m_{\phi_r} = \{\phi_r\}^T [M] \{\phi_r\} \quad (5.16)$$

takes a specified value, often unity, where  $\{\phi_r\}$  is the *r*th mode vector.

The choice of normalization scheme, if any, is immaterial, and any scheme may be used according to personal preference in the given circumstances.

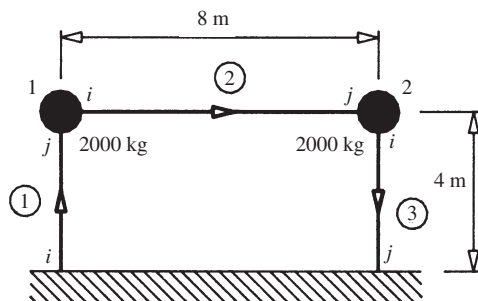
The number of natural frequencies which may be obtained in the above manner will be equal to the number of coordinates in equations (5.5) which are associated with non-zero masses. In formulating the dynamic model there is generally some freedom in the choice of the number and type of both the coordinates and the masses employed, and the selections made will affect both the number and the types of the natural frequencies which are obtainable. Considerable judgement may therefore be required in the establishment of a suitable model, as will be demonstrated by the examples given in the following sections.

### 5.3.3 Example 5.1 – single-storey sway frame

The natural frequencies and modes of the single-storey sway frame shown in Fig. 5.13 are to be determined. It is assumed that standard computer routines are available for the determination of eigenvalues and vectors, so that, from equation (5.12), the problem becomes one of determining the stiffness and mass matrices for an appropriate dynamic model.

The usual plane frame representation (Ghali and Neville, 1997) using a three-component joint displacement representation will be employed, so that, taking the non-restrained displacement components only, the coordinate set becomes

$$\{x\} = \begin{Bmatrix} u_1 \\ v_1 \\ \theta_1 \\ u_2 \\ v_2 \\ \theta_2 \end{Bmatrix} \quad (5.17)$$



For all members:  $E = 200 \text{ kN/mm}^2 = 200 \times 10^9 \text{ N/m}^2$   
 $A = 1 \times 10^4 \text{ mm}^2 = 1 \times 10^{-2} \text{ m}^2$ ,  $I = 3 \times 10^8 \text{ mm}^4 = 3 \times 10^{-4} \text{ m}^4$

Fig. 5.13 Sway frame example



$$\begin{aligned}
 \{f^e\} &= \begin{Bmatrix} f_i \\ f_j \end{Bmatrix} = \begin{Bmatrix} f_{xi} \\ f_{yj} \\ m_i \\ f_{xj} \\ f_{yj} \\ m_j \end{Bmatrix} = \begin{Bmatrix} k_{ii} & k_{ij} \\ k_{ji} & k_{jj} \end{Bmatrix} \begin{Bmatrix} u_i \\ v_i \\ \theta_i \\ u_j \\ v_j \\ \theta_j \end{Bmatrix} = [k] \{\delta^e\} \quad (5.18)
 \end{aligned}$$

where

$$[k] = \begin{bmatrix}
 c^2 \frac{EA}{L} + s^2 \frac{12EI}{L^3} & \frac{EA}{L} & \frac{12EI}{L^3} & \frac{6EI}{L^2} & s \frac{6EI}{L^2} & -c^2 \frac{EA}{L} + s^2 \frac{12EI}{L^3} & -s \frac{6EI}{L^2} \\
 \frac{EA}{L} & \frac{12EI}{L^3} & \frac{12EI}{L^3} & \frac{6EI}{L^2} & -c \frac{6EI}{L^2} & \frac{EA}{L} + c^2 \frac{12EI}{L^3} & \frac{6EI}{L^2} \\
 \frac{12EI}{L^3} & \frac{12EI}{L^3} & \frac{12EI}{L^3} & \frac{6EI}{L^2} & -c \frac{6EI}{L^2} & \frac{EA}{L} + s^2 \frac{12EI}{L^3} & -c \frac{6EI}{L^2} \\
 \frac{6EI}{L^2} & \frac{6EI}{L^2} & \frac{6EI}{L^2} & \frac{4EI}{L} & -s \frac{6EI}{L^2} & \frac{6EI}{L^2} & \frac{2EI}{L} \\
 s \frac{6EI}{L^2} & -c \frac{6EI}{L^2} & -c \frac{6EI}{L^2} & \frac{4EI}{L} & -s \frac{6EI}{L^2} & \frac{6EI}{L^2} & \frac{2EI}{L} \\
 -c^2 \frac{EA}{L} + s^2 \frac{12EI}{L^3} & \frac{EA}{L} & \frac{12EI}{L^3} & \frac{6EI}{L^2} & -s \frac{6EI}{L^2} & -c^2 \frac{EA}{L} + s^2 \frac{12EI}{L^3} & -s \frac{6EI}{L^2} \\
 \frac{EA}{L} & \frac{12EI}{L^3} & \frac{12EI}{L^3} & \frac{6EI}{L^2} & -c \frac{6EI}{L^2} & \frac{EA}{L} + c^2 \frac{12EI}{L^3} & \frac{6EI}{L^2} \\
 \frac{12EI}{L^3} & \frac{12EI}{L^3} & \frac{12EI}{L^3} & \frac{6EI}{L^2} & -c \frac{6EI}{L^2} & \frac{EA}{L} + s^2 \frac{12EI}{L^3} & -c \frac{6EI}{L^2} \\
 \frac{6EI}{L^2} & \frac{6EI}{L^2} & \frac{6EI}{L^2} & \frac{4EI}{L} & -s \frac{6EI}{L^2} & \frac{6EI}{L^2} & \frac{2EI}{L} \\
 s \frac{6EI}{L^2} & -c \frac{6EI}{L^2} & -c \frac{6EI}{L^2} & \frac{4EI}{L} & -s \frac{6EI}{L^2} & \frac{6EI}{L^2} & \frac{2EI}{L}
 \end{bmatrix}$$

and  $c = \cos \alpha$ ,  $s = \sin \alpha$  (see Fig. 5.14)

For the plane frame element shown in Fig. 5.14, the element stiffness equations are as given in equation (5.18) (page 232), while the sub-matrix form of the overall structure stiffness matrix may be established (by the methods described above) to be

$$[K] = \begin{matrix} & \begin{matrix} 1 & 2 \end{matrix} \\ \begin{matrix} 1 \\ 2 \end{matrix} & \begin{bmatrix} k_{ii}^1 + k_{ii}^2 & & k_{ij}^2 \\ & k_{ji}^2 & \\ & & k_{jj}^2 + k_{ii}^3 \end{bmatrix} \end{matrix} \quad (5.19)$$

The stiffness matrix may be obtained in numeric form by appropriate substitution from equation (5.18) into equation (5.19). However, it must be borne in mind that for dynamic equations of the form of equations (5.5) to be valid, a consistent set of units must be employed. Since a force of 1 N produces an acceleration of 1 m/s<sup>2</sup> when acting on a mass of 1 kg, newtons, metres and seconds are a consistent set of units and should be used throughout any problem involving dynamics. Thus from equation (5.18), using newton and metre units,

$$[k_{ij}^1] = 10^5 \begin{bmatrix} 112.5 & & \text{sym.} \\ 0 & 5000 & \\ -225 & 0 & 600 \end{bmatrix}$$

$$[k_{ii}^2] = 10^5 \begin{bmatrix} 2500 & & \text{sym.} \\ 0 & 14.1 & \\ 0 & -56.3 & 300 \end{bmatrix}, \quad [k_{jj}^2] = 10^5 \begin{bmatrix} -2500 & 0 & 0 \\ 0 & -14.1 & 56.3 \\ 0 & -56.3 & 150 \end{bmatrix}$$

$$[k_{ij}^3] = 10^5 \begin{bmatrix} 2500 & & \text{sym.} \\ 0 & 14.1 & \\ 0 & 56.3 & 300 \end{bmatrix}, \quad [k_{ii}^3] = 10^5 \begin{bmatrix} 112.5 & & \text{sym.} \\ 0 & 5000 & \\ -225 & 0 & 600 \end{bmatrix}$$

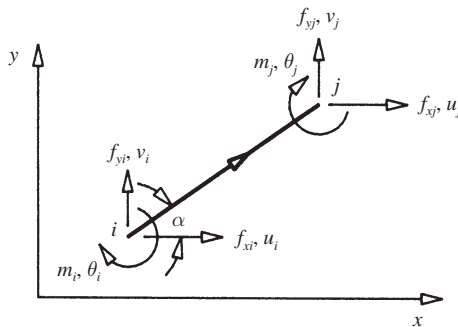


Fig. 5.14 Plane frame element

Whence, by substituting into equation (5.19),

$$[K] = 10^5 \begin{bmatrix} 2612.5 & & & & & & & \\ & 0 & 5014.1 & & & & & \\ & -225 & -56.3 & 900 & & & & \\ & -2500 & 0 & 0 & 2612.5 & & & \\ & 0 & -14.1 & 56.3 & 0 & 5014.1 & & \\ & 0 & -56.3 & 150 & -225 & 56.3 & 900 & \end{bmatrix} \quad (5.20)$$

The mass matrix may be formed by considering the nodal equations of motion, which have the general form given in equations (5.5). For the sway frame under consideration, these equations become

$$\begin{aligned} F_{x1} &= -m_1 \ddot{u}_1 \\ F_{y1} &= -m_1 \ddot{v}_1 \\ M_1 &= -I_{m1} \ddot{\theta}_1 \\ F_{x2} &= -m_2 \ddot{u}_2 \\ F_{y2} &= -m_2 \ddot{v}_2 \\ M_2 &= -I_{m2} \ddot{\theta}_2 \end{aligned} \quad (5.21)$$

where  $I_m$  is the mass moment of inertia

Since a lumped-mass model is to be used, the mass moment of inertias will be presumed to be zero, so that the mass matrix is given by

$$[M] = \begin{bmatrix} 2000 & & & & & & & \\ & 0 & 2000 & & & & & \\ & 0 & 0 & 0 & & & & \\ & 0 & 0 & 0 & 2000 & & & \\ & 0 & 0 & 0 & 0 & 2000 & & \\ & 0 & 0 & 0 & 0 & 0 & 0 & 0 \end{bmatrix} \\ = \text{diag}[2000, 2000, 0, 2000, 2000, 0] \quad (5.22)$$

Since there are four coordinates associated with a non-zero mass (equations (5.21)), it will be possible to determine four natural frequencies and modes if the stiffness and mass matrices given by equations (5.20) and (5.22) are substituted into equation (5.12). When evaluated from this equation by a standard computer routine, the natural frequencies are

$$\omega^2 = 3.21 \times 10^3, 2.50 \times 10^5, 2.51 \times 10^5 \text{ or } 2.52 \times 10^5 \quad (5.23a)$$

Whence, since  $f = \omega/2\pi$ ,

$$f = 9.01, 79.6, 79.7 \text{ or } 79.8 \text{ Hz} \quad (5.23a)$$

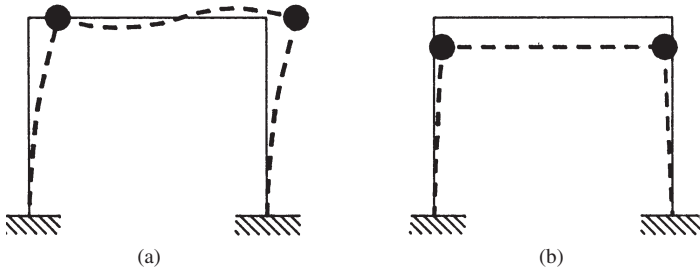


Fig. 5.15 Example 5.1—fundamental and higher modes

From the natural frequencies of equation (5.23), it may be observed that the lowest frequency is considerably less than the remaining three natural frequencies, which happen to be very close to each other in this case.

The mode associated with the lowest natural frequency is shown in Fig. 5.15(a), and is a flexural mode involving sideways of the frame and consequent bending of the columns and beam of the frame. The frame members do not undergo axial deformation in this mode, since the column sideways are equal, at any instant, and hence the beam is not distorted axially. Furthermore, nodes 1 and 2 do not displace vertically during the motion, so that the columns are also axially undistorted. The higher modes all involve axial deformation, and a typical mode shape is shown in Fig. 5.15(b), where the vertical displacements of the nodes deform the columns axially, while the opposing sense of the horizontal displacements results in axial deformation of the beam member.

The lower natural frequencies of a system are commonly those of most interest, since these modes tend to dominate in any general vibration of the system, and, as seen already, resonance effects are most severe (Fig. 5.12(b)) at the lower natural frequencies. The lowest frequency of all is, in fact, often termed the *fundamental* frequency to emphasize its significance. For this sway frame example, it has already been pointed out that the fundamental mode is a purely flexural one, and it is therefore reasonable to consider the possibility of constructing a simpler analytical model which treats bending deformations only. The analysis of the frame under these conditions is treated in the next section, together with the dynamic analysis of beams, where it is also reasonable to disregard axial modes.

### 5.3.4 Simplified analysis of sway frames

If axial deformations are assumed negligible, the nodes of a general sway frame (Fig. 5.16(a)) do not displace vertically and the horizontal

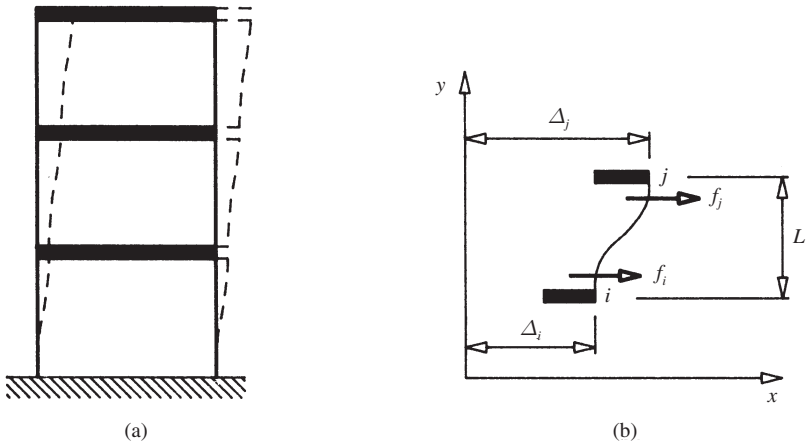


Fig. 5.16 (a) General sway frame. (b) Column element under sway

displacements of the nodes at any one storey are equal. A further simplification may be made if it is also assumed that the nodes do not rotate, which will be the case if the beam bending stiffnesses are very much greater than those of the columns. In these circumstances, there is only one coordinate for each storey – its horizontal displacement – and the element stiffness matrix for a column element which sways without end rotation (Fig. 5.16(b)) is given by

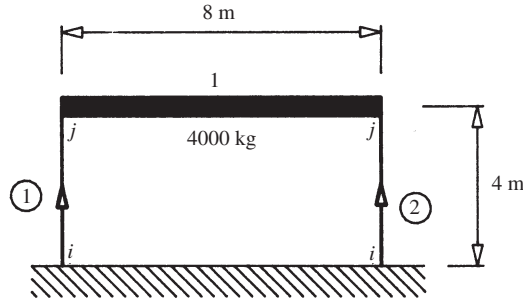
$$\begin{aligned} \{f^e\} &= \begin{Bmatrix} f_i \\ f_j \end{Bmatrix} = 12 \frac{EI}{L^3} \begin{bmatrix} 1 & -1 \\ -1 & 1 \end{bmatrix} \begin{Bmatrix} \Delta_i \\ \Delta_j \end{Bmatrix} \\ &= \begin{bmatrix} k_{ii} & k_{ij} \\ k_{ji} & k_{jj} \end{bmatrix} \begin{Bmatrix} \Delta_i \\ \Delta_j \end{Bmatrix} = [k] \{\delta^e\} \end{aligned} \quad (5.24)$$

Since there is one coordinate per storey, it is only necessary to use nodes at each storey level of a sway frame and there is hence just one node involved in the single-storey frame of example 5.1 (Fig. 5.17). The total mass will also be assumed to be located at the rigid beam level, as shown in Fig. 5.17. If the rigid foundation node is excluded, the stiffness ‘matrix’ becomes the scalar of equation (5.25) and the mass matrix the scalar of equation (5.26):

$$[K] = [k_{ij}^1 + k_{ij}^2] = 12 \frac{EI}{L^3} [2] = 24 \frac{EI}{L^3} \quad (5.25)$$

$$[M] = [4000] \text{ kg} \quad (5.26)$$

Substituting for the stiffness and mass matrices from equations (5.25) and (5.26) in the natural frequency equation (5.12), the circular natural frequencies are given by



For both columns:  $E = 200 \text{ kN/mm}^2 = 200 \times 10^9 \text{ N/m}^2$   
 $A = 1 \times 10^4 \text{ mm}^2 = 1 \times 10^{-2} \text{ m}^2$ ,  $I = 3 \times 10^8 \text{ mm}^4 = 3 \times 10^{-4} \text{ m}^4$

Fig. 5.17 Example 5.1—simplified model

$$24 \frac{EI}{L^3} - \omega^2 \times 4000 = 0 \quad (5.27)$$

Since this model involves only one coordinate with an associated non-zero mass, it is only possible to determine a single natural frequency, which is given by the positive root of equation (5.27):

$$\omega = \left( \frac{24 \times 200 \times 10^9 \times 3 \times 10^{-4}}{4^3 \times 4000} \right)^{1/2} = 75 \text{ rad/s} \quad (5.28)$$

Whence

$$f = \frac{\omega}{2\pi} = 11.9 \text{ Hz} \quad (5.29)$$

The natural frequency of 11.9 Hz derived from this simplified model is not a particularly good approximation to the fundamental frequency of 9.0 Hz obtained earlier (equation (5.23)). However, due to its greater length, the beam bending stiffness used in the earlier analysis was actually less than that of the columns and was hence far from satisfactory in respect of the rigid beam assumption of the simplified model. Simplified models therefore need to be used with care (Hurty and Rubinstein, 1964) and comparisons of calculated with observed values can be poor (Ellis, 1980) unless very considerable care is taken with the modelling, which may have to include the stiffening effect of non-structural building components.

#### Example 5.2 – two-storey sway frame

As a further example of the use of the simplified sway frame model, the natural frequencies and modes for the two-storey frame shown in Fig. 5.18

will be determined. Assuming consistent units, the stiffness matrix may be established as shown by

$$\begin{aligned}
 [K] &= \begin{matrix} & \begin{matrix} 1 & 2 \end{matrix} \\ \begin{matrix} 1 \\ 2 \end{matrix} & \begin{bmatrix} k_{jj}^1 + k_{jj}^2 + k_{ii}^3 + k_{ii}^4 & k_{ij}^3 + k_{ij}^4 \\ k_{ji}^3 + k_{ji}^4 & k_{jj}^3 + k_{jj}^4 \end{bmatrix} \end{matrix} \\
 &= 12 \frac{EI}{L^3} \begin{bmatrix} 4 & -2 \\ -2 & 2 \end{bmatrix} = \beta \begin{bmatrix} 2 & -1 \\ -1 & 1 \end{bmatrix} \quad (5.30)
 \end{aligned}$$

where  $\beta = 24EI/L^3$ . Assuming that the equal masses,  $m$  (Fig. 5.18), are concentrated at the beam levels, the mass matrix is given by

$$[M] = \begin{bmatrix} m & 0 \\ 0 & m \end{bmatrix} \quad (5.31)$$

For this case, the natural frequency relationship corresponding to equation (5.12) becomes

$$[K - \omega^2 M] \{x\} = \beta \begin{bmatrix} 2 - \frac{m\omega^2}{\beta} & -1 \\ -1 & 1 - \frac{m\omega^2}{\beta} \end{bmatrix} \begin{Bmatrix} \Delta_1 \\ \Delta_2 \end{Bmatrix} = \{0\} \quad (5.32)$$

For an equation such as equation (5.32) to have a non-trivial solution:

$$\det[K - \omega^2 M] = 0 \quad (5.33)$$

In this case then

$$\left( 2 - \frac{m\omega^2}{\beta} \right) \left( 1 - \frac{m\omega^2}{\beta} \right) - 1 = 0 \quad (5.34)$$

or

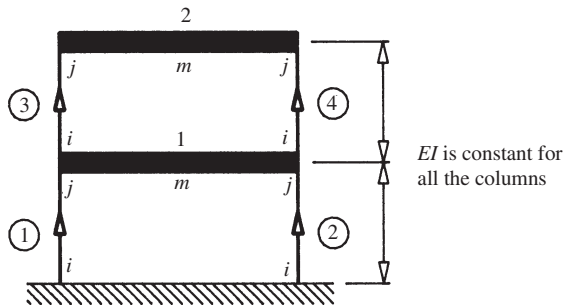


Fig. 5.18 Example 5.2—two-storey sway frame

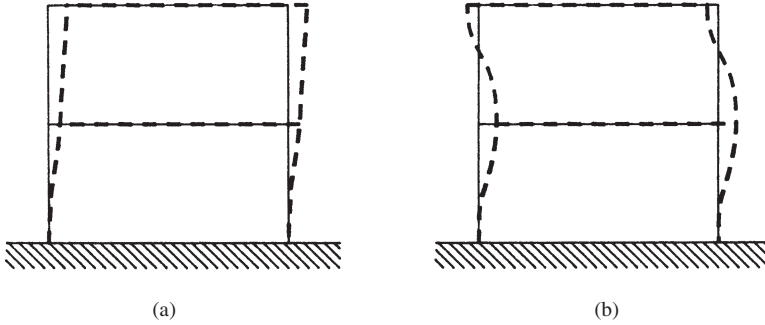


Fig. 5.19 Example 5.2—principal modes

$$\alpha^2 - 3\alpha + 1 = 0 \quad (5.35)$$

where

$$\alpha = \frac{m\omega^2}{\beta}$$

Whence

$$\alpha = 0.382 \quad \text{or} \quad 2.62 \quad (5.36)$$

So that

$$\omega = 3.03 \left( \frac{EI}{mL^3} \right)^{1/2} \quad \text{or} \quad 7.93 \left( \frac{EI}{mL^3} \right)^{1/2} \quad (5.37)$$

As expected, this two-coordinate problem has resulted in two natural frequencies, and the associated modes may now be determined by substitution in equation (5.32) for the two frequencies. Since only ratios of the dynamic displacements may be obtained from a set of equations such as equations (5.32), normalization of the modes may be conveniently carried out at this stage by allocating a particular displacement the value of unity according to the normalization scheme (a) above. If the displacement at storey 1 is given the value unity, then the relative displacement at storey 2 may be determined from either of the equations (5.32), to give the modes for the two natural frequencies:

$$\{\phi\} = \begin{Bmatrix} 1.00 \\ 1.62 \end{Bmatrix} \quad \text{or} \quad \begin{Bmatrix} 1.00 \\ -0.62 \end{Bmatrix} \quad (5.38)$$

The similar signs involved in the first (fundamental) mode for the frame imply that the frame vibrates such that the two storeys always sway in the same direction (Fig. 5.19(a)), in contrast to the second mode, where the opposing signs indicate dissimilar sway directions (Fig. 5.19(b)) for the two storeys.



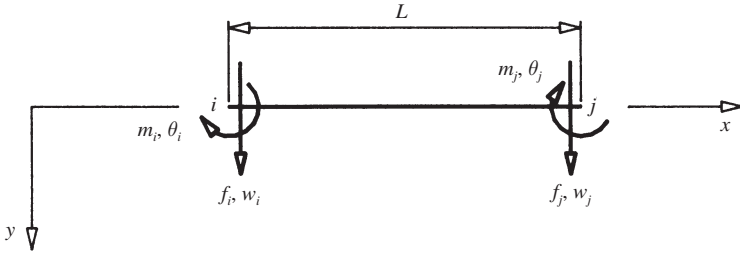


Fig. 5.20 Beam element

### 5.3.5 Analysis of beams

Modes involving axial components of vibration will normally have significantly higher natural frequencies than purely flexural modes, and therefore only bending stiffness will be included in beam problems. For a beam element (Fig. 5.20), the element stiffness matrix is

$$\begin{Bmatrix} f_i \\ f_j \\ m_i \\ m_j \end{Bmatrix} = \begin{Bmatrix} f_i \\ m_i \\ f_j \\ m_j \end{Bmatrix} = \begin{bmatrix} k_{ii} & k_{ij} \\ k_{ji} & k_{jj} \end{bmatrix} \begin{Bmatrix} w_i \\ \theta_i \\ w_j \\ \theta_j \end{Bmatrix} = [k] \begin{Bmatrix} \delta_i \\ \delta_j \end{Bmatrix} \quad (5.39)$$

where

$$[k] = EI \begin{bmatrix} \frac{12}{L^3} & \frac{6}{L^2} & -\frac{12}{L^3} & \frac{6}{L^2} \\ \frac{6}{L^2} & \frac{4}{L} & -\frac{6}{L^2} & \frac{2}{L} \\ -\frac{12}{L^3} & -\frac{6}{L^2} & \frac{12}{L^3} & -\frac{6}{L^2} \\ \frac{6}{L^2} & \frac{2}{L} & -\frac{6}{L^2} & \frac{4}{L} \end{bmatrix}$$

The structure stiffness and mass matrices for beam analysis may be assembled in a similar fashion to that employed previously to eventually yield the natural frequencies and modes, as will be illustrated in the following example.

#### Example 5.3 – cantilever beam

The beam considered in this example (Fig. 5.21) is of the same form as the two-mass cantilever beam discussed in general terms in the introduction (Fig. 5.3 *et seq.*). The general form of the stiffness matrix may be established either from

first principles or by noting that the element interconnection for a beam has a similar linear, unbranched form as the shell problems studied in Chapter 4:

$$[k] = \begin{matrix} & \begin{matrix} 1 & 2 \end{matrix} \\ \begin{matrix} 1 \\ 2 \end{matrix} & \begin{bmatrix} k_{ij}^1 + k_{ii}^2 & k_{ij}^2 \\ -k_{ji}^2 & k_{jj}^2 \end{bmatrix} \end{matrix} \quad (5.40)$$

and the stiffness matrices therefore also take the same form (equation (4.69)). For a beam structure, there are two resultant ‘forces’ at each node (Fig. 5.20), a vertical force and a moment, so that, at a typical node  $i$ , the equations of motion corresponding to equations (5.21) become

$$F_1 = -1500\ddot{w}_1, \quad M_1 = -I_{M_1}\ddot{\theta}_1, \quad F_2 = -1000\ddot{w}_2, \quad M_2 = -I_{M_2}\ddot{\theta}_2 \quad (5.41)$$

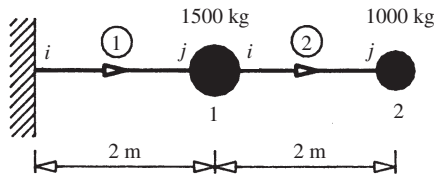
Again assuming negligible mass moment of inertias for the point masses, the mass matrix is therefore

$$[M] = \text{diag}[1500, 0, 1000, 0] \quad (5.42)$$

The natural frequencies may now be evaluated either by using a standard computer routine for eigenvalue determination or by using the condition of equation (5.33), as will be employed here. Using equations (5.41), (5.42) and (5.39), the natural frequency relationship corresponding to equation (5.12) may be expressed as

$$EI \begin{bmatrix} 3 & 0 & -\frac{3}{2} & \frac{3}{2} \\ 0 & 4 & -\frac{3}{2} & 1 \\ -\frac{3}{2} & -\frac{3}{2} & \frac{3}{2} & -\frac{3}{2} \\ \frac{3}{2} & 1 & -\frac{3}{2} & 2 \end{bmatrix} \begin{Bmatrix} w_1 \\ \theta_1 \\ w_2 \\ \theta_2 \end{Bmatrix} - \omega^2 \begin{bmatrix} 1500 & 0 & 0 & 0 \\ 0 & 0 & 0 & 0 \\ 0 & 0 & 1000 & 0 \\ 0 & 0 & 0 & 0 \end{bmatrix} \begin{Bmatrix} w_1 \\ \theta_1 \\ w_2 \\ \theta_2 \end{Bmatrix} = \{0\} \quad (5.43)$$

The labour involved in determining the fourth-order determinant which results from the application of equation (5.33) to this problem may be minimized by the use of a ‘reduction’ process. To see how such a process works, a generalization of equations (5.43) will be considered in which all the equations involving zero-mass components have been segregated as indicated in



$$E = 200 \text{ kN/mm}^2 = 200 \times 10^9 \text{ N/mm}^2, \quad I = 2 \times 10^8 \text{ mm}^4 = 2 \times 10^{-4} \text{ m}^4$$

Fig. 5.21 Example 5.3—cantilever beam

$$\begin{bmatrix} K_{aa} & K_{ab} \\ K_{ba} & K_{bb} \end{bmatrix} \begin{Bmatrix} x_a \\ x_b \end{Bmatrix} - \omega^2 \begin{bmatrix} M_{aa} & 0 \\ 0 & 0 \end{bmatrix} \begin{Bmatrix} x_a \\ x_b \end{Bmatrix} = \begin{Bmatrix} 0 \\ 0 \end{Bmatrix} \quad (5.44)$$

It is now possible to eliminate the coordinates associated with the zero-mass components by use of the lower sub-matrix expression in equation (5.44) to give

$$\{x_b\} = -[K_{bb}]^{-1}[K_{ba}]\{x_a\} \quad (5.45)$$

Substituting for the coordinates to be eliminated from equation (5.45) into the upper sub-matrix expression of equation (5.44) gives

$$[K_{aa} : K_{ab}] \begin{Bmatrix} x_a \\ -[K_{bb}]^{-1}[K_{ba}]\{x_a\} \end{Bmatrix} - \omega^2 [M_{aa}]\{x_a\} = \{0\} \quad (5.46)$$

A natural frequency relationship involving a reduced set of coordinates may now be established from equation (5.46) as

$$[K_{aa} - K_{ab}K_{bb}^{-1}K_{ba}]\{x_a\} - \omega^2 [M_{aa}]\{x_a\} = \{0\} \quad (5.47)$$

To apply this reduction process to the example under consideration, equation (5.43) is first reorganized along the lines of equation (5.44). This requires the exchange of the second and third *columns* of each of the matrices to ensure that the variables associated with non-zero masses are in the upper sub-matrix. The second and third *rows* are then exchanged to ensure that the non-zero masses occupy the upper sub-matrix position:

$$EI \begin{bmatrix} 3 & -\frac{3}{2} & 0 & \frac{3}{2} \\ -\frac{3}{2} & \frac{3}{2} & -\frac{3}{2} & -\frac{3}{2} \\ 0 & -\frac{3}{2} & 4 & 1 \\ \frac{3}{2} & -\frac{3}{2} & 1 & 2 \end{bmatrix} \begin{Bmatrix} w_1 \\ w_2 \\ \theta_1 \\ \theta_2 \end{Bmatrix} - \omega^2 \begin{bmatrix} 1500 & 0 & 0 & 0 \\ 0 & 1000 & 0 & 0 \\ 0 & 0 & 0 & 0 \\ 0 & 0 & 0 & 0 \end{bmatrix} \begin{Bmatrix} w_1 \\ w_2 \\ \theta_1 \\ \theta_2 \end{Bmatrix} = \{0\} \quad (5.48)$$

In this case then

$$[K_{bb}] = EI \begin{bmatrix} 4 & 1 \\ 1 & 2 \end{bmatrix} \quad (5.49a)$$

hence

$$[K_{bb}]^{-1} = \frac{1}{7EI} \begin{bmatrix} 2 & -1 \\ -1 & 4 \end{bmatrix} \quad (5.49b)$$

and

$$\begin{aligned} [K_{ab}][K_{bb}]^{-1}[K_{ba}] &= \frac{EI}{7} \begin{bmatrix} 0 & \frac{3}{2} \\ -\frac{3}{2} & -\frac{3}{2} \end{bmatrix} \begin{bmatrix} 2 & -1 \\ -1 & 4 \end{bmatrix} \begin{bmatrix} 0 & -\frac{3}{2} \\ \frac{3}{2} & -\frac{3}{2} \end{bmatrix} \\ &= \frac{9EI}{28} \begin{bmatrix} 4 & -3 \\ -3 & 4 \end{bmatrix} \end{aligned}$$

So that

$$\begin{aligned}
 [K_{aa}] - [K_{ab}][K_{bb}]^{-1}[K_{ba}] &= \frac{3EI}{28} \left( \begin{bmatrix} 28 & -14 \\ -14 & 14 \end{bmatrix} - \begin{bmatrix} 12 & -9 \\ -9 & 12 \end{bmatrix} \right) \\
 &= \frac{3EI}{28} \begin{bmatrix} 16 & -5 \\ -5 & 2 \end{bmatrix}
 \end{aligned} \tag{5.50}$$

By substituting from equation (5.50) in equation (5.47), the reduced natural frequency relationship therefore becomes as shown in equation (5.51) and it will be noted that it is the rotational dynamic displacements which have been eliminated by the reduction process, since the rotations are associated with zero contributions to the mass matrix.

$$\begin{bmatrix} 16 - \frac{28}{3EI} 1500\omega^2 & -5 \\ -5 & 2 - \frac{28}{3EI} 1000\omega^2 \end{bmatrix} \begin{Bmatrix} w_1 \\ w_2 \end{Bmatrix} = \{0\} \tag{5.51}$$

Applying the condition of equation (5.33) to equation (5.51) gives the *characteristic* equation:

$$(16 - 3\alpha)(2 - 2\alpha) - 25 = 0 \tag{5.52}$$

where

$$\alpha = \frac{28}{3EI} 500\omega^2$$

Whence

$$\alpha = 0.1899 \quad \text{or} \quad 6.143$$

So that

$$\omega = 0.00638(EI)^{1/2} \quad \text{or} \quad 0.0363(EI)^{1/2} \tag{5.53}$$

and

$$f = \frac{\omega}{2\pi} = 6.42 \quad \text{or} \quad 36.5 \text{ Hz} \tag{5.54}$$

taking

$$E = 200 \times 10^9 \text{ N/m}^2 \quad \text{and} \quad I = 2 \times 10^{-4} \text{ m}^4$$

As previously, the corresponding modes may be obtained by setting the vertical displacement coordinate at, say, node 1 to unity and then substituting in either of the two equations (5.51) for the circular natural frequencies of equation (5.53). The resulting modes are

$$\{\phi\} = \begin{Bmatrix} 1.000 \\ 3.086 \end{Bmatrix} \quad \text{or} \quad \begin{Bmatrix} 1.000 \\ -0.486 \end{Bmatrix} \tag{5.55}$$

and have been displayed previously in Fig. 5.3.

### 5.3.6 Example 5.4 – cantilever slab

As a final example of natural frequency and mode determination, the square, isotropic slab shown in Fig. 5.22 will be analysed by the finite element method, using the division into four equal elements shown in the figure. It is presumed that the natural frequencies are required for vibration under self-mass only, the latter being presumed to be uniformly distributed and of intensity metres per unit area. Following the procedures of example 3.6 (see p. 145), the sub-matrix form of the stiffness matrix for the slab may be shown to be

$$\begin{matrix}
 & \begin{matrix} 1 & 2 & 3 & 4 & 5 & 6 \end{matrix} \\
 \begin{matrix} 1 \\ 2 \\ 3 \\ 4 \\ 5 \\ 6 \end{matrix} & \begin{bmatrix}
 k_{kk}^1 & k_{ki}^1 & k_{kj}^1 & k_{kl}^1 & 0 & 0 \\
 k_{ik}^1 & k_{ii}^1 + k_{kk}^2 & k_{ij}^1 + k_{kl}^2 & k_{il}^1 & 0 & 0 \\
 k_{jk}^1 & k_{ji}^1 + k_{lk}^2 & k_{jj}^1 + k_{ll}^2 + k_{kk}^3 + k_{ii}^4 & k_{jl}^1 + k_{ik}^4 & k_{kl}^3 + k_{ij}^4 & k_{il}^4 \\
 k_{lk}^1 & k_{li}^2 & k_{lj}^1 + k_{ki}^4 & k_{ll}^1 + k_{kk}^4 & k_{kj}^4 & k_{kl}^4 \\
 0 & 0 & k_{lk}^1 + k_{ji}^4 & k_{jk}^4 & k_{ll}^3 + k_{jj}^4 & k_{jl}^4 \\
 0 & 0 & k_{ii}^4 & k_{ik}^4 & k_{ij}^4 & k_{il}^4
 \end{bmatrix}
 \end{matrix} \quad (5.56)$$

Appropriate substitutions from Fig. 3.26(b) (see p. 143) then give the numerical form of the stiffness matrix to be as equation (5.57) (page 245), where the modified type of displacement variables used in example 3.6 (see Fig. 3.29(c), p. 148) have again been employed.

To construct the mass matrix on the lumped-mass type of model described above it is necessary to obtain suitable nodal point masses, which will approximate the uniformly distributed self-mass of the slab. The simplest way of doing this is to allocate to each node the mass of a region of slab surrounding

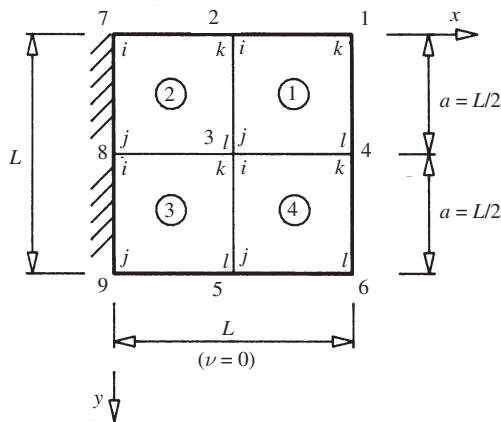


Fig. 5.22 Example 5.4—cantilever slab

$$[K] = \frac{D}{15a^2} \times \begin{bmatrix} 162 & 33 & 33 & -72 & 12 & 12 & -18 & 12 & 12 & -72 & 33 & 12 & 0 & 0 & 0 & 0 & 0 & 0 \\ 33 & 0 & 12 & 6 & 0 & -33 & 9 & 0 & 0 & -33 & 9 & 0 & 0 & 0 & 0 & 0 & 0 & 0 \\ 24 & 24 & -33 & 0 & 9 & -12 & 0 & 6 & 12 & 0 & 6 & 0 & 0 & 0 & 0 & 0 & 0 & 0 \\ \hline 324 & 66 & 0 & -144 & 66 & 0 & -18 & 12 & -12 & -18 & 12 & -12 & 0 & 0 & 0 & 0 & 0 & 0 \\ 48 & 0 & -66 & 18 & 0 & -12 & 6 & 0 & 0 & 0 & 0 & 0 & 0 & 0 & 0 & 0 & 0 & 0 \\ \hline 48 & 0 & 0 & 12 & 12 & 0 & 6 & 0 & 0 & -144 & 66 & 0 & -18 & 12 & -12 & 0 & 0 & 0 \\ \hline 648 & 0 & 0 & 0 & 0 & -144 & 0 & -66 & -144 & 66 & 0 & -18 & 12 & -12 & 0 & 0 & 0 & 0 \\ \hline 96 & 96 & 0 & 12 & 0 & 0 & 12 & 0 & -66 & 18 & 0 & -12 & 6 & 0 & 0 & 0 & 0 & 0 \\ \hline 324 & 0 & 66 & 0 & 18 & 0 & 0 & 12 & 12 & 0 & 0 & 12 & 12 & 0 & 0 & 6 & 0 & 6 \\ \hline 48 & 48 & 0 & 0 & 66 & -18 & 12 & 12 & -72 & 33 & 12 & 0 & 0 & 0 & 0 & 0 & 0 & 0 \\ \hline 48 & 48 & -12 & 0 & 6 & 12 & 0 & 6 & 12 & 0 & 6 & 12 & 0 & 6 & 0 & 0 & 0 & 0 \\ \hline 324 & -66 & 0 & -72 & -12 & -33 & 48 & 0 & -12 & 6 & 0 & -33 & 9 & 0 & 0 & 0 & 0 & 0 \\ \hline 48 & 48 & 0 & -12 & & 6 & 0 & 48 & 0 & -12 & 6 & 0 & 0 & 0 & 0 & 0 & 0 & 0 \\ \hline 162 & -33 & 33 & 48 & 33 & 0 & 9 & 162 & -33 & 33 & 33 & 0 & 9 & 0 & 0 & 0 & 0 & 0 \\ \hline 24 & 24 & 0 & 24 & 0 & 24 & 0 & 24 & 0 & 24 & 0 & 24 & 0 & 24 & 0 & 24 & 0 & 24 \end{bmatrix}$$

symmetric

(5.57)

(where  $a = L/2$ ,  $D = Et^2/12$ )

the node, the region being a square of the same side as the elements used. If this procedure is followed, then the mass matrix becomes

$$[M] = \text{diag}[0.25, 0, 0, 0.5, 0, 0, 1, 0, 0, 0.5, 0, 0, 0.5, 0, 0, 0.25, 0, 0]ma^2 \quad (5.58)$$

In this model, it should be noted that there are three dynamic acceleration components associated with each node, corresponding to the normal displacement and two rotational displacements of the finite element used (see fig 3.24(b)). There are thus 18 possible mass components in equation (5.58), of which 12 are zero, since they represent assumed negligible mass inertias associated with the rotational accelerations. It will hence be possible to determine six natural frequencies, since there are six non-zero mass components.

The natural frequency relationship may now be established from the stiffness and mass matrices of equations (5.57) and (5.58) and standard computer routines then used to determine the natural frequencies and modes. The circular natural frequencies determined in this way are

$$\omega = 3.16, 7.64, 16.3, 16.8, 20.5 \text{ or } 27.2 \left( \frac{D}{mL^4} \right)^{1/2} \quad (5.59)$$

and the first four modes are shown in Fig. 5.23. It must, however, be emphasized that the approximations involved in the finite element and lumped-mass idealizations used in the analysis will result in errors which become progressively more severe for the higher modes and are more pronounced for mode

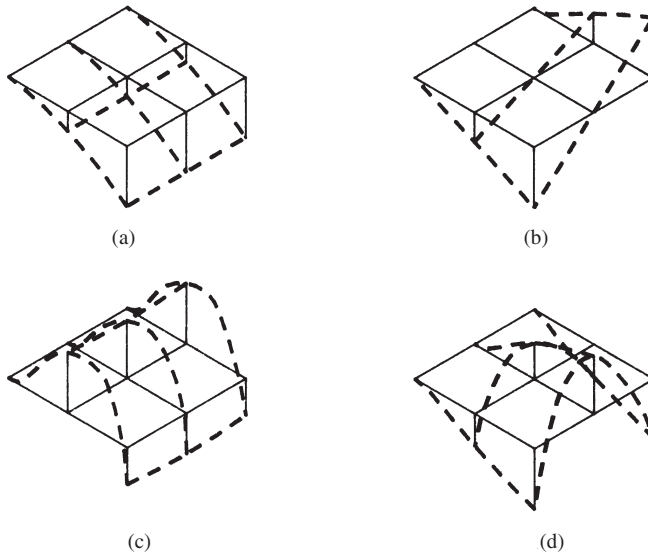


Fig. 5.23 Example 5.4—first four modes

shapes than for frequencies. The accuracy of an analysis such as that just undertaken would therefore, in practice, need to be checked by progression to a finer element net and, possibly, by the use of a more sophisticated mass representation (see Section 5.3.9).

### 5.3.7 Orthogonality of the principal modes

The principal modes of vibration of a structure possess an *orthogonal* property with respect to the structure's stiffness and mass matrices such that

$$\{\phi_r\}^T [K] \{\phi_s\} = 0 \quad (r \neq s) \quad (5.60)$$

and

$$\{\phi_r\}^T [M] \{\phi_s\} = 0 \quad (r \neq s) \quad (5.61)$$

These orthogonality relationships may be established by noting that two distinct modes will both satisfy the natural frequency relationship of equation (5.33) such that

$$[K] \{\phi_r\} = \omega_r^2 [M] \{\phi_r\} \quad (5.62)$$

and

$$[K] \{\phi_s\} = \omega_s^2 [M] \{\phi_s\} \quad (5.63)$$

Pre-multiplying equation (5.62) by  $\{\phi_s\}^T$  gives

$$\{\phi_s\}^T [K] \{\phi_r\} = \omega_r^2 \{\phi_s\}^T [M] \{\phi_r\} \quad (5.64)$$

and, transposing both sides of equation (5.64),

$$[\{\phi_s\}^T [K] \{\phi_r\}]^T = \omega_r^2 [\{\phi_s\}^T [M] \{\phi_r\}]^T \quad (5.65)$$

So that

$$\{\phi_r\}^T [K] \{\phi_s\} = \omega_r^2 \{\phi_r\}^T [M] \{\phi_s\} \quad (5.66)$$

since  $[K] = [K]^T$  and  $[M] = [M]^T$  due to the symmetry of these matrices. However, from equation (5.63),

$$\{\phi_r\}^T [K] \{\phi_s\} = \omega_s^2 \{\phi_r\}^T [M] \{\phi_s\} \quad (5.67)$$

Hence, subtracting equations (5.66) and (5.67),

$$(\omega_r^2 - \omega_s^2) \{\phi_r\}^T [M] \{\phi_s\} = 0 \quad (5.68)$$

Equation (5.68) proves the orthogonality of the principal modes with respect to the mass matrix, provided that the structure does not possess repeated natural frequencies, a possibility which will not be considered here but which can be accommodated (Craig, 1987). The orthogonality of the principal modes with respect to the stiffness matrix follows by substitution from equation (5.61) into equation (5.64).



An illustration of these orthogonality properties may be obtained by considering the (reduced) stiffness and mass matrices of the cantilever beam treated in example 5.3, together with the beam's principal modes (equation (5.46)). In this case then

$$\begin{aligned} \{\phi_1\}^T [K] \{\phi_2\} &= \{1.000 \quad 3.086\} \frac{3EI}{28} \begin{bmatrix} 16 & -5 \\ -5 & 2 \end{bmatrix} \begin{Bmatrix} 1.000 \\ -0.486 \end{Bmatrix} \\ &= \frac{3EI}{28} \{1.000 \quad 3.086\} \begin{Bmatrix} 18.43 \\ -5.98 \end{Bmatrix} = 0 \end{aligned}$$

and

$$\begin{aligned} \{\phi_1\}^T [M] \{\phi_2\} &= \{1.000 \quad 3.086\} 500 \begin{bmatrix} 3 & 0 \\ 0 & 2 \end{bmatrix} \begin{Bmatrix} 1.000 \\ -0.486 \end{Bmatrix} \\ &= 500 \{1.000 \quad 3.086\} \begin{Bmatrix} 3.000 \\ -0.972 \end{Bmatrix} = 0 \end{aligned}$$

### 5.3.8 Rayleigh quotient

From equation (5.62), it follows that

$$\omega_r^2 = \frac{\{\phi_r\}^T [K] \{\phi_r\}}{\{\phi_r\}^T [M] \{\phi_r\}} = \frac{k_{\phi_r}}{m_{\phi_r}} \quad (5.69)$$

where  $k_{\phi_r}$ ,  $m_{\phi_r}$  are the *modal* stiffness and mass for mode  $r$ .

The expression of equation (5.69) is usually known as the Rayleigh quotient, since, on energy grounds, Lord Rayleigh suggested that equation (5.69) could be used to evaluate the circular fundamental frequency, even if the mode shape used was only an approximate representation of the actual fundamental mode, provided that the approximating mode satisfied the geometric constraints on the structure. This concept may be expressed as

$$\omega_R^2 = \frac{\{\phi_R\}^T [K] \{\phi_R\}}{\{\phi_R\}^T [M] \{\phi_R\}} \simeq \omega_1^2 \quad (5.70)$$

where  $\phi_R$  indicates Rayleigh approximation.

In single-span beam analysis, the static displacements, which certainly satisfy the beam's geometric constraints, will often provide a suitable approximation to the fundamental mode. In the case of the cantilever beam (Fig. 5.21), for example, the stiffness equations for the static displacement of the beam (using the reduced stiffness matrix of equation (5.50)) are

$$\frac{3EI}{28} \begin{bmatrix} 16 & -5 \\ -5 & 2 \end{bmatrix} \begin{Bmatrix} w_1 \\ w_2 \end{Bmatrix} = 500 \begin{Bmatrix} 3 \\ 2 \end{Bmatrix} g \quad (5.71)$$

By solving equations (5.71), it may be shown that the vertical displacements at nodes 1 and 2 are in the ratio of 1:2.94, so that an approximate fundamental mode is

$$\{\phi_R\}^T = \{1.00, 2.94\}$$

Hence

$$\{\phi_R\}^T [K] \{\phi_R\} = \{1.00 \quad 2.94\} \frac{3EI}{28} \begin{bmatrix} 16 & -5 \\ -5 & 2 \end{bmatrix} \begin{Bmatrix} 1.00 \\ 2.94 \end{Bmatrix} = 0.416EI$$

and

$$\{\phi_R\}^T [M] \{\phi_R\} = \{1.00 \quad 2.94\} 500 \begin{bmatrix} 3 & 0 \\ 0 & 2 \end{bmatrix} \begin{Bmatrix} 1.00 \\ 2.94 \end{Bmatrix} = 10100$$

Whence

$$\omega_R = 0.00642\sqrt{(EI)}, \quad \omega_{\text{exact}} = 0.00638\sqrt{(EI)} \quad (5.72)$$

The approximate circular fundamental frequency of equation (5.72) may be seen to compare very favourably with the exact value, which is reproduced from equation (5.53).

For structures other than single-span beams, the static displacements will not necessarily provide an approximation to the fundamental mode, as, for example, in the case of the two-storey sway frame of Fig. 5.18. In such cases, displacements from a hypothetical loading may be used, where the loading is chosen such that the resulting displaced shape may be expected to approximate to the fundamental mode. The fundamental mode of the sway frame might be expected to involve sways in the same direction for each storey, a type of displacement which would result from a, perhaps improbable, assumption that gravity acts horizontally temporarily, so that the equal-storey masses produce equal lateral forces. The stiffness equations for this loading may be obtained, by use of the stiffness matrix from equation (5.30), as

$$24 \frac{EI}{L^3} \begin{bmatrix} 2 & -1 \\ -1 & 1 \end{bmatrix} \begin{Bmatrix} \Delta_1 \\ \Delta_2 \end{Bmatrix} = \begin{Bmatrix} 1 \\ 1 \end{Bmatrix} mg \quad (5.73)$$

From the equations (5.73), it may be shown that the storey sways produced by the lateral loading are in the ratio of 2:3, so that a suitable approximate mode is

$$\{\sigma_R\}^T = \{2, 3\} \quad (5.74)$$

Using this mode shape in the Rayleigh quotient of equation (5.70), together with the stiffness and mass matrices from equations (5.30) and (5.31), results in the approximate circular natural frequency

$$\omega_R = 3.04\sqrt{\frac{EI}{mL^3}}, \quad \omega_{\text{exact}} = 3.03\sqrt{\frac{EI}{mL^3}} \quad (5.75)$$

which is again close to the exact value, reproduced from equation (5.37).

### 5.3.9 Distributed-mass models

Distributed masses may be approximated by lumped-mass models if the structural element is sub-divided (see Fig. 5.24, for example). The accuracy of this approximation obviously increases with the fineness of the sub-division but also decreases significantly for higher modes. If the structure involves relatively few nodes and/or distributed masses form a significant proportion of the total mass, then a more accurate distributed-mass representation is warranted, which may be obtained by the use of ‘consistent’ mass matrices (Ross, 1998; Zienkiewicz and Taylor, 1991).

## 5.4 Free, undamped vibration analysis

By combining equations (5.4) and (5.6), the equations of motion of an undamped structural system undergoing free vibration may be expressed as

$$[K]\{x\} = -[M]\{\ddot{x}\} \quad (5.76)$$

It will be presumed that the free vibration commences from a prescribed displacement configuration and that the effect causing the vibration produces known initial velocities. If the coordinates in equation (5.76) are the dynamic displacements, then the problem of free, undamped vibration analysis results in the solution of equations (5.76) subject to initial conditions which may be represented by

$$\{x\}_{t=0} = \{x\}_0 \quad \text{and} \quad \{\dot{x}\}_{t=0} = \{\dot{x}\}_0 \quad (5.77)$$

Equations (5.76) are interdependent (or *coupled*), since the stiffness matrix contains off-diagonal terms, as may the mass matrix if the lumped-mass approximation described above is not being employed. If formulated in dynamic displacement coordinates, then the free, undamped vibration problem involves the simultaneous solution of the set of second-order differential equations represented by equations (5.76), subject to the initial conditions of equation (5.77). The problem may, however, be simplified by the use of *principal* coordinates, which have the effect of *uncoupling* the equations so that they may be considered individually rather than simultaneously.

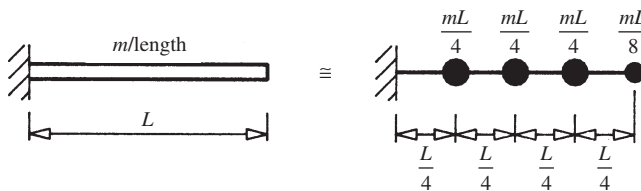


Fig. 5.24 Lumping of a distributed mass

### 5.4.1 Analysis by mode superposition

Principal coordinates may be related to the dynamic displacement coordinates by the transformation

$$\{x\} = [\Phi]\{\eta\} \quad (5.78)$$

where  $[\Phi] = [\phi_1, \dots, \phi_r, \dots, \phi_n]$  is the modal matrix.

To see why equations (5.76) become uncoupled in principal coordinates, it is first necessary to note that, by virtue of the orthogonality condition (equation (5.60)),

$$\begin{aligned} [\Phi]^T [K] [\Phi] &= [\phi_1^T, \dots, \phi_r^T, \dots, \phi_n^T] [K] [\phi_1, \dots, \phi_r, \dots, \phi_n] \\ &= \text{diag}[\phi_1^T K \phi_1, \dots, \phi_r^T K \phi_r, \dots, \phi_n^T K \phi_n] \\ &= \text{diag}[k_{\phi_1}, \dots, k_{\phi_r}, \dots, k_{\phi_n}] = [K_\phi] \end{aligned} \quad (5.79)$$

where  $[K_\phi]$  is the modal stiffness matrix, and

$$[\Phi]^T [M] [\Phi] = [\phi_1^T M \phi_1, \dots, \phi_r^T M \phi_r, \dots, \phi_n^T M \phi_n] = [M_\phi] \quad (5.80)$$

where  $[M_\phi]$  is the modal mass matrix.

Transforming equations (5.76) to principal coordinates and pre-multiplying by  $[\phi]^T$  gives

$$[\Phi]^T [K] [\Phi] \{\eta\} = -[\Phi]^T [M] [\Phi] \{\ddot{\eta}\} \quad (5.81)$$

or

$$[K_\phi] \{\eta\} = -[M_\phi] \{\ddot{\eta}\} \quad (5.82)$$

Due to the diagonal nature of the modal stiffness and mass matrices, equation (5.82) represents the required set of uncoupled equations which may be written as

$$\begin{aligned} k_{\phi_1} \eta_1 &= -m_{\phi_1} \ddot{\eta}_1 \\ \dots \\ k_{\phi_r} \eta_r &= -m_{\phi_r} \ddot{\eta}_r \\ \dots \\ k_{\phi_n} \eta_n &= -m_{\phi_n} \ddot{\eta}_n \end{aligned} \quad (5.83)$$

The solutions to all these equations are similar, and the solution to a typical equation (as may be verified by substitution in equation (5.83)) is

$$\eta_r = A_{\phi_r} \sin(\omega_r t + \alpha_r) \quad (5.84)$$

where

$$\omega_r^2 = \frac{k_{\phi_r}}{m_{\phi_r}}$$

An equivalent and, for the present purpose, more convenient form of the solution is

$$\eta_r = a_r \cos(\omega_r t) + b_r \sin(\omega_r t) \quad (5.85)$$

where  $a_r$  and  $b_r$  are constants.

The complete set of principal coordinates is therefore given by

$$\{\eta\} = [\cos \omega t] \{a\} + [\sin \omega t] \{b\} \quad (5.86)$$

where

$$[\cos \omega t] = \text{diag}[\cos \omega_1 t, \dots, \cos \omega_r t, \dots, \cos \omega_n t]$$

$$[\sin \omega t] = \text{diag}[\sin \omega_1 t, \dots, \sin \omega_r t, \dots, \sin \omega_n t]$$

To complete the solution, it remains to obtain the constants in equation (5.86), which may be determined from the initial conditions, since, from equation (5.86),

$$\begin{aligned} \{\eta\}_0 &= \{a\} \\ \{\dot{\eta}\}_0 &= \text{diag}[\omega_1, \dots, \omega_r, \dots, \omega_n] \{b\} = [\omega] \{b\} \end{aligned} \quad (5.87)$$

where  $\{\eta\}_0$ ,  $\{\dot{\eta}\}_0$  are the modal initial conditions.

The solution may therefore be expressed, in terms of the nodal initial conditions, as

$$\{\eta\} = [\cos \omega t] \{\eta\}_0 + [\sin \omega t] [\omega]^{-1} \{\dot{\eta}\}_0 \quad (5.88)$$

Using equation (5.78), the modal initial conditions may be related to the initial conditions in the original coordinates by

$$\{x\}_0 = [\Phi] \{\eta\}_0 \quad \text{and} \quad \{\dot{x}\}_0 = [\Phi] \{\dot{\eta}\}_0 \quad (5.89)$$

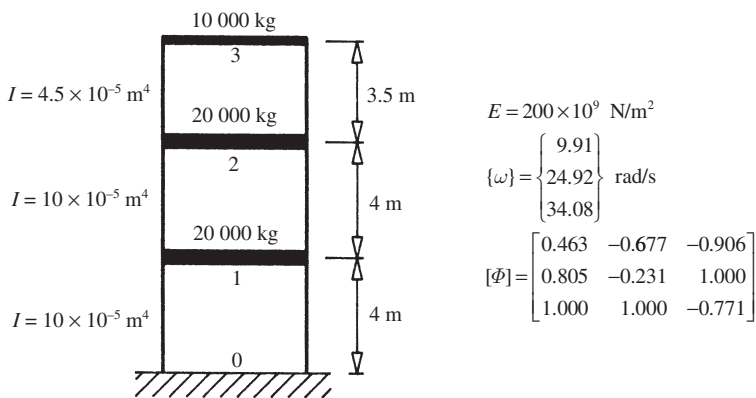


Fig. 5.25 Example 5.5—three-storey sway frame

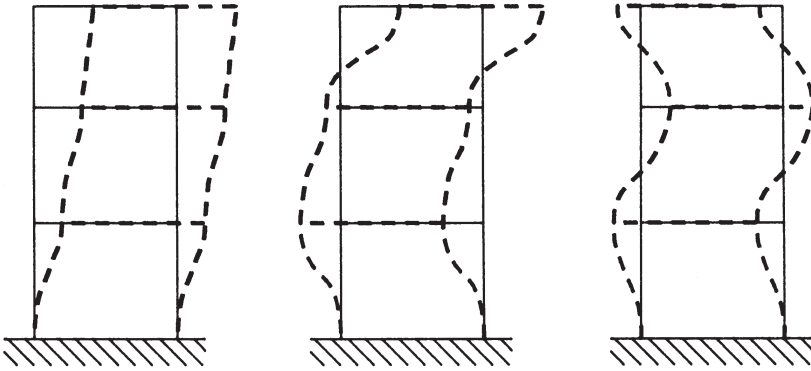


Fig. 5.26 Example 5.5—principal modes

If the first of equations (5.89) is pre-multiplied by  $[\Phi]^T[M]$ , then

$$[\Phi]^T[M]\{x\}_0 = [\Phi]^T[M][\Phi]\{\eta\}_0 = [M_\phi]\{\eta\}_0 \quad (5.90)$$

Whence

$$\{\eta\}_0 = [M_\phi]^{-1}[\Phi]^T[M]\{x\}_0 \quad (5.91)$$

Similarly,

$$\{\dot{\eta}\}_0 = [M_\phi]^{-1}[\Phi]^T[M]\{\dot{x}\}_0 \quad (5.92)$$

Substitution from equations (5.91) and (5.92) into equation (5.88) therefore provides the full principal coordinate solution, and the dynamic displacement solution follows from equation (5.78), a procedure which is illustrated in the following example.

#### 5.4.2 Example 5.5 – three-storey sway frame

It is required to determine the undamped motion of the three-storey sway frame shown in Fig. 5.25 when the top storey is given an initial sway velocity of 0.5 m/s from its static position while the lower two storeys remain at rest in their static positions. The natural frequencies and principal modes are given in Fig. 5.25, and an illustration of the principal modes is provided as Fig. 5.26.

The modal mass matrix is first constructed from equation (5.80) by calculating the diagonal terms as, for example,

$$m_{\phi_1} = \{\phi_1\}^T[M]\{\phi_1\} = \{0.463, 0.805, 1.000\}10^3 \begin{bmatrix} 20 & 0 & 0 \\ 0 & 20 & 0 \\ 0 & 0 & 10 \end{bmatrix} \begin{Bmatrix} 0.463 \\ 0.805 \\ 1.000 \end{Bmatrix}$$

$$= 27.2 \times 10^3$$

Whence

$$[M_\phi] = \text{diag } 10^3 [27.2, 20.2, 42.4] \quad (5.93)$$

In this case the dynamic displacement coordinates are the sway displacements of the three storeys, so that the stipulated initial conditions may be specified as

$$\begin{aligned} \{x\}_0 &= \begin{Bmatrix} \Delta_1 \\ \Delta_2 \\ \Delta_3 \end{Bmatrix}_0 = \{0\} \\ \{\dot{x}\}_0 &= \begin{Bmatrix} 0 \\ 0 \\ 0.5 \end{Bmatrix} = \{0\} \end{aligned} \quad (5.94)$$

Hence, from equation (5.91),

$$\{\eta\}_0 = [M_\phi]^{-1} [\Phi]^T [M] \{x\}_0 = \{0\} \quad (5.95)$$

and, from equation (5.92),

$$\begin{aligned} \{\dot{\eta}\}_0 &= [M_\phi]^{-1} [\Phi]^T [M] \{\dot{x}\}_0 \\ &= [M_\phi]^{-1} \begin{bmatrix} 0.463 & 0.805 & 1.000 \\ -0.677 & -0.231 & 1.000 \\ -0.906 & 1.000 & -0.771 \end{bmatrix} 10^3 \begin{bmatrix} 20 & 0 & 0 \\ 0 & 20 & 0 \\ 0 & 0 & 10 \end{bmatrix} \begin{Bmatrix} 0 \\ 0 \\ 0.5 \end{Bmatrix} \\ &= 10^{-3} \begin{bmatrix} 27.2^{-1} & 0 & 0 \\ 0 & 20.2^{-1} & 0 \\ 0 & 0 & 42.4^{-1} \end{bmatrix} 10^3 \begin{Bmatrix} 5.000 \\ 5.000 \\ -3.855 \end{Bmatrix} \\ &= \begin{Bmatrix} 0.184 \\ 0.248 \\ -0.091 \end{Bmatrix} \end{aligned} \quad (5.96)$$

Substituting from equations (5.95) and (5.96) in equation (5.88), the solution in principal coordinates is therefore given by

$$\begin{aligned} \{\eta\} &= [\sin \omega t] \begin{bmatrix} 9.91^{-1} & 0 & 0 \\ 0 & 24.92^{-1} & 0 \\ 0 & 0 & 34.08^{-1} \end{bmatrix} \begin{Bmatrix} 0.184 \\ 0.248 \\ -0.091 \end{Bmatrix} \\ &= 10^{-3} \begin{Bmatrix} 18.55 \sin 9.91t \\ 9.93 \sin 24.92t \\ -2.67 \sin 34.08t \end{Bmatrix} \end{aligned}$$

Finally, the solution in the original coordinates is obtained by substitution in equation (5.78):

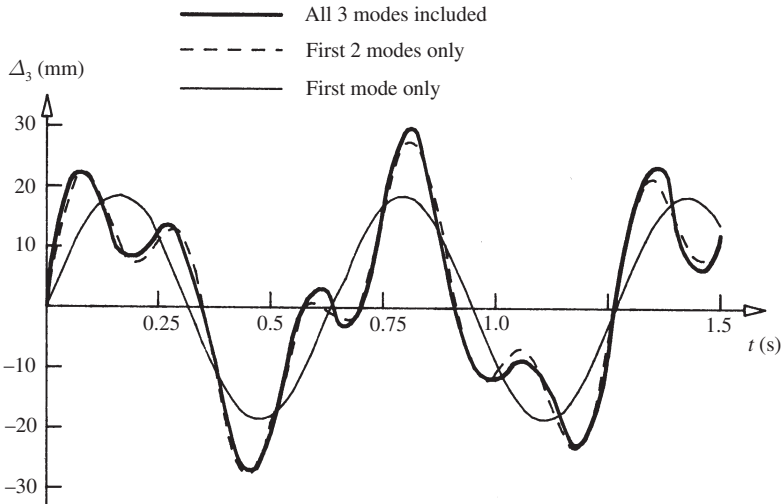


Fig. 5.27 Example 5.5—displacement solution

$$\{x\} = \begin{Bmatrix} \overset{1}{+8.59 \sin 9.91t} & \overset{2}{-6.72 \sin 24.92t} & \overset{3}{+2.42 \sin 34.08t} \\ +14.93 \sin 9.91t & -2.29 \sin 24.92t & -2.67 \sin 34.08t \\ +18.55 \sin 9.91t & +9.93 \sin 24.92t & +2.06 \sin 34.08t \end{Bmatrix} 10^{-3} \text{ m} \quad (5.97)$$

The solution given by equation (5.97) may be seen to consist of linear combinations of contributions (numbered 1–3) from the three principal modes, a feature which gives mode superposition analysis its name. The top-storey displacement solution is plotted in Fig. 5.27, which also shows the contributions of the modes to this displacement. It will be seen that neglecting the third mode contribution has little effect on the solution, but that neglect of the second and third mode contributions reduces the solution to the harmonic form of the first mode, which cannot accurately model the full solution. It is generally the case that higher modes have a reducing effect on the dynamic response of a structure, and, when large numbers of coordinates are involved, it is usual to determine the response using only a fraction of the total number of modes. In reducing the number of modes, however, it is obviously important that all modes be included which are likely to be significantly excited.

## 5.5 Forced, undamped vibration analysis

If the structure is subjected to a set of time-dependent forcing functions,  $\{p\}$ , which correspond in type and positive directions to the coordinates,  $\{x\}$ , then the equations of motion (equation (5.76)) become



$$[M]\{\ddot{x}\} + [K]\{x\} = \{p\} \quad (5.98)$$

### 5.5.1 Analysis by mode superposition

Using the procedures of Section 5.4.1 to transform to principal coordinates gives

$$[\Phi]^T [M] [\Phi] \{\ddot{\eta}\} + [\Phi]^T [K] [\Phi] \{\eta\} = [\Phi]^T \{p\} = \{p_\phi\} \quad (5.99)$$

where  $\{p_\phi\}$  is the vector of modal forcing functions, or

$$[M_\phi] \{\ddot{\eta}\} + [K_\phi] \{\eta\} = \{p_\phi\} \quad (5.100)$$

As before, equations (5.100) are uncoupled due to the diagonal nature of the modal mass and stiffness matrices, so that the solutions of all the equations are similar and it suffices to consider a typical equation:

$$m_{\phi_r} \ddot{\eta}_r + k_{\phi_r} \eta_r = p_{\phi_r} \quad (5.101)$$

If the forcing function in equation (5.101) is an analytically straightforward function of time, then a closed-form solution can be obtained by the use of standard differential equation solution techniques. However, in the case of more complex or non-analytically defined functions, a more general approach is to interpret the forcing function as the sum of an infinite number of impulses, since the response to an isolated impulse may be readily determined as follows.

A single degree of freedom system of stiffness,  $k$ , will be considered, in which the position of a mass,  $m$ , is defined by a coordinate,  $x$ . The effect of an impulse,  $I$ , applied to the mass under zero initial conditions will be to impart a momentum to the mass given by

$$m\dot{x}_0 = I$$

So that

$$\dot{x}_0 = \frac{I}{m} \quad (5.102)$$

Subsequent to the action of the impulse, the system is unforced, so that its equation of motion takes the form

$$m\ddot{x} + kx = 0 \quad (5.103)$$

Equation (5.103) has the solution

$$x = a \cos \omega t + b \sin \omega t \quad (5.104)$$

where  $\omega^2 = k/m$ . Using the initial conditions

$$x = 0 \quad \text{and} \quad \dot{x} = \dot{x}_0 \quad \text{when} \quad t = 0$$

Then

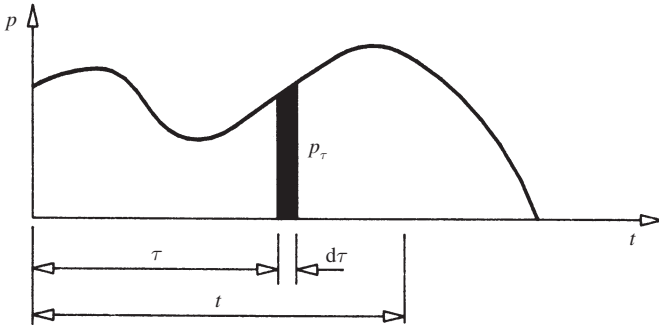


Fig. 5.28 Forcing function idealization

$$a = 0 \quad \text{and} \quad b = \frac{I}{m\omega} \quad (5.105)$$

So that the solution becomes

$$x = \frac{I}{m\omega} \sin \omega t \quad (5.106)$$

If the action of a forcing function,  $p$ , on the mass is now considered, the equation of motion is given by

$$m\ddot{x} + kx = p \quad (5.107)$$

The solution to equation (5.107) may be obtained by the idealization of the forcing function into an infinite number of impulses. From equation (5.106), the response due to the typical impulse shown in Fig. 5.28 is given by

$$x = \frac{p_\tau d\tau}{m\omega} \sin \omega(t - \tau) \quad (5.108)$$

So that the total response is given by

$$x = \frac{1}{m\omega} \int_0^t p_\tau \sin \omega(t - \tau) d\tau \quad (5.109)$$

where the integral is known as *Duhamel's* integral.

Since equation (5.101) has the same form as equation (5.107), its solution is

$$\eta_r = \frac{1}{m_{\phi_r} \omega_{\phi_r}} \int_0^t (p_{\phi_r})_\tau \sin \omega_r(t - \tau) d\tau \quad (5.110)$$

Although closed-form solutions to equation (5.110) are only readily obtainable for simple forcing functions, more complex functions may either be represented as Fourier series or the integral may be evaluated numerically (Craig, 1981).

The solution provided by equation (5.110) is for zero initial conditions but may readily be generalized, since the effects of any non-zero initial conditions may be treated as resulting in a free response (obtainable by the methods of Section 5.4.1) which may be superimposed on the forced motion.

### 5.5.2 Example 5.6 – sway frame under ground motion

As an example of transiently forced, undamped vibration, the three-storey sway frame of Fig. 5.25 will be considered under the influence of an isolated horizontal ground movement. The dynamic history of the ground movement is described by a ground acceleration plot which will be taken to be as shown in Fig. 5.29.

The restoring forces developed in the frame when the ground moves will be proportional to the *relative* sway displacements between the ground and the storey levels, so that the equations of motion may be represented by

$$[K](\{\Delta\} - \{e\}\Delta_0) = -[M]\{\ddot{\Delta}\} \quad (5.111)$$

where  $\{e\} = \{1, 1, 1\}^T$ .

The most convenient coordinates in this case are the relative sway displacements, so that

$$\{x\} = \{\Delta\} - \{e\}\Delta_0 \quad \text{and} \quad \{\ddot{x}\} = \{\ddot{\Delta}\} - \{e\}\ddot{\Delta}_0 \quad (5.112)$$

Substituting in equation (5.111) for the relative displacement coordinates gives

$$[K]\{x\} = -[M](\{\ddot{x}\} + \{e\}\ddot{\Delta}_0) \quad (5.113)$$

Hence, the equations of motion may be expressed as

$$[M]\{\ddot{x}\} + [K]\{x\} = -[M]\{e\}\ddot{\Delta}_0 = -10^3 \begin{Bmatrix} 20 \\ 20 \\ 10 \end{Bmatrix} \ddot{\Delta}_0 = \{p\} \quad (5.114)$$

Equation (5.114) shows that the ground motion results in inertial forcing

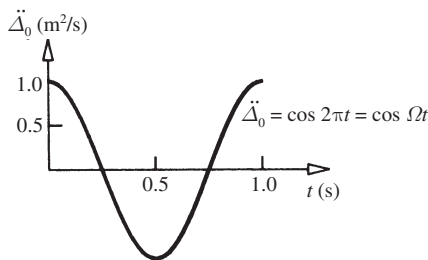


Fig. 5.29 Example 5.6—ground acceleration plot

functions at each storey, whose magnitudes are equal to the product of the storey masses and the ground acceleration. On the assumption that the contribution of mode 3 is negligible, only the first two modes will be used, so that there will be just two principal coordinates, defined by the transformation

$$\{x\} = \begin{bmatrix} 0.463 & -0.677 \\ 0.805 & -0.231 \\ 1.000 & 1.000 \end{bmatrix} \begin{Bmatrix} \eta_1 \\ \eta_2 \end{Bmatrix} = [\Phi]\{\eta\} \quad (5.115)$$

Transforming the equations of motion (equation (5.114)) to principal coordinates gives

$$[M_\phi]\{\ddot{\eta}\} + [K_\phi]\{\eta\} = [\Phi]^T\{p\} = \{p_\phi\} \quad (5.116)$$

So that the modal forcing functions are

$$\{p_\phi\} = - \begin{bmatrix} 0.463 & 0.805 & 1.000 \\ -0.677 & -0.231 & 1.000 \end{bmatrix} 10^3 \begin{Bmatrix} 20 \\ 20 \\ 10 \end{Bmatrix} \cos \Omega t = \{f_\phi\} \cos \Omega t \quad (5.117)$$

where  $\{f_\phi\} = 10^3\{-35.36, 8.16\}^T$ .

To obtain the solution for a typical principal coordinate, substitution from equation (5.117) into equation (5.110) gives

$$\eta_r = \frac{f_{\phi_r}}{m_{\phi_r} \omega_{\phi_r}} \int_0^t \cos \Omega \tau \sin \omega_r (t - \tau) d\tau \quad (5.118)$$

Since

$$\cos A \sin B = \frac{1}{2} [\sin(A + B) - \sin(A - B)]$$

$$\eta_r = \frac{f_{\phi_r}}{2m_{\phi_r} \omega_r} \int_0^t \sin[(\Omega - \omega_r)\tau + \omega_r t] - \sin[(\Omega + \omega_r)\tau - \omega_r t] d\tau$$

Hence

$$\eta_r = \frac{f_{\phi_r}}{2m_{\phi_r} \omega_r} \left[ \frac{-\cos[(\Omega - \omega_r)\tau + \omega_r t]}{\Omega - \omega_r} + \frac{\cos[(\Omega + \omega_r)\tau - \omega_r t]}{\Omega + \omega_r} \right]_0^t$$

Whence

$$\eta_r = \frac{f_{\phi_r}}{m_{\phi_r} (\Omega^2 - \omega_r^2)} (\cos \omega_r t - \cos \Omega t)$$

or

$$\eta_r = \frac{f_{\phi_r}}{k_{\phi_r} (1 - \Omega^2 / \omega_r^2)} (\cos \Omega t - \cos \omega_r t) \quad \text{since } k_{\phi_r} = m_{\phi_r} \omega_r^2 \quad (5.119)$$

The full principal coordinate solution may be obtained by substituting successively in equation (5.119) for the modal forcing function amplitudes of equation (5.117), the modal masses of equation (5.93) and the natural frequencies given in Fig. 5.25:

$$\{\eta\} = \begin{Bmatrix} -22.14(\cos \Omega t - \cos \omega_1 t) \\ 0.69(\cos \Omega t - \cos \omega_2 t) \end{Bmatrix} 10^{-3} \text{ m} \quad (5.120)$$

Transforming back to the original relative displacement coordinates, by use of equation (5.115), gives the final solution:

$$\{x\} = \begin{Bmatrix} -10.25(\cos 2\pi t - \cos 9.91t) & -0.47(\cos 2\pi t - \cos 24.92t) \\ -17.82(\cos 2\pi t - \cos 9.91t) & -0.16(\cos 2\pi t - \cos 24.92t) \\ -22.14(\cos 2\pi t - \cos 9.91t) & +0.69(\cos 2\pi t - \cos 24.92t) \end{Bmatrix} 10^{-3} \text{ m} \quad (5.121)$$

since  $\Omega = 2\pi$ .

Equation (5.121) shows that the first mode contribution predominates. Also, since modal stiffness increases with frequency and the forcing frequency is, in this case, less than any of the natural frequencies, the form of equation (5.119) indicates that higher-mode contributions will rapidly diminish, so that the omission of the third mode is retrospectively justified. The solution obtained is only valid during the time the ground motion occurs but may be readily extended beyond this. The subsequent motion is free, so that one way of extending the solution is to determine the modal state of the vibration at the end of the forced motion and use this state as the initial conditions for the free-vibration solution given by equation (5.88). Alternatively, the upper limit in the solution of equation (5.118) may be amended to the time limit of the forcing effect (1 s in this case).

The forced and free regimes for the vibration of the top storey are illustrated for the initial stages of the motion in Fig. 5.30. It will be seen that the relative

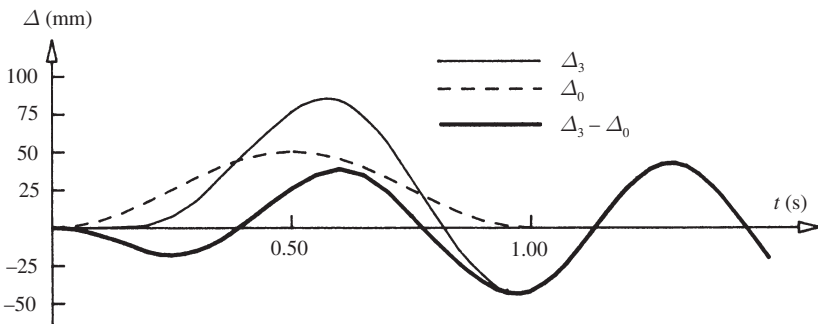


Fig. 5.30 Example 5.6—displacement solution

displacement response is close to being harmonic after approximately 0.5 s. In practice, the vibration would decay due to damping, and the maximal response would be at one of the peaks occurring during the forced motion. The ground displacement profile may be obtained by integration of the acceleration history (Fig. 5.29) and is given by

$$\Delta_0 = \frac{1}{4\pi^2}(1 - \cos 2\pi t) \text{ m} \quad (5.122)$$

By adding the ground and relative displacements during the forced motion, the absolute displacement response may be obtained, and this is plotted, for the top storey, in Fig. 5.30. From Fig. 5.30, it may be observed that the maximum absolute displacement of the top storey occurs well within the forced motion and is significantly greater than subsequent peak values, in contrast to the approximately repeated peaks of the corresponding relative displacement.

## 5.6 Harmonically forced, undamped vibration analysis

As described in Section 5.2.3, harmonic forcing will result in a transient response on initiation of the excitation which is quickly damped into a steady-state response such that the vibration becomes harmonic and has the same frequency as the excitation. Even on an undamped assumption, it is possible to assume a steady-state solution, since, although damping rapidly eliminates transient effects, it has relatively little impact on the steady state, provided that the excitation frequency is not close to any of the natural frequencies of the system (Fig. 5.10(a)). The analysis presented below therefore assumes that steady-state vibration has been achieved and that the forcing frequency is not in the vicinity of any of the system's natural frequencies.

### 5.6.1 Analysis by mode superposition

If the forcing function is harmonic, then the forcing function vector has the form

$$\{p\} = \{f\} \sin \Omega t \quad (5.123)$$

where  $\{f\}$  is the vector of the forcing function amplitudes.

Following transformation of the equations of motion to principal coordinates, a typical equation of motion will be

$$m_{\phi_r} \ddot{\eta}_r + k_{\phi_r} \eta_r = f_{\phi_r} \sin \Omega t \quad (5.124)$$

Due to the steady-state assumption, the solution must be harmonic and have the same frequency as the excitation. Further, due to the undamped

assumption, the response will be in phase (or 180° out of phase) with the excitation (Fig. 5.10(b)), so that the solution must take the form

$$\eta_r = a_r \sin \Omega t \quad (5.125)$$

The constant in equation (5.125) may be determined by substituting the solution in equation (5.124) to give

$$-m_{\phi_r} a_r \Omega^2 + k_{\phi_r} a_r = f_{\phi_r}$$

Whence

$$a_r = \frac{f_{\phi_r}}{k_{\phi_r} - \Omega^2 m_{\phi_r}} = \frac{f_{\phi_r}}{k_{\phi_r} (1 - \Omega^2 / \omega_r^2)} \quad (5.126)$$

since

$$m_{\phi_r} = \frac{k_{\phi_r}}{\omega_r^2}$$

Substituting in equation (5.125) gives the solution as

$$\eta_r = \frac{f_{\phi_r} \sin \Omega t}{k_{\phi_r} (1 - \Omega^2 / \omega_r^2)} \quad (5.127)$$

Successive substitution in equation (5.127) for the various modes of the system therefore produces the complete solution in principal coordinates. This may then, as before, be transformed back to the original coordinates by use of equation (5.78).

### 5.6.2 Example 5.7 – harmonically forced cantilever beam

The two-mass cantilever beam of example 5.3 will be analysed for its steady-state response to a harmonic force excitation applied to node 2 (Fig. 5.31). The analysis will utilize the reduced displacement coordinates only, that is, the vertical nodal displacements.

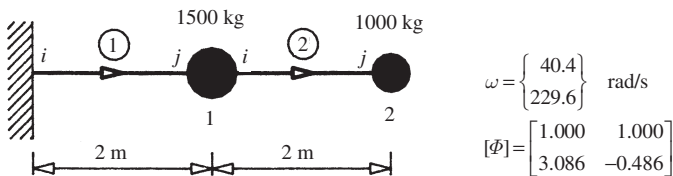


Fig. 5.31 Example 5.7—two-mass cantilever beam

From the system parameters given in Fig. 5.31, the modal mass and stiffness matrices may be readily determined as

$$[M_\phi] = \text{diag}[11.02, 1.74] \times 10^3 \quad (5.128)$$

and

$$[K_\phi] = [\omega^2][M_\phi] = \text{diag}[17.94, 91.71] \times 10^6 \quad (5.129)$$

The modal forcing function vector is

$$\{p_\phi\} = \begin{bmatrix} 1 & 3.086 \\ 1 & -0.486 \end{bmatrix} \begin{Bmatrix} 0 \\ p_2 \end{Bmatrix} \sin \Omega t = \{f_\phi\} \sin \Omega t \quad (5.130)$$

By substituting from equations (5.128), (5.129) and (5.130) into equation (5.127), the solution in principal coordinates is obtained as equation (5.131) which, in displacement coordinates, becomes equation (5.132):

$$\begin{Bmatrix} \eta_1 \\ \eta_2 \end{Bmatrix} = \begin{Bmatrix} \frac{3.086 p_2}{10^6 \times 17.94(1 - \Omega^2/\omega_1^2)} \sin \Omega t \\ \frac{-0.486 p_2}{10^6 \times 91.71(1 - \Omega^2/\omega_2^2)} \sin \Omega t \end{Bmatrix} \quad (5.131)$$

$$\{x\} = \begin{Bmatrix} w_1 \\ w_2 \end{Bmatrix} = \begin{Bmatrix} \frac{0.172}{1 - \Omega^2/\omega_1^2} - \frac{0.0053}{1 - \Omega^2/\omega_2^2} \\ \frac{0.531}{1 - \Omega^2/\omega_1^2} + \frac{0.0026}{1 - \Omega^2/\omega_2^2} \end{Bmatrix} 10^{-6} \sin \Omega t p_2 \text{ m} \quad (5.132)$$

Equation (5.132) shows that the first mode predominates, provided that the forcing frequency is not close to the second natural frequency. In fact, as pointed out already, the solution will not hold for forcing frequencies close to either of the natural frequencies, due to the sensitivity of the solution to damping. In such circumstances, it therefore becomes imperative to include damping effects in the solution, and ways in which this may be accomplished are outlined, with other more advanced topics, in the next section.

## 5.7 Specialized problems

If viscous damping is included in the analysis, damping forces of the type described by equation (5.2) must be incorporated in the analysis, with the result that the equations of motion, in displacement coordinates, will take the form

$$[M]\{\ddot{x}\} + [C]\{\dot{x}\} + [K]\{x\} = 0 \quad (5.133)$$

If mode superposition is to be used, it is essential that the damping matrix,  $[C]$ , is orthogonal with respect to the modal matrix so that the equations



(5.133) become uncoupled on transformation to principal coordinates. In practice, it is often desirable to define damping coefficients (equation (5.2)) for the principal modes of a structure directly, and these therefore become the modal damping coefficients in uncoupled equations of motion, a typical example of which would be

$$m_{\phi_r} \ddot{\eta}_r + c_{\phi_r} \dot{\eta}_r + k_{\phi_r} \eta_r = 0 \quad (5.134)$$

where  $c_{\phi_r}$  is the modal damping coefficient for mode  $r$ .

In certain problems, however, notably soil–structure interaction investigations (Warburton, 1976), it becomes unrealistic to specify modal damping coefficients, and the damping matrix,  $[C]$ , will not be uncoupled on transformation to principal coordinates. In such cases, the equations of motion may be integrated numerically (Clough and Penzien, 1993) or approximating solutions may be obtained by mode superposition, an approach which is often preferred due to the greater efficiency of this method. Direct integration must be used, however, if non-linear problems are to be tackled, since the superposition process undertaken in the modal method is then invalid. Finally, it should be emphasized that the analysis developed in this chapter has assumed that the forcing effects are known functions of time alone. This excludes a thorough treatment of random effects such as waves, wind and earthquakes, which will often require a statistical treatment (Gould and Abu-sitta, 1980) and *self-excited* vibration in which the forcing effect depends upon the state of the vibration as well as on time. Self-excitation is experienced primarily by structures subjected to fluid or air flow and requires specialized treatment (Blevins, 1977).

## References and further reading

- Beards, C. F. (1996) *Structural Vibration – Analysis and Damping*, 2nd edn. Arnold, London. A concise, introductory account which gives particular emphasis to modelling and damping.
- Bishop, R. E. D. (1979) *Vibration*, 2nd edn. Cambridge University Press, Cambridge. A fascinating qualitative description of vibration phenomena; Chapters 2 and 3 are most relevant to the above.
- Blevins, R. D. (1977) *Flow Induced Vibration*. Van Nostrand Reinhold, New York. A specialized text which includes (Chapter 8) data on the damping properties of typical structures.
- Chopra, A. K. (1981) *Dynamics of Structures – A Primer*. EERI, Berkeley. An excellent, mainly qualitative introduction which concentrates on multi-storey buildings and earthquake response.
- Clough, R. W. and Penzien, J. (1993) *Dynamics of Structures*, 2nd edn. McGraw-Hill, New York. A comprehensive text which includes a treatment of the linear-acceleration method of numerical integration.

- Craig, R. R. (1981) *Structural Dynamics*. Wiley, New York. A thorough but accessible description which emphasizes computer applications and gives an introduction to earthquake analysis.
- Ellis, B. R. (1980) An assessment of the accuracy of predicting natural frequencies of buildings and the implications concerning the dynamic analysis of structures. *Proceedings of the Institution of Civil Engineers* **69**, Part 2, 763–776.
- Ghali, A. and Neville, A. M. (1997) *Structural Analysis*, 4th edn. Spon, London. Chapter 21 includes an analytical treatment of single degree of freedom vibration which may be used to supplement the qualitative approach of this chapter. Chapter 4 describes the displacement method, including its application to plane frames.
- Gould, P. L. and Abu-sitta, S. H. (1980) *Dynamic Response of Structures to Wind and Earthquake Loading*. Pentech Press, Plymouth. A practically orientated introduction to the dynamic analysis of random loading.
- Hurty, W. C. and Rubinstein, M. F. (1964) *Dynamics of Structures*. Prentice Hall, New Jersey. Chapter 12 includes an examination of the effects of different theoretical assumptions on the analysis of a large sway frame.
- Irvine, H. M. (1986) *Structural Dynamics for the Practising Engineer*. Allen and Unwin, London. Basic theory supported by some intriguing examples drawn from the author's practice.
- Jennings, A. (1977) *Matrix Computation for Engineers and Scientists*. Wiley, Chichester. Chapters 8–10 give a detailed treatment of eigenvalue and mode determination methods.
- Paz, M. (1991) *Structural Dynamics*, 3rd edn. Van Nostrand Reinhold, New York. A general text which emphasizes the use of response spectra and includes random vibration.
- Prentis, J. M. and Leckie, F. A. (1963) *Mechanical Vibrations: An Introduction to Matrix Methods*. Longman, London. Chapter 2 gives an introduction to the power (iterative) method of eigenvalue and mode determination.
- Ross, C. T. F. (1996) *Finite Element Programs in Structural Engineering and Continuum Mechanics*. Albion, Chichester. Includes BASIC programs for the natural frequency and mode analysis of skeletal structures.
- Ross, C. T. F. (1998) *Advanced Applied Finite Element Methods*. Horwood, Chichester. Includes mass matrices for a variety of structural elements.
- Warburton, G. B. (1976) *The Dynamical Behaviour of Structures*, 2nd edn. Pergamon Press, Oxford. Chapter 6 gives an introduction to dynamic interaction problems.
- Zienkiewicz, O. Z. and Taylor, R. L. (1991) *The Finite Element Method*, 4th edn, Vol. 2. *Solid and Fluid Mechanics Dynamics and Non-linearity*. McGraw-Hill, London. Chapter 9 treats dynamic problems and includes the mass matrix for a rectangular plate element.

### Problems

5.1 Figure 5.32 shows a structure housing ore-crushing machinery. Each floor has a mass of 10 000 kg and the column stiffness parameter  $k = (12EI/L^3) = 1$  MN/m. The ore-crusher is permanently fixed to the lower floor, adding its mass of 10 000 kg to that floor. The crusher operates at 1.75 Hz but sets up large resonant vibrations in the structure.

In an effort to reduce the vibrations it is proposed to attach a large mass of 10 000 kg to the structure. Calculate whether it is better to attach the extra mass to the upper or the lower floor.

(LIVERPOOL)

5.2 The plane structure shown in Fig. 5.33 consists of rigid beams of mass  $m$ , rigidly joined to elastic columns having the second moments of area shown.  $E$  is constant throughout. The top storeys are connected by a member AB, hinged at A and B, having only axial stiffness. The cross-sectional area of AB is equivalent to  $36I/L^2$ . If  $k = 12EI/L^3$ :

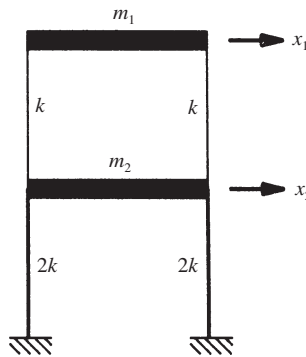


Fig. 5.32

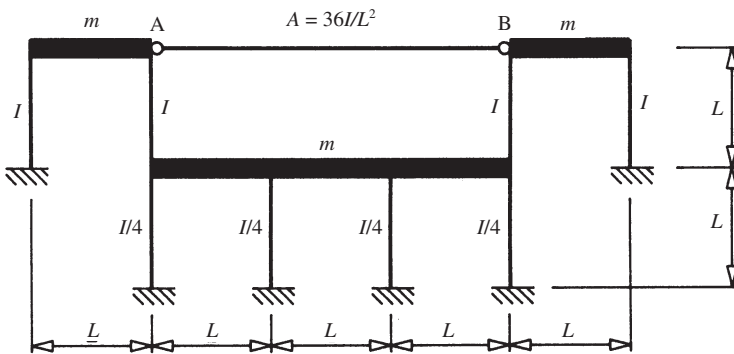


Fig. 5.33

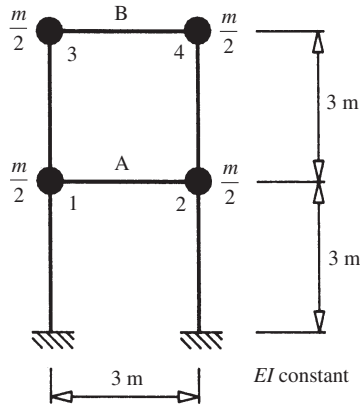


Fig. 5.34

- (a) Calculate the circular natural frequencies, given that one of the circular natural frequencies is  $2\sqrt{(k/m)}$ .
- (b) Given that the higher modes may be determined by symmetry/asymmetry considerations, find the natural modes of vibration and sketch their shapes.

(BRIGHTON)

- 5.3 The two-storey sway frame shown in Fig. 5.34 consists of similar, rigidly jointed beam and stanchion members. Use the beam element stiffness matrix of equation (5.39) to show that the structure stiffness equations for the frame may be expressed as

$$\begin{Bmatrix} F_A \\ F_B \\ M_1 \\ M_2 \\ M_3 \\ M_4 \end{Bmatrix} = \frac{6EI}{3^3} \begin{bmatrix} 8 & -4 & 0 & 0 & 3 & 3 \\ -4 & 4 & -3 & -3 & -3 & -3 \\ \hline 0 & -3 & 18 & 3 & 3 & 0 \\ 0 & -3 & 3 & 18 & 0 & 3 \\ 3 & -3 & 3 & 0 & 12 & 3 \\ 3 & -3 & 0 & 3 & 3 & 12 \end{bmatrix} \begin{Bmatrix} \Delta_A \\ \Delta_B \\ \theta_1 \\ \theta_2 \\ \theta_3 \\ \theta_4 \end{Bmatrix}$$

Given that

$$\begin{bmatrix} 18 & 3 & 3 & 0 \\ 3 & 18 & 0 & 3 \\ 3 & 0 & 12 & 3 \\ 0 & 3 & 3 & 12 \end{bmatrix}^{-1} = 7 \times 10^{-3} \begin{bmatrix} 8.6 & -1.6 & -2.4 & 1.0 \\ -1.6 & 8.6 & 1.0 & -2.4 \\ -2.4 & 1.0 & 13.4 & -3.6 \\ 1.0 & -2.4 & -3.6 & 13.4 \end{bmatrix}$$

determine the stiffness and mass matrices for the structure using the storey sway displacements only as reduced dynamic coordinates. Hence calculate the circular natural frequencies and principal modes for the frame and comment on the comparison between the results obtained and the corresponding values as calculated from equations (5.37) and (5.38).

- 5.4 The uniform cantilever beam of Fig. 5.35(a) is of length  $2L$  and supports a point mass,  $m$ , at its mid-point. The beam is supported at its free end by a spring of axial stiffness  $kEI$  where  $I$  is the second moment of area of the beam and  $E$  is the Young's modulus of the beam material. Show that the circular natural frequency of the beam is given by

$$\omega = \left[ \frac{12EI}{mL^3} \left( \frac{3 + 8kL^3}{12 + 7kL^3} \right) \right]^{1/2}$$

Hence determine the circular natural frequencies for the beams shown in Figs 5.35(b) and 5.35(c).

(UEL)

- 5.5 Figure 5.36 shows an idealization of an off-shore structure to be used for a preliminary dynamic analysis. It includes the five coordinates and associated lumped masses shown in the figure. The corresponding stiffness matrix (in units of meganewtons per metre) is given by

$$[K] = \begin{bmatrix} 1166 & -1216 & -81 & 121 & 0 \\ -1216 & 1544 & -214 & -100 & -7 \\ -81 & -214 & 1027 & -756 & 17 \\ 121 & -100 & -756 & 1756 & -608 \\ 0 & -7 & 17 & -608 & 1366 \end{bmatrix}$$

- (a) Obtain an approximation to the fundamental frequency of vibration of the structure. You may use some results from a static analysis,

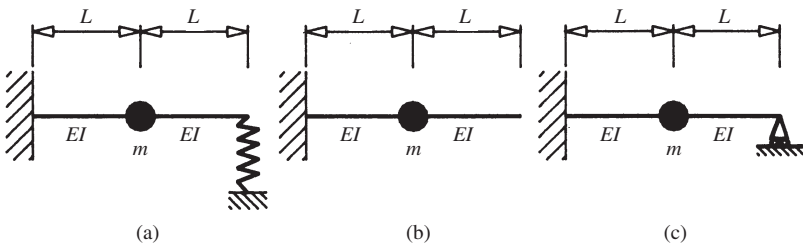


Fig. 5.35

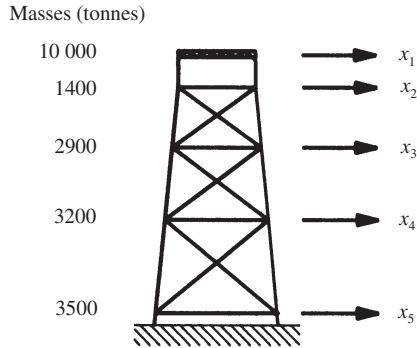


Fig. 5.36

giving displacements  $\{x\}$  caused by a load of 1 MN applied at the topmost degree of freedom, thus

$$\{F\} = \{1, 0, 0, 0, 0\}^T \text{ MN}$$

$$\{x\} = \{8.20, 6.98, 3.10, 1.37, 0.61\}^T \text{ mm}$$

are corresponding loads and displacements.

- (b) What is the percentage change in fundamental natural frequency if the 10 000 tonne mass is increased to 15 000 tonnes?

(UCL)

5.6 A structural system has mass and stiffness matrices as follows:

$$[M] = 10^5 \begin{bmatrix} 1 & 0 \\ 0 & 1.5 \end{bmatrix} \text{ kg}$$

$$[K] = 10^8 \begin{bmatrix} 1 & -1 \\ -1 & 3 \end{bmatrix} \text{ N/m}$$

For the system evaluate the natural frequencies and corresponding mode shapes.

Assuming that the structure is undamped, derive expressions for the displacements of the system when the system executes free vibration following arbitrary initial conditions on displacement and velocity of

$$\{x_0\} = \begin{Bmatrix} 0.015 \\ 0.014 \end{Bmatrix} \text{ m}$$

$$\{\dot{x}_0\} = \begin{Bmatrix} 0 \\ 0.1 \end{Bmatrix} \text{ m/s}$$

(UCL)

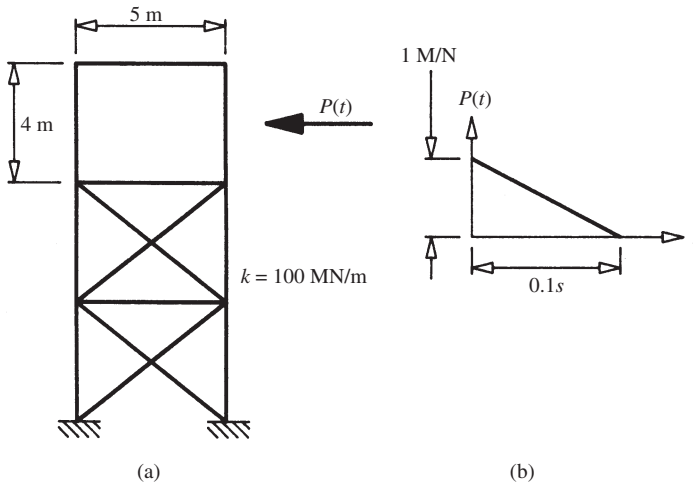


Fig. 5.37

- 5.7 A water tower shown in Fig. 5.37(a) is 5 m square in plan and has sides 4 m high. The mass of the tank itself is 10 000 kg and the lateral stiffness of the skeletal supporting structure is 100 MN/m.

As a result of an external explosion the tank is subjected to a horizontal time-varying force of maximum value 1 MN as shown in Fig. 5.37(b). Assuming zero damping, calculate the maximum horizontal displacement of the tank when it is (a) empty and (b) full of water.

(LIVERPOOL)

- 5.8 A system has inertia and stiffness matrices given by

$$[M] = \begin{bmatrix} 22 & -4 \\ -4 & 3 \end{bmatrix}$$

$$[K] = \begin{bmatrix} 17 & 1 \\ 1 & 3 \end{bmatrix}$$

The principal modes may be expressed by

$$\{\phi_1\} = \{1, -2\}^T, \quad \{\phi_2\} = \{1, 3\}^T$$

Confirm that these satisfy the orthogonality relations and find the corresponding natural frequencies. The system is excited by the forces

$$\{F\} = \begin{Bmatrix} 3 \\ -1 \end{Bmatrix} \sin \Omega t$$

Obtain the resulting undamped displacement responses and comment on the contribution from the second mode.

(UCL)

- 5.9 Figure 5.38 shows an idealization of a fixed-fixed beam with three finite elements each of length  $L$  and flexural rigidity  $EI$ . Using the element stiffness matrix given in equation (5.39), obtain the total stiffness matrix corresponding to the coordinates shown in the figure.

In a particular case  $L = 1$  m and the first two modes of vibration are given as

$$\{\phi_1\} = \{0.719, 0.763, 0.719, -0.763\}$$

$$\{\phi_2\} = \{0.863, -0.688, -0.863, -0.688\}$$

corresponding to circular natural frequencies of 2.496 rad/s and 6.989 rad/s. Obtain an expression for the harmonic response  $q_s$  to the load  $F \sin \Omega t$  applied as shown, neglecting damping and ignoring contributions from all but the lowest two modes. It may be assumed that  $\phi_1$  and  $\phi_2$  are normalized to give the same modal mass in each mode.

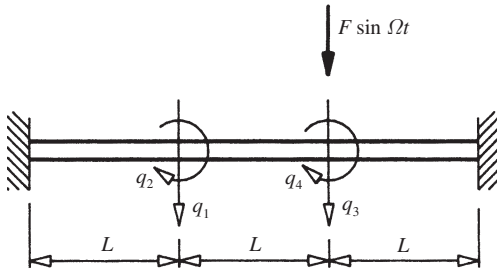


Fig. 5.38

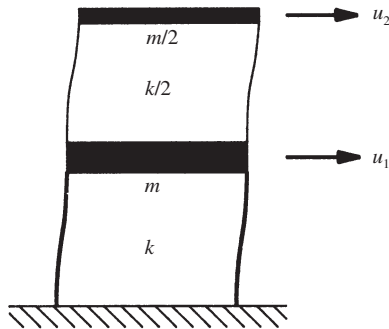


Fig. 5.39



Show that at  $\Omega = 1$  rad/s the contribution to  $q_s$  from the second mode is approximately 14% of the total.

(UCL)

- 5.10 The single-bay, two-storey building shown in Fig. 5.39 has concentrated masses of  $m$  at first-storey level and  $m/2$  in the second floor. If the shear stiffness of the first floor is  $k$ , and  $k/2$  for the second storey, and each storey undergoes only horizontal displacement  $u_1$  and  $u_2$  as shown in Fig. 5.39, find the natural frequencies and principal modes of vibration.

If, initially, a force is applied to the second floor such that  $u_2$  is 1, show that  $u_1$  is  $1/3$ . The structure is then released from this initial position; use modal summation to determine the subsequent motion of the floors. Repeat the calculation with  $u_1$  initially forced to have unit value.

If the ground oscillates in the horizontal direction according to  $u = U_0 \sin \Omega t$ , determine the steady-state response of the building and plot the displacement amplitude of the second floor against  $\omega_1/\Omega$ , where  $\omega_1$  is the lower circular natural frequency.

(KCL)

# Appendix A. Finite difference method

## A.1 Theory

### A.1.1 Functions of a single variable

The finite difference method replaces differential equations by a set of simultaneous linear equations in terms of a finite number of values of the unknown function. In the case of a function of a single variable, the differential equation will be of the ordinary variety and the unknown function values to be determined are taken to be those corresponding to prescribed intervals in the independent variable. In the following, equal prescribed intervals will be used, but, more generally, unequal intervals can also be employed. Thus, in Fig. A.1(a), equal spacings,  $h$ , in the independent variable,  $x$ , are used and the values of the function  $w (= f(x))$  to be determined are  $w_0, w_1, w_2$  and so on.

To obtain a finite difference representation of a given differential expression, the function is locally replaced by an approximating function, which could, in general, be a polynomial of any order, but which will here be taken to be of second order (parabolic). Hence, if point 0 is being considered, then a unique parabolic curve can be constructed through 0 and the immediately preceding (-1) and following (1) points (Fig. A.1(a)). If the approximating parabolic curve is assumed to have the form

$$w = \alpha_1 + \alpha_2 x + \alpha_3 x^2 \quad (\text{A.1})$$

where  $\alpha_1, \alpha_2$  and  $\alpha_3$  are constants, then the coefficients,  $\alpha$ , may be expressed in terms of unknown function values by substituting in equation (A.1) for the points -1, 0, 1:

$$\begin{aligned} w_{-1} &= \alpha_1 - h\alpha_2 + h^2\alpha_3 \\ w_0 &= \alpha_1 \\ w_1 &= \alpha_1 + h\alpha_2 + h^2\alpha_3 \end{aligned} \quad (\text{A.2})$$

Solving equations (A.2) for the coefficients,  $\alpha$ , gives

$$\alpha_1 = w_0, \quad \alpha_2 = \frac{w_1 - w_{-1}}{2h}, \quad \alpha_3 = \frac{w_1 - 2w_0 + w_{-1}}{2h^2} \quad (\text{A.3})$$

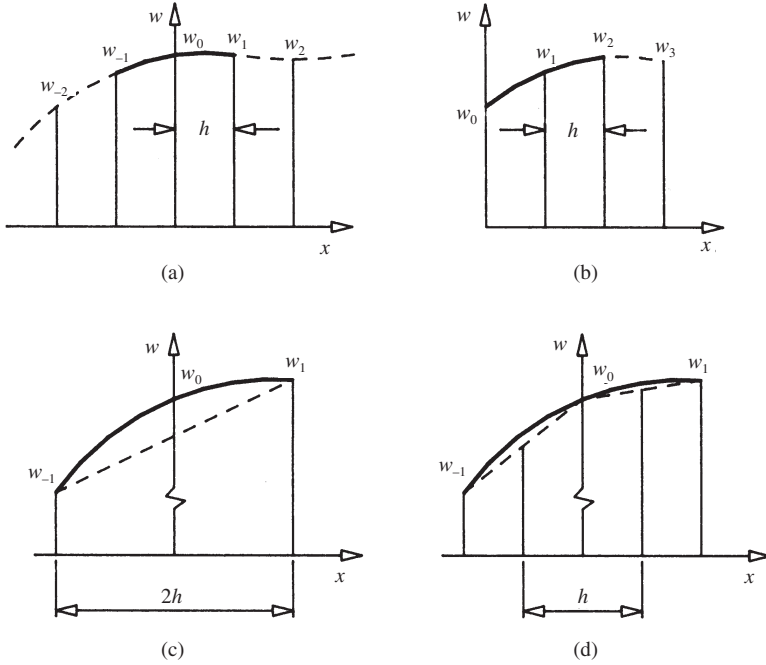


Fig. A.1 Single-variable function

but, from equation (A.1), differentiation gives

$$\frac{dw}{dx} = \alpha_2 + 2\alpha_3 x, \quad \frac{d^2w}{dx^2} = 2\alpha_3 \quad (\text{A.4})$$

so that, substituting from equations (A.3),

$$\left(\frac{dw}{dx}\right)_0 = \alpha_2 = \frac{w_1 - w_{-1}}{2h} = \frac{1}{2h} \Delta w_0 \quad (\text{A.5})$$

$$\left(\frac{d^2w}{dx^2}\right)_0 = 2\alpha_3 = \frac{w_1 - 2w_0 + w_{-1}}{h^2} = \frac{1}{h^2} \Delta^2 w_0 \quad (\text{A.6})$$

Equation (A.5) may be interpreted geometrically (Fig. A.1(c)) as representing the slope of the function at 0 by the slope of the chord connecting points  $-1$  and  $1$ . Also, if equation (A.6) is re-arranged as

$$\left(\frac{d^2w}{dx^2}\right)_0 = \frac{(w_1 - w_0)/h - (w_0 - w_{-1})/h}{h}$$

then equation (A.6) may be geometrically interpreted as representing the small-slope curvature at 0 by the change of chord slope (Fig. A.1(d)) over the

interval length,  $h$ , thus approximating the rate of change of slope (curvature) at 0.

Higher-order differential functions may be readily obtained by use of the first and second *central difference* operators ( $\Delta$  and  $\Delta^2$ ) defined by equations (A.5) and (A.6) respectively. Thus

$$\begin{aligned} \left(\frac{d^3w}{dx^3}\right)_0 &= \left[\frac{d}{dx}\left(\frac{d^2w}{dx^2}\right)\right]_0 = \frac{\Delta}{2h} \frac{w_1 - 2w_0 + w_{-1}}{h^2} \\ &= \frac{1}{2h^3} [\Delta w_1 - 2\Delta w_0 + \Delta w_{-1}] \\ &= \frac{1}{2h^3} [(w_2 - w_0) - 2(w_1 - w_{-1}) + (w_0 - w_{-2})] \\ &= \frac{1}{2h^3} [w_2 - 2w_1 + 2w_{-1} - w_{-2}] \end{aligned} \quad (\text{A.7})$$

and

$$\begin{aligned} \left(\frac{d^4w}{dx^4}\right)_0 &= \left[\frac{d^2}{dx^2}\left(\frac{d^2w}{dx^2}\right)\right]_0 = \frac{\Delta^2}{h^2} \frac{w_1 - 2w_0 + w_{-1}}{h^2} \\ &= \frac{1}{h^4} [(w_2 - 2w_1 + w_0) - 2(w_1 - 2w_0 + w_{-1}) + (w_0 - 2w_{-1} + w_{-2})] \\ &= \frac{1}{h^4} [w_2 - 4w_1 + 6w_0 - 4w_{-1} + w_{-2}] \end{aligned} \quad (\text{A.8})$$

Occasionally, especially at boundaries, points are not available to either side of the point under consideration. The use of the above central difference expressions then becomes impractical and recourse must be made to *forward* difference expressions. Thus, with reference to Fig. A.1(b), the points 0, 1 and 2 may be substituted in equation (A.1) and, solving as before, it may be shown that, for this case,

$$\left(\frac{dw}{dx}\right)_0 = \frac{-3w_0 + 4w_1 - w_2}{2h} \quad (\text{A.9})$$

The corresponding *backward* expression may be similarly derived as

$$\left(\frac{dw}{dx}\right)_0 = \frac{3w_0 - 4w_{-1} + w_{-2}}{2h} \quad (\text{A.10})$$

### A.1.2 Functions of two variables

The extension of the method to the two-variable case requires the function evaluation points to be located at the nodes of a finite difference *net*. The

logical extension of the one-variable case, as described above, is to use a square net (Fig. A.2(a)) but rectangular, oblique, triangular or other net shapes (Salvadori and Baron, 1961) are all possible. The type of net employed will principally depend upon the shape of the region to be considered.

The differential functions of interest are now of the partial variety, with respect to two independent variables, say  $x$  and  $y$ . By straightforward extension of the one-variable case, partial difference operators  $\Delta_x$ ,  $\Delta_y$  and so on may be appropriately defined and used to determine any given partial differential function. Thus, using the portion of a square net shown in Fig. A.3, the Laplace function may be approximated by

$$\begin{aligned} \left( \frac{d^2 w}{dx^2} + \frac{d^2 w}{dy^2} \right)_0 &= \frac{\Delta_x^2 w_0}{h^2} + \frac{\Delta_y^2 w_0}{h^2} = \frac{w_1 - 2w_0 + w_3}{h^2} + \frac{w_2 - 2w_0 + w_4}{h^2} \\ &= \frac{-4w_0 + (w_1 + w_2 + w_3 + w_4)}{h^2} \end{aligned} \quad (\text{A.11})$$

While the biharmonic function may be constructed as follows:

With reference to Fig. A.3 and by analogy to equation (A.8),

$$\left( \frac{\partial^4 x}{\partial x^4} \right)_0 = \frac{1}{h^4} [w_9 - 4w_1 + 6w_0 - 4w_3 + w_{11}] \quad (\text{A.12})$$

and

$$\left( \frac{\partial^4 x}{\partial y^4} \right)_0 = \frac{1}{h^4} [w_{10} - 4w_2 + 6w_0 - 4w_4 + w_{12}] \quad (\text{A.13})$$

while

$$\begin{aligned} \left( \frac{\partial^4 x}{\partial x^2 \partial y^2} \right)_0 &= \frac{\partial^2}{\partial y^2} \left( \frac{\partial^2 w}{\partial x^2} \right)_0 = \frac{\Delta_y^2}{h^2} \frac{w_1 - 2w_0 + w_3}{h^2} \\ &= \frac{1}{h^4} [(w_5 - 2w_1 + w_8) - 2(w_2 - 2w_0 + w_4) + (w_6 - 2w_3 + w_7)] \end{aligned}$$

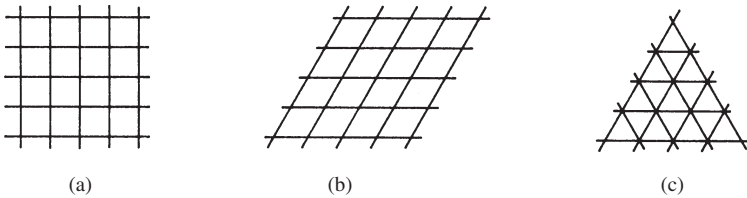


Fig. A.2 Finite difference nets: (a) square; (b) oblique; (c) triangular

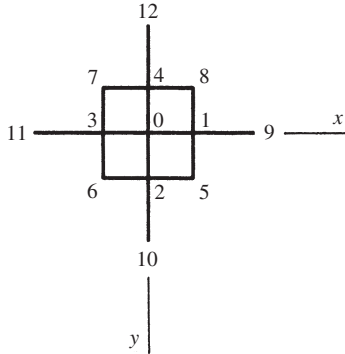


Fig. A.3 Part of difference net

$$= \frac{1}{h^4} [4w_0 - 2(w_1 + w_2 + w_3 + w_4) + (w_5 + w_6 + w_7 + w_8)] \quad (\text{A.14})$$

Hence, from equations (A.12), (A.13) and (A.14),

$$\left( \frac{\partial^4 w}{\partial x^4} + 2 \frac{\partial^4 w}{\partial x^2 \partial y^2} + \frac{\partial^4 w}{\partial y^4} \right) = \frac{1}{h^4} [20w_0 - 8(w_1 + w_2 + w_3 + w_4) + 2(w_5 + w_6 + w_7 + w_8) + (w_9 + w_{10} + w_{11} + w_{12})] \quad (\text{A.15})$$

## A.2 Practical application

Single-variable function applications are generally straightforward, but applications involving two independent variables need some care, and an indication of the most effective procedures will be given in this section. First, a suitable net (square in this case) is superimposed on the region to be considered. The node points so created are then numbered for reference with the following conventions. All nodes at which the function values are expected to differ are given unique reference numbers, normally sequentially numbered from 1. However, should there be nodes at which symmetry, or other considerations, require that the function take identical values at the stipulated nodes, then these nodes are given the same reference number. In Fig. A.4, for instance, the values of a function  $w (= f(x, y))$  at the points on the first (top) row of the net are being constrained to take the same values as the corresponding points on the third row of the net. Similarly, should there be nodes at

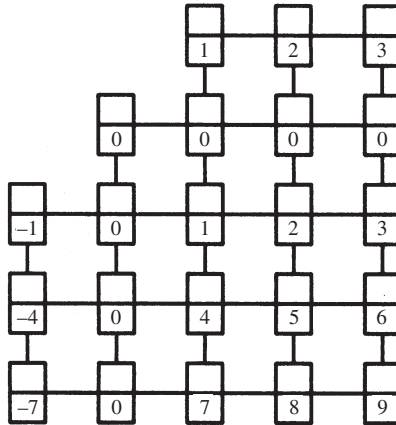


Fig. A.4 Example difference net

which anti-symmetry requires the function to possess equal and opposite values, then equal and opposite reference numbers are used. Referring to Fig. A.4 again:

$$w_{-1} = -w_1, \quad w_{-4} = -w_4, \quad w_{-7} = -w_7 \tag{A.16}$$

Also, should there be nodes at which the function is required to be zero, then this is indicated by a zero reference number. Thus, in Fig. A.4,

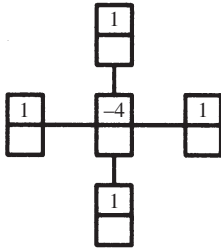
$$\text{For all points } 0: \quad w_0 = 0 \tag{A.17}$$

Once a suitable numbering scheme has been established, the next step is to form the linear difference equations which approximate both the partial differential equation and also the appropriate boundary conditions. This formation process is most easily accomplished by the use of difference operators, typical examples of which are shown in Figs A.5 and A.6. The numbers on the operators in the figures refer to the coefficients by which the function values at the respective nodes must be multiplied to produce the desired difference approximation. It is to be understood that the approximations are being made in respect of the central node of the operator in each case. The most reliable technique for using the operators is to make tracings which are then superimposed on nets of the same scale, such as Fig. A.4. If, for example, it is required to approximate the Laplace function at node 2 of Fig. A.4, then superimposing the appropriate operator (Fig. A.5(a)) gives

$$-4w_2 + w_3 + w_5 + w_1 + 0 = w_1 - 4w_2 + w_3 + w_5$$

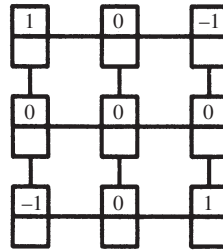
Similarly, if the biharmonic equation is to be represented at node 1, then superimposition of Fig. A.5(c) gives

$$\frac{\partial^2}{\partial x^2} + \frac{\partial^2}{\partial y^2} = \frac{1}{h^2} \Delta^2 x$$

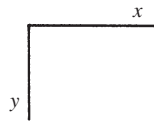


(a)

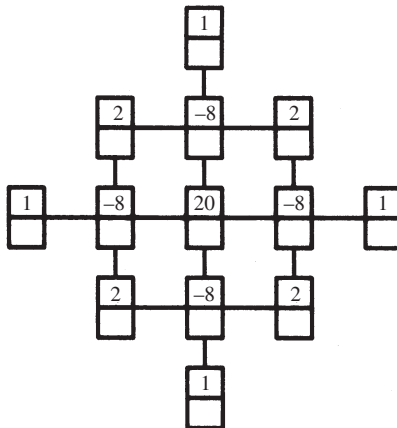
$$\frac{\partial^2}{\partial x \partial y} = \frac{1}{4h^2} \Delta^2 x$$



(b)



$$\frac{\partial^4}{\partial x^4} + \frac{\partial^4}{\partial x^2 \partial y^2} + \frac{\partial^4}{\partial y^4} = \frac{1}{h^4} \Delta^4 x$$



(c)

Fig. A.5 Finite difference operators



$$\frac{\partial^3 w}{\partial x^3} + 2 \frac{\partial^3 w}{\partial x \partial y^2} = \frac{1}{2h^3} x$$

$$\frac{\partial^3 w}{\partial y^3} + 2 \frac{\partial^3 w}{\partial y \partial x^2} = \frac{1}{2h^3} x$$

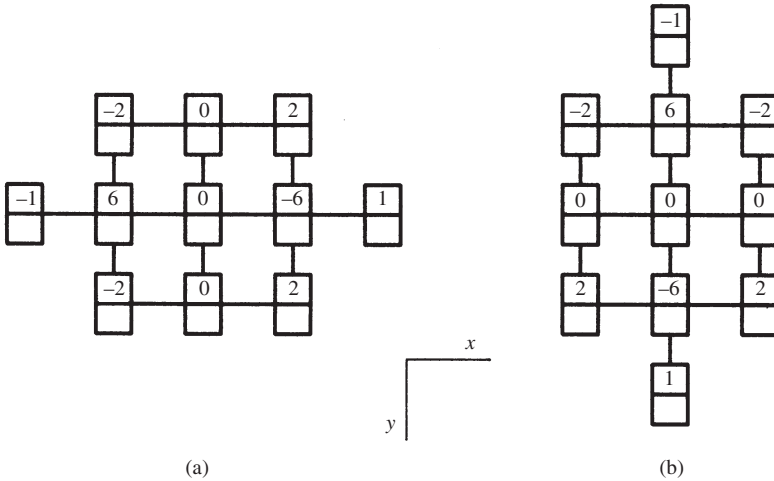


Fig. A.6 Finite difference operators

$$20w_1 - 8(w_2 + w_4 + 0 + 0) + 2(w_5 + 0 + 0 + 0) + (w_3 + w_7 - w_1 + w_1) = 20w_1 - 8w_2 + w_3 - 8w_4 + 2w_5 + w_7$$

### References and further reading

- Ghali, A. and Neville, A. M. (1997) *Structural Analysis*, 4th edn. Spon, London. Chapter 16 covers the finite difference method and provides applications to beam, plate and shell problems.
- Salvadori, M. G. and Baron, M. L. (1961) *Numerical Methods in Engineering*, 2nd edn. Prentice-Hall, New York. A thorough treatment of the finite difference method and its application to engineering problems.
- Ugural, A. C. and Fenster, S. K. (1981) *Advanced Strength and Applied Elasticity – The SI Version*. Arnold, London. Chapter 7 contains a concise introduction to the finite difference method and its application to the torsion of solid sections by the stress function formulation.

# Appendix B. Finite element method

## B.1 Introduction

The finite element method is outlined here as applied to the stress analysis of a surface type of structural continuum. The presentation also assumes that the method is being employed as a displacement (stiffness) type approach. For a more general treatment of the finite element method the reader is referred to other texts (Hinton and Owen, 1980; Reddy, 1985).

The finite element method seeks to replace a continuous type of structural problem, which is alternatively represented by a set of partial differential equations, by a set of discrete, simultaneous linear equations which may be readily solved by computer. The discretization is achieved by sub-dividing the surface to be considered into a number of regions and so creating a set of elements and nodes (Fig. B.1). It is important to realize that the sub-division process is not a physical separation of the surface so that it becomes joined only at the nodes. The intention is purely to create regions in which the deformation will be assumed to be represented by a particular algebraic function of position. The deformation within different regions (elements) will be represented by different functions, although these will all be of the same general

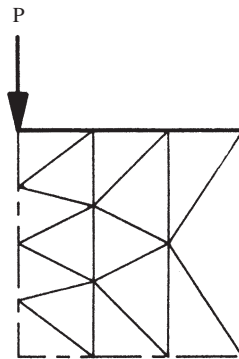


Fig. B.1 Finite element sub-division

form and will normally be chosen such that displacement continuity is preserved along the element boundaries so that the possibility of element separation will not arise.

On the basis of the assumed displacement function, it is possible to derive an element stiffness matrix linking element nodal ‘forces’ to element nodal ‘displacements’. The analysis then closely follows the normal stiffness method as applied to skeletal structures, in that the element stiffness matrices are used to assemble a set of *structure* (system, overall) stiffness equations which represent, in terms of the nodal displacements, the conditions of equilibrium of the total forces acting at the nodes with the applied nodal loads. The solution of this set of linear equations yields the nodal displacements from which the internal element forces may be determined.

## B.2 Theory

For a typical element (Fig. B.2), an example displacement component,  $u$ , at a general point P within the element is assumed to be represented by a polynomial function of the position variables  $x$  and  $y$ . The function will include a number of undetermined coefficients equal in number to the number of nodal displacement components possessed by the element. Thus

$$u = \{c_u\} \{\alpha\} \tag{B.1}$$

where  $\{c_u\}$  is the row vector of polynomial terms with unit coefficients, and  $\{\alpha\}$  is the column vector of undetermined coefficients.

If the remaining displacement components are also represented by polynomial functions of position, which involve the same undetermined coefficients,  $\{\alpha\}$ , then the complete displacement vector at P will be given by

$$\{\delta\} = [C] \{\alpha\} \tag{B.2}$$

where  $\{\delta\}$  is the column vector of displacement components at P, and  $[C]$  is the matrix of polynomial terms with unit coefficients.

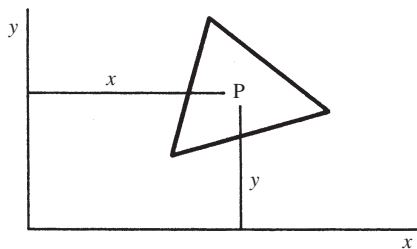


Fig. B.2 Typical finite element

Since  $P$  is a general point, it may be successively chosen to be each of the element nodes in turn, and, by substituting the known nodal position coordinates successively in  $[C]$ , the element nodal displacement components may be related to the undetermined coefficients by

$$\{\delta^e\} = [C^e]\{\alpha\} \quad (B.3)$$

where  $^e$  indicates successive evaluation at each node of an element.

Since the number of undetermined coefficients was (purposely) chosen to be equal to the number of element nodal displacement components, matrix  $[C^e]$  is square. Provided the matrix is also non-singular, it is therefore possible to relate the undetermined coefficients to the element nodal displacement components by

$$\{\alpha\} = [C^e]^{-1}\{\delta^e\} \quad (B.4)$$

The strain at  $P$  will be related to the displacement at that point by known strain–displacement relationships which may be applied to equation (B.2) to give

$$\{\varepsilon\} = [Q]\{\alpha\} \quad (B.5)$$

where  $\{\varepsilon\}$  is the column vector of strain components at  $P$ , and  $[Q]$  is the matrix derived from  $[C]$ , or, using equation (B.4),

$$\{\varepsilon\} = [Q][C^e]^{-1}\{\delta^e\} = [B]\{\delta^e\} \quad (B.6)$$

where  $[B] = [Q][C^e]^{-1}$  is the strain matrix.

The stress–strain relationships of elasticity may also be invoked to relate the stress and strain components at  $P$  by

$$\{\sigma\} = [D]\{\varepsilon\} \quad (B.7)$$

where  $\{\sigma\}$  is the column vector of stress components at  $P$ , chosen such that  $\{\varepsilon\}^T\{\sigma\}dv$  represents a work scalar, and  $[D]$  is the elasticity matrix, and, using equation (B.6),

$$\{\sigma\} = [D][B]\{\delta^e\} = [H]\{\delta^e\} \quad (B.8)$$

where  $[H] = [D][B]$  is the stress matrix.

Equations (B.6) and (B.8) relate the strain and stress components at the point,  $P$ , to the element nodal displacement components. An element stiffness matrix relates element nodal forces to element nodal displacements. Such a stiffness matrix may be derived by applying the principle of virtual displacements to the *complete* element to establish the element nodal forces which are statically equivalent to the stress field throughout the element. By use of equations (B.6) and (B.8), it is then possible to relate these element nodal forces to the element nodal displacement components, as required for the construction of an element stiffness matrix.

Thus, equating external and internal work by the principle of virtual displacements,

$$\{\delta_v^e\}^T \{f^e\} = \int_{\text{vol}} \{\varepsilon_v\}^T \{\sigma\} dv \quad (\text{B.9})$$

where  $\{f^e\}$  is the column vector of statically equivalent nodal forces such that  $\{\delta_v^e\}^T \{f^e\}$  represents a work scalar,  $\delta_v$  is a virtual quantity, and  $\int_{\text{vol}}$  is an integral through the element volume.

From equations (B.6) and (B.8)

$$\{\delta_v^e\}^T \{f^e\} = \int_{\text{vol}} \{[B]\{\delta_v^e\}\}^T [D][B]\{\delta^e\} dv$$

or

$$\{\delta_v^e\}^T \{f^e\} = \int_{\text{vol}} \{\delta_v^e\}^T [B]^T [D][B]\{\delta^e\} dv$$

so that

$$\{\delta_v^e\}^T \{f^e\} = \{\delta_v^e\}^T \int_{\text{vol}} [B]^T [D][B] dv \{\delta^e\}$$

and, since the virtual displacements are arbitrary,

$$\{f^e\} = \int_{\text{vol}} [B]^T [D][B] dv \{\delta^e\} \quad (\text{B.10})$$

Equation (B.10) is the required relationship between element nodal forces and displacement components and may be written as

$$\{f^e\} = [k]\{\delta^e\} \quad (\text{B.11})$$

where

$$[k] = \int_{\text{vol}} [B]^T [D][B] dv$$

is the element stiffness matrix.

The stiffness matrices for all the elements may therefore be determined by repeated application of equation (B.11) and these may be used to assemble (see example 1.1 or Astley (1992)) the complete structure stiffness equations which link total structure nodal forces to the complete set of structure nodal displacement components. Thus

$$\{F\} = [K]\{\Delta\} \quad (\text{B.12})$$

where  $\{F\}$  is the column vector of structure nodal forces,  $\{\Delta\}$  is the column vector of structure nodal displacements, and  $[K]$  is the structure stiffness matrix.

Since the structure nodal forces must, for equilibrium, be equivalent to the applied nodal forces

$$\{W\} = [K]\{\Delta\} \quad (\text{B.13})$$

where  $\{W\}$  is the column vector of nodal applied loads.

Solving equations (B.13) for the unknown nodal displacements in terms of the known applied loading and specified boundary conditions gives

$$\{\Delta\} = [K]^{-1}\{W\} \quad (\text{B.14})$$

To complete the solution, it is necessary to evaluate the stresses in each element. Equation (B.8) gives the stresses at a general point within an element in terms of the element nodal displacements. These element displacements may be extracted from the complete set of structure displacements provided by equation (B.14), and expressions for the stresses at a general point are thereby generated. Often it is convenient to determine stresses at element nodal positions, in which case equation (B.8) is used repeatedly, the coordinates of the various nodes of the elements being successively substituted in matrix  $[B]$ . If this procedure is followed for all the elements, it will result in multiple values of nodal stresses being derived at any given node according to the number of elements which the node interconnects. By the nature of the finite element process, these nodal stresses will not agree exactly, and normal practice is to average the values obtained.

## References and further reading

Astley, R. J. (1992) *Finite Elements in Solids and Structures*. Chapman and Hall, London. Chapter 4 covers displacement finite elements and, in particular, the assembly of stiffness matrices.

Hinton, E. and Owen, D. R. J. (1980) *A Simple Introduction to Finite Elements*. Pineridge Press, Swansea. The finite element method is explained using variational and weighted residual methods, and the application of the method is illustrated through heat flow examples.

Cook, R. D. (1995) *Finite Element Modeling for Stress Analysis*. Wiley, Chichester. Concentrates on the use of finite element programs, emphasizing topics such as modelling, mesh specification, element selection and assessment of results.

Reddy, J. N. (1985) *An Introduction to the Finite Element Method*. McGraw-Hill, New York. Thorough account of the finite element method on a variational formulation basis.

# Solutions to problems

1.1

$$[k^1] = \frac{1}{40} \begin{bmatrix} 1.5 & -0.5 & -1.0 & 0 & -0.5 & 0.5 \\ -0.5 & 1.5 & 1.0 & -2.0 & -0.5 & 1.0 \\ -1.0 & 1.0 & 2.0 & 0 & -1.0 & -1.0 \\ 0 & -2.0 & 0 & 4.0 & 0 & -2.0 \\ -0.5 & -0.5 & -1.0 & 0 & 1.5 & 0.5 \\ 0.5 & 1.0 & -1.0 & -2.0 & 0.5 & 1.5 \end{bmatrix} \text{ kN/mm}$$

$$[k^2] = [k^3] = \frac{1}{40} \begin{bmatrix} 1.5 & 0.5 & -0.5 & -0.5 & -1.0 & 0 \\ 0.5 & 1.5 & 0.5 & 0.5 & -1.0 & -2.0 \\ -0.5 & 0.5 & 1.5 & -0.5 & -1.0 & 0 \\ -0.5 & 0.5 & -0.5 & 1.5 & 1.0 & -2.0 \\ -1.0 & -1.0 & -1.0 & 1.0 & 2.0 & 0 \\ 0 & -2.0 & 0 & -2.0 & 0 & 4.0 \end{bmatrix} \text{ kN/mm}$$

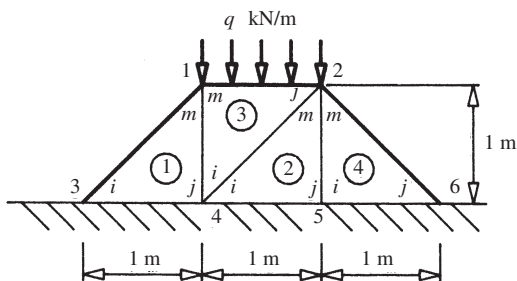


Fig. P.1

1.2 With reference to Fig. P.1:

(a)

$$[k] = \begin{bmatrix} k_{mn}^1 + k_{mn}^3 & k_{mj}^3 & k_{mi}^1 & k_{mj}^1 + k_{mi}^3 & 0 & 0 \\ & k_{jj}^3 + k_{nm}^2 + k_{nm}^4 & 0 & k_{ji}^3 + k_{mi}^2 & k_{mj}^2 + k_{mi}^4 & k_{mj}^4 \\ & & k_{ii}^1 & k_{ij}^1 & 0 & 0 \\ & \text{sym.} & & k_{jj}^1 + k_{ii}^3 + k_{ii}^2 & k_{ij}^2 & 0 \\ & & & & k_{jj}^2 + k_{ii}^4 & k_{ij}^4 \\ & & & & & k_{ij}^4 \end{bmatrix}$$

(b) Final four rows and columns of the stiffness matrix of (a) should be deleted in view of the constraints at nodes 3, 4, 5 and 6.

1.3 The part stiffness matrix is

$$\begin{bmatrix} 1.5 & 0.5 & -0.5 & 0 & 0 & 0 & -1.0 & -0.5 & 0 & 0 & 0 & 0 & 0 & 0 & 0 \\ & 1.5 & -0.5 & -1.0 & 0 & 0 & 0 & -0.5 & 0 & 0 & 0 & 0 & 0 & 0 & 0 \\ & & 3.0 & 0.5 & -0.5 & 0 & 0 & 0.5 & -2.0 & -0.5 & 0 & 0 & 0 & 0 & 0 \\ & & & 3.0 & -0.5 & -1.0 & 0.5 & 0 & -0.5 & -1.0 & 0 & 0 & 0 & 0 & 0 \\ & & & & 1.5 & 0 & 0 & 0 & 0 & 0.5 & -1.0 & 0 & 0 & 0 & 0 \\ & \text{sym.} & & & & 1.5 & 0 & 0 & 0.5 & 0 & -0.5 & -0.5 & 0 & 0 & 0 \\ & & & & & & 3.0 & 0.5 & -1.0 & -0.5 & 0 & 0 & -1.0 & -0.5 & 0 \\ & & & & & & & 3.0 & -0.5 & -2.0 & 0 & 0 & 0 & -0.5 & 0 \end{bmatrix}$$

1.4

$$\{\sigma^1\} = \begin{Bmatrix} 160 \\ 0 \\ -0.1 \end{Bmatrix}, \quad \{\sigma^5\} = \begin{Bmatrix} 154 \\ -0.9 \\ -2.5 \end{Bmatrix}, \quad \{\sigma^9\} = \begin{Bmatrix} 94 \\ -4.5 \\ -17 \end{Bmatrix} \quad \text{N/mm}^2$$

1.5

$$\{\sigma^3\} = \begin{Bmatrix} 0.99 \\ -15.2 \\ 3.73 \end{Bmatrix}, \quad \{\sigma^4\} = \begin{Bmatrix} 1.48 \\ -5.98 \\ 1.45 \end{Bmatrix}, \quad \{\sigma^5\} = \begin{Bmatrix} 2.45 \\ -12.5 \\ 0 \end{Bmatrix} \quad \text{N/mm}^2$$

1.6  $P = 1.21$  kN; small tensile principal stress ( $0.21$  N/mm<sup>2</sup>) produced in element 7 by the action of pre-stress alone.

1.7

$$[B] = \begin{bmatrix} -\frac{1}{a} + \frac{y}{ab} & 0 & -\frac{y}{ab} & 0 & \frac{1}{a} - \frac{y}{ab} & 0 & \frac{y}{ab} & 0 \\ 0 & -\frac{1}{b} + \frac{x}{ab} & 0 & \frac{1}{b} - \frac{x}{ab} & 0 & -\frac{x}{ab} & 0 & \frac{x}{ab} \\ -\frac{1}{b} + \frac{x}{ab} & -\frac{1}{a} + \frac{y}{ab} & \frac{1}{b} - \frac{x}{ab} & -\frac{y}{ab} & -\frac{x}{ab} & \frac{1}{a} - \frac{y}{ab} & \frac{x}{ab} & \frac{y}{ab} \end{bmatrix}$$



1.8 The global constrained stiffness matrix is

$$\begin{bmatrix} k_{jj} & k_{jm} & 0 & k_{ji} & k_{jl} & 0 & 0 & 0 & 0 \\ k_{mm} + k_{jj} & k_{jm} & k_{mi} & k_{ml} + k_{ji} & k_{jl} & 0 & 0 & 0 & 0 \\ & k_{mm} & 0 & k_{mi} & k_{ml} & 0 & 0 & 0 & 0 \\ & & k_{ii} + k_{jj} & k_{il} + k_{jm} & 0 & k_{ji} & k_{jl} & 0 & 0 \\ & & & k_{il} + k_{ii} + k_{mm} + k_{jj} & k_{il} + k_{jm} & k_{ml} & k_{ji} + k_{ml} & k_{jl} & k_{jl} \\ & & & & k_{il} + k_{mm} & 0 & k_{mi} & k_{ml} & k_{ml} \\ & \text{sym.} & & & & k_{ii} + k_{jj} & k_{il} + k_{jm} & 0 & 0 \\ & & & & & & k_{il} + k_{ii} + k_{mm} + k_{jj} & k_{jm} + k_{il} & k_{il} + k_{mm} \end{bmatrix}$$

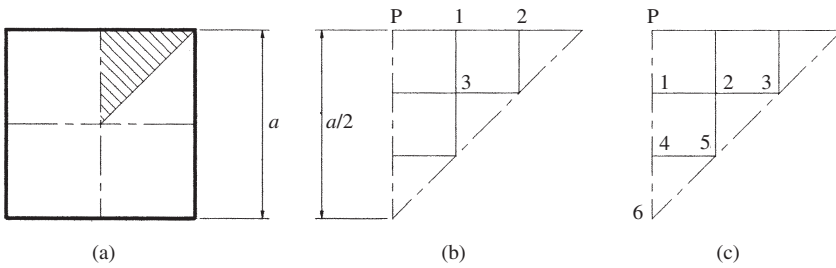


Fig. P.2

2.1 With reference to Fig. P.2(b),

$$\{w\} = \{-0.0256, -0.0342, -0.0064\}^T a^2 \theta'$$

$$\tau_{\max} = |\tau_p| = 0.654aG\theta', \quad J = 0.135a^4$$

With reference to Fig. P.2(c),

$$\{\phi\} = \{0.0856, 0.0781, 0.0528, 0.130, 0.118, 0.144\}^T a^2 G\theta'$$

$$\tau_{\max} = |\tau_p| = 0.636aG\theta', \quad J = 0.137a^4$$

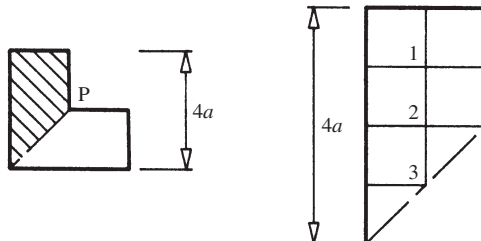


Fig. P.3

2.2 With reference to Fig. P.3,

$$\{\phi\} = \{0.731, 0.923, 0.962\}^T a^2 G \theta'$$

$$\tau_{\max} = |\tau_p| = 1.85 a G \theta', \quad J = 11.1 a^4$$

By 'combined rectangles',

$$\tau_{\max} = |\tau_p| = 2.00 a G \theta', \quad J = 16.0 a^4$$

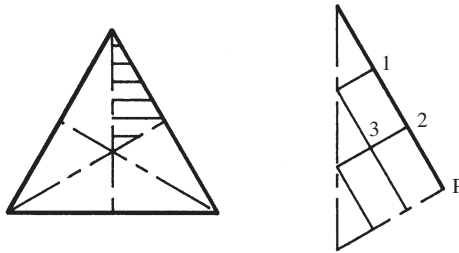


Fig. P.4

2.3 With reference to Fig. P.4,

$$\{w\} = \{0.0267, 0.0214, 0.0080\}^T s^2 \theta'$$

$$\tau_{\max} = |\tau_p| = 0.415 s G \theta'$$

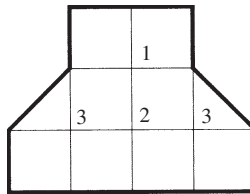


Fig. P.5

2.4 With reference to Fig. P.5,

$$\{\phi\} = \{0.0308, 0.0431, 0.0308\}^T G \theta'$$

$$J = 0.0137 m^4$$

2.5 For open section:  $T = 0.86 \text{ kN m}$ ;  $\theta = 21.1^\circ$ .

For closed section:  $\tau_{\max} = 2.99 \text{ N/mm}^2$ ;  $\theta = 0.18^\circ$ .

2.6 For closed section:  $J = 0.0791 \text{ m}^4$ .

For open section:  $J = 0.00245 \text{ m}^4$ .

- 2.7 In order of increasing torsional stiffness, ranking is D, A, B, E, C.  
 2.8 Torsional rigidity =  $1.27 \text{ kN m}^2/\text{degree}$ .  
 2.9 Torsional rigidity =  $1.41 \times 10^5 \text{ kN m}^2/\text{degree}$ .

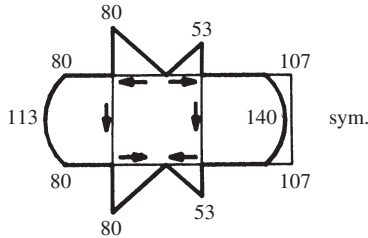


Fig. P.6

- 2.10 Shear flows in kilonewtons per metre are as shown in Fig. P.6.

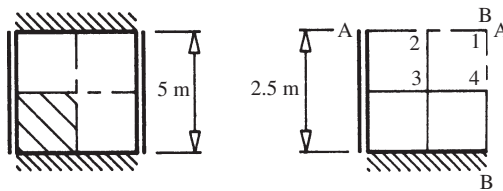


Fig. P.7

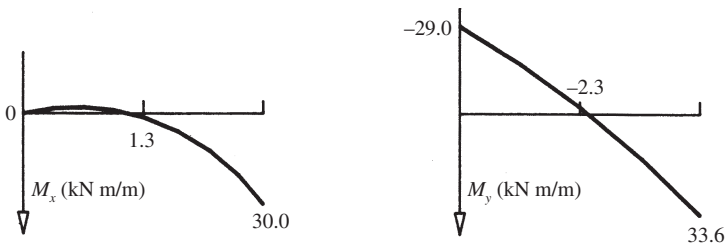


Fig. P.8

- 3.1 With reference to Fig. P.7,  $\{w\} = \{29.33, 15.28, 7.83, 13.58\}^T \text{ mm}$ .  
 Bending moments along and in the direction of AA and BB (Fig. P.7) are as shown in Fig. P.8.  
 3.2

$$w_1 = -\frac{1}{162} \frac{PL^2}{D} \quad \text{and} \quad w_2 = -\frac{1}{108} \frac{PL^2}{D}$$

3.3 The difference equations are as shown below where the alternative vectors are for cases (i) and (ii):

$$\frac{1}{(a/4)^4} \begin{bmatrix} -20 & -8 & 1 & -8 & 2 & 1 \\ -8 & 21 & -8 & 3 & -8 & 0 \\ 2 & -16 & 18 & 0 & 2 & 0 \\ -8 & 3 & 0 & 23 & -8 & -8 \\ 4 & -16 & 2 & -16 & 20 & 2 \\ 2 & 0 & 0 & -16 & 2 & 22 \end{bmatrix} \{w\} = \begin{cases} \begin{bmatrix} 1 \\ 1 \\ 1 \\ 1 \\ 1 \\ 1 \end{bmatrix} \frac{q}{D} \\ \text{or} \\ \begin{bmatrix} 0 \\ 0 \\ 0 \\ 0 \\ 1 \\ 0 \end{bmatrix} \frac{16P}{a^2 D} \end{cases}$$

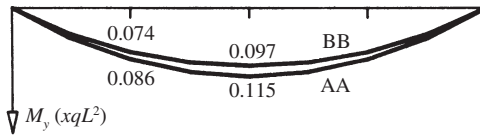


Fig. P.9

3.4

$$\{w\} = \{0.01232, 0.00881, 0.00729, 0.01018\}^T \frac{qL^4}{D}$$

Bending moments along and in the direction of AA and BB are as shown in Fig. P.9.

For a plate of infinite length

$$M_1 = \frac{qL^2}{8} = 0.125qL^2$$

Table P.1

Position	$w (\times 10^{-5} qL^4/D)$	$M_x (\times 10^{-4} qL^2)$	$M_y (\times 10^{-4} qL^2)$
Centre	88	118	116
Column	0	0	-21

3.5  $L/4$  grid finite difference analysis results are given in Table P.1.

3.6 For the typical grid shown in Fig. P.10, sample member properties are given in Table P.2 and sample joint loads, calculated on the basis set out in Fig. 4.28 are given in Table P.3.

Restraints are: joints 10–16 are fully restrained; joints 1, 4 and 7 have  $\theta_y$  restrained (symmetry).

3.7 With reference to the sample element mesh shown in fig. P.11:

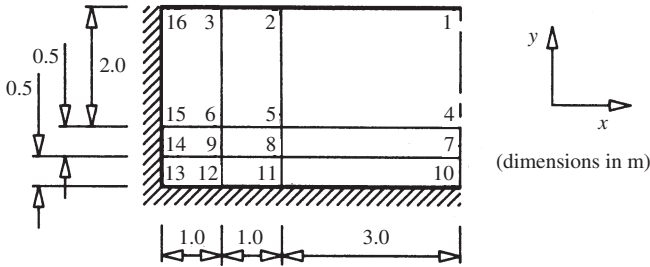


Fig. P.10

Table P.2

Member	$I (\times 10^{-3} m^4)$	$J (\times 10^{-3} m^4)$
16-3	0.16	0.32
6-5	0.62	1.24
8-7	0.47	0.94
6-3	0.28	0.56
8-5	1.60	3.20
10-7	1.69	3.38

Table P.3

Joint	Load (kN)
1	9.81
2	13.08
4	27.59
5	36.79
7	18.39
8	24.53

All elements have thickness  $t = 125$  mm, except elements 1, 2 and 3, where the column head may be roughly modelled by  $t_1 = t_2 = 200$  mm and  $t_3 = 162.5$  mm.

Nodes 36, 42 and 43 (around the column) are fully restrained.

Along 1-48 and 37-42,  $\theta_x = 0$  (symmetry).

Along 1-37 and 43-48,  $\theta_y = 0$  (symmetry).

Typical nodal loads due to a uniform applied load  $q$  (kN/m<sup>2</sup>) are shown in Table P.4.

3.9 With reference to Fig. P.7:

$$\{w_1, w_2, w_3, w_4\} = \{22.42, 12.51, 6.62, 10.39\} \text{ mm.}$$

Averaged bending moments along and in the direction of AA and BB (Fig. P.7) are as shown in Fig. P.12.

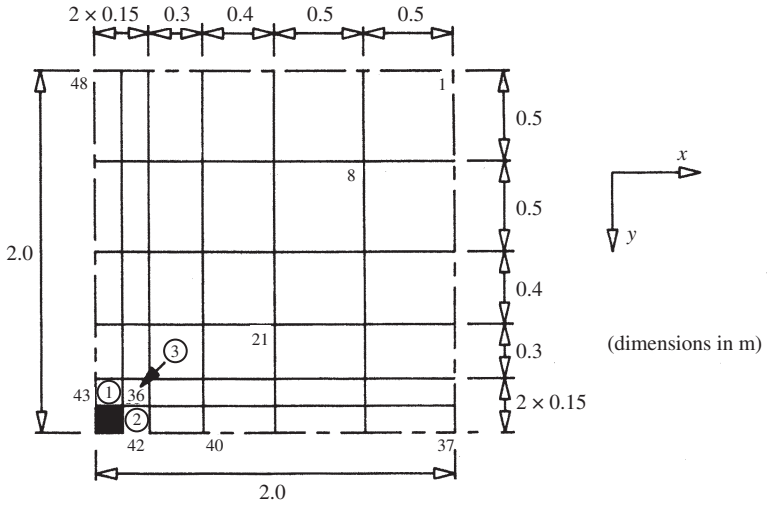


Fig. P.11

Table P.4

Node	Load (kN)
1	$0.0625q$
8	$0.25q$
21	$0.1575q$
40	$0.02625q$

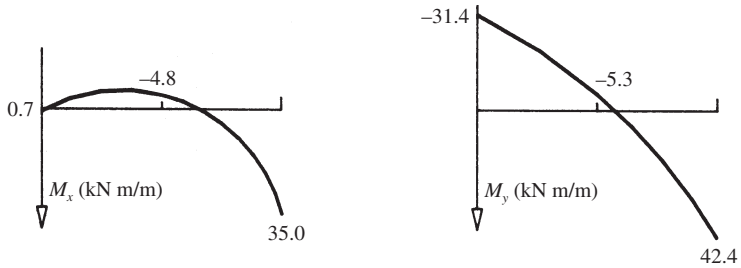


Fig. P.12

3.10 The reduced stiffness matrix is

$$\begin{bmatrix} 162 & -144 & 66 & -18 & 24 \\ -72 & 306 & 12 & -144 & 66 \\ 33 & 12 & 48 & 0 & 12 \\ -18 & -288 & 0 & 648 & 0 \\ 12 & 66 & 12 & 0 & 96 \end{bmatrix}$$



4.10 (b)

$$\begin{Bmatrix} N_{t1} \\ M_{m1} \\ N_{t13} \\ M_{m13} \end{Bmatrix} = \begin{Bmatrix} 2998 \\ -0.1 \\ 0 \\ 27.2 \end{Bmatrix} \begin{matrix} \text{kN/m} \\ \text{kN m/m} \\ \text{kN/m} \\ \text{kN m/m} \end{matrix}$$

(c)  $N_t = 3000 \text{ kN/m}$

- 5.1 Without additional mass, fundamental frequency = 1.59 Hz.  
 With extra mass on lower storey, fundamental frequency = 1.46 Hz.  
 With extra mass on upper storey, fundamental frequency = 1.22 Hz (best).

5.2

$$\{\omega\}^T = \{1, 2, 2\}\sqrt{k/m}$$

$$[\Phi] = \begin{bmatrix} 1 & 1 & 0 \\ 1 & -0.5 & 1 \\ 1 & -0.5 & -1 \end{bmatrix}$$

5.3

$$\{\omega\}^T = \{0.42, 1.35\}\sqrt{EI/m}$$

$$[\Phi] = \begin{bmatrix} 1.00 & 1.00 \\ 2.04 & -0.49 \end{bmatrix}$$

5.4

$$\omega_b = \sqrt{\frac{3EI}{mL^3}}$$

$$\omega_c = \sqrt{\frac{96EI}{7mL^3}}$$

- 5.5 For 10 000 tonne mass, fundamental circular frequency = 3.23 rad/s.  
 For 15 000 tonne mass, fundamental circular frequency = 2.70 rad/s, a 16.4% decrease.

5.6

$$\{\omega\} = \begin{Bmatrix} 23.3 \\ 49.6 \end{Bmatrix} \text{ rad/s}$$



$$[\Phi] = \begin{Bmatrix} 1.000 & -0.689 \\ 0.457 & 1.000 \end{Bmatrix}$$

$$\{x\} = \begin{Bmatrix} 18.74 \cos 23.3t + 2.25 \sin 23.3t - 3.74 \cos 49.6t - 1.06 \sin 49.6t \\ 8.56 \cos 23.3t + 1.03 \sin 23.3t + 5.43 \cos 49.6t + 1.53 \sin 49.6t \end{Bmatrix} \text{ mm}$$

- 5.7 Maximum displacement when empty = 17.1 mm.  
Maximum displacement when full = 11.7 mm.

5.8

$$\{\omega\} = \begin{Bmatrix} 0.707 \\ 1.414 \end{Bmatrix} \text{ rad/s}$$

$$\{x\} = \begin{Bmatrix} 1 \\ -2 \end{Bmatrix} \frac{\sin \Omega t}{5(1 - 2\Omega^2)}$$

- 5.9 Constrained stiffness matrix is

$$EI = \begin{bmatrix} \frac{24}{L^3} & 0 & -\frac{12}{L^3} & \frac{6}{L^2} \\ 0 & \frac{8}{L} & -\frac{6}{L^2} & \frac{2}{L} \\ -\frac{12}{L^3} & -\frac{6}{L^2} & \frac{24}{L^3} & 0 \\ \frac{6}{L^2} & \frac{2}{L} & 0 & \frac{8}{L} \end{bmatrix}$$

$$q_3 = \left( \frac{0.719^2}{\omega_1^2 - \Omega^2} + \frac{0.863^2}{\omega_2^2 - \Omega^2} \right) \frac{\sin \Omega t}{m_\phi}$$

5.10

$$\{\omega\} = \begin{Bmatrix} 1 \\ 2 \end{Bmatrix} \sqrt{\frac{k}{m}}, \quad [\Phi] = \begin{bmatrix} 1 & 1 \\ 2 & -1 \end{bmatrix}$$

$$\{x\} = \begin{Bmatrix} u_1 \\ u_2 \end{Bmatrix} = \frac{1}{9} \begin{Bmatrix} 4 \cos \omega_1 t - \cos \omega_2 t \\ 8 \cos \omega_1 t + \cos \omega_2 t \end{Bmatrix}$$

If a force is applied to the lower storey such that  $u_1 = 1$ , then  $u_2 = 1$ , and

$$\{x\} = \begin{Bmatrix} u_1 \\ u_2 \end{Bmatrix} = \frac{1}{3} \begin{Bmatrix} 2 \cos \omega_1 t + \cos \omega_2 t \\ 4 \cos \omega_1 t - \cos \omega_2 t \end{Bmatrix}$$

The steady state response is

$$\{x\} = \begin{Bmatrix} u_1 \\ u_2 \end{Bmatrix} = \begin{Bmatrix} \frac{2}{\omega_1^2 - \Omega^2} + \frac{1}{\omega_2^2 - \Omega^2} \\ \frac{4}{\omega_1^2 - \Omega^2} - \frac{1}{\omega_2^2 - \Omega^2} \end{Bmatrix} \frac{u_0 \Omega^2}{3} \sin \Omega t$$

# Index

- adaptive meshing, 45
- amplitude, 219
- anti-clastic, 104
- anti-symmetry, with finite differences, 278
- area projection rule, 174
- axial mode, 220, 235, 240
- axis, of axisymmetric shell, 169
- axisymmetric shells, 166, 168–169, 204, 205
  - membrane analysis of, 169–185
- axisymmetry, in shells, 171–172, 186, 188
  
- backward differences, 275
- basis element, 38–39
- beam analogy, for plates, 102
- beams, 9
  - by Rayleigh's method, 248–249
  - harmonically forced vibration of, 262–263
  - interaction of with slabs, 126, 136, 151
  - lateral instability of, 60
  - natural frequencies of, 240–243
- bending,
  - in shells, 167–169, 178–179, 185, 186–204
  - in shells, classical solutions for, 186
- biharmonic equation, 112, 277, 279
  
- body force, 12
- boundary conditions, 15
  - for plates, 114–117, 118–119, 128–129, 145
  - for torsion, 68, 70–71, 73
  - modification of stiffness matrix for, 29–32, 148–149, 201
- box girders, 59, 94
  - under applied torque, 81–83
  - under general load, 87
  - under shear load, 84–87
  
- central differences, 275
- centre of rotation, 61
- characteristic equation, 243
- circular cylindrical shells, 166, 186
  - finite element analysis of, 186–204, 211–215
- circular natural frequency, 219
- circular sections, torsion of, 62–63
- circular tank
  - of non-uniform thickness, 199–204
  - of uniform thickness, 193–199
- circumferential stress resultant, 172
- closed cylindrical shells, 166
- closed sections, 59, 77
- closed-form solution, 15
- co-factor method, 18, 50
- coordinates, in dynamics, 218, 228, 231

- compatibility, 12
  - equation in plane stress, 13
- complementary shear stress, 3
- concrete core construction, 59
- concrete cube analysis, 36, 45–47
- concrete cylinder analysis, 43–45
- conical shells, 208
  - under fluid pressure, 182–185
- consistent loads, 151, 200
- consistent mass matrix, 250
- contour, 78
- coupling, 251
  - of damping matrix, 263–264
- critical damping, 222
- curvature
  - in axisymmetric shells, 170
  - in circular cylindrical shells, 189
  - in plates, 104–105, 109–110, 119, 133, 139, 152
  - in shells, 168, 170, 179
- curved boundaries
  - in plane stress, 36
  - in plates, 126, 136
- damping, 218, 221–223, 226–227, 264
  - coefficient of, 221, 264
  - critical coefficient of, 222
  - matrix, 263
  - ratio, 222
- dashpot model, 221
- deep beam, 9
- degrees of freedom, 218, 220
- design moments in slabs, 152–154
- direct strain, 4
- direct stress, 3
  - in shells, 167, 171–172, 188, 202
- distributed mass model, 250
- Duhamel integral, 257
- dynamic loading, 218
- dynamic matrix, 230
- eigenvalue, 230
  - determination of, 230, 265
- eigenvector, 230
- elasticity, 2
  - theory, 2–7
- elasticity matrix, 283
  - circular cylindrical shell, 190
  - plate bending, 141
  - square slab bending, 141
  - triangular plane stress, 19, 24
- element numbering, 22
- element stiffness matrix, 282, 284
  - beam, 240
  - circular cylindrical shell, 192
  - plane frame, 232
  - square slab bending, 143
  - sway column, 236
  - triangular plane stress, 21
- element stress solution, 285
  - circular cylindrical shell, 198–199
  - square slab, 149–151
  - triangular plane stress, 33–36
- error estimators, 45
- excitation, 223
- fatigue, 218
- finite difference method
  - for plates and slabs, 118–126
  - for shells, 186, 205, 206
  - for torsion, 69–76
  - nets for, 275–276
  - theory, 273–280
- finite element method
  - accuracy of, 45–48
  - for dynamic analysis, 228, 244–247, 250
  - for plane strain, 50
  - for plane stress, 16
  - for plate bending, 136, 152
  - for shells, 186, 204, 206
  - for torsion, 71, 95
  - theory, 281–285
- finite elements, 281
  - circular cylindrical shell, 186–204, 205, 211–215

- eight-noded isoparametric plane stress, 37–45  
 plane strain, 50  
 rectangular plane stress, 36, 56, 58  
 square slab, 136–151  
 triangular plane stress, 16–36  
 types of, 36–37  
 flexural mode, 220, 235, 240  
 flexural rigidity, 109  
 folded plates, 166, 167, 168  
 forced damped vibration, 223–228  
 forced undamped vibration, 255–265  
 forcing frequency, 226  
 forcing function, 223–227, 256, 259, 261  
 forward differences, 275  
 Fourier series analysis, 204, 225, 257  
 free damped vibration, 221–223, 224  
 free undamped vibration, 218–221, 250–255  
 frequency, 219  
   of damped vibration, 222  
   ratio, 226  
 frustum of shell, 173  
 fundamental frequency, 235, 248  
  
 Gaussian curvature, 168  
 Gaussian integration, 42–45  
 grid analogy,  
   for plates and slabs, 103–105  
   for slabs, 126–136, 152, 155  
 ground motion, 258–261  
  
 harmonic excitation, 224–225, 262  
 harmonic vibration, 219  
 harmonically forced undamped vibration, 261–263  
 homogeneous material, 7  
 hoop stress resultant, 172  
 hyperboloid shell, under fluid pressure, 209–211  
  
 impulse, dynamic response to, 256–258  
  
 Intze-type container, 210–211  
 isoparametric elements, 36–45, 151  
 isotropic material, 7  
  
 Jacobian matrix, 40–44  
  
 Kirchoff assumption, 87, 152  
  
 Laplace equation, 14, 66, 276, 279  
 line element, 1  
 line of curvature, 170  
 linear elastic behaviour, 2, 6–7  
 lines of distortion, 178–179  
 load representation  
   with finite differences, 118, 121  
   with finite elements, 147, 200  
   with grid analogy, 129, 131  
 lumped mass model, 228, 234  
  
 magnification factor, 226  
 mapping of co-ordinates, 36–37, 40  
 mass matrix, 229, 234, 265  
 mass moment of inertia, 234  
 membrane action, 167  
 membrane analogy for torsion, 91–93  
 membrane forces  
   in circular cylindrical shells, 188  
   in circular tank, 198–199, 202–204  
   in conical tank, 184–185  
   in paraboloid dome, 181–182  
   in shells, 171–172, 178–179  
   in spherical dome, 176–177  
 membrane shell theory, 169–185, 202–204  
   limitations of, 178–179  
 meridian, 169  
 meridional stress resultant, 171, 173  
   *see also* membrane forces  
 middle surface, 106  
 Mindlin plate theory, 151–152  
 modal damping, 264  
 modal damping coefficients, 264  
 modal forcing function, 259

- modal mass, 230
- modal mass matrix, 251, 253
- modal matrix, 251
- modal stiffness matrix, 251, 253
- mode, 219
  - shape, 220
- mode superposition analysis
  - of forced undamped vibration, 255–261
  - of free undamped vibration, 251–255
  - of harmonically forced undamped vibration, 261–263
  - reduced modes in, 255
- modulus of elasticity, 6
- modulus of rigidity, 7
- moments
  - in circular cylindrical shells, 186, 188–189
  - in circular tank, 198–199, 202
  - in plates, 107–110, 120
  - in slabs, 121–122, 129–130, 132–135
- multiply-closed sections, 59
  - torsion of, 81–86, 95
- natural frequencies, 219, 220, 230
  - by Rayleigh's method, 248–249
  - determination of, 228–247, 265
  - number of, 231, 235, 239, 246
  - repeated, 247
- natural mode, 220
  - see also* principal mode
- Newton's second law, in dynamics, 229, 263
- non-uniform torsion, 94–95
- normal mode, *see* principal mode
- normal mode method, *see* mode superposition analysis
- normal stress, 3
- normalization of modes, 230–231, 239
- numeric integration, 72, 75–76, 186, 257, 264
- open sections, 59, 77–78
  - torsion of, 87–90
  - under shear load, 84
- orthogonality of modes, 247–248
- orthotropic plates and slabs, 126, 136, 151, 155
- packages, 20
- paraboloid domes
  - under internal pressure, 180–182
  - under snow load, 208
- parallel, 170
- period, 219
- periodic excitation, 224
- phase angle, 219, 226
- plane sections, assumption of, 1
- plane strain, 48–50
- plane stress, 9–10
  - elasticity theory, 10–14
- plates, 101
  - beam analogy for, 102
  - bending theory, 105–117
  - classical solutions, 117, 155
  - grid analogy for, 103–105
  - see also* slabs
- Poisson equation, 68
- Poisson's ratio, 6
  - effect in plates, 104–105, 110
- Prandtl membrane analogy, 91–93
- principal axes, 84
- principal coordinates, 250–252, 256, 259–261, 263
- principal curvatures, 168
- principal modes, 220
  - approximate, 248–249
  - determination of, 230, 265
  - inaccuracy in, 246, 250
  - see also* orthogonality of modes
- principal moments, 110
- principal radii of curvature, 167–168, 170
  - of circular cylindrical shell, 203
  - of cone, 184–185
  - of paraboloid, 181

- of sphere, 176
- principal stress, 10–11
- plot, 34–35, 46–47
- radii of curvature, *see* principal radii of curvature
- random excitation, 227, 265
- Rayleigh quotient, 248–249
- reactions
  - in plates and slabs, 114–117
  - in slabs, 123, 129, 133
- rectangular sections, torsion of, 69–76
- reduced stiffness matrix, 248
- reduction of natural frequency relationship, 241–243, 268
- resonance, 225–228
- ring beam, 178, 207
- Saint–Venant
  - principle of, 9–10, 50, 94
  - torsion, 61, 65, 94
- self-excitation, 264
- semi-inverse method, 16
- shallow shells, 179
- shear centre, 61, 81, 87
- shear flow, 79, 80–82
  - direction of, 86
- shear forces
  - in plates, 111, 113
  - in shells, 172, 178, 188, 203, 204
  - in slabs, 120, 122–123, 129–130, 132–133
- shear load, 84
- shear modulus, 7
- shear strain, 5
- shear stress, 3–4
  - for circular section under torsion, 62
  - in closed sections under torsion, 88, 91, 93
  - in open sections under torsion, 88, 90–91, 92
  - in shells, 167, 172
  - in singly-closed sections under torsion, 78–79, 93
  - in solid sections under torsion, 64–66, 71–72, 75
  - in thin-walled sections under torsion, 78
  - sign convention, 3
  - trajectories in torsion, 72, 77–78
- shear wall analysis, 58
- shells, classification of, 165, 166
- shells of rotation, 165
- simple support
  - in plates, 103, 114
  - in shells, 178
- Simpson’s rules for integration, 72, 75–76
- singly-closed sections, 59
  - torsion of, 78–80
- slabs, 102
  - design moments for, 152–154
  - finite difference analysis of, 118–126
  - finite element analysis of, 136–152
  - grid analogy for, 103–105, 126–136, 152, 155
  - natural frequencies of, 244–246
  - torsional stiffness of, 127–128
  - see also* plates
- small deflection theory, 2
- soap-bubble analogy, 91
- soil–structure interaction, in dynamics, 264
- solid sections, 61
  - torsion of, 62–76
  - torsional properties of, 76
- spherical domes
  - under dead load, 176–177
  - under normal pressure, 206
- spring, 223
- steady-state, 225, 261
  - frequency, 225
- strain matrix, 283
  - circular cylindrical shell, 190

- square slab bending, 140
- triangular plane stress, 19
- stress concentration, in torsion, 89
- stresses
  - in plates, 107–110
  - in shells, 167, 202
  - see also* direct stress, shear stress
- stress function
  - for plane stress, 15–16
  - for torsion, 67–69, 91–93
- stress matrix, 283
  - circular cylindrical shell, 191
  - square slab bending, 141–143
- structure stiffness equations, 282
- structure stiffness matrix, 284
  - construction of, 25–29, 146–147, 194–196, 284
  - general properties of, 27, 29
- sub-matrix, form of structure stiffness matrix, 26–29
- support excitation, 227
- surface element, 1
- sway frames
  - by Rayleigh's method, 249
  - forced undamped vibration of, 258–261
  - free undamped vibration of, 253–255
  - natural frequencies of, 231–239
  - simplified analysis of, 235–239
  - under ground motion excitation, 258–261
- symmetry
  - in plane stress, 22, 29, 32
  - in plates and slabs, 103, 120, 121, 130, 133
  - of shear flows, 82, 86
  - of stress function in torsion, 74
  - warping along lines of, 62, 63, 70
  - with finite differences, 120, 277
- system stiffness matrix, *see* structure stiffness matrix
- Tacoma Narrows bridge, 48
- tangential stress resultant, 171–172, 174
  - see also* membrane forces
- tangential stress, 3
- thick plate theory, 151–152
- thin walled sections, 61
  - torsional properties of, 91
  - torsion of, 77–91
- time-dependent loading, 223
- torque, 61, 62
- torsion, elasticity theory, 63–69
- torsion constant, 62
  - for closed sections, 80, 91
  - for open sections, 89–91
  - for solid sections, 68–69, 72–73, 75–76
- torsional mode, 220
- transient excitation, 223
- underdamping, 222
- undetermined coefficients, 282
- uniform torsion, 61
- units, in dynamics, 219, 233
- vertical load on shell, 174, 175
  - due to fluid pressure, 175–176, 183–184
  - due to normal pressure, 174–175, 181
- virtual work
  - in plane stress, 14–15
  - principle of, 283–284
- viscous damping, 221
- von Mises failure criterion, 152
- warping, 61
  - displacement distributions, 63, 66–67, 69–71, 77
  - of thin-walled sections, 78
  - restraint of, 93–94
- Wood–Armer moments in slabs, 153
- Young's modulus, 6